

UNIVERSITY OF SOUTHAMPTON

**FACULTY OF ENGINEERING AND APPLIED SCIENCE
DEPARTMENT OF AEROSPACE ENGINEERING**

Doctor of Philosophy

**A THEORETICAL AND EXPERIMENTAL APPRAISAL OF
AIRWORTHINESS EVALUATION TECHNIQUES
FOR SMALL LIGHT AEROPLANES**

by

By Guy Brian Gratton

February 2005

This thesis has been completed as a requirement for a higher degree of the
University of Southampton

ABSTRACT

A thorough evaluation of the airworthiness of a manned aircraft is vitally important, regardless of the size or function of the aircraft. However, the methods used in light and particularly microlight aircraft certification were largely based upon rules of thumb or methods better suited to larger, higher energy, aircraft programmes.

A programme of research has been carried out to develop means by which microlight aircraft certification could be carried out appropriately to this class of aircraft.

The stall and immediately post-stall behaviour of an aircraft are shown to be a function of the deceleration rate prior to the stall; therefore it is necessary to use a representative deceleration rate when determining the acceptability of stall and post-stall handling qualities. This research has found means by which the range of deceleration rates likely to be seen in a particular type can be estimated, so that flight test programmes can ensure these rates are included, and thus aircraft are confirmed to have acceptable stalling characteristics.

Weightshift controlled microlight aeroplanes, using a Rogallo type wing, rarely show a conventional (square law) relationship between stalling speed and loading; the reason being identified as aeroelastic deformation of the wing with loading. A means by which stalling speed may be estimated for such aircraft at a variety of loadings has been developed. This will allow designers the maximum flexibility in determining operating limits and shows how the stall speed at various flight conditions may be predicted in aircraft operating documentation.

The spin is a serious and potentially fatal mode of flight; a spinning evaluation, even for non-aerobatic aeroplanes, is therefore essential. A best practice has been developed and tested for the spin-resistance or spinning evaluation of microlight aeroplanes, including equipment, aircraft and crew preparation, and reporting. The developed methodology is shown to be successful, using the results of certification flight test programmes, and the in-service safety record of aircraft which had been evaluated using these methods.

The tumble mode is a little known mode of departure from controlled flight experienced by weightshift controlled microlight aeroplanes. It has been a very significant factor in fatal accident records, being non-recoverable without the use of external safety devices. The mode consists of a nose-down autorotation at a rate of up to 400°/s. The tumble entry mechanism is explained, and advice to operators developed which should prevent tumble entry. Evidence is shown of the nature of the developed tumble – both modelled and through wind tunnel results, which explain how the autorotation occurs. It is also shown how this theory may be applied during testing of an aircraft to develop a tumble resistant aircraft.

VERBUM SAPIENTI

This thesis contains advice regarding the conduct of certain aspects of aeroplane flight trials and airworthiness assessment. Used within the context of formal training in these subjects, it is intended that this information will permit aircraft safety investigations to be carried out more safely and efficiently. Used without that supporting education and training, it has potential to do the opposite.

Use of the information herein cannot replace proper training in the fields of airworthiness, aircraft certification and flight testing, only supplement it.

In addition, it is cautioned that no theoretical method should be used to prove the safety (or otherwise) of an aircraft without substantiation by flight test.

AUTHOR'S DECLARATION

The work contained within this thesis is substantially the author's own, and is original. In particular the following are claimed as original work by the author.

- Modelling of the deceleration rate of a microlight aircraft between engine failure and the stall.
- Experimental proof of the Venton-Walters relationship between loading and stall speed for Rogallo wings, and demonstration of how this may be used within the aircraft certification process.
- Proposal and experimental justification of the controls-central spin recovery actions for microlight aeroplanes.
- Identification of the characteristics of the tumble mode in weightshift controlled microlight aeroplanes, together with the means of entry. Proposal of commonality between the microlight tumble mode, and departures from controlled flight previously seen on rigid flying wing aircraft.
- The GPS racetrack method for airspeed indicator calibration.
- The timed / segmented method for conservative estimation of aircraft take-off and landing distances.

TABLE OF CONTENTS

Notation	12
1 The “small light aeroplane” or “microlight aeroplane”	20
1.1 The legal definition of a microlight aeroplane.	20
1.2 The practical definition of a microlight aeroplane.	20
1.3 A brief history of microlight aviation in the United Kingdom	22
1.4 The environment within which a microlight aeroplane operates.....	26
1.5 General Peculiarities of microlight aircraft performance and handling.	26
1.6 Description Of The Main Design Features And Operation Of Weightshift Controlled Microlight Aeroplanes.....	28
2 Rate of deceleration towards the stall of a microlight aeroplane.	42
2.1 The fact and significance of stall entry rate.....	42
2.2 The definition of the stall and stall warning from the perspective of the pilot..	43
2.3 The significance and magnitude of the stall entry rate.....	46
2.4 Measuring and Estimating Stall Entry Rate.....	46
2.5 Physical significance of τ_d	62
2.6 Recommendations.....	62
3 Stalling speeds and determination of manoeuvre speed for conventional flexwing microlight aeroplanes.	63
3.1 Back ground to non-square-law stalling speed to loading relationship.....	63
3.2 The significance of V_A	65
3.3 Experimental investigations into a non-square-law stall speed to loading relationship for three aircraft: the Air Creation KISS-400, KISS 450 and iXess	67
3.4 Problems with developing a theoretical model.....	78
3.5 An alternative application of the non square law relationship between V_s and N_z : modification of N_1 and N_2	79
3.6 Historical precedent – normal acceleration limits for the Pegasus Quantum 15.	81
4 Spinning evaluation of 3-axis controlled microlight aeroplanes.....	83
4.1 The Spin Mode.	83
4.2 Scope of this Research.....	89
4.3 The spin recovery technique for microlight aeroplanes.	90
4.4 Certification requirements.	93
4.5 The philosophy behind spinning assessment for a non-aerobatic aircraft	93
4.6 Preparation for a spinning trial	94
5 The tumble departure mode in weightshift controlled microlight aeroplanes	99
5.1 Introduction to the tumble.	99
5.2 The mechanism of the established tumble.....	101
5.3 A simple estimate of the magnitude of induced camber during the tumble.	105
5.4 Longitudinal static stability of a weightshift microlight: development of a model intended to aid analysis of tumble entry	111
5.5 Wind tunnel testing of a scaled model to consider the flow around a tumbling aircraft.....	122
5.6 Discussion, induced inflow and vortex generation during the tumble entry	130

5.7	Discussion – behaviour of the aircraft during the sustained tumble.....	131
5.8	Avoiding the tumble.	131
5.9	Effect of aircraft mass upon the tumble.....	132
5.10	A simple model of the tumble equations of motion	135
5.11	Effect of wing settings.	141
5.12	Initiation of the tumble.	144
5.13	First proposed mechanism, the whip-stall.	144
5.14	Second proposed mechanism, Spiral instability combined with loss of visual horizon.....	145
5.15	Third proposed mechanism – failed loop manoeuvre.....	148
5.16	Fourth proposed mechanism, flight through own wake vortex.	153
5.17	Historical note 1 – the Northrop YB-49 “Flying Wing Bomber”	154
5.18	Historical Note 2, the Northrop XP-79 “Flying Ram” experimental fighter.....	156
5.19	Historical Note 3, The de Havilland DH108 “Swallow”	158
5.20	Historical Note 4, the BKB-1	160
5.21	Conclusions concerning the tumble.....	162
6	Conclusions	164
6.1	Stall entry rates in the planning of flight testing.....	164
6.2	Form of the O-A curve in Rogallo winged micro light aeroplanes.	164
6.3	Spinning evaluation of 3-axis controlled micro light aeroplanes.	165
6.4	The tumble mode.	165
7	Scope for further work in the fields of research described in this thesis..	167
7.1	Use of stall entry rates in the planning of flight testing.....	167
7.2	Form of the O-A curve in Rogallo winged micro light aeroplanes.	167
7.3	Spinning evaluation of 3-axis controlled micro light aeroplanes.	168
7.4	The tumble mode.	169
8	Acknowledgements	171
Appendix A – Other test techniques developed to assist in the investigation of aircraft flying qualities.		174
A1	Manual methods for data recording.....	177
A2	Use of GPS for airspeed indicator calibration. (The racetrack method)....	187
A3	Alternative GPS based methods for ASI calibration: the triangular, and box-pattern methods, also the non-GPS based ground course method.....	193
A4	Methodology for Spin-Testing of Microlight Aeroplanes.....	197
A5	A timed method for the conservative estimation of take-off distances, eliminating the requirement for external measurement devices.	214
A6	A timed method for the conservative estimation of landing distances, eliminating the requirement for external measurement devices.	224
Appendix B – Characteristics And Illustrations Of The Main Aircraft Types Referred To In This Thesis.....		228
B1	Aviasud Mistral.	229
B2	Eurowing Goldwing.....	230
B3	Easy Raider.....	231
B4	KISS-400	233
B5	Air Creation iXess	234
B6	Mainair Gemini Flash 2 and Flash 2a.....	235
B7	Mignet HM 1000 Balerit.	236
B8	CFM Shadow	237
B9	Raj Hamsa X’ Air Mk.1 and Mk.2. (Falcon).....	238

B10	Southdown (now Medway) Raven-X.....	240
B11	Spectrum T1.....	241
B13	Thruster TST Mk.1 and Thruster T300.....	242
B12	Thruster T600 and T600 Sprint.....	243
B13	Flightdesign / Pegasus CT2K.....	244
B14	Sky Ranger UK.....	245
B15	Naval Aircraft Factory N3N-3.....	246

Tables - Contents

<u>No.</u>	<u>Title</u>	<u>Page No</u>
Table 1,	CAS:TAS comparison for different heights	53
Table 2,	Comparison of theory with test data for stall deceleration rates.....	55
Table 3,	determination of deceleration time constant	57
Table 4,	Wing loadings for test aircraft at time of each stalling test	58
Table 5,	Demonstrating the accuracy of (2-27)	59
Table 6,	Stalling Speeds at various loadings for Air Creation KISS-400.....	68
Table 7,	Stalling Speeds at various loadings for Air Creation KISS-450.....	68
Table 8,	Stalling Speeds at various loadings for iXess	69
Table 9,	Spin Terminology	86
Table 10,	Inertia and aileron effects upon the spin mode.....	95
Table 11,	Conditions used for tumble simulation	109
Table 12,	Local angle of attack (degrees)	109
Table 13,	Pitching moments about hangpoint.....	116
Table 14,	Effect of trike mass upon inflow angle for constant pitching moment	134
Table 15,	Characteristics of typical aircraft	139
Table 16,	Results of test to demonstrate weightshift spiral instability	147
Table 17,	ASI calibration data reduction table	192
Table 18,	Test grid for a simple flapless aeroplane	200
Table 19,	Test grid for a simple flapped aeroplane.....	202
Table 20,	Summary of known spinning test results.....	207
Table 21,	Take-off test data for HM1000 Balerit at 420kg.	219
Table 22,	Take-off test data for N3N-3 Aeroplane.....	221
Table 23,	Landing test data for HM 1000 Balerit at 420kg.....	225
Table 24,	Landing test data for N3N-3 Aeroplane.....	226

Figures - Contents

<u>No.</u>	<u>Title</u>	<u>Page No</u>
Figure 1,	Mainair Gemini Flash 2 alpha	21
Figure 2,	Chevvron 2-32c 3-axis microlight aeroplane	22
Figure 3,	Raj Hamsa X'Air Mk.1 3-axis microlight aeroplane	22
Figure 5,	size of British registered microlight aircraft fleet.....	24
Figure 6,	Mainair Blade 912 in side view (courtesy of Mainair Sports Ltd).....	28
Figure 7,	Wing internal structure in planform.	29
Figure 8,	Typical flexwing pitching moment curve.....	30
Figure 9,	Aircraft with Raven wing, showing fin.	31
Figure 10,	Wing Frame main components.....	33
Figure 11,	Rear end view of Southdown Raven-X aircraft.....	34
Figure 12,	Conventional trike “breaking” mechanism.	40
Figure 13,	Rear View of Mainair Gemini Trike Main Undercarriage	41
Figure 14,	Generic polar for total drag upon a subsonic aircraft	49
Figure 15,	Deceleration constant versus wing loading (Goldwing and Thruster TST Omitted).....	58
Figure 16,	Deceleration constant versus wing loading (Goldwing and Thruster TST Omitted), with straight lines plotted giving greatest and least magnitude acceleration rates.	61
Figure 17,	Theoretical stalling speeds for Raven wing.....	64
Figure 18,	Classical flight envelope diagram.....	66
Figure 19,	Actual and classically predicted stalling speeds for Air Creation KISS-400	70
Figure 20,	Actual and classically predicted stalling speeds for Air Creation KISS-450	71
Figure 21,	Actual and classically predicted stalling speeds for Air Creation iXess....	72
Figure 22,	Stall Speed versus bank angle diagram from KISS-400 operators manual	73
Figure 23,	Stall Speed versus bank angle diagram from KISS-450 operators manual	75
Figure 24,	Stalling section from UK operators manual for Air Creation iXess.....	76
Figure 25,	Illustration of variation in stall speed with loading for three different values of C_{Ac} - with $V_s=30kn$	81
Figure 26,	Illustration of lift, drag and angle of attack of an autorotative spinning aeroplane	84
Figure 27,	Illustration of lift, drag and angle of attack at the wings of an aeroplane likely to enter a spiral dive from an attempted spin entry.....	85
Figure 28,	Illustration of aircraft flightpath and main parameters during a developed erect spin to the right.....	88
Figure 29,	Excerpt from BCAR Section S, showing spinning requirements.....	93
Figure 30,	Tail shape considered with relation to rudder blanking and thus spin recovery (diagrams are illustrative only and not to scale)	96
Figure 31,	Sycamore Seed with wing casing, showing similarity to trike with damaged wing.....	101
Figure 32,	Positions of aircraft in normal flight(A) and tumble(B).....	102
Figure 33,	position of whole aircraft CG	102
Figure 34,	illustration of induced camber during tumble.....	103
Figure 35,	Illustration of the effect of localised induced camber	104
Figure 36,	Illustration of aerodynamic forces sustaining the tumble.....	105

Figure 37, Illustration of tumble parameters.....	106
Figure 38, Local velocity components of airflow over a wing element	107
Figure 39, Determination of local angle of attack.	108
Figure 40, Local angle of attack variation	110
Figure 41, BHPA hang-glider test facility at Rufforth, Yorkshire.....	112
Figure 42, Sign conventions used in tumble analysis	113
Figure 43, Forces, distances and angles relevant to the longitudinal stability model	114
Figure 44, typical aircraft (Mainair Gemini Flash 2a) in flight	119
Figure 45, Pitching Moment of trike about hangpoint, zero thrust.....	120
Figure 46, Characteristics of Mainair Flash 2 alpha wing	121
Figure 47, Illustration of induced flow, superimposed upon aircraft image (Pegasus Quantum 15-912).....	122
Figure 48, Scale model of Mainair Gemini Flash 2 alpha aircraft, used in wind tunnel tests.....	123
Figure 49, Illustration of flow near the wing root during nose-down tumble rotation	124
Figure 50, Illustration of flow near the wing tip during nose-down tumble rotation	125
Figure 51, Series of illustrations of flow around aircraft during one tumble cycle. (All illustrations in same orientation).....	126
Figure 52, Illustrating the shift in vertical CG with passenger and fuel loading changes.....	133
Figure 53, Co-ordinate system for tumbling aircraft	135
Figure 54, Defining motion of the wing	135
Figure 55, Coordinate System in Wing.....	137
Figure 56, Illustration of tumble motion, $X_{CG}=0.5m$	139
Figure 57, Illustration of tumble motion, $X_{CG}=0.7m$	140
Figure 58, Illustration of tumble motion, $X_{CG}=0.3m$	141
Figure 59, Effect of different rigging conditions upon Mainair Flash 2 alpha wing.	142
Figure 60, Illustration of spiral instability as a function of engine power: Raven-X	148
Figure 61, Illustration of a fatal tumble after a failed loop	150
Figure 62, Northrop YB-49 experimental flying wing bomber.	155
Figure 63, Northrop XP-79B "Flying Ram"	157
Figure 64, de Havilland DH108 Swallow	158
Figure 65, Illustration of BKB-1.....	161
Figure 66, BKB-1 in flight	162
Figure 67, Typical kneeboards	177
Figure 68, Typical spring balance.....	178
Figure 69, Illustration of sawtooth flightpath.....	179
Figure 70, Typical test cards showing sawtooth climbs and glides	180
Figure 71, Analysed results of sawtooth climbs for N3N-3 aircraft	181
Figure 72, Analysed results of sawtooth glides for N3N-3 aircraft	182
Figure 73, Results from a continuous climb for the N3N-3 aircraft	183
Figure 74, Results from two continuous long glides for N3N-3 aircraft	184
Figure 75, Climb performance section from N3N-3 operators manual (UK public transport version).....	186
Figure 76, Typical modern handheld GPS receivers	187
Figure 77, Met office form 214 wind forecast, showing (columns from left) altitude, wind heading, wind strength, and OAT at specific locations.	189
Figure 78, Typical pressure chart (USAFE type)	190
Figure 79, Illustration of "racetrack" flightpath.....	191

Figure 80, Sample ASI calibration plot from GPS method	193
Figure 81, Sample kneeboard test card for spinning tests.....	203
Figure 82, Photographs of a whole-aircraft recovery parachute being deployed	205
Figure 83, Illustration of take-off segments.....	215
Figure 84, Geometry of Sandown airport as used for N3N field performance estimation (not to scale)	222
Figure 85, Aerial View of Sandown Airport, in similar orientation to figure above, showing approximate camera position.....	223
Figure 86, Chart of distance along runway centreline versus distance across video monitor screen, showing quadratic best fit curve.	223
Figure 87, Aviasud Mistral	229
Figure 88, Eurowing Goldwing fitted with Rotax 377 engine.....	230
Figure 89, Easy Raider J2.2(1).....	232
Figure 90, Air Creation KISS-400	233
Figure 91, Air Creation iXess	234
Figure 92, Mainair Gemini Flash 2.....	235
Figure 93, Mignet HM 1000 Balerit	236
Figure 94, Shadow CD	237
Figure 95, Raj Hamsa X'Air Mk.1 (UK) with Rotax 582/48-2V engine and Ivoprop propeller	239
Figure 96, Southdown Raven-X with Rotax 447 engine.	240
Figure 97, Spectrum T1	241
Figure 98, Thruster TST Mk.1.....	242
Figure 99, Thruster T600N Sprint.....	243
Figure 100, Flightdesign CT2K	244
Figure 101, Sky Ranger UK.....	245
Figure 102, Naval Aircraft Factory N3N-3.....	246

Notation

θ	Angle between local airflow, and a forward perpendicular line from the hangpoint. = $\alpha - \phi_w$
α	Wing angle of attack
ϕ_w	Wing control angle (0 places wing perpendicular to monopole)
η_p	Propeller efficiency
ϕ_g	Angle between monopole and earth Z-Axes
ϕ_T	Thrust angle (0 places thrustline perpendicular to monopole)
σ	Relative air density
ϕ	Bank angle
τ_d	Deceleration time constant (defined at equation 2-25)
ρ	Air density
$\frac{\partial IAS}{\partial CAS_s}$	Partial derivative of Indicated airspeed with respect to Calibrated Air Speed, determined at or near to the stall condition.
ω	(Pitch) Rotational velocity during tumble
ψ	Azimuth angle during sustained tumble.
ζ	Vorticity
η_p	Propeller efficiency
A	Rotational inertia of an aircraft about the longitudinal axis (rolling inertia)
A&AEE	Aeroplane and Armaments Experimental Establishment, located at Boscombe Down Airfield, Wiltshire. Now part of Qinetiq.
a_1	(During take-off) Acceleration from brakes off to rotation (Must be positive).
a_1	(During landing) Acceleration along flightpath from point at which aircraft descends through screen height to touchdown point.

a_2	(During take-off) Acceleration from rotation to unstick
a_2	(During landing) Acceleration along ground for segment of ground roll whilst aircraft is running on two wheels.
a_3	(During take-off) In flightpath acceleration from unstick to achieving screen height
a_3	(During landing) Acceleration along ground from point at which all three wheels touch the ground until aircraft stops. (Must be negative).
AAIB	(United Kingdom) Air Accidents Investigations Branch
ARB	(UK) Airworthiness Requirements Board (mandatory review body until it was dissolved in 2003 for new and changed airworthiness legislation). [Note, this abbreviation was also previously used to refer to the Air Registration Board, a precursor of the CAA. It is not used in this context within this thesis.]
ARB LAC	Light Aircraft Committee of the ARB
ASI	Air Speed Indicator
B	Rotational inertia of an aircraft about the lateral axis (pitching inertia)
BCAR	British Civil Airworthiness Requirements
BHPA	British Hang-gliding and Paragliding Association
BMAA	British Microlight Aircraft Association
BRS	Ballistic Recovery (parachute) System
C	Rotational inertia of an aircraft about the vertical axis (yawing inertia)
CAA	(United Kingdom) Civil Aviation Authority
C_{Ae}	Aeroelastic coefficient for a wing (used in determining stalling speed under load).
CAS	Calibrated Air Speed (also see RAS)
C_D	Drag coefficient of aircraft
C_{Di}	Induced drag coefficient
C_{Do}	Zero lift drag coefficient of aircraft
C_{Ds}	Drag coefficient of aircraft at point of stall
CG	Centre of Gravity (Centre of Mass)

C_L	Lift Coefficient of aircraft
$C_{L,max}$	Maximum (stall point) lift coefficient of aircraft
C_{LE}	Lift coefficient at the best range glide condition
CofA	Certificate of Airworthiness (the term normally implies an ICAO compliant document)
CR	Cruise Configuration, normally flaps-up gear up airbrakes retracted. In an aircraft lacking retractable gear, flaps or airbrake this will co-incide with all other normally referred configurations (PA, LAND, TO), in which case the terminology of configurations will not be used.
D_T	Trike drag
D_W	Wing drag
ETPS	Empire Test Pilots School (based at Boscombe Down, Wiltshire, UK)
FAI	Fédération Aéronautique Internationale (European Airports Federation)
FTO	Flight Test Observer (in aircraft)
g	Acceleration due to gravity (9.80665 N/kg, or m/s ²)
G	Best glide ratio
GPS	Global Positioning System (satellite navigation)
GS	Ground Speed
H	Altitude
IAS	Indicated Air Speed
ICAO	International Civil Aviation Organisation (International treaty based organisation setting international standards for overflight)
IMC	Instrument Meteorological Conditions (defined by being below acceptable minima of visibility or clearance from cloud for visual flight control)
ISA	International Standard Atmosphere (also sometimes known as US Standard Atmosphere).
JAA	Joint (European) Aviation Authorities
JAR	Joint (European) Aviation Requirements

k	Gradient of C_{Di}/C_L^2 ($\frac{\partial C_D}{\partial (C_L^2)}$)
k	Radius of gyration
K_{DT}	Trike drag coefficient = D/V^2
L	Lift
LAND	Configuration for landing, normally full flaps gear down. Usually co-incident with PA in a fixed-gear aircraft.
L_{CG_w}	Distance of wing CG behind the hangpoint
M	Wing aerodynamic pitching moment
M	Mass
MAUW	Maximum Authorised Weight (effectively an alternative term to MTOW for any conventional aircraft)
MCP	Maximum Continuous Power
MTOP	Maximum Permitted Take-Off Power
MTOW	Maximum (Authorised) take-off weight. (Also see MAUW)
n	Alternative term for Normal acceleration
N_1	Aircraft structural positive normal acceleration design limit at V_A
N_2	Aircraft structural positive normal acceleration design limit at V_D
N_3	Aircraft structural negative normal acceleration design limit at V_D
N_4	Aircraft structural negative normal acceleration design limit at V_A
N_Z	Normal acceleration.
NACA	National Advisory Committee for Aeronautics (US government research organisation, existing from circa WW1 until 1950s when superseded by NASA, the National Aeronautics and Space Administration).
NTPS	National Test Pilots School (based at Mojave, California, USA)
OAT	Outside Air Temperature
P	Engine power output

PA	Configuration Powered Approach, normally flaps down gear up airbrake deployed. Usually co-incident with LAND in a fixed-gear aircraft.
PFA	Popular Flying Association: UK representative body for amateur constructed light aircraft.
PFL	Practice Forced Landing (normally following a simulated engine failure)
PLF	Power required to maintain Level Flight
POH	Pilots Operating Handbook
PPL	Private Pilot's License
QFE	Altimeter setting giving an indication of zero height on the ground at a destination aerodrome. Given in hPa (hectopascals) or mb(millibars) the units being identical, ISA sea-level value being 1013.25
R ²	Coefficient of determination, defining the quality of a line fit ¹ , has value R ² =1 for perfect line fit, R ² =0 for totally random distribution.
RAS	Rectified Air Speed, alternative term to CAS.
S	Reference wing area (including a canard, if fitted, but not tailplane)
S ₁	(During take-off) Distance from brakes-off to rotation
S ₁	(Landing) Distance along ground from directly below point at which aircraft descends through screen height, until touchdown
S ₁ '	(Landing) Straight line distance from point at which aircraft descends through screen height, until touchdown.
S ₂	(During take-off) Distance from rotation to unstick
S ₂	(Landing) Distance aircraft is on two wheels during ground roll
S ₃	(During take-off) Straight line distance measured along the ground from unstick point to directly below point at which screen height is achieved
S ₃	(Landing) Distance from all three wheels being on the ground until aircraft is stopped

¹ Defined by $R = \frac{n \sum xy - \sum x \sum y}{\sqrt{n(\sum x^2) - (\sum x)^2} \sqrt{n(\sum y^2) - (\sum y)^2}}$

S_3'	(During take-off) Straight line distance from unstick point to point at which screen height is achieved
sHp	Standard Pressure Altitude (altimeter reading with 1013.25 hPa set on subscale)
t_1	(During take-off) Time from brakes off to rotation
t_1	(During landing) Time from screen height to touchdown
t_2	(During take-off) Time from rotation to unstuck
t_2	(During landing) Time spent on two wheels during ground roll
t_3	(During take-off) Time from unstick to achieving screen height
t_3	(During landing) Time spent from all three wheels touching down until aircraft stops.
TAS	True Air Speed
TO	Configuration for take-off, normally mid flaps gear down.
TP	Test Pilot
USAFTPS	United States Air Force Test Pilots' School
V	Aircraft translational velocity
V_1	(During take-off) True airspeed at rotation.
V_1	(During landing) True airspeed at screen height
V_2	(During take-off) True airspeed at unstick
V_2	(During landing) True airspeed at touchdown
V_3	(During take-off) True airspeed at screen height.
V_3	(During landing) True airspeed at point when all three wheels touch the ground.
V_A	Manoeuvre Speed (maximum speed at which aircraft will stall before exceeding structural limits in the normal axis)
V_D	Design airspeed limit (normally quoted in EAS)
V_{DF}	Flight test maximum achieved airspeed (normally quoted in CAS or EAS)
V_E	Best range glide speed

V_F	Maximum permitted speed with flaps selected. (May be a single value, or specified at different speeds for different flap settings, depending upon aircraft type).
VFR	Visual Flight Rules
V_H	Maximum achievable airspeed in level flight.
VMC	Visual Meteorological Conditions ² (defined as a minimum visibility of 3km below 3,000ft or 5km above 3,000ft, clear of cloud below 3,000ft or 1000ft vertical separation and 1.5km horizontal separation above 3,000 ft, maintaining sight of the surface at all times). In most countries this also implies daylight.
V_{NE}	Maximum permitted operating speed (Velocity, Never Exceed).
VOR	VHF (radio frequency) Omni-directional Range (navigation device)
V_{RA}	Recommended maximum speed for flight in severe turbulence (“Rough Air”).
V_{REF}	Recommended final approach speed (normally given in IAS)
V_S	Stalling speed
V_{SI}	Stalling speed at MTOW in a defined (or by default, cruise) configuration.
V_{SO}	Stalling speed, at MTOW, in the landing configuration.
W	Actual weight of an aircraft.
W/S	Wing loading (normally quoted for MTOW)
W_f	Mass (or quantity) of fuel carried on board an aircraft.
W_T	Weight of trike
W_w	Weight of wing
W_x	Weather
$X_{CG,T}$	Perpendicular distance of trike CG forwards of monopole
$Z_{CG,T}$	Distance below hangpoint of trike CG (in axis parallel to the monopole)

² Note: altitude is conventionally quoted in feet and visibility in kilometres. Whilst not standard SI units, this convention is continued in this definition of VMC.

Z_{DT} Distance from hangpoint to intercept between monopole and line of action of drag (assumed to be the centroid of area in front view)

Z_T Distance from hangpoint to intercept between monopole and thrustline

1 The “small light aeroplane” or “microlight aeroplane”

1.1 The legal definition of a microlight aeroplane.

Microlight aircraft are artificially defined: that is a low energy aircraft definition which allows simplified (and hence reduced cost) certification, construction, and operating rules. Whilst the existence of reduced regulation (or deregulated) low energy aircraft occurs in most countries, the precise definition and the terminology used varies. Terms used outside the United Kingdom include ultralight (USA, Australia, Canada), ultra-leger motorisée (France) and ultraleichtflugzeuge (Germany, Austria)

The terms “small light aeroplane” (sometimes abbreviated to “SLA”) and “microlight aeroplane” may be considered interchangeable. In practice, the term “microlight aeroplane” is most commonly used, whilst “small light aeroplane” is used by BCAR Section S[1], the UK certification standard for aeroplanes in this class (it was also a temporary legal definition used in the UK between 1999 and 2002 to indicate aircraft meeting the definition below but not the previous definition as described in 1.3 below .

- For landplanes: MTOW not exceeding 450kg for 2-seat aircraft, or 300kg for single seat aircraft
- For seaplanes and amphibians, MTOW not exceeding 495kg, or 330kg for single seat aircraft.
- V_{so} not exceeding 35 kn CAS. (Note, in the UK only, an acceptable alternative is a wing loading not exceeding 25 kgf.m⁻²).
- A maximum of 2 seats.

1.2 The practical definition of a microlight aeroplane.

Microlight aeroplanes have become a mainstream part of recreational aviation. At July 2004, they account for 23% of civil aircraft registered in the United Kingdom, and a similar proportion in most other affluent countries. They may be divided into three different control systems, although only two are considered in the course of this thesis, that is, three-axis and weightshift. The United Kingdom has 6 manufacturers of such aircraft, and numerous others exist worldwide.

The most common type of microlight aircraft is the “weightshift” or “flexwing aircraft”, an example of which is shown in **Figure 1**. A description of these aircraft and their operation may be found in [2]. In the UK, about 2,600 such aircraft exist.

Figure 1, Mainair Gemini Flash 2 alpha



Less common, but still very popular (about 1,100 such aircraft in the UK), is the 3-axis controlled aeroplane. These have much in common with a conventional light aircraft, and in many cases are indistinguishable save by an inspection of documentation – the dividing line being only the legal definition given above. Two typical aircraft are shown below in Figure 2 and Figure 3.

Figure 2, Chevron 2-32c 3-axis microlight aeroplane



Figure 3, Raj Hamsa X'Air Mk.1 3-axis microlight aeroplane



Further examples of typical aircraft, particularly those referred to within the text of this thesis, are included in Appendix B, with illustrations and main technical details.

1.3 A brief history of microlight aviation in the United Kingdom

Whilst recreational aviation in various forms has existed in the United Kingdom since the 19th century, there was a particular surge in interest in the early 1970s. Operating outside of regulation, two imported technologies in particular appealed to a desire amongst certain

people to fly without restriction. The first was the Rogallo winged hang-glider, which had been developed from some NASA research into foldable lightweight wings, the second was attempts primarily in the USA and Australia to develop very lightweight single-seat fixed wing aircraft such as the Australian Wheeler Scout, and the American Chotia Weedhopper. These two technologies to some extent converged, with powered hang-gliders and lightweight aeroplanes becoming relatively commonplace by the late 1970s, and sharing flying sites, and many components – particularly engines, propellers and undercarriage

Figure 4. Chotia Weedhopper

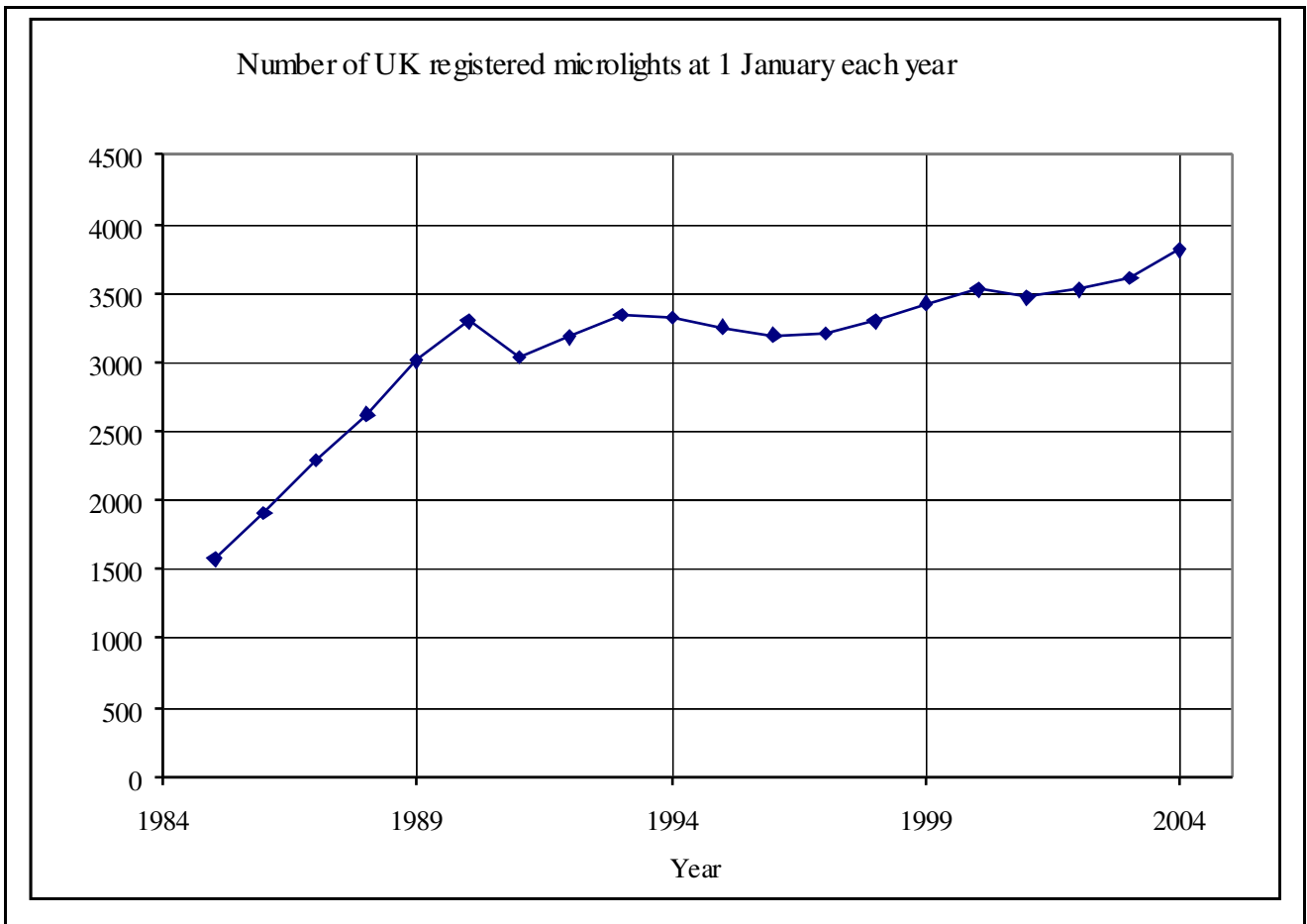


By the early 1980s, microlight aeroplanes were becoming increasingly common, but they were also becoming a matter of public concern. A combination of noise nuisance, and a high fatal accident rate (peaking at 18 deaths in the UK in one year[3]) caused questions to be asked in the houses of parliament. As a result, the UK Civil Aviation Authority was instructed to regulate microlight aeroplanes; therefore in 1981 mandatory pilot licensing was introduced, in 1984 it became mandatory that all aircraft with a empty weight exceeding 70kg met newly introduced safety requirements (BCAR Section S, based upon JAR-VLA and JAR-22) and in 1987 it became mandatory that all microlight aeroplanes should meet these requirements – albeit that “grandfather rights” were granted to aircraft with some established history of safe operation. During the same period mandatory noise emission testing was also introduced, as were requirements for periodic (usually annual) inspection and flight testing of all microlight aeroplanes. After some variation, the microlight definition was established as being a single or two-seat aeroplane, with an MTOW not exceeding 390kg and a wing loading (W/S) not greater than 25 kg/m². Additional limitations permitted a fuel capacity of no more than 50 litres and required that with a maximum seat occupancy of 90kg per seat (later revised to 86kg) and full fuel the aircraft should not exceed its MTOW.

Hence by 1987 the current pattern of regulation in British microlight aviation was established. That is that in order to fly (except under flight test conditions) all aircraft had to have been issued with a permit to fly, the basis for issuance of which was BCAR Section S[4]. That permit requires revalidation annually via an inspection and check flight, both by qualified persons [5].

During the late 1980s and the early 1990s the British industry matured, and numerous new designs were introduced, mostly indigenous, the overall size of the fleet increasing substantially as indicated by **Figure 5** below. The reasons were various, including improved public perception, improved accident rates, and reduced noise nuisance, as well as a continued large cost advantage relative to conventional General Aviation.

Figure 5. size of British registered microlight aircraft fleet



A further change was forced by the fact that this British microlight definition had diverged significantly from that which had become standardised across Europe – the European definition being based upon a sporting definition adopted by the Fédération Aéronautique

Internationale (FAI). Therefore in 1999, after several years of national debate, the UK adopted the European microlight definition, which included [6] aeroplanes having no more than two seats, V_{so} not exceeding 35 knots CAS, and a maximum take-off mass of no more than:-

- 300 kg for a landplane, single seater; or
- 450 kg for a landplane, two-seater; or
- 330 kg for an amphibian or floatplane, single seater; or
- 495 kg for an amphibian or floatplane

The previous wing loading limits and fuel limitation ceased to apply, and the empty weight limit was revised to require that with 86kg per seat and one hours fuel at maximum continuous power the aircraft should not exceed its MTOW.

This revision to the British microlight definition also co-incided with a re-issue of BCAR Section S at issue 2, which had been substantially revised to reflect the (correctly) anticipated greater kinetic energy and complexity of these “450kg” aircraft that started to appear, primarily through imports from the European mainland, once the microlight definitions had converged.

During the same period, various countries other than the United Kingdom also developed indigenous microlight safety standards. Of greatest significance was Germany (formerly West Germany) which developed a standard initially very similar to BCAR Section S, named BFU-95[7]; this was more recently superseded by a newer standard named RTF-UL [8]. The other country known to have introduced a rigorous design code against a similar microlight definition to the United Kingdom was the Czech Republic, whose design code UL2 part 1 is essentially a translation into Czech of the German code BFU-95. There has not been any successful attempt to converge the various requirements for microlight aeroplanes, but a degree of natural convergence has tended to occur, primarily because these various requirements have all to a greater or lesser extent been based upon JAR-22[9] and JAR-VLA[10].

1.4 The environment within which a microlight aeroplane operates.

It is not possible to properly understand the design of an aircraft without also understanding the operating environment. In many respects microlight aircraft are operated in a similar manner to any other privately owned light aeroplane. However, there are significant differences which are important when considering the design of these aircraft.

In the United Kingdom, as in many other countries, the law prevents the use of microlight aircraft for commercial work, other than for flight training, or during airworthiness flight testing (although the hiring of aircraft has recently become permissible under certain circumstances [11]). For this reason, and the low cost of ownership compared to other classes of aircraft, most aircraft are privately owned by individual pilots. Because these aircraft are associated with the search for low-cost aviation, this usually means that the aircraft are stored in less than ideal facilities (trailers, barns, sheds) and they are operated from what are normally semi-prepared or unprepared short (below 500m) grass airstrips which would probably be impracticable for larger or more conventional aircraft.

In addition, the routine maintenance on these aircraft is most often conducted by the aircraft owner, who often will have very little formal training or experience in aircraft maintenance.

These characteristics demand certain features from most microlight aircraft; specifically portability, ruggedness, and simplicity.

The pilots who fly microlight aircraft should also be considered. In the United Kingdom, they are trained to a relatively simple syllabus which can be completed in as few as 25 flying hours [12]. This relative lack of training and experience that can be expected from some private pilots puts a large onus upon those evaluating the airworthiness of an aircraft to ensure great clarity of operating instructions, and a good level of flying qualities.

1.5 General Peculiarities of microlight aircraft performance and handling.

Microlight aircraft inevitably possess low mass, and usually possess a relatively high form drag. This combination means that the speed and height can change very quickly, particularly in the event of power loss.

Such aeroplanes are almost universally fitted with uncertified engines, which may then be maintained by the operator who does not hold formal servicing qualifications. The

consequence of this is that such aircraft are more prone to engine failure than other classes. This necessitates good engine-off handling qualities, and relatively good (or at least predictable) glide performance.

Associated with the requirement for good glide performance, is the need for good low speed handling qualities. This is partly ensured by the certification requirement that either V_{SO} does not exceed 35 kn CAS, or that W/S does not exceed 25 kg/m². However equally, it is necessary that aircraft have flying controls which will allow full control to be maintained in all axes controlled down to a very low stalling speed – this implies in many cases greater control authority over the aircraft at low speeds than most larger “light” aircraft would possess.

A further effect of the low mass combined with the requirement for a low stall speed (implying a generally low wing loading), is that the effects of turbulence or other air disturbance is comparatively great. Pilots become familiar with large lateral or normal disturbances (potentially 45° of undemanded bank or $\pm 1g N_z$) during flying in visual conditions. These not only require sufficient structural integrity and strength, but sufficient control authority to correct such disturbances quickly enough to prevent loss of control.

However, whilst the above impose particular restrictions, in some areas designers and airworthiness investigators may be more relaxed. Microlight aircraft are not permitted to fly other than in day-VMC conditions whilst maintaining sight of the surface at all times. This means that navigation instruments need not be approved to the standards required for other aircraft classes (or in some cases, fitted at-all). Handling qualities need not be suitable for flight in IMC (for example, many microlight aircraft suffer neutral to divergent spiral stability, a characteristic only normally acceptable in aircraft flown with a constant visual horizon). Also, microlight aircraft (including all flexwing microlight aircraft, due to the tumble mode) are normally prohibited from flying aerobatics, so inverted oil and fuel systems, extreme handling characteristics beyond moderate pilot mishandling, and large propeller manoeuvring loads need not be considered with great rigour.

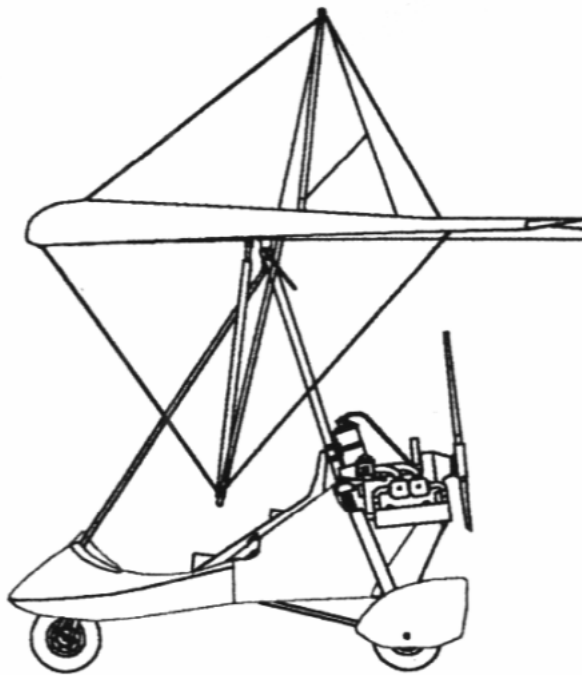
1.6 Description Of The Main Design Features And Operation Of Weightshift Controlled Microlight Aeroplanes.

The main components

Figure 6 below, shows a typical weightshift microlight aircraft (a Mainair Blade 912).

The aircraft comprises of two distinct parts, the trike and the wing. Whilst the interaction between them is essential to the characteristics of the aircraft, it is convenient initially to consider them separately.

Figure 6, Mainair Blade 912 in side view (courtesy of Mainair Sports Ltd)



The Wing - Aerodynamics

The weightshift wing is a tailless delta which has positive static stability in all three axes, it is normally of 8-10m wingspan, and 2.5 - 3.5m from nose to tip trailing edge. There is no pendular stability, since the *trike* (the unit hung below the wing, containing crew, undercarriage and powerplant) is suspended at the *hangpoint* through a joint which is free to rotate in pitch and roll without hindrance.

Longitudinal stability is provided by a combination of washout and wingsweep (thus producing a downforce at the wingtips, which are significantly behind the CG), and reflex (a reversed curvature of the aerofoil section at the inboard trailing edge). At high speeds, the fabric covering of the wing (the *sail*) will tend to flatten, reducing static stability. This is unacceptable and therefore two devices are incorporated into the wing design to prevent this loss of longitudinal stability. Firstly tipsticks (see **Figure 7**), also known as *minimum washout rods* are cantilever rods protruding perpendicular to the leading edge of the wing beneath (or occasionally within) the sail. These prevent the washout at the tips reducing below a preset value (usually about 3°) at low or negative angles of attack. Secondly, *luff lines* are a series of fixed length lines attached to the *kingpost* (a rod perpendicularly above the centre of the wing) and the trailing edge. These are effective in maintaining reflex at low angles of attack. Although luff lines have always been used in microlight aircraft, their advent in hang-gliders in the early 1980s produced a marked reduction in the hang-glider fatal accident rate [13]. The *luffing dive* was a neutral pitch control point, at which the pilot was denied any pitch control over the wing, usually resulting into an unrecoverable accelerating dive. **Figure 8** shows a typical pitching moment .v. AoA curve for a flexwing microlight wing.

Figure 7, Wing internal structure in planform.

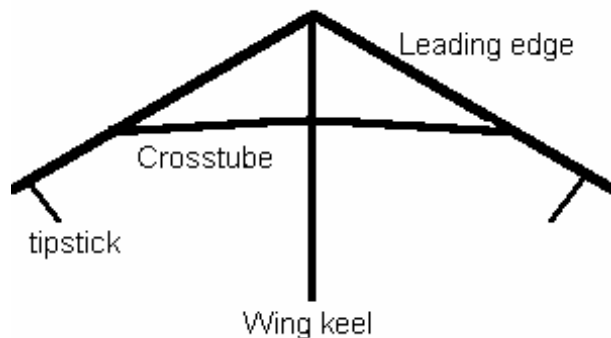
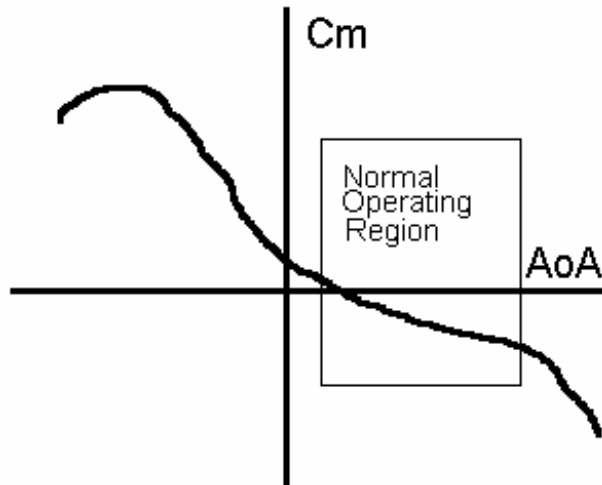


Figure 8. Typical flexwing pitching moment curve

On some modern wings (most notably the Pegasus Q2 wing, Mainair Blade wing, and the KISS series of wings) the luff lines also are used to provide a pitch trim mechanism. A tensioning device, controlled from the cockpit, can alter the *trim speed* through alteration of the amount of reflex – although sometimes with the undesirable side-effect of modifying roll power as a function of pitch trimmer setting [14]. Some hang-gliders make use of the washout rods to control pitch trim in flight [15], but no microlight aeroplane is currently believed to be using this mechanism.

Directional Stability is provided in the known fashion of any swept wing. This is usually supplemented by either a keel pocket (a weighted pocket suspended from the wing's structural keel) such as may be seen in **Figure 6**, or less commonly a fin, protruding above the aft part of the wing (**Figure 9**). Directional stability of current designs seems to have reached an ideal mid point between the requirement for adequate directional stability to ensure balanced turns, and the need to provide adequate control in turbulence; there have been attempts to fit “tip-fins” to such wings, which have largely resulted in aircraft virtually uncontrollable in turbulence due to excessive directional stability.

Figure 9, Aircraft with Raven wing, showing fin.



Photograph courtesy of Medway Microlights

Lateral Stability is provided primarily by a combination of wingsweep and angle of attack, in the same manner as for any classical delta winged aeroplane. It is extremely significant that at high angles of attack the lateral stability becomes extremely high such that roll power becomes weak, whilst susceptibility of the wing to undemanded rolling due to gusts becomes high. For this reason, pilots must fly at comparatively high speeds (occasionally as high as $2.0V_s$), and thus low AoA during approach or climb-out in particularly turbulent conditions, so that adequate control over the aeroplane can be maintained [16]. Nonetheless, lateral stability can still be unacceptably high, for which reason the wing will employ *billow shift*. The billow shift mechanism is as follows: -

- a) Bank is initiated by direct application of a rolling moment through the basebar.
- b) The trailing edge of the downgoing wing tends to move upwards, whilst the trailing edge of the upgoing wing tends to move downwards.
- c) This movement, is amplified by the lufflines, which are able to slide through a mechanism at the top of the kingpost. In effect, the wing has differential ailerons!

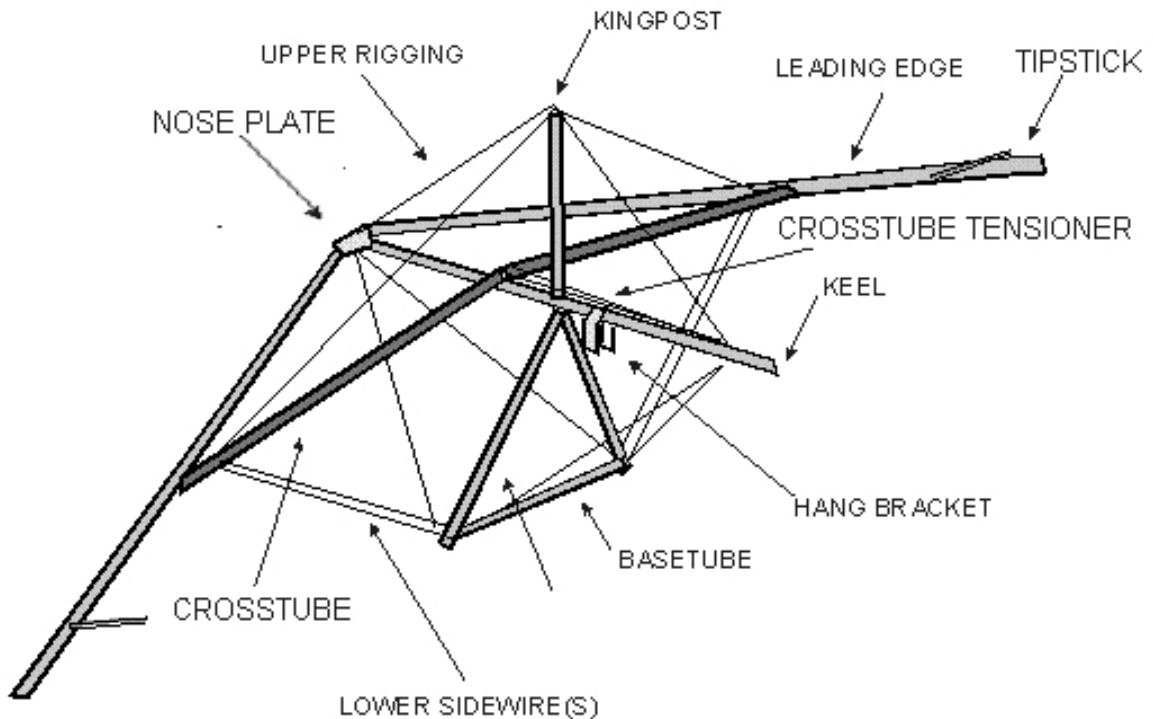
A similar mechanism also occurs at the wingtips, which are outboard of the lufflines, and thus provided with no automatic differential. This is known as *Leach*.

These mechanisms reduce lateral stability and so permits reasonably low control forces and deflections for comparatively high bank angles (most wings should be able to achieve 60° of bank with perhaps 200mm of lateral bar deflection). In a wing with low sail tension, this mechanism can however lead to an excessively high value of Roll Mode Time Constant (τ_R) giving handling problems - because of this it is a certification requirement that such aircraft do not require centring or reversal of roll control when rolling from 60° to 60° before passing through wings level [17, 18].

The Wing - Structure

The wing structure of a flexwing microlight (**Figure 10**) is complex, and somewhat unlike a that of a conventional wing. The primary parts of the structure are the *leading edges* - two segmented tubes typically 4.5 - 5.5 metres long, which are joined at the nose to the *keel tube* which runs the length of the wing and can be seen protruding from the trailing edge in **Figure 96**, **Figure 6**, and **Figure 9**. Stretched over these is the *sail* manufactured from a high-strength synthetic nonporous fabric such as Polyester Dacron. The whole structure is put under considerable internal loads during rigging, ensuring rigidity and form by *cross-tubes* which are hinged at approximately half span to the leading edges, and hinged to each other above the keel tube. Although they can and must move laterally relative to the keel tube, they are attached to the rear of the keel with a tensioning cable - it is this cable, running the length of the keel which ensures the form of the wing. The mechanism by which the cross-tubes and keel may move laterally compared to each other is referred to as a *floating keel*.

Figure 10. Wing Frame main components



Above the wing is a kingpost, attached through a flexible joint above the keel tube. To this is attached the lufflines, landing wires (which are attached to the leading edge / cross-tube junction), and usually leading and trailing edge wires to hold it in position. This can be seen in **Figure 6** and **Figure 10**

Looking at the wing in end view (see **Figure 11** below), the *A-frame*, consisting of two *uprights* and a *basebar* are clearly visible. In normal flight, the basebar is not only the primary flight control, providing both roll and pitch control, but also is primary structure, carrying in tension, via the *flying wires* much of the wing loads outboard of the cross-tube / leading edge junction. The inboard sections of the leading edge, and the A-frame uprights are for the most part in compression.

Figure 11. Rear end view of Southdown Raven-X aircraft



The position of the basebar is critical to correct control of the aeroplane, the ideal position relative to the pilot being referred to as the “piano playing position”. Adjustment of the position of the basebar, when developing a wing, can usually be done by adjusting the *front wires* and *rear wires* which run from the ends of the basebar to the nose and rear keel respectively. These wires locate the basebar, whilst also transmitting pitch control forces to the wing.

It can clearly be seen that the “wires” in the weightshift wing are extremely critical to the structure of the aircraft. All the structural wires are normally duplicated by parallel wires, perhaps 20 - 60mm away. The exception to this is the lufflines which, whilst aerodynamically critical, take very little actual load in flight. These are generally simplex, and of considerably reduced diameter compared to other structural wires (perhaps 2mm diameter, compared to 4 - 6mm diameter for flying wires).

The sail in older designs is usually of a single surface, that is the upper surface of the aerofoil with no separate lower surface. As the design of flexwings developed during the 1980s, increasingly the forward part of the sail used a lower surface also; modern wings almost universally have both upper and lower aerofoil surfaces throughout. The aerofoil section is maintained by *battens*, which are formed rods

inserted into pockets in the sail then put under compressive load. A modern wing may have 12 - 20 battens per side. The shape of these battens is highly critical, and they are subject to regular removal and checking as part of the routine inspection and maintenance of the wing [19].

The Trike - Aerodynamics

To the whole aircraft, the trike does not contribute significant lift, but inevitably a large segment of the drag and all of the thrust through a pusher engine / propeller combination in the 30 - 75 kW (40 - 100 hp) range. Propellers are usually large (1.5 - 1.7m diameter) compared to light aircraft propellers, and connected to either a 2 or 4 stroke engine through a reduction drive. 2 stroke engines are considerably more common, as are gearbox reduction mechanisms (as compared to belt reduction mechanisms). The reduction mechanism is necessary because of the high (typically 4000 - 7000 rpm) operating speeds of aircraft two stroke engines, which would otherwise cause supersonic tip speeds. Reduction ratios vary, although the most common value is 2.58:1. Ratios as high as 3.47:1 are used, but “simple” values such as 2:1, 3:1 or 4:1 are avoided because of the risk of sympathetic vibrations between engine and propeller, given that most propellers are either 2 or 3 bladed. An additional advantage for the designer, of a gearbox between propeller and engine, is the ability to easily introduce a torsional shock absorber, protecting the engine crankshaft from torque fatigue-inducing torque fluctuations; this is particularly necessary with modern composite propellers which may possess rotational inertia as high as 5000 kg.cm², compared to perhaps 2000 kg.cm² for a simple 2-bladed wooden propeller.

Aerodynamically the trike often has a significant effect upon directional stability [20]. The *pod*, which protrudes considerably forward of the trike CG, can often have a destabilising effect in yaw, particularly combined with a powerful engine. For this reason more modern, powerful aircraft, tend to use large aerofoil section wheel spats (as may be seen on the Mainair Blade in **Figure 6**). Older, less highly powered aircraft such as the Raven in **Figure 11** have less need of this. An interesting demonstration of this problem was the Pegasus XL-Q, an aircraft manufactured in

the late 1980s / early 1990s which had a comparatively powerful engine and a large forward pod area. Some examples of this aircraft would display a divergent Dutch Roll mode at high speeds, driven partly by poor trike directional stability, and partly by poor wing roll damping. The latter was particularly noticeable on aircraft with a multicoloured undersurface, the dyeing process of which had marked effects upon the fabric's elastic properties. This is one of the few recorded cases of an aircraft's colour scheme affecting the handling qualities - but any Engineer dealing with fabric covered aircraft should be aware of the risk. The author's personal experience of flying a "Rainbow-Q" aircraft, was also of a high τ_R giving less 'crisp' roll control than more soberly coloured wings..

In pitch, the trike mass has the effect of setting the trim speed of the aircraft. The hangpoint (point on the trike keel at which the trike's *monopole* is attached to the wing) is not at CP, therefore the pitching moment of the trike as suspended from the wing affects the trim speed of the aircraft. In practice it is the position of the hangpoint which affects the trim speed far more than the weight of the trike. In a Medway Raven-X aircraft (**Figure 9**), a 70 mm change in hangpoint position could alter the trim speed in the range 35 - 60 knots, whilst a 50% increase in trike suspended weight might increase the trim speed by 3 - 4 knots; a similar response has been found during flight testing of an experimental variable hangpoint on a Mainair Gemini Flash 2 alpha . This effect will be discussed in greater depth later in this appendix. However at this point it is important to appreciate that the wing aerodynamics alone, whilst important, cannot just be regarded separately from the dynamics of the whole, combined system.

Because of the nature of the hangpoint, the trike has no effect upon lateral stability other than by increasing or decreasing the load upon the wing, and thus the trimmed AoA value.

The Trike - Structure

The most important part of the trike is the *monopole*: this is the "vertical" mast extending from the mainwheels to the hangpoint. Engine, wing, seat frame and

mainwheels are all attached to this component which is structurally highly critical. Generally, the monopole will consist of two concentric aluminium alloy tubes, with an interference fit between them. Whilst this design should give adequate protection against failure due to fatigue crack propagation around the monopole, most designers also fit a further backup cable through the centre of the monopole which connects the lower engine mount, or sometime undercarriage attachment, to the hangpoint.

Horizontally from the base of the monopole runs the *trike keel tube* to which will be attached the forward part of the *seat frame*, and the nosewheel. From the front of the trike keel tube (also known as the *snoot*) to the monopole, just below the hangpoint, runs the *front strut*. Although this has the appearance of primary structure, in most flight modes its primary function is of a control stop - preventing the basebar from travelling so far forward that the propeller may strike the rear part of the wing keel. It does however serve a function in preventing collapse or inadvertent distortion of the trike frame during either heavy landings, or high normal acceleration manoeuvres. The front strut is held in place by a single removable pin at top and bottom; it is essential that it can be easily removed to permit the wing to be removed during derigging. The rigging and derigging operations will be discussed later.

The Combined Aircraft

The combined structure of the wing and trike become a complete aircraft. They are joined by a single bolt in quadruple shear at the hangpoint, known as the “hangbolt” or more commonly and colloquially as the “Jesus Bolt”, reflecting the available alternatives in the event of a bolt failure - thankfully an almost unknown occurrence. Most designs will also incorporate a backup strap or cable, attached to the monopole below the hangpoint, which runs loosely around the keel tube. This, in case of a hangbolt failure, is expected to keep the wing and trike together, albeit with control restriction and likely damage to the keel, is intended to keep the wing and trike together long enough for a landing to be executed. No recorded instance can be found of this backup mechanism being tested following an actual hangbolt failure.

So far as the wing and its longitudinal stability is concerned, the CG is located at the hangpoint. The trike CG, compared to that of a conventional aeroplane, is comparatively unimportant. It is essential that the trike CG is such that when suspended, the mainwheels hang at least 30mm below the nosewheel (so as to prevent any risk of a nosewheel-first landing), but beyond that current theory does not consider trike longitudinal CG to be significant in aircraft stability. However, it is important that the basebar position, which the designer may alter by changing the lengths of front and rear flying wires, is in a roughly central position between the pilot's chest and the front strut, thus ensuring adequate longitudinal control in both the nose-up and nose-down senses. Thrust does have a significant effect upon the "hang-angle" of the trike, and thus although not affecting the trim speed, will alter the ratio of pitch control authority in the nose-up to nose-down directions (i.e. at higher thrust, the trike tends to hang more nose-up, and thus the nose-up pitch authority increases since there is greater distance between the basebar and front strut in the trimmed condition.)

The trim speed of the aircraft is the airspeed at which the aircraft will tend to fly hands-off, variations from which requiring a continuous force to be applied at the control bar. Apart from some modern types which use the lufflines to provide a pitch trimmer effect, the majority of weightshift microlights do not have any kind of trimmer and thus the pilot will tend to climb, cruise, and descend at constant speed. The value of the trim speed is dictated by four factors: -

- The form of the C_M - α curve for the wing.
- The form of the C_L - α curve for the wing.
- The weight of the trike.
- The distance from the hangpoint to the wing Centre of Pressure (CP).

The trim speed will be that speed at which the form of the C_M - α curve shows a pitching moment at the value of C_L necessary for 1g flight at the aircraft weight, equal and opposite to the pitching moment generated by the weight of the trike multiplied by the moment arm between the hangpoint and CP. Both the C_M - α and C_L - α curves will

vary in shape and dimensions as a function of airspeed, due to the aeroelastic deformation of the wing surface.

The subject of longitudinal static stability of the weightshift aircraft is obviously far more complex than the simplified explanation above, but it is not proposed to discuss the subject, which is still not well understood, further herein. However reference [21] attempts to analyse the problem for hang-gliders which, although lacking a propulsion device, have similar characteristics.

Design Implications of the Operating Environment

In the United Kingdom, as in many other countries the use of microlight aeroplanes is restricted; specifically to private use, instruction, airworthiness flight testing [22], and hire only under certain limited conditions [23]. For this reason, and the low cost of ownership compared to other classes of aircraft, most aircraft are privately owned by individual pilots. Because these aircraft are associated with the search for “cheap” aviation, this usually means that the aircraft are stored in less than ideal facilities (trailers, barns, sheds) and they are operated from what are normally semi-prepared or unprepared short (<500m) grass airstrips which would probably be impracticable for larger or more conventional aircraft.

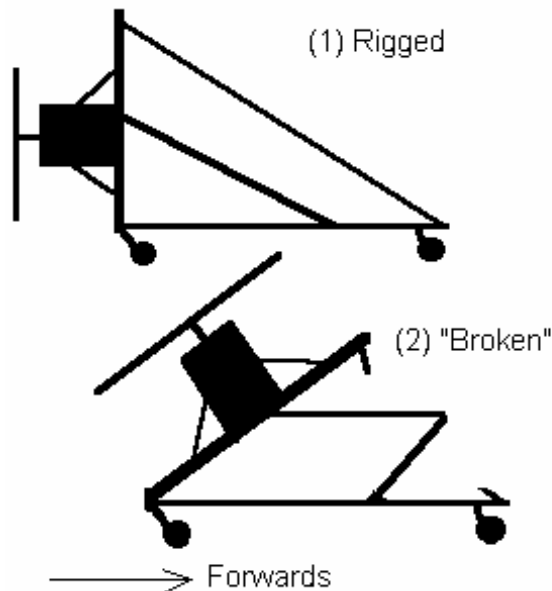
Almost universally also, the routine maintenance on these aircraft is conducted by the aircraft owner, who often will have very little formal training or experience in aircraft maintenance.

These characteristics demand certain features from a flexwing microlight aircraft; specifically portability, ruggedness, and simplicity.

Derigging of a weightshift microlight is in two stages. Firstly the front strut is removed, permitting the monopole to be inclined forwards until the basebar and nose of the wing rest upon the ground. This allows the hangbolt to be removed, and the wing and trike separated. The monopole inclines forward by use of hinged joints at the base of the monopole, and at the centre and each end of the seat frame (see **Figure**

12 below). Some more modern trikes such as the Pegasus Quantum eliminate the seat-folding mechanism by locating the monopole slightly further forward and using a gas-filled compression strut between the monopole and trike keel.

Figure 12, Conventional trike “breaking” mechanism.



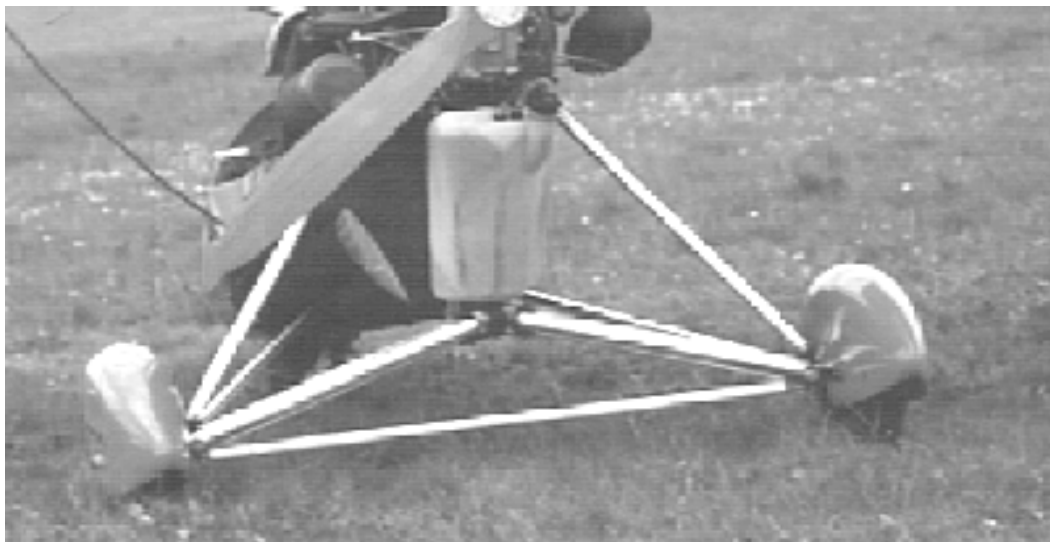
The second stage of derigging is for the link between the nose and crosstubes to be removed, taking the tension from the system, permitting the leading edges and crosstubes to be folded parallel with the wing keel, and allowing the battens to be removed. The A-frame is also collapsed by removal of the forward flying wire, and then removal of the basebar, permitting the pin-jointed A-frame structure to be folded again parallel with the wing keel. This entire process, including folding of the fabric, which remains attached to the wing frame takes 20-30 minutes and leaves the wing in readily transportable state - a cylinder roughly 5.5m x 0.3m. The two component parts (wing and trike) of a 2-seat aircraft will have empty weights of approximately 50kg and 100-130kg respectively and are now easily storable or transportable.

The advantages of this system of routine derigging are routine removal of the wing fabric from exposure to degrading UV radiation, the forced regular inspection of much of the primary aircraft structure by the pilot, and the ability to store or transport the aircraft inexpensively. The primary disadvantages are inconvenience to the pilot, and wear and tear upon the aircraft structure, particularly the sail.

Ruggedness and simplicity in the design of flexwing microlights go together. Virtually all of the structure of the aircraft is constructed from bolted or pinjointed alloy tube, which is a form of structure that tends to be very elastic under load. Also, because of the simplicity of this, in the event of structural damage, repair is almost invariably by direct replacement, a task which requires very little skill. Virtually all primary structure is duplicated, usually by internal or external sleeving, or internal backup cables.

Undercarriages, which traditionally are the most damage susceptible parts of a light aircraft are again manufactured from a pin-jointed tubular structure. Shock absorption is from large tyres, with spring action created by steel cables between the mainwheel hubs (see **Figure 13** below). This system is aerodynamically very inefficient, but is capable of sustaining very large landing shocks, whilst being inexpensive to construct, and largely maintenance free. More modern microlights have used undercarriage shock absorption more similar to that used on a light aircraft, but the system described continues to be the most common and inexpensive design solution.

Figure 13. Rear View of Mainair Gemini Trike Main Undercarriage



2 Rate of deceleration towards the stall of a microlight aeroplane.

2.1 The fact and significance of stall entry rate.

The stall entry rate of any aircraft is critical in determining the stall and post-stall characteristics. This is because of the “deepness” of the stall, i.e. the minimum airspeed actually achieved before the aircraft starts to recover, and its being affected by the deceleration rate prior to the stall. This may be demonstrated by examining the stalling characteristics of an X’Air Mk.1 (see Appendix B9) aircraft shown in Table 1 below.

2.1.1.1 Table 1, X’Air Mk.1 stalling characteristics

Stalling Characteristics, G-BYCL		
Type: X’Air 582(1), mid CG, MTOW, flight idle.		
Source of data: Type Certification flight test reports.		
<u>Engine Power</u>	<u>Stall Entry Rate</u>	<u>Stall Characteristics</u>
Flight idle (throttle closed)	1 kn/s	Ran out of control authority in level flight attitude
Flight idle (throttle closed)	2 kn/s	5° nose down pitch at the point of stall
Flight idle (throttle closed)	5 kn/s	20° nose down pitch at the point of stall

In general, more rapid stall entries tend to cause greater nose-down pitching moments at the point of stall, whilst slower stall entries (typically the conventional 1 kn/s deceleration primarily used during certification testing) causes a reduced pitching moment, but in some circumstances a greater tendency for the aircraft to suffer a wing-drop. During the flight test parts of this research, no general relationship between the stall entry rate and any tendency to enter a spin has been observed, but certain types of aeroplane (for example the Spectrum T1 as shown in Appendix B11) will certainly enter an

incipient spin mode from a rapid stall entry, whilst this does not occur following a more gradual deceleration.

2.2 The definition of the stall and stall warning from the perspective of the pilot.

It is important to appreciate that the stall, as seen by the pilot, is not identical to the stall as would be understood classically by an aerodynamicist. The following definition, which is extracted from BCAR Section S, is typical of the definitions contained in most civil certification standards:-

(From S201(a)) Stall demonstrations must be conducted by reducing the speed by approximately 1kn/s from straight and level flight until either a stall results as evidenced by a downward pitching motion or downward pitching and rolling motion not immediately controllable or until the longitudinal control reaches the stop.

A more simple definition, which is a variation upon that taught in the military test pilots schools such as the Empire Test Pilots School at Boscombe Down, Wiltshire (ETPS), is that *a stall is the point following deceleration at which the pilot ceases to have full control over the aeroplane.* This is compatible with the definition above, since an uncontrolled motion or the longitudinal control being on the stop are clear indicators that the pilot does not have full control over the aircraft in all axes; however, wing rocking (undemanded rolling oscillations, initially of low amplitude but potentially enough to roll an aircraft inverted if not controlled), or other low-speed departures from controlled flight may also be included.

This definition is different to the stall as commonly explained in purely aerodynamic terms. Such conventional explanations (for example section 8.2. of [24]) would most normally either define the stall when considering lift versus AoA characteristics as the point at which lift ceases to increase with increasing AoA, by reference to a flow visualisation as the point where a given degree of flow detachment occurs from the lifting surface, or as the point at

which there is a marked increase in the gradient of $\frac{\partial C_M}{\partial \alpha}$. However, whilst these features are essential to aerodynamic research, not all (or sometimes any) of these will be immediately apparent in those forms to a pilot and depending upon severity may not be considered by a pilot to mark the stall in any case.

During a test programme, the test team must define the stall for a specific aircraft. Notwithstanding that other definitions may be useful in certain circumstances, the three most common definitions are:-

- The longitudinal control being on the nose-up control stop (often termed “mush” by pilots). This is most common at forward CG / hangpoint states where insufficient nose-up control authority exists to fully aerodynamically stall the wing.
- A downward pitching motion (often termed a “pitch break”). This is caused by a loss of lift at the mainplane (or canard) altering the balance of forces and moments on the aircraft and causing a net nose-down pitching moment. This is most common at aft CG/hangpoint states, where there is sufficient nose-up control authority to fully aerodynamically stall the wing.
- A wing drop, sometimes accompanying a pitch break. This occurs where the two sides of the mainplane do not stall simultaneously and may be caused by a small amount of uncorrected sideslip, a rigging asymmetry in the wings and airframe, or by an inadvertent control input.

The term stall warning describes those characteristics of the aircraft which indicate to a pilot that he or she is flying at conditions close to the stall and caution may be needed. Stall warning characteristics will vary between

aircraft and should normally be noted in the operators manual. The following are typical stall warnings:-

- Airframe buffet, as localised airflow starts to detach.
- Stick buffet, as localised airflow, usually over the wing root in a conventional 3-axis/tailplane aircraft, detaches and strikes the tail control surfaces.
- Artificial stall warning devices, normally either based upon an AoA sensor [25] or a localised airflow pressure sensor [26], [27].
- An aircraft pitch attitude which is perceptibly more nose-up than that normally seen in level flight.
- The aircraft's primary pitch control being noticeably displaced in the nose-up sense compared to its position in level flight.
- Lack of control responsiveness.

During the airworthiness evaluation process for any aircraft, the following questions need to be addressed:-

- What are the stalling characteristics at representative deceleration rates? Are these characteristics acceptable?
- What are the stall warning cues? Are they adequate?
- Is the aircraft fully controllable during deceleration down to the point of stall?
- Can the aircraft, post-stall, be returned to controlled flight without the use of exceptional piloting skill, or whilst suffering an unacceptable degree of height loss or uncommanded manoeuvre?

Finally, operating data (most particularly the Pilots Operating Handbook, or POH) must be confirmed to accurately and safely address the stalling characteristics of the aeroplane.

2.3 The significance and magnitude of the stall entry rate

Historical experience[28] is that in most light aircraft, the combination of inertia and drag are such that in the event of mishandling or sudden loss of power, the rate of deceleration can reasonably be expected to be around the 1kn/s used for the determination of stall speed (and acceptable handling characteristics at the point of stall) contained within most certification codes. However, for microlight aircraft, this is not necessarily true; the combination of low mass and relatively high drag (particularly caused by unfaired or externally braced structures) can result in far higher deceleration rates. The consequence of this is that the handling characteristics following a genuinely inadvertent stall, can differ significantly from those which would be found if testing was only carried out at 1kn/s deceleration.

Realising this, most accepted test schedules such as [29],[30] insist upon acceptable stalling characteristics at increased deceleration rates of up to 5kn/s. This value however is entirely empirical and the reason for this value has not historically been justified. To address this lack of rigour, the following investigation seeks to establish a means to estimate a deceleration rate, representative of what would occur in a mishandling or sudden loss of power case, which might be used during certification flight testing to determine whether stalling characteristics are acceptable.

2.4 Measuring and Estimating Stall Entry Rate

The following assumptions are made:

- In this class of aircraft, the pilot will initially either enter a descent or maintain level flight in the event of a sudden engine failure. (In high energy aircraft such as fighters the immediate action would be to climb to increase

potential energy; however this behaviour is inappropriate and is not taught in small light aeroplanes.)

- C_{D0} is constant between V_S and V_E
- The partial derivative of lift with respect to induced drag squared is constant between V_S and V_E
- The aircraft is moving within a fixed air mass (i.e. inertial effects due to movement of that air mass are insignificant).

Basic equations:

Basic lift equation $L = \frac{1}{2} \rho V^2 S C_L$ (2-1)

Basic drag equation $D = \frac{1}{2} \rho V^2 S C_D$ (2-2)

Components of Drag $C_D = C_{D0} + k C_L^2$ (2-3)

Note that the term k above represents something more complex than a simple coefficient, however for the purposes of this analysis will be treated as a constant value for $\frac{\partial C_D}{\partial (C_L^2)}$ and its greater physical significance will not be discussed. A detailed

discussion of the significance of this constant may be found particularly in chapter XI of reference [31] and also repeated in more recent texts.

Consider the Aircraft at the stall

Drag at the point of stall $C_{D_s} = C_{D0} + k C_{L_{max}}^2$ (2-4)

[from (2-3)], assuming

$C_{L_{max}}$ occurs at the stall.

Re-arranging (2-1):- $C_{L_{max}} = \frac{Mg}{\frac{1}{2} \rho V_S^2 S}$ (2-5)

Inserting (2-5) into (2-4):-

$$C_{Ds} = C_{Do} + k \left(\frac{Mg}{\frac{1}{2} \rho V_s^2 S} \right)^2 \quad (2-6)$$

Inserting (2-6) into (2-2):-

$$D_s = \frac{1}{2} \rho V_s^2 \left(C_{Do} + k \left(\frac{Mg}{\frac{1}{2} \rho V_s^2 S} \right)^2 \right) \quad (2-7)$$

Applying Newton's second law to (2-7)

$$\left(\frac{dV}{dt} \right)_s = - \left(\frac{\frac{1}{2} \rho V_s^2 S}{M} \right) \left(C_{Do} + k \left(\frac{Mg}{\frac{1}{2} \rho V_s^2 S} \right)^2 \right) \quad \text{Where} \quad (2-8)$$

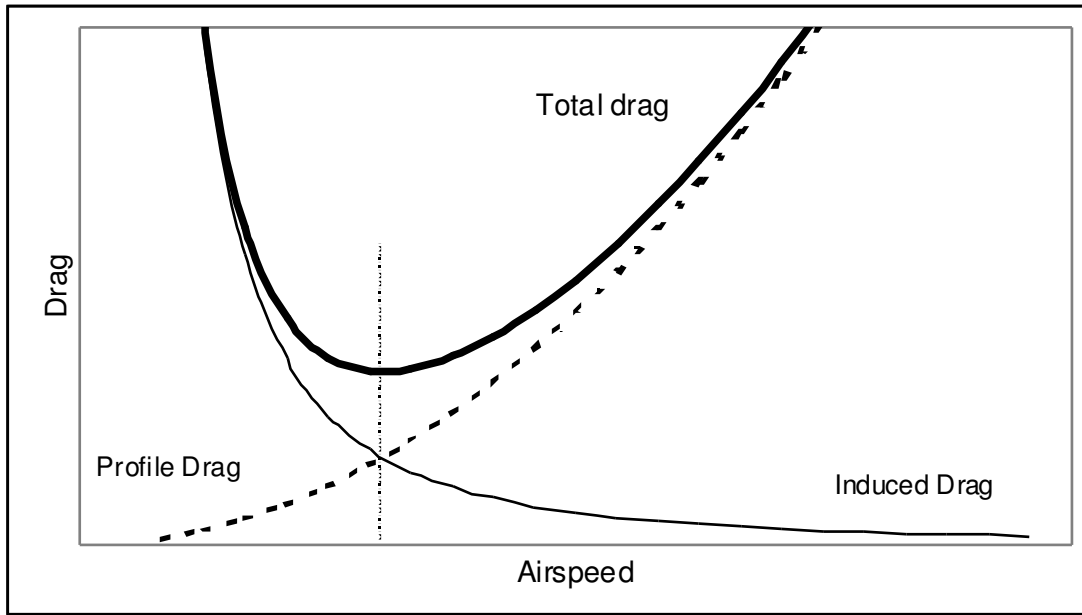
the acceleration rate, $\frac{dV}{dt}$ should have a

negative sign during the deceleration towards the stall.

In order to solve equation (2-8) we only require C_{Do} and k , since all other parameters are known. These missing terms will be found by use of the best range glide condition - since at this condition $C_{Do} = kC_L^2$ and the best glide ratio, G , exists. G will normally have been determined and is quoted in the aircraft operating manual.

(Note: proof that $C_{Do} = kC_L^2$. Total subsonic aircraft drag is conventionally regarded as being made up of two components [32] which are induced drag, defined by $D_i = \frac{1}{2} \rho V^2 S \cdot k \cdot C_L^2$ and profile (or form) drag which is defined by $D_p = \frac{1}{2} \rho V^2 S C_{D_p}$. **Figure 14** below is shown a generic graph for these two components and the total value of drag, defined by $D = D_i + D_p$.)

Figure 14. Generic polar for total drag upon a subsonic aircraft



By inspection, total drag is at a minimum at the airspeed where Profile drag is equal to induced drag. Therefore at this speed,

$$\frac{1}{2}\rho V^2 S .k.C_L^2 = \frac{1}{2}\rho V^2 S C_{D_o} \text{ and hence, } k.C_L^2 \equiv C_{D_o} .)$$

(Note: proof that $(L/D)_{MAX}$ is identical to the best glide ratio. The curve of total drag against speed is known from all available experimental data to show a clear minimum. Since $D = L\left(\frac{D}{L}\right)$ and assuming level flight or a shallow glide angle $L = W$, $D = W\left(\frac{D}{L}\right)$. Thus the speed at which the minimum value of drag occurs is co-incident with the point where L/D is at a maximum. It is known that L/D is identical to the glide ratio, and thus to the best glide ratio since it is at a maximum at this speed.)

Hence, at this condition: $C_{D_o} = k C_{LE}^2$ (2-9)

And also, from (2-1) $L = nMg = \frac{1}{2}\rho V_e^2 S C_{LE}$ (2-10)

Therefore, and assuming that $n=1$ (nominally level flight)

$$C_{LE} = \frac{Mg}{\frac{1}{2}\rho V_E^2 S} \quad (2-11)$$

We know that at this condition, $C_{Do} = k C_{LE}^2$

$$k = \frac{C_{Do}}{C_{LE}^2} \quad (2-12)$$

thus:-

And since $G = \frac{C_L}{C_D}$ at this point

$$G = \frac{C_{LE}}{C_D} = \frac{C_{LE}}{2C_{Do}} \quad (2-13)$$

Thus:-

$$C_{Do} = \frac{C_{LE}}{2G} \quad (2-14)$$

Substituting (2-14) into (2-12) gives:-

$$k = \frac{C_{LE}}{2G C_{LE}^2} = \frac{1}{2G C_{LE}} \quad (2-15)$$

and substituting (2-11) into (2-15) gives:-

$$k = \left(\frac{1}{2G}\right) \frac{\frac{1}{2}\rho V_E^2 S}{Mg} \quad (2-16)$$

So, from (2-16) one may now calculate k, since all other terms are known.

Now, from (2-9), (2-16) and (2-11):-

$$C_{Do} = k C_{LE}^2 = \left(\frac{1}{2G}\right) \left(\frac{\frac{1}{2}\rho V_E^2 S}{Mg}\right) \left(\frac{Mg}{\frac{1}{2}\rho V_E^2 S}\right)^2$$

$$\therefore C_{Do} = \left(\frac{1}{2G}\right) \left(\frac{Mg}{\frac{1}{2}\rho V_E^2 S}\right) \quad (2-17)$$

Then, inserting (2-16) and (2-17) into (2-8) this gives an estimate for the aircraft's longitudinal acceleration at the point of stall:-

$$\left(\frac{dV}{dt}\right)_s = \left(\frac{\frac{1}{2}\rho V_s^2 S}{M}\right) \left(\left(\frac{1}{2G}\right) \left(\frac{Mg}{\frac{1}{2}\rho V_E^2 S}\right) + \left(\frac{1}{2G}\right) \left(\frac{\frac{1}{2}\rho V_E^2 S}{Mg}\right) \left(\frac{Mg}{\frac{1}{2}\rho V_s^2 S}\right)^2 \right) \quad (2-18)$$

It may be seen, that all terms in M , $\frac{1}{2}\rho$, S cancel out in (2-18), giving:-

$$\left(\frac{dV}{dt}\right)_s = V_s^2 \left(\left(\frac{1}{2G}\right) \left(\frac{g}{V_E^2}\right) + \left(\frac{1}{2G}\right) \left(\frac{V_E^2}{V_s^4}\right) g \right) \quad (2-19)$$

$$= \frac{g}{2G} \left(\frac{V_s^2}{V_E^2} + \frac{V_E^2}{V_s^2} \right) \quad (2-20)$$

This gives a value, from readily available aircraft data for the maximum magnitude of acceleration (which will have a negative sign) immediately prior to the stall event, when an aircraft is not in manoeuvring or climbing flight. The airspeed values, since they divide into each other may be treated in any convenient unit, g is conventionally in ms^{-2} and the value is for all normal purposes fixed. However, the equation (2-20) will give a value in ms^{-2} , which is inconvenient for flight use. Therefore a standard value of $g=9.80665$ will be applied and a conversion of 0.514 from ms^{-2} to kn/s will be applied. This gives the following:-

$$\text{Therefore:-} \quad \left(\frac{dV}{dt}\right)_s = \frac{9.54}{G} \left(\frac{V_s^2}{V_E^2} + \frac{V_E^2}{V_s^2} \right) \text{kn/s} \quad (2-21)$$

Before progressing further, it is appropriate to consider the nature of the airspeeds under discussion. An aircraft will indicate results in IAS, which for current purposes will be treated as CAS (Calibrated Airspeed) and the errors disregarded. It is theoretically possible that deceleration could instead be measured using an accelerometer, but the combination of a comparatively low rate of deceleration and presence of pre-stall airframe buffet are such that this is not considered a sensible possibility. This would also entail fitting non-standard flight instrumentation; this has therefore not been explored. The origin of this analysis - equations (2-1) to (2-4) use TAS. In equation (2-20) the values are worked upon as ratios and so it is unimportant whether they are TAS or CAS since the ratio will be identical. But the result is expressed as

TAS. Since for flight purposes TAS is rarely useable, it is necessary to transform this into a value in CAS. So, considering equation (2-21):-

The relationship between CAS and TAS is:-

$$CAS = (TAS)\sqrt{\sigma} \quad (2-22)$$

So, a more useful form of equation (2-21) incorporates (2-22) allowing the result to be expressed in terms of CAS:-

$$\frac{dV_{ind}}{dt} = -\frac{9.54\sqrt{\sigma}}{G} \left(\frac{V_S^2}{V_E^2} + \frac{V_E^2}{V_S^2} \right)$$

However, it has been found on occasion that the form of the ASI calibration curve (see Appendix A2) is such that the gradient of IAS versus CAS is not near to unity. Therefore for test work this gradient must be known, and incorporated into this transitional result, to become:-

$$\frac{dV_{ind}}{dt} = \frac{-\partial IAS}{\partial CAS_s} \cdot \frac{9.54\sqrt{\sigma}}{G} \left(\frac{V_S^2}{V_E^2} + \frac{V_E^2}{V_S^2} \right) \quad (2-23)$$

(Although the low speed IAS:CAS gradient at or near to the stall,

$\frac{\partial IAS}{\partial CAS_s}$ may often be found to be near unity and may sometimes therefore be disregarded.)

ISA defines σ by an exponential equation in terms of height (which should be borne in mind for any computer modelling purposes) however for the current purpose of considering overall altitude effect, look-up tables will suffice, as shown in Table 1 below.

Table 1, CAS:TAS comparison for different heights

Assuming that a value of 2.4 kn/s TAS had been obtained.

Standard Pressure Altitude (ft) (a)	TAS deceleration (kn/s) (b)	σ (c)	$\sqrt{\sigma}$ (d)	CAS Deceleration = TAS $\sqrt{\sigma}$ (kn/s) (e)
0	2.4	1	1	2.4
5,000	2.4	0.862	0.928	2.23
10,000	2.4	0.738	0.859	2.06
15,000	2.4	0.629	0.793	1.90

Thus: (1) The sea level condition (represented by TAS) is the worst case
 (2) Up to 10,000 ft the IAS stall entry rate may reduce by up to 14% - which is significant enough to require adjustment of flight test results. However, since an accuracy of deceleration rate of 30% is as good as might reasonably be hoped for from a test pilot, the sea level result may be used when calculating the stall entry rates to be used for flight test planning at any altitude. Microlight flight testing will not normally be carried out above 10,000 ft because above that height supplementary oxygen is required, which is not normal equipment in this class of aircraft. In any case, a normal height bracket for stall tests would be 3,000 to 5,000 ft sHp (Standard Pressure Altitude) where the maximum error is trivially small.

Notwithstanding the table above, a -1kn/s acceleration rate (1 kn/s deceleration) towards the stall event will still be required (for determination of performance stalling speeds). The worst case sea level value of deceleration rate should therefore be used when determining the safe proof case for flight test purposes (i.e. that is the deceleration rate into the stall up to which the aircraft must not show unacceptable stalling characteristics). Any further

adjustments for CAS should be performed only where quantitative comparison with actual flight test data is required.

In order to provide any confidence in this result, it is essential to compare this to actual flight test data. **Table 2** following is based upon flight test data for individual aircraft as listed.

Table 2. Comparison of theory with test data for stall deceleration rates

Type	Reg.	V _s (kn CAS)	V _E (kn CAS)	ht (ft sHp)	$\sqrt{\sigma}$	G	$\left(\frac{dv}{dt}\right)_{calc}$ (kn/s)	$\frac{\delta t^3}{\delta t^3}$ (s)	$\left(\frac{dv}{dt}\right)_{true}$ (kn/s)
X'Air 582 ⁴ (1)	G-BYCL	33.5	43	3000	0.949	6.7	3.05	7.75	1.22
Spectrum ⁵	G-MWTE	35	30 ⁶	1500	0.992	7.4 ²	2.68	6.25	1.28
Thruster TST ⁷	G-MTGR	28	45	2000	0.971	8.66	3.18	8.0	2.13
Cyclone AX3-503	Several	27	34	2800	0.959	6.92	2.93	4.75 ⁸	2.74
Avasud Mistral	G-MWIB	30	44	3000	0.957	11.1	2.15	8.38	1.69
Goldwing	G-MJRS	30	35	2000	0.971	12.1	1.60	6.3 ⁹	3.17
X'Air Jabiru (1) ¹⁰	G-HITM	33	43	1800	0.974	6.8	3.12	6.0	2.5
Thruster TST Mk1 ¹¹	G-MVBT	33	40	2000	0.971	8.1	2.45	3.5	3.43
Sky Raider II(UK) ¹²	G-SRII	38	48	1500	0.992	8.2	2.56	12	1.18

(Note: illustrations and general data on each of these types may be found in part 9 of this thesis.)

³ Mean value from several tests.

⁴ From certification testing of first UK example.

⁵ From testing by the author in a privately owned example.

⁶ These are estimated values by extrapolation of test data, the aircraft stalled whilst still on the right hand side of the drag curve. Stalls were carried out from a trim speed of 43 kn.

⁷ From testing a modified aircraft for approval under MAAN 1404. ASI calibration not available, so IAS is used.

⁸ Deceleration in the AX3 was from 50 mph IAS (43 kn). Apparent stall was at 35 mph IAS = 30kn, which compares only moderately well to the TADS value of 31 mph at MTOW.

⁹ Deceleration from 50 kn IAS. (Data obtained during performance testing of an example privately owned by the author).

¹⁰ From certification flight test reports, aircraft was trimmed to 48 kn CAS prior to throttle closure.

¹¹ Example modified by fitment of BMW R100 engine, enclosed rear fuselage and doors, data extracted from flight testing for approval of the modifications. Throttle closed at 45 kn V_{trim}.

¹² During certification testing of the first UK example, flown at light weight (345kg), trim speed 55 mph IAS = 52 kn CAS. This aircraft developed into the Easy Raider before certification.

During flight tests, it was often noted that for microlight aircraft, the stalling characteristics are poorly defined, such that there is some uncertainty concerning the precise starting moment of the stall event. Therefore there was probably considerable lag between the aerodynamic stall and the perception of the stall. It must be remembered that at all times, apparent characteristics must be used in flight testing. Also however, it is known from published literature on unsteady aerodynamics that $C_{L_{max}}$ is greater when a rapid pitch-up occurs; clearly the greater the deceleration rate, the greater the pitch rate and so a greater deceleration rate is likely to result in a lower apparent stalling speed. A lack of appropriate facilities (e.g. a 15m+ section wind tunnel combined with a movable sting capable of pitch rates better than 30°/s nose-down motion in order to meaningfully simulate the post-stall pitch break) for conducting tests for this on wings with a 9 - 12m wingspan prevent this being quantified.

Therefore it is proposed to insert an additional term into (2-23), as shown below:-

$$\frac{dV_{ind}}{dt} = \frac{-9.54\tau_d\sqrt{\sigma}}{G} \left(\frac{V_S^2}{V_E^2} + \frac{V_E^2}{V_S^2} \right) \text{kn/s} \quad (2-24)$$

Where the new term, τ_d is introduced, which will be termed the “deceleration time constant”. This is estimated for the types previously considered in **Table 3** below.

Table 3, determination of deceleration time constant

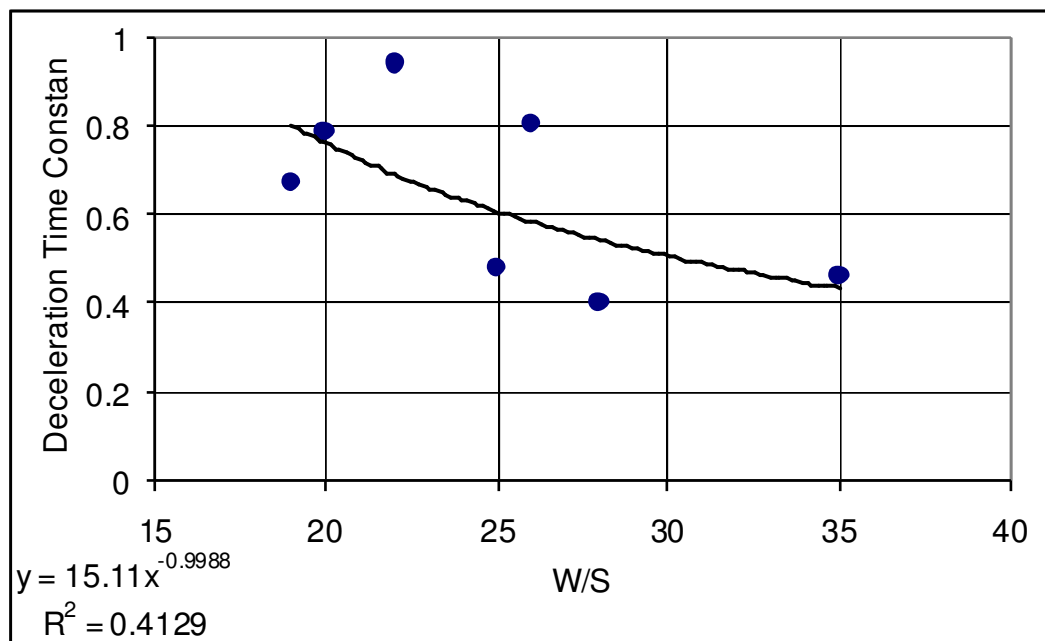
<u>Type</u>	<u>Reg.</u>	<u>V_s</u> (kn CAS)	$\left(\frac{dv}{dt}\right)_s^{calc}$ (kn/s)	$\left(\frac{dv}{dt}\right)_s^{true}$ (kn/s)	$\frac{\left(\frac{dv}{dt}\right)_s^{true}}{\left(\frac{dv}{dt}\right)_s^{calc}} = \tau_d$
X'Air 582 (1)	G-BYCL	33.5	3.05	1.22	0.400
Spectrum	G-MWTE	35	2.68	1.28	0.478
Thruster TST	G-MTGR	28	3.18	2.13	0.670
Cyclone AX3-503	Various	29	2.93	2.74	0.935
Aviasud Mistral	G-MWIB	30	2.15	1.69	0.785
Goldwing	G-MJRS	30	1.60	3.17	1.98
X'Air Jabiru(1)	G-HITM	33	3.12	2.50	0.801
Thruster TST Mk1	G-MVBT	33	2.45	3.43	1.4
Sky Raider II(UK)	G-SRII	38	2.56	1.18	0.461

At first sight this shows a very large variation in values of τ_d , hence this was explored further. Personal experience had shown that aircraft in this class tend to show a far more well-defined stall at higher wing loadings, and so the relationship with wing loading was explored. **Table 4** shows the wing loading of each of the test aircraft described above, and **Figure 15** plots the determined value of τ_d versus the wing loading W/S at the time of each test. (The figure omits the results for the Goldwing and Thruster TST.1, which otherwise significantly skew the best-fit curve away from all other points. Both of these are older designs which are known to have pitch control characteristics that might not necessarily be accepted if current practices were followed – very shallow apparent longitudinal static stability in the case of the Goldwing, and a very wide trim speed band in the case of the Thruster TST. It is suspected that the unusual pitch control characteristics of these aircraft significantly affect the pilot's perception of the stalling characteristics.)

Table 4. Wing loadings for test aircraft at time of each stalling test

<u>Type</u>	<u>Reg.</u>	<u>W/S</u> (kg/m ²)
X'Air 582 (1)	G-BYCL	28
Spectrum	G-MWTE	25
Thruster TST	G-MTGR	19
Cyclone AX3-503	Various	22
Aviasud Mistral	G-MWIB	20 ¹³
Goldwing ¹⁴	G-MJRS	20
X'Air Jabiru (1)	G-HITM	26
Thruster TST Mk1	G-MVBT	25
Sky Raider II(UK)	G-SRII	35

Figure 15. Deceleration constant versus wing loading (Goldwing and Thruster TST Omitted)



The curve shown is a power regression of the form $y = Ax^{-1}$, which gives a moderate ($R^2 = 0.413$) fit. The relationship, shown on the graph is

¹³ The Aviasud Mistral is a biplane.

¹⁴ Including Canard. The Goldwing is the only canard aircraft listed.

(2-25)

$$\tau_d = \frac{A}{W/S}$$

Where A is a derived term of value A=15.1 m²/kg.

Final form of the equation

We therefore find that the acceleration rate of a micro light aircraft as it approaches the stall, is defined by the following equation, where the aircraft has suffered a sudden power failure and the pilot attempts to maintain level flight.

$$\frac{dV_{ind}}{dt} = \frac{9.54 \tau_d \sqrt{\sigma}}{G} \left(\frac{V_S^2}{V_E^2} + \frac{V_E^2}{V_S^2} \right) \tag{2-27}$$

Where, τ_d , the deceleration time constant is determined by the formula

$$\tau_d = \frac{15.1}{W/S}; G \text{ is the best glide ratio for the aircraft; } V_s \text{ is the stall speed; and}$$

V_E is the best range glide speed. Although the term is retained for analysis purposes, when planning flight tests, it is safe and more convenient to assume that $\sigma = 1$. The accuracy of (2-27) is investigated in **Table 5** below.

Table 5, Demonstrating the accuracy of (2-27)

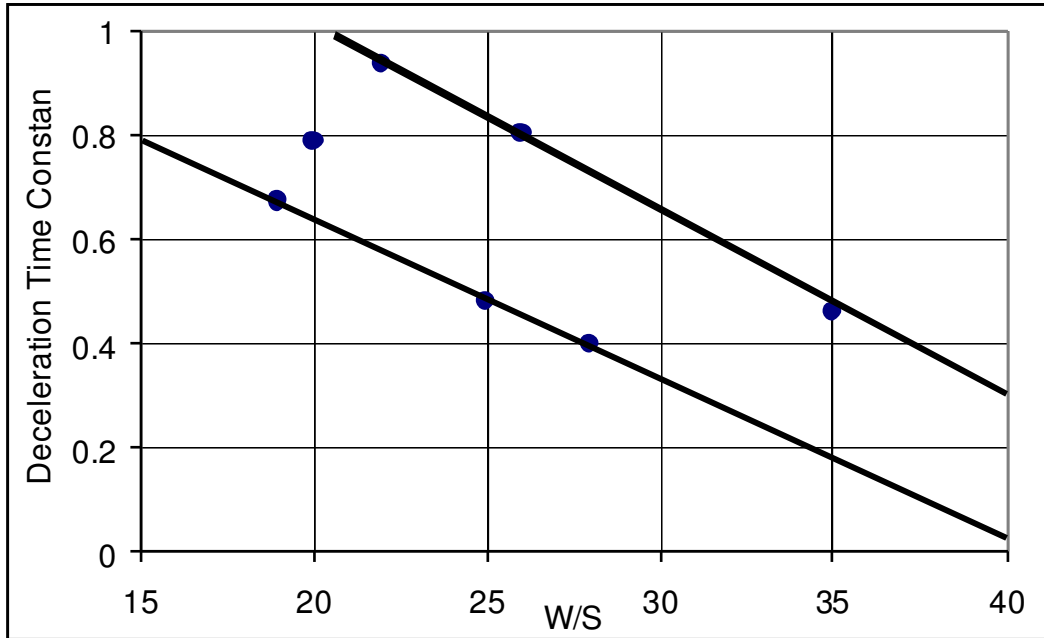
<u>Type</u>	<u>Reg.</u>	<u>V_s</u> (kn CAS)	<u>V_E</u> (kn CAS)	<u>ht</u> (ft sHp)	<u>√σ</u>	<u>G</u>	<u>W/S</u> (kg/m ²)	$\left(\frac{dv}{dt}\right)_{calc}$ (kn/s)	$\left(\frac{dv}{dt}\right)_{true}$ (kn/s)
X'Air 582 (1)	G-BYCL	33.5	43	3000	0.949	6.7	28	1.2	1.2
Spectrum	G-MWTE	35	30	1500	0.992	7.4	25	1.6	1.3
Thruster TST	G-MTGR	28	45	2000	0.971	8.66	19	2.5	2.1
Cyclone AX3-503	Various	27	34	2800	0.959	6.92	22	2.0	2.7
Aviasud Mistral	G-MWIB	30	44	3000	0.957	11.1	20	1.6	1.7

<u>Type</u>	<u>Reg.</u>	<u>V_S</u> (kn CAS)	<u>V_E</u> (kn CAS)	<u>ht</u> (ft sHp)	<u>$\sqrt{\sigma}$</u>	<u>G</u>	<u>W/S</u> (kg/m ²)	$\left(\frac{dv}{dt}\right)_{calc}$ (kn/s)	$\left(\frac{dv}{dt}\right)_{true}$ (kn/s)
Goldwing	G-MJRS	30	35	2000	0.971	12.1	20	1.2	2.0
X'Air Jabiru (1)	G-HITM	33	43	1800	0.974	6.8	26	1.8	2.5
Thruster TST Mk1	G-MVBT	33	40	2000	0.971	8.1	25	1.5	3.4
Sky Raider II(UK)	G-SRII	38	48	1500	0.992	8.2	35	1.1	1.2

However this formula (demonstration of the accuracy of which is given in the next table) gives the best estimate; this is by definition since it uses the best fit curve to the available data. What is actually needed is the worst-case deceleration rate.

Given that in most cases the stalling characteristics are more severe at higher deceleration rates (and if they are not, then the 1kn/s case must in any case be examined so as to satisfy specific certification requirements) an alternative approach is to determine a value of \mathcal{T}_d which will give the greatest magnitude value of deceleration. This can be achieved by defining the linear relationship (data not existing to justify a higher order curve in this case) which gives the greatest value of deceleration amongst the values in the analysis above. A worst-case straight line may be marked on the previous figure as shown in **Figure 16:-**

Figure 16. Deceleration constant versus wing loading (Goldwing and Thruster TST Omitted), with straight lines plotted giving greatest and least magnitude acceleration rates.



These two lines define the bounds of maximum and minimum acceleration that should be experienced in the event of level flight being maintained following an engine failure. These may be defined by the following:-

Greatest magnitude acceleration: $\tau_d = 1.74 - 0.036 W/S$ (2-28)

Least magnitude acceleration: $\tau_d = 1.28 - 0.032 W/S$ (2-29)

Inserting (2-28) and (2-29) into (2-27) one obtains two predictions for the greatest and least magnitude level-flight acceleration rate that are likely to be experienced prior to an inadvertent stall, which are:-

(Greatest)
$$\frac{dV_{ind}}{dt} = \frac{(12.2 - 0.34 W/S) \sqrt{\sigma}}{G} \left(\frac{V_S^2}{V_E^2} + \frac{V_E^2}{V_S^2} \right)$$
 (2-30)

$$\text{(Least)} \quad \frac{dV_{ind}}{dt} = \frac{(12.2 - 0.31W/S)\sqrt{\sigma}}{G} \left(\frac{V_S^2}{V_E^2} + \frac{V_E^2}{V_S^2} \right) \quad (2-31)$$

2.5 Physical significance of τ_d

An investigation has not been attempted into the physical significance of τ_d ; however, the fact that it is shown to be a function of wing loading indicates that there must be some relationship to an aircraft's design and loading; it is likely that other variables will also be significant – for example the apparent longitudinal static stability, and the severity of the aircraft's post-stall gyrations (in particular of any pitch break) are likely to be significant in determining τ_d 's value. Whilst not explored herein, it is likely that the physical significance, and the factors leading to a given value of τ_d will adopt greater importance within any subsequent development of this work.

2.6 Recommendations.

Whilst the conventional 1kn/s deceleration rate stall is still required, it is also recommended that handling of a microlight aircraft immediately prior to, at the point of, and immediately following a piloting stall is investigated where the tests are carried out using a decelerations of the aircraft immediately prior to the stall event, in knots per second, at least as great and as small as given by (2-30) and (2-31) above.

3 Stalling speeds and determination of manoeuvre speed for conventional flexwing microlight aeroplanes.

3.1 Back ground to non-square-law stalling speed to loading relationship.

It has been observed for many years that the stall speed of weightshift controlled microlight aeroplanes does not necessarily follow the pattern considered “normal” for a fixed wing aeroplane as loading is increased, that is:-

$$V_s = V_{SO_{MTOW.1g}} \left(\frac{W}{MTOW} N_Z \right)^{1/2} \quad (3-1)$$

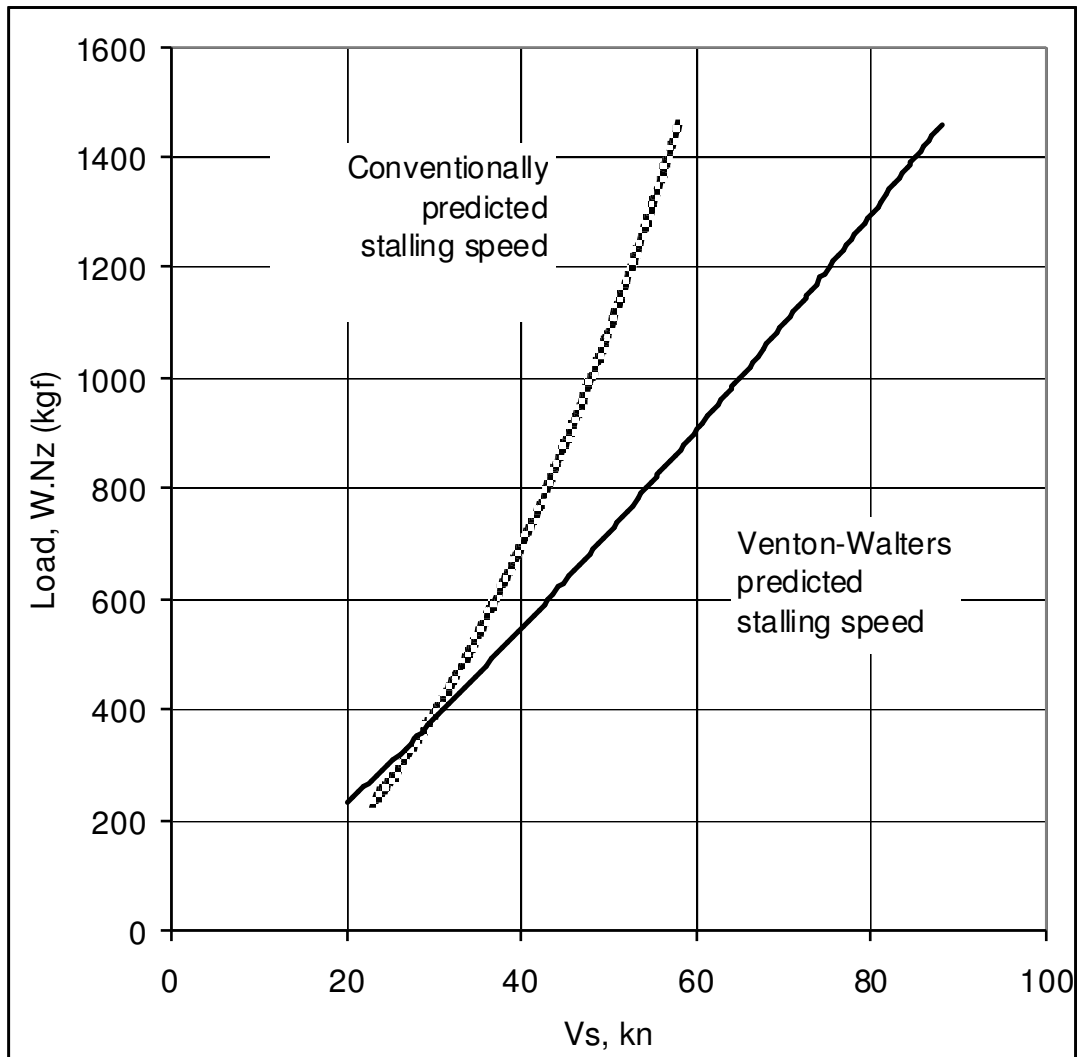
In practice, this class of aircraft is known to display higher stalling speeds at high loadings (for example in a steep turn) than are necessarily predicted by (3-1) above and would be considered normal for a conventional, rigid-winged, aeroplane. It is believed that this phenomenon was first observed by Roy Venton-Walters, who designed the Sprint and Raven wings in the early 1980's (for greater detail of the Raven aircraft, see Appendix B10). Venton-Walters stated that the behaviour could be shown to follow the following relationship [33]:-

$$V_s = V_{SO_{MTOW.1g}} \left(\frac{W}{MTOW} N_Z \right)^{C_{Ae}} \quad (3-2)$$

C_{Ae} will be referred to here as the “Aeroelastic Coefficient” for the wing (author's terminology, not Venton-Walters' who uses α). In discussion with Venton-Walters [34], he has stated that he does not know of a formal aeroelastic model which supports the relationship, but nonetheless had found this empirical model to work extremely well. It is however Venton-Walter's assertion that the term C_{Ae} will have a fixed value which is dependent upon the characteristics of the wing. He has stated that the value of this coefficient, which would be 0.5 for a perfectly stiff wing, has

greater values for wings which tend at higher aircraft weights, ; for the Raven wing (the more modern of his two designs) he states the value to be $C_{Ac}=0.80$. Taking the known value that $V_{so}=29\text{kn}$ at the MTOW of 367 kgf, a theoretical comparison may be made as shown in **Figure 17**.

Figure 17, Theoretical stalling speeds for Raven wing.



One significance of this is that greater caution needs to be observed by pilots during steep turns. For example, in an aircraft loaded to 350 kgf, making a 2g (60° banked) turn, conventional theory would give a stall speed of about 40 kn, whilst the Venton-Walters approach would give a stall speed of about 50 knots. Given that a 60° banked turn is a permitted manoeuvre, and a typical cruising speed would be about 40-45 knots, the risk of an inadvertent stall

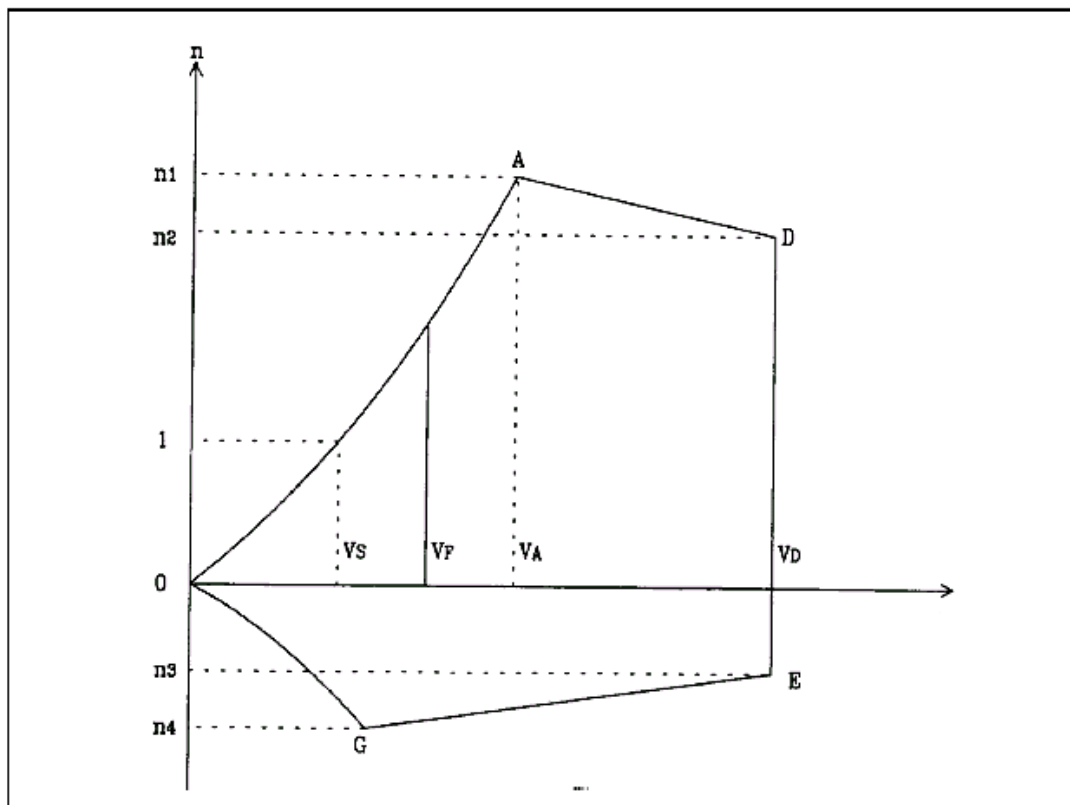
during a turn is very real. Although the reasons for this have not historically been quantified, pilots in this class of aircraft are indeed taught to pull the bar in (accelerate) before initiating a steep turn[35].

Further significance is seen when considering the operating limits for the aircraft. V_{ne} for the Raven wing is 87 kn and the positive normal acceleration limit is +4g [36]. Using the more conventional model for stalling speed, this combination necessitates a manoeuvre speed, V_A to be defined, in this case at 58 kn. However if the Venton-Walters model is accepted, then at 4g and MTOW, the total loading is 1460 kgf and the stalling speed at this loading would be 88 kn – or slightly greater than V_{NE} . The consequence of this, if the relationship is truly the case, is a degree of natural protection which may be used to allow “carefree” handling of the aircraft with respect to structural limits up to V_{NE} – particularly in regard to gust limits (the normal practice in microlights and simpler light aircraft being to limit flight in turbulent conditions to below V_A , rather than introduce a separate V_{RA} term.) The potential usefulness of this characteristic, if it could be proven, led this research effort to explore means of doing so.

3.2 The significance of V_A

V_A which is termed the manoeuvre speed is highly significant both to the technical certification effort, and to the operation of the aircraft. It is defined by all fixed wing airworthiness requirements (such as [37],[38], [39], [40]) as the airspeed at which, on the conventional V-N (flight-envelope) diagram [41], the positive g stall line (often referred to as the O-A curve, see **Figure 18** below) intercepts the maximum permitted positive normal acceleration limit. Thus it is the speed above which structural limits may be exceeded before aerodynamic characteristics in the form of a stall will reduce lift.

Figure 18. Classical flight envelope diagram



It has further structural significance in an aircraft with movable primary control surfaces (generally not the case in a weightshift aircraft) because it is conventional for airworthiness requirements to mandate that these surfaces and their supporting or controlling structure can withstand full deflection up to V_A (as well as up to $1/3$ deflection at V_{NE}).

To a pilot, the primary significance of V_A is that up to this speed he or she has the ability to apply full primary control deflection without risk of overstressing the airframe; it being taught that at any speed above that only $1/3$ control deflection should be applied. Additionally, it is conventionally taught [42] in the operation of most smaller aircraft types, including microlights, that V_A is the maximum speed at which the aircraft should be flown in severe turbulence, so as to reduce the risk of airframe overstress due to gust loadings.

However, the conventional definition of V_A , is $V_A = V_{S0} N_1^{1/2}$. In such aircraft, both lateral and directional stability are proportional to angle of attack [43], [44], and thus inversely proportional to airspeed. At low speeds, rolling and yawing excursions will thus be more severe. For that reason a high speed,

greater than would be permitted by this classical definition of V_A , may be advisable in some conditions. This is particularly the case when descending at speed through particularly turbulent air, for example when approaching to land through rotor¹⁵, descending through an inversion or thermal, or attempting to dive out of rising air at the base of a cumulonimbus cloud [45].

Hence, if justification can be found for an increase in V_A for a weightshift controlled microlight aeroplane, then operating safety of the aircraft can be improved by allowing flight through severe turbulence at speeds that reduce the risk of uncommanded and potentially dangerous rolling or yawing excursions. There is at least one incidence reported of a flexwing microlight suffering a severe rolling excursion close to the ground (on that occasion during the initial climb-out after take-off) which was attributed to flight at too low an airspeed through moderate to severe turbulence, causing a fatal accident [46].

3.3 Experimental investigations into a non-square-law stall speed to loading relationship for three aircraft: the Air Creation KISS-400, KISS 450 and iXess

During UK certification testing of the Air Creation KISS-400 (for illustration and details see Appendix B4), KISS-450 and later iXess aircraft (Appendix B5) the aircraft were stalled over as large a range of wing loading as could safely be achieved – from single crew / minimum fuel at 1g, to MTOW in steep turns with an installed g-meter providing a value for N_z immediately prior to the stall. The results in **Table 6**, **Table 7** and **Table 8** were obtained:-

¹⁵ “Rotor” in this context refers to a large closed eddy in the prevailing airflow, which commonly exists downwind of a large obstruction to the wind (such as trees, hills or large buildings). A fuller explanation of this effect may be found in pp38-40 of reference [45].

Table 6. Stalling Speeds at various loadings for Air Creation KISS-400

<u>Test No.</u>	<u>W.N_Z</u> <u>(kgf)</u>	<u>V_s</u> <u>(kn CAS)</u>
1	315	29.6
2	400	32.2
3	560	39.1
4	800	52.2
5	1000	62.6

Table 7. Stalling Speeds at various loadings for Air Creation KISS-450

<u>Test No.</u>	<u>W.N_Z</u> <u>(kgf)</u>	<u>V_s</u> <u>(kn CAS)</u>
1.	300	27.7
2.	345	29.8
3.	450	32.7
4.	450	34.2
5.	450	34.2
6.	518	35.6
7.	675	42.2
8.	900	56.7
9.	1125	63.9

Table 8. Stalling Speeds at various loadings for iXess

<u>Test No.</u>	<u>W.N_Z</u> <u>(kgf)</u>	<u>V_s</u> <u>(kn CAS)</u>
1	320	28.0
2	450	33.0
3	457	34.0
4	480	35.0
5	640	41.0
6	675	39.0
7	685	40.4
8	900	45.2
9	914	52.2
10	1143	61.0

These results are plotted in **Figure 19**, **Figure 22** and **Figure 20** below, showing in each case both the best fit curve using 3-2 above, and also the curve which would have been predicted using conventional theory, based upon the known value of V_{so} at MTOW.

Figure 19. Actual and classically predicted stalling speeds for Air Creation KISS-400

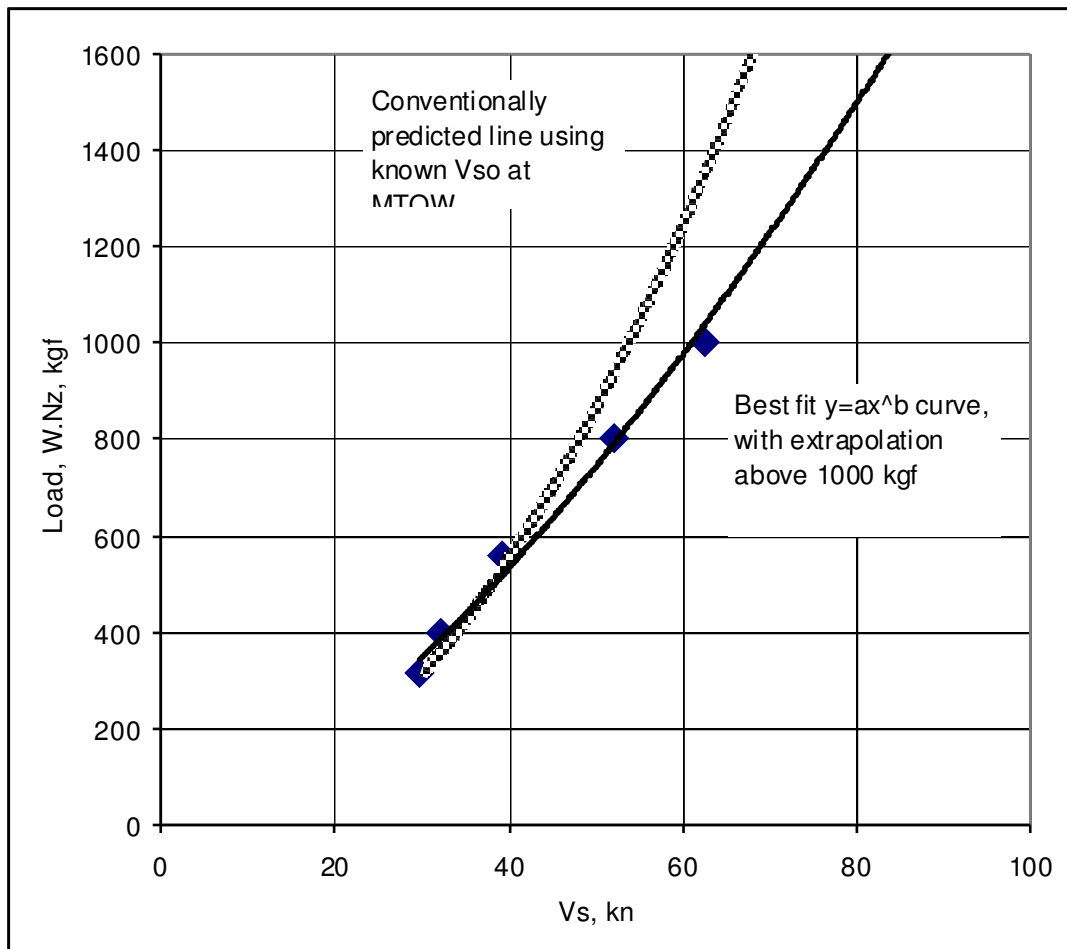


Figure 20. Actual and classically predicted stalling speeds for Air Creation KISS-450

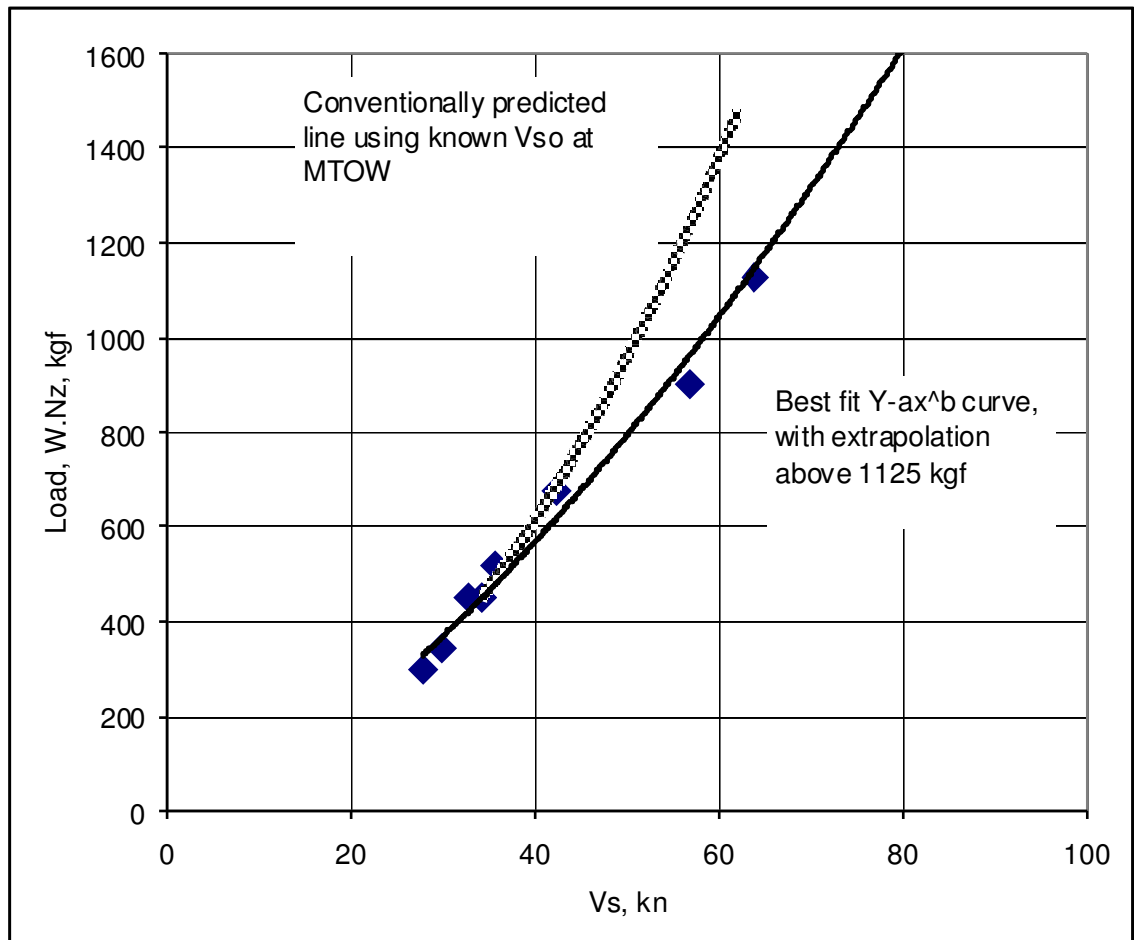
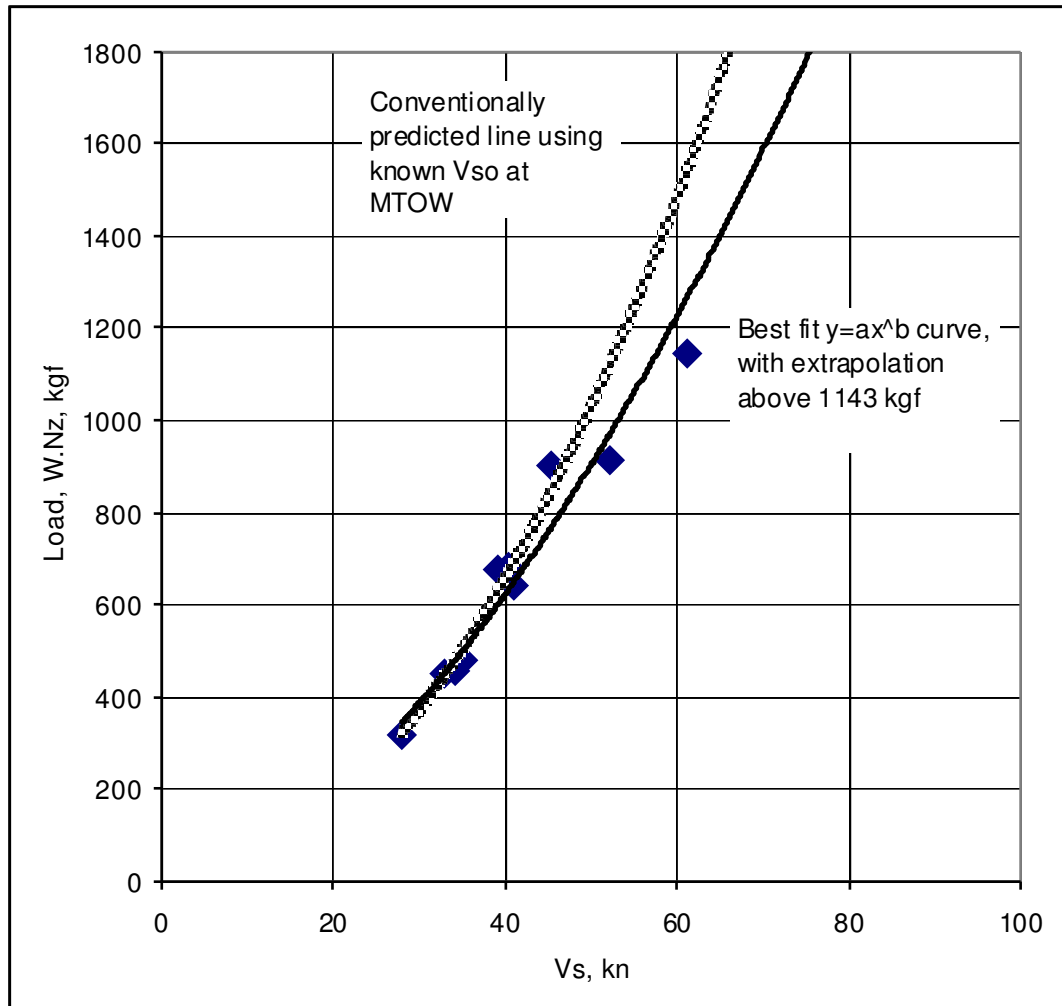


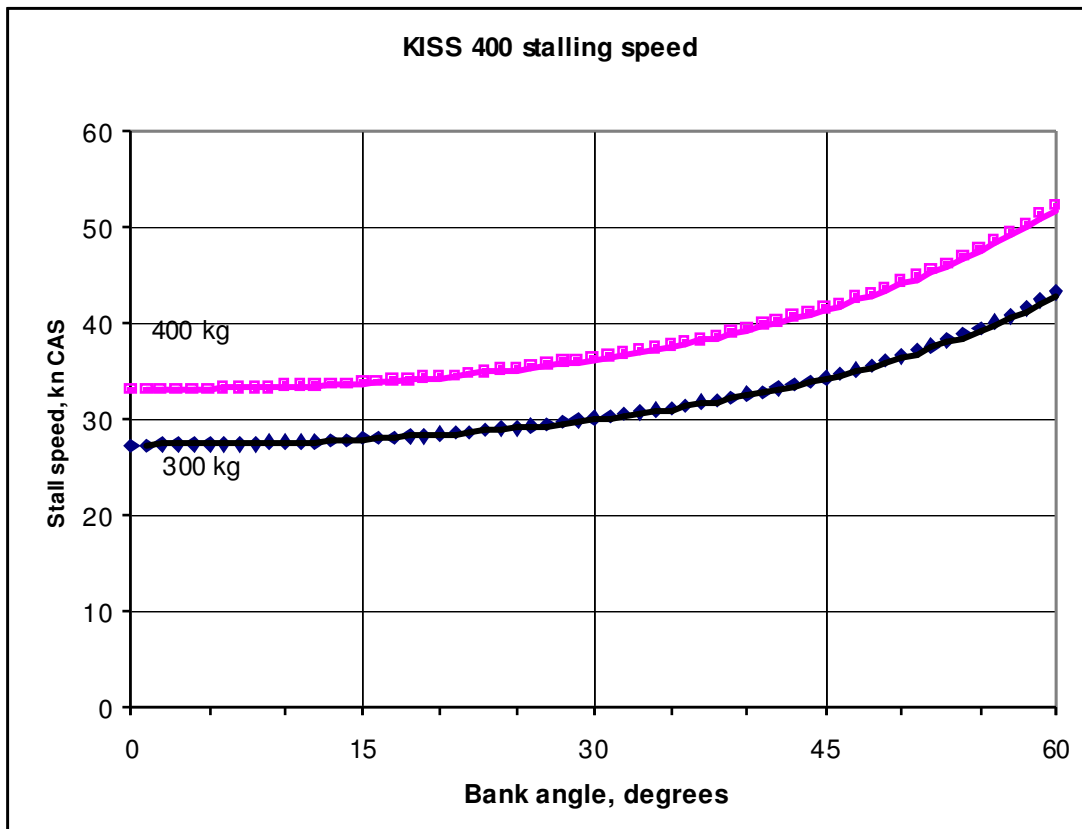
Figure 21. Actual and classically predicted stalling speeds for Air Creation iXess**Discussion – KISS-400**

The best fit curve to the actual results shown in **Figure 19** above is indeed of the form of 3-2, although in this case the aeroelastic constant, $C_{Ae}=0.66$. The $R^2>0.98$ line-fit is extremely good and gives high confidence in the result, although it should again be emphasised that no theoretical basis exists for this relationship. In this case a value of V_A for the wing of 83 kn CAS is shown, which is greater than V_{NE} of 76 kn CAS [47]. Carefree handling in pitch may therefore be assumed for this aircraft insofar as any pitch mishandling or flight in turbulence, up to V_{NE} may be considered unlikely to cause any overstress of the aircraft through exceedence of the normal acceleration limit.

Based upon the work above, which was carried out during the UK certification programme for the aircraft, two decisions were made with regard to the

operating limitations. These were firstly that because the V_A has been calculated at 83 kn CAS, which is greater than the V_{NE} of 76 kn CAS it was not included in the normal operating documentation (although it still lies slightly below the flight test limit of $V_{DF}=85$ kn CAS, and therefore is still listed in the series test schedule and type data sheet). Secondly, that specific data based upon this relationship was included in the operators manual showing stalling speeds at various bank angles, so as to warn pilots of the risk of inadvertent stall in steep turns. Below, in **Figure 22** is reproduced the diagram which was included in the operators manual [48], the bank angle limit for the aircraft, as is common practice for most microlight aircraft, is 60° , which is why the bank-angle scale does not extend beyond this value. The actual relationship plotted is given in 3-3, below the graph.

Figure 22. Stall Speed versus bank angle diagram from KISS-400 operators manual



Reproduced courtesy of Flylight Airports Ltd

(Note: $MTOW=400kgf$, typical empty weight= 200kgf).

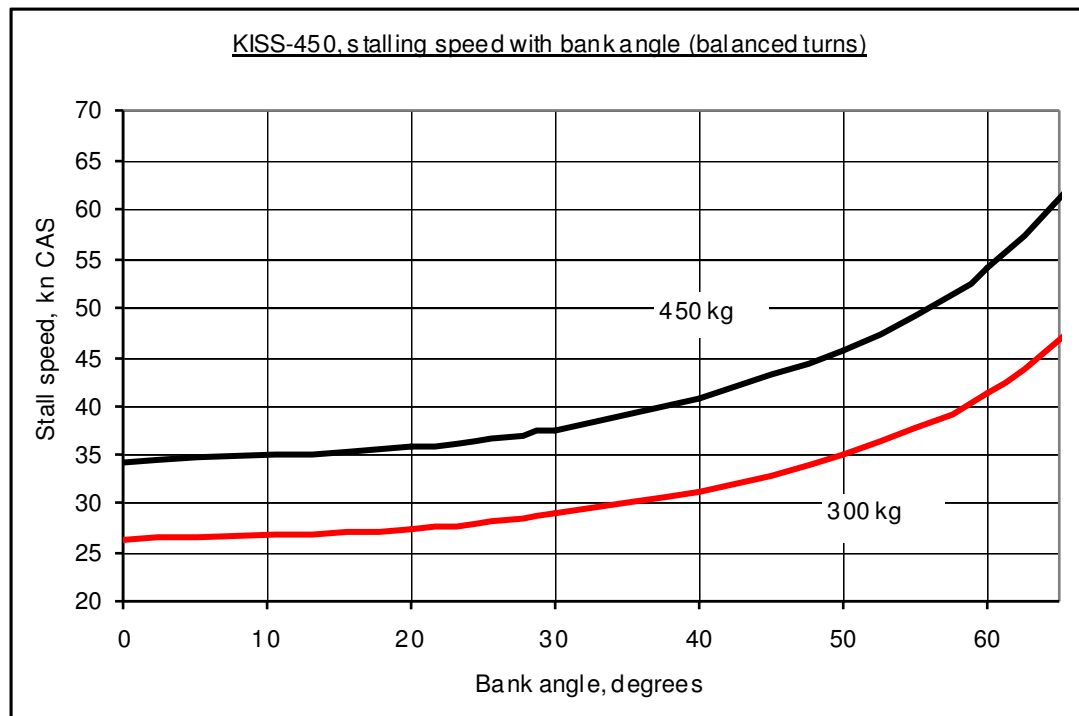
$$V_s = V_{s0} \left(\frac{W}{\cos\phi.MTOW} \right)^{C_{st}} \quad (3-3)$$

Discussion – KISS-450

The best fit curve to this is of the form of 3-2 above, although in this case the aeroelastic constant, $C_{Ae}=0.65$. The $R^2>0.97$ line-fit again gives high confidence in the result, whilst not disregarding that theoretical justification does not exist. In this case a value of V_A for the wing of 84 kn CAS is predicted, which is, as with the KISS 400 described in paragraph 3.3 above, greater than the V_{NE} of 75 kn CAS [49]. Carefree handling in pitch may therefore be assumed for this aircraft insofar as any pitch mishandling or flight in turbulence, up to V_{NE} may be considered unlikely to cause any overstress of the aircraft through exceedence of the normal acceleration limit.

As a result V_A was calculated at 84 kn CAS, which is well above the V_{NE} of 75 kn CAS it was thus not included in the normal operating documentation (although it still lies slightly below the flight test limit of $V_{DF}=83$ kn CAS, and therefore is still listed in the series test schedule and type data sheet). Below in **Figure 23** is reproduced the diagram which was included in the operators manual [50], the bank angle limit for the aircraft, as is common practice for most microlight aircraft, is again 60° , for which reason the bank-angle scale does not extend much beyond this value.

Figure 23. Stall Speed versus bank angle diagram from KISS-450 operators manual



Reproduced courtesy of Flylight Airports Ltd

(Note: MTOW=450kgf, typical empty weight = 200kgf)

Discussion - iXess

The Air Creation iXess is a new type that was certified in the UK under BMAA supervision during 2003 and 2004. It is a relatively high performance aircraft compared to the KISS-400 and KISS-450 aircraft previously mentioned, designed to fly at greater speeds using larger powerplants than most weightshift controlled aircraft of the 1980's and 1990's; it would appear that this performance improvement (in both level speed and climb rate) is mostly achieved through modification of the aerofoil section and stiffness of the wing, supplemented by profile drag reduction measures throughout the aircraft.

Whilst showing a less marked departure from "convention", the iXess still displays the same general characteristics as were seen for other types. In this case, it shows a value of $CA_e=0.751$. Relating to the V_{so} of 33 KCAS, this shows a V_A of 72 KCAS. This difference is not marked, but does show an increased safety margin for flight in

turbulent conditions where a pilot might wish to fly up to 60-65kn if flying an approach through particularly severe turbulence. Based upon these results, **Figure 24** below shows an excerpt from the operators manual for the iXess, as certified in the United Kingdom.

Figure 24, Stalling section from UK operators manual for Air Creation iXess

(The document from which this is extracted is at Reference [51])

4.14 Fully developed stalls. If the iXess is decelerated at a rate greater than 1kn/sec, a fully developed stall will occur. This is usually in the form of a smooth nose down rotation, proportional to the deceleration rate. There is not normally a wing drop tendency.

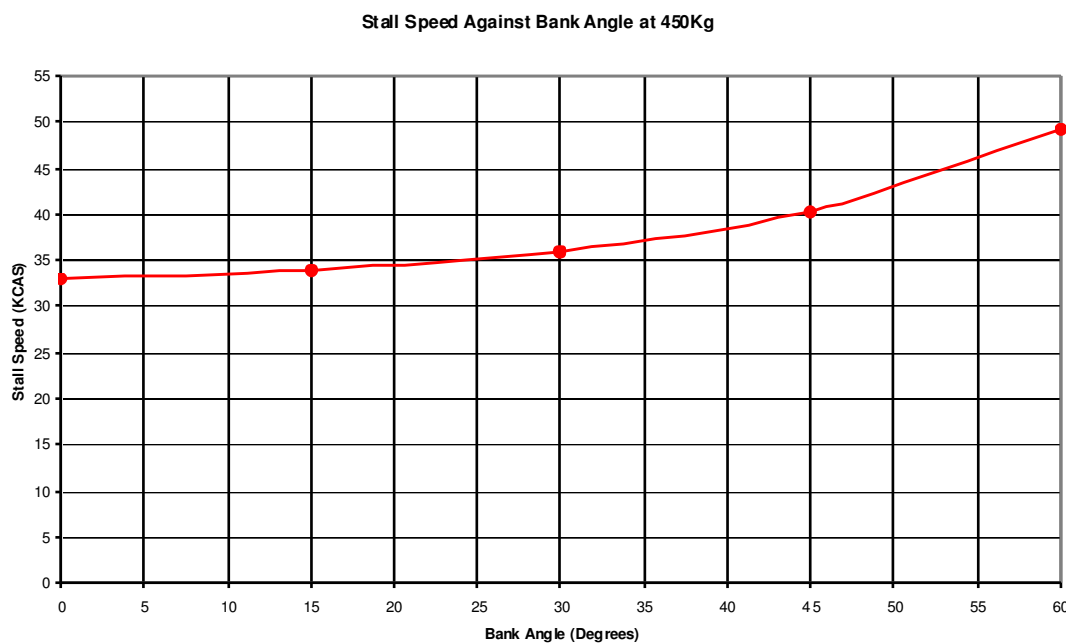
Power on stalls at maximum takeoff weight and low deceleration rates are usually quite safe. However never suddenly close the throttle at the point of stall. This will result in a greatly increased nose down rotation rate. Avoid also full power stalls at light cockpit weights and deceleration rates over 1kn/sec, otherwise very nose high pitch attitudes can be generated prior to the stall break with correspondingly high nose down rotation rates generated post stall break. In common with all flexwing aircraft extreme examples of this can result in aircraft inversion, loss of control and massive structural failure.

The iXess has relatively high wing loading when compared to older generations of UK flexwing aircraft. This means that it exhibits relatively high stalling speeds. This is most noticeable when the aircraft is flown at its maximum takeoff weight (Kg) and when load is being applied in manoeuvres. Pilots should beware of performing high G manoeuvres close to the ground where the energy loss of encountering stall buffet may be of significance.

Pilots should also be aware that as with all aircraft, overloading the aircraft with baggage / heavy occupants will further increase

the stalling speeds, as well as the usual drawbacks of reduced performance and structural safety margins.

4.15 *In Turning Flight. Stalling speeds are increased with bank angle. Flexwing aircraft do not increase stalling speed in proportion to load factor in the same way as conventional aircraft. Below is a graph specific to the iXess .*



Reproduced courtesy of Flylight Airsports Ltd

3.4 Problems with developing a theoretical model.

The author has made several unpublished attempts to develop a theoretical justification for the relationship between V_s and N_z which is described above. To date, these attempts have been unsuccessful.

Such a model might be constructed by dividing the wing into chordwise strips. Each strip may then be considered to be a small finite aerofoil section which has discrete aerodynamic characteristics.

Starting at a fixed reference (the wing root, fixed as it is to the keel tube, being the obvious datum), it may be assumed that the strip immediately outboard of the keel will then have the same angle of attack as at the root and aerodynamic characteristics as determined by the airspeed, angle of attack, and aerodynamic characteristics of the aerofoil.

Considering then the next strip outboard, a further piece of information is required – that is the aeroelastic relationship from the first strip. Integration of this aerodynamic and aeroelastic model spanwise would then permit estimation of total lift. However, to do so requires the following information:-

- An accurate model or sufficient test data of the relationship between shape, angle of attack and chordwise pressure distribution (or at-least the lift and pitching moment characteristics) for any section under given airspeed conditions.
- An accurate model of the chordwise and spanwise torsional stiffness of the wing at any section.
- An accurate estimation of the torsional centre of the wing at any section.

Whilst the last item may reasonably be assumed to act at the leading edge tube (being torsionally rigid) the first two of these quantities are presently

unobtainable. Facilities do not currently exist to measure the shape of a full scale wing under aerodynamic load, to determine the chordwise pressure distribution of a full scale wing, or to determine the torsional stiffness characteristics of a wing section under aerodynamic loads. Equally the time and resources required to produce a finite element model of the whole wing, for aeroelastic prediction purposes, would be significant.

It may be possible to produce a general demonstration of the general (rather than type specific) characteristics using an instrumented scale model of a wing within a wind tunnel. This would not necessarily permit accurate extrapolation to a full scale wing (since the aerodynamic and aeroelastic characteristics will not scale identically), but would allow a further justification of the form of (3-2). This would be of academic interest, however at present is outside of the resources available to the microlight aircraft industry; in addition there is little justification to expend such resources when (notwithstanding the lack of theoretical justification) the experimental form of the curve can be determined relatively inexpensively – as has been demonstrated in section 3.3 above.

3.5 An alternative application of the non square law relationship between V_s and N_z : modification of N_1 and N_2 .

Having defined the true form of the O-A curve using this relationship, it has been found that there are two ways in which the theory may usefully be applied in the certification of an aircraft.

Modification of N_1 and N_2

N_1 and N_2 define the positive N_z limits for an aircraft at V_A and V_D respectively. Light aircraft certification standards will define minimum values of N_1 , N_2 (in general $N_1=N_2= +4g$ for this aircraft class) and V_A . However, V_A typically is defined within certification codes (such as BCAR Section S) by:-

$$V_A = V_S \sqrt{N_1} \quad (3-4)$$

Where N_1 in this context is the minimum value

And even when V_A is permitted to vary from this value, it is normal that it is only required not to have a value less than that defined by (3-4) and is not necessarily required to have any greater value (for example, JAR-VLA [10]).

Thus, it is possible to define V_A as given in (3-4) but to use the form of O-A curve as given in (3-2). It is possible to combine (3-2) and (3-4), whilst treating N_1 as a variable. To do this, first assume that the aircraft is at MTOW and modify (3-2), giving the following result:-

$$V_A = V_{S_0} N_1^{C_{Ae}} \quad (3-5)$$

These are apparently incompatible, but can be made to work together if it is accepted that the value of N_1 in (3-4) is a variable, and that in (3-4) is based upon the requirements given in the certification standard, which will now be re-termed $N_{1,cert}$. Thus:-

$$V_A = V_{S_0} \sqrt{N_{1,CERT}} = V_{S_0} N_1^{C_{Ae}} \quad (3-6)$$

Which becomes:

$$N_{1,CERT}^{0.5} = N_1^{C_{Ae}} \quad (3-7)$$

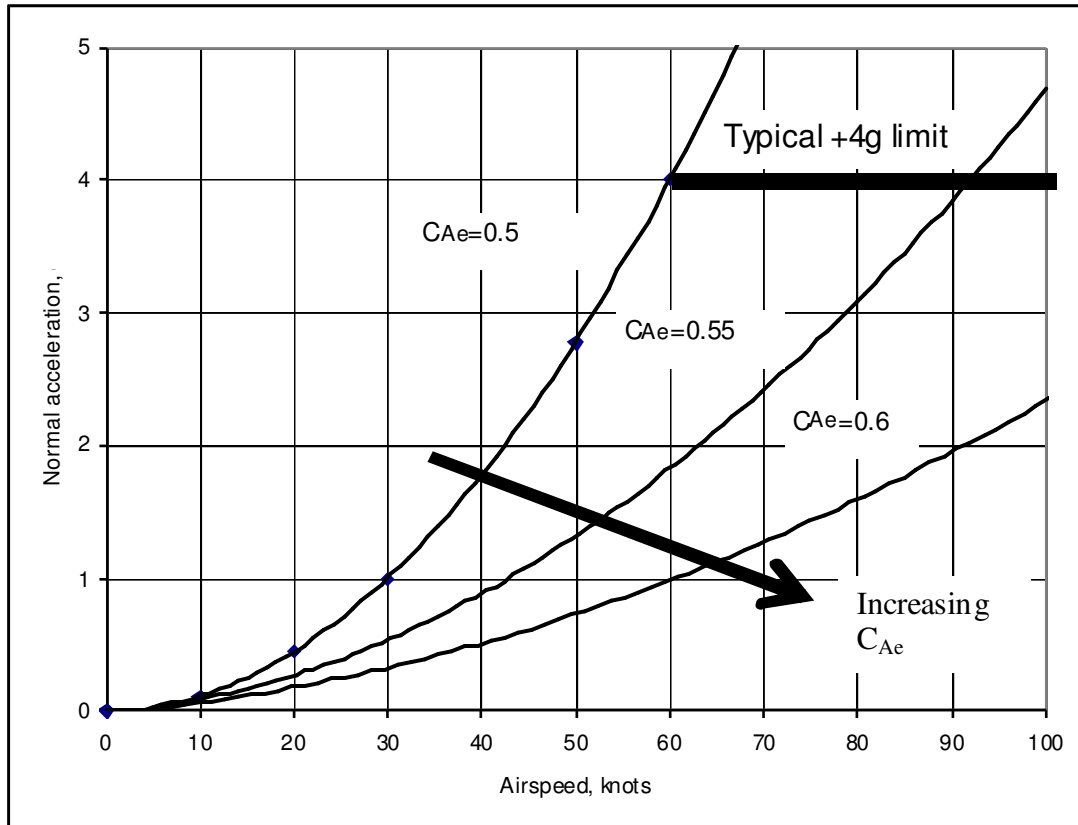
And thus:

$$N_1 = N_{1,CERT}^{\frac{1}{2 \cdot C_{Ae}}} \quad (3-8)$$

Thus, it is justifiable to reduce the value of N_1 and thus reduce primary structural mass, without reducing the magnitude of V_A . It may be noted that as C_{Ae} tends towards 0.5 (a perfectly rigid wing), the relationship tends towards $N_{1,cert} = N_1$. This is illustrated below in **Figure 25** (which effectively shows the upper left part of the V-N diagram as shown in **Figure 18** above).

It may be seen from this figure, that the stalling speed, and thus V_A , will be greater for any given value of $W.N_Z$, for a greater value of C_{Ae} .

Figure 25, Illustration of variation in stall speed with loading for three different values of C_{Ae} - with $V_s=30kn$



3.6 Historical precedent – normal acceleration limits for the Pegasus Quantum 15.

A variation upon this method was successfully carried out in 1991 by Pegasus Aviation during the certification programme for the Pegasus Quantum-15 aircraft[52]. During that programme it was demonstrated experimentally that the maximum normal acceleration that could be achieved through diving the aircraft to V_{NE} or above and applying a step input of the pitch control to maximum nose-up (the basebar to the front strut) the aircraft was capable of a transient loading not exceeding 2.4g before a stall occurred.

Following this demonstration by the manufacturer, Pegasus Aviation, it was successfully argued to the CAA that it was not necessary to require a value of $N_1=4g$, and it was reduced to $3.8g$, although V_A remained at $2V_S$. This may be considered conservative since if $N_1 = 3.8g$, then there is a structural redundancy factor of 1.58 above the maximum achievable N_Z , combined with which it may be considered that although the true value of co-incidence of the O-A curve with N_1 is unknown, it will certainly be at a speed greater than $2V_S$. Subsequent service experience, which has comprised manufacture of over 1000 aircraft, the oldest of which have, at time of writing, been in service for over 12 years, without any in-flight structural failure, tends to support the belief that the aircraft's structure is capable of withstanding loads significantly in excess of maximum flight loads.

There is an important additional point made by this specific experience. It should be noted that in this case $V_A = 2V_S = 4^{1/2}V_S > 3.8^{1/2}V_S$. So, N_1 has been reduced (thus permitting a lighter structure on the aircraft), whilst V_A is greater than the minimum value permitted (thus permitting higher speed flight in turbulence, albeit by only 2 mph). Whilst the most appropriate values of V_A and N_1 are subject to the judgement of the certification team, this example demonstrates that it can be acceptable to modify both V_A and N_1 away from the "classical" values without jeopardising the operational safety of the aircraft. The methods presented in 3.3 above may equally be applied in this manner, if it is necessary or appropriate to do so. This gives the certification team the ability to fine-tune limitations to give the maximum operating flexibility for the aircraft without degrading necessary structural safety factors. Clearly conservatism is reduced by this approach, but only to a value not less than that accepted by the certification basis, and thus acceptable; as with any class of aircraft, greater than essential conservatism in flying limitations has potential to either increase mass or to restrict operating limitations, and thus is deliberately avoided.

4 Spinning evaluation of 3-axis controlled microlight aeroplanes

4.1 The Spin Mode.

The spin mode is well understood [53, 54, 55, 56, 57, 58, 59, 73]; that is a combined roll:yaw autorotation occurring post-stall. It is known historically that most 3-axis controlled aeroplanes have the potential to enter a spin, although the characteristics such as apparent pitch attitude, oscillations, rate of rotation, readiness to spin, and ease of recovery, can vary widely. Because of the known risk of spin entry from manoeuvring flight or flight at or near the stall, it is an almost universal requirement in the certification of fixed wing aircraft that the spin is investigated. The rigour and nature of this investigation will, however, vary considerably between aircraft; whilst an aerobatic aircraft would be subjected to a wide range of spinning tests including prolonged fully developed spins, an airliner would probably not be tested beyond the first signs of incipient spin. A non-aerobatic light aircraft would normally be tested for resistance to spin entry, and for recovery from one and two-turn spins.

The entry to the spin occurs normally when the main lifting surface is stalled whilst there is significant sideslip. This might inadvertently occur when an aircraft is stalled in an unbalanced turn, or the rudder is not correctly set to balanced flight when an aircraft is stalled in level flight, or airframe asymmetry causes an aircraft to stall markedly one wing first causing large wing-drop, due to slow-flight in turbulence, or following a mishandled aerobatic manoeuvre.

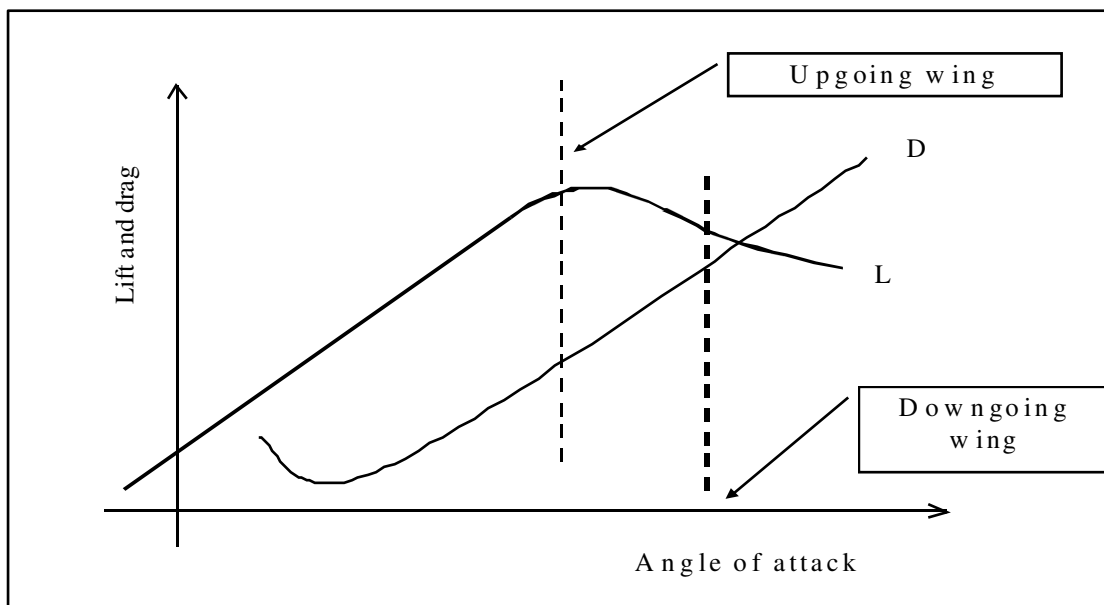
A deliberate spin entry will normally be attempted in one of two ways. Either full rudder will be applied as the aircraft is decelerating and the airspeed is about 5 knots above the stall, or full rudder, opposite to the direction of turn is applied at or just above a turning flight stall.

Following entry, the aircraft will normally pitch up, suffer some brief rolling or yawing motion, before normally after several seconds establishing a spin in

one direction, at which the nose with pitch down giving an apparently steep nose-down pitch attitude (although this should not be confused with angle of attack, the wing is still stalled). Rotation rates vary, extremes being from around $200^\circ/\text{s}$ (in the Bulldog T Mk.1, Cessna 152 and MXP 740 Savannah) to $40^\circ/\text{s}$ (in the X'Air Mk.1). However, most smaller (microlight and light) aircraft will tend to spin at rates of around $100^\circ/\text{s}$ to $150^\circ/\text{s}$ where the spin rate is defined as the rate of heading change as identified from the cockpit.

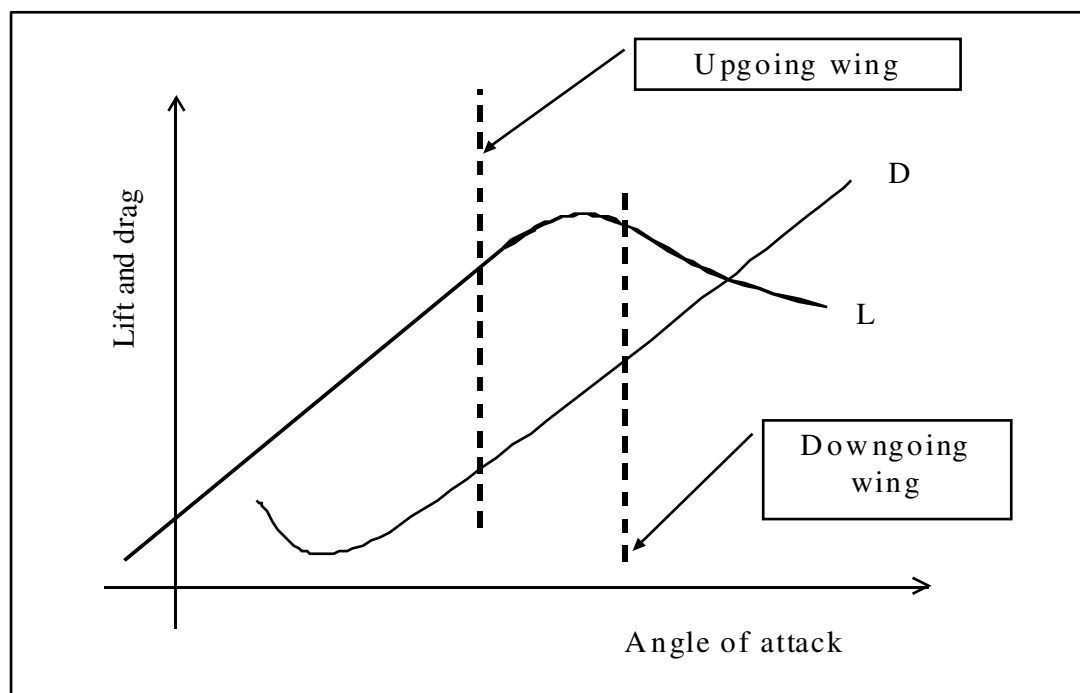
Aerodynamically, the yaw rate causing the sideslip induces the outer wing of the yawing motion to be flying faster than the inner wing. Lateral stability then causes the aircraft to roll in the direction of the yaw, causing the outer wing (due to roll rate) to experience a lower angle of attack than the inner wing. This stalls the inner wing and may stall the outer wing, but probably does not. The result is a difference in angle of attack between the wings, and hence a difference in lift and drag. This is shown below in ; as may be seen, lift is greater on the upgoing wing and drag is greater on the downgoing wing. This is normal and essential to the spin.

Figure 26. Illustration of lift, drag and angle of attack of an autorotative spinning aeroplane



If, however both lift and drag are greater on the downgoing wing, then the aircraft is more likely to enter a spiral dive during which airspeed will increase. This is particularly associated with “elevator limited” aircraft such as the CFM Shadow which lack sufficient pitch authority to fully stall the mainplane. The risk with such aeroplanes is primarily that the spin mode cannot be investigated and may be met for the first time in-service through unrepeatable factors such as a sudden upgust during low speed unbalanced flight.

Figure 27. Illustration of lift, drag and angle of attack at the wings of an aeroplane likely to enter a spiral dive from an attempted spin entry



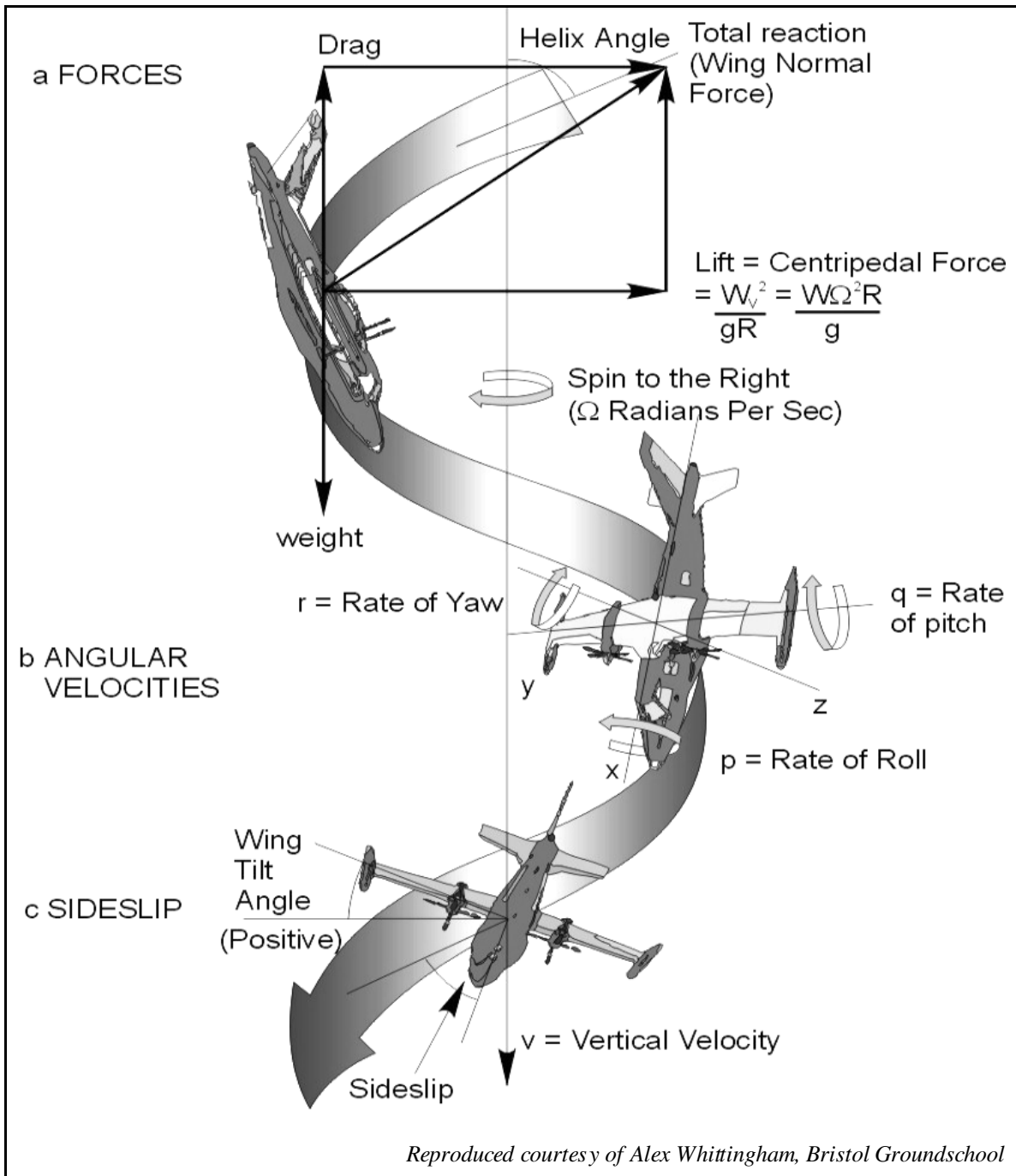
It is useful, prior to a detailed discussion of the subject, to define some of the terminology associated with the spin mode. Table 9 and Figure 28 below show the main terms in regular use.

Table 9, Spin Terminology

<u>Term</u>	<u>Meaning</u>
Developed Spin	The period of sustained autorotation between the incipient spin, and recovery.
Erect Spin	A spin where the rolling and yawing motions are in the same sense
Flat spin	A spin where the pitch attitude is close to that of normal flight. These tend to be associated with difficulty in recovering.
Incipient spin	The period of time between spin-entry, and a steady and developed spin being achieved. This can last between 1 and 6 turns although most test pilots and authorities do not consider it to extend beyond 2 turns.
In-spin aileron	Deflection of the roll control with the direction of the spin (e.g. a right stick input = starboard aileron up in a left hand spin).
Inverted Spin	A spin where the rolling and yawing motions are in opposite senses. These are normally only assessed on aerobatic aeroplanes unless an inverted spin has been found to occur, possibly as a result of a mishandled spin-entry.
Left Hand Spin	A spin where the yawing motion is in the sense nose to the left
Oscillatory spin	A spin where the rates of roll and/or yaw are varying, causing a potentially violent and apparently random motion of the aircraft during the spin.
Out-spin aileron	Deflection of the roll control opposite to the direction of the spin. (E.g. a left-stick input = port aileron up in a left hand spin).
Pull-out	Recovery from the dive or spiral-dive which is normally the attitude found immediately following a spin recovery.
Recovery	The point at which the spin has stopped, insofar as the mainplane has become unstalled. It does not imply a recovery to normal level flight.

<u>Term</u>	<u>Meaning</u>
Right Hand Spin	A spin where the yawing motion is in the sense nose to the right
Spiral Dive	An accelerating (or constant high speed) descent combined with a continuous turn. This mode can be mistaken for a spin when considering only visual cues, and is often the mode into which an aircraft recovers from the spin.
Standard Entry	Where a spin is induced by making a full yaw inceptor (rudder) input when a decelerating aircraft is just above the stall.
Turning Entry	Where a spin is induced by applying full yaw inceptor (rudder) input opposite to the turn, when in a steep turn just above the stall.

Figure 28. Illustration of aircraft flightpath and main parameters during a developed erect spin to the right



Note that although this diagram, as is the convention, shows that the spin axis lies permanently outside of the airframe; this is not necessarily true. During a test flight in July 1995, the author observed sustained reverse flow at a sidlip vane forward of the port wing during a left hand erect spin in a Tucano T Mk.1 No. ZF510, indicating that on that occasion the spin axis lay somewhere inboard of that vane (which was at about $\frac{2}{3}$ span).

4.2 Scope of this Research

This discussion will reserve itself to the spinning assessment of smaller aircraft which are not intended for deliberate spinning or aerobatics, and primarily microlight aeroplanes. It might be (and often is) asked why this is considered necessary when these aircraft will not be deliberately spun in service. The answer to this is that if an aircraft is capable of entering a spin, it should be known what conditions will cause the spin to occur, how it can be identified, and what actions should be taken by the pilot to recover the aircraft from the spin. The evidence of accident reports such as references [60], [61], [62], [63], [64], [65] in addition to anecdotal evidence show that it would not be a safe assumption that all spins will be intentional, or that pilots will be sufficiently knowledgeable or skilful to identify a spin without prior guidance. This is further supported by the fact that none of the private pilots licence (PPL) syllabi as used in Britain [66], require a pilot to have experienced (or recovered from) a developed spin.

This research is limited entirely to 3-axis controlled microlight aeroplanes. At present, all weightshift controlled microlight aeroplanes in the United Kingdom, and the majority worldwide, use Rogallo type delta planforms. These possess very high lateral and directional stability values, which simultaneously makes the aircraft prone to enter and remain in a stable spiral dive mode, yet extremely reluctant to enter a spin. There is no recorded instance of a spin to a weightshift controlled microlight aeroplane in the United Kingdom, and thus the topic cannot readily be studied, neither is there any good reason to do so. Some weightshift controlled aircraft may, if subjected to what might be considered typical pro-spin actions (a rapid stall entry in conditions where sideslip is present) enter an initial loss of control which rapidly becomes an accelerating spiral dive [67], despite the pitch control remaining in the fully nose-up position. Whilst to an extent anecdotal, this re-enforces the view that weightshift aircraft are inherently spin-resistant.

The spiral dive mode has historically caused safety problems in that class of aircraft [68], but is not currently considered a matter for concern – for this reason no research funding is available, and equally the spiral dive mode is considered outside of the scope of this thesis.

Assessments have been carried out on 2-axis controlled microlight aeroplanes, such as the HM 1000 Balerit, however data available for study is limited, and also no such aircraft has as-yet shown any tendency to spin. For these reasons, the spinning characteristics of these aircraft are also not considered here.

Whilst this section restricts itself to the theory and general practice of spinning assessments, appendix A4 shows in greater detail specific spinning test plans developed in the course of this research, the results of test plans, and detail of the advice now being given to microlight test pilots conducting spinning assessments, which is based upon the detailed experience of spinning trials in microlight aeroplanes. So far, the results contained in that Appendix indicate full success in that the controls-central spin recovery drill has been universally successful, and no aircraft considered satisfactory following these assessments has subsequently suffered any spinning related accident.

4.3 The spin recovery technique for microlight aeroplanes.

The “standard spin recovery” or SSR, as defined since before 1939 by many texts on aerobatics or the operators manuals for many light aircraft [69],[70], [71], [72] is “close throttle, centralise stick, apply full opposite rudder, move stick forward until the rotation stops”. This recovery presents three problems for the pilot of a microlight aircraft:-

- (i) It assumes a degree of recognition of the spin (and spin direction) which an average microlight pilot may not possess - also many microlights are not equipped with a turn co-ordinator or sideslip gauge (slip ball). Indeed, even for pilots whose training should have supposedly

included spin awareness and spin recovery, there is significant evidence that those pilots also lack sufficient familiarity [73] that a rapid and correct spin recovery can be relied upon on each occasion.

- (ii) Because of the tendency of a microlight to change energy state very quickly combined with strong rudder power at low speeds, there is a theoretical risk that use of opposite rudder may simply reverse the direction of spin.
- (iii) The standard spin recovery is only useful in the developed spin; in the incipient spin stage many aircraft will not yet have fallen into a particular spin direction. It is unhelpful to force a pilot to wait until the spin is properly established before being able to recover, particularly if the aircraft may be close to the ground.

Because of these factors, it has been concluded within the UK microlight certification community that, where possible, the following spin recovery should be used for microlight aeroplanes.

- Close throttle
- Centralise all controls
- Wait for spin to stop.

Both spin recoveries are then followed by some variation on *“roll wings level and gently ease out of any ensuing dive, applying power as the level flight attitude is reached”*.

So far, all microlight aeroplane assessment programmes during the course of this research have found this recovery to be successful in all cases where the aircraft was able to enter a spin. The largest concern then becomes the failure of a pilot to identify and take proper recovery action from a spiral dive if that

proves to be the mode of recovery from the spin. However, the spiral dive and recovery are a part of the training syllabus for microlight pilots, so this risk is considered small. There has however been at-least one occasion where a pilot who *may* have recovered from an inadvertent spin at low level into a spiral dive, failed to realise the change in flight mode and as a consequence flown into the ground [74]. However on that occasion the pilot was qualified in larger aircraft types, and had received no formal training in microlight aircraft. This was legal (although considered poor practice) at the time. Future recurrence should be prevented by subsequent regulatory changes [75], [76] that now require pilots of other aircraft classes to receive formal training in microlight aircraft handling, and to pass an assessment of competence, before being permitted to fly as an unsupervised pilot in command.

4.4 Certification requirements.

Figure 29 is an excerpt from BCAR Section S, being the most common standard used in the approval of microlight aircraft.

Figure 29. Excerpt from BCAR Section S, showing spinning requirements.

S221 General

For any aeroplane that is not controlled by weightshift:

- a) The aeroplane must be able to recover from a one-turn erect spin or a 3 second erect spin, whichever takes longer, in not more than one additional turn, with the controls used in the manner normally used for recovery. The recovery must be demonstrated with flaps, airbrakes and undercarriage in any allowable position and without exceeding the pilot effort limits for temporary application under S143 and the applicable airspeed and positive manoeuvring load factor limitation.
- b) It must be impossible to obtain unrecoverable spins with any use of the controls.

For the flaps and airbrakes extended condition, the flaps and airbrakes may be retracted during the recovery.

Note: S143 refers to maximum temporary and sustained control forces which should be demanded of a pilot. Most significantly in this case are a maximum temporary pitch control force of 200N and yaw control force of 400N.

4.5 The philosophy behind spinning assessment for a non-aerobatic aircraft

S221 is a short text to cover a complex subject. In summary however what needs to be established is

- Will the aircraft spin from a normal spin entry?
- Will the aircraft spin from a mishandled manoeuvre (most commonly from either stalling off a steep turn or a power-on rapid stall entry)?

- How may a pilot recognise the spin?
- How may the spin recovery be performed?

Regardless of the simplistic wording in BCAR Section S, spin assessment is considered vitally important in the assessment of a new aeroplane; it has ceased to be regarded within the airworthiness community acceptable (as has happened in the past) for the first experience of the spin to be accidental and some time after introduction of the type into service. It was for this reason that this programme of test method development, partly out of perceived necessity and partly in response to a direct tasking from the Light Aircraft Committee of the UK Airworthiness Requirements Board (ARB LAC) [77], that the author initiated the development of spinning guidance for microlight aircraft in 1998. This guidance is contained in reference [78], but the following indicates the main components of this, and actual test results obtained since then.

4.6 Preparation for a spinning trial

An examination of the direction of propeller rotation will show that one spin direction will be against the propeller torque reaction, the other in the same direction. Spins should always be executed with the roll direction against the propeller first, then with it. Spins “with” the propeller may be more stable but more resistant to recovery, spins “against” the propeller rotation may be more oscillatory but should recover more quickly [79]. If an aircraft recovers from the spin against the torque, but is reluctant to recover with the torque, preparation and briefing must have included the possibility of needing to switch the engine off in flight.

Also, the ratio of pitching to rolling inertias B/A must be considered. The yawing inertia is the largest – approximately being defined by $C \approx B + A$, and thus its actual value tends not be significant in determining the spinning characteristics. It is the two smaller rotational inertia values, B and A , and specifically their ratio, which tends to define the spin mode and the response to roll (aileron) input during the spin. When $B/A < 1$, the aircraft may be

referred to as “wing dominated” which tends to imply a spin-prone aircraft. When $B/A > 1$, the aircraft may be referred to as “fuselage dominated” or “pitch dominated”, which tends to imply spin-resistance. One obvious implication of this is that biplanes or aircraft with wing-mounted engines will tend to be more spin-prone than monoplanes or aircraft with fuselage mounted engines; although, it is important to appreciate that this is a trend and not an absolute rule.

Ailerons act in the normal sense during the spin. Thus if the aircraft is wing-dominant, in-spin aileron will tend to cause the roll to couple with yaw, increasing the spin rate (an aircraft well documented for showing this characteristic is the Scottish Aviation Bulldog [80]), also tending to flatten the spin. The converse will also be true, this is illustrated in **Table 10**.

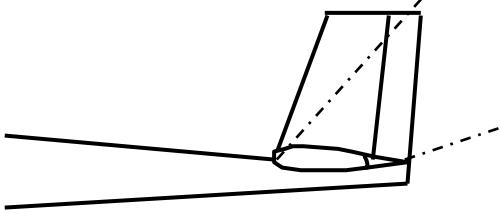

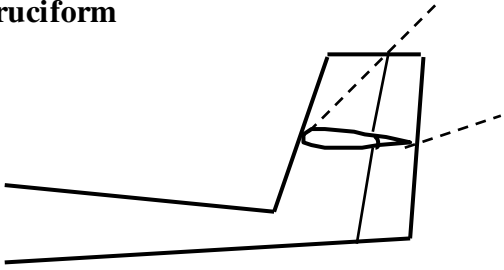

Table 10, Inertia and aileron effects upon the spin mode.

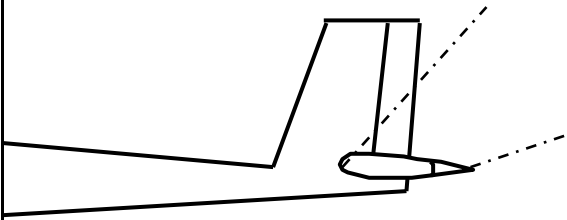

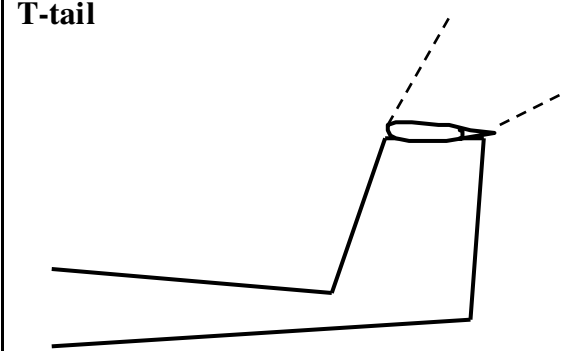

	Fuselage dominant aircraft	Wing dominant aircraft
In-spin aileron	Reduces spin rate	Increases spin rate and flattens spin
Out-spin aileron	Increases spin rate and flattens spin	Reduces spin rate

A further consideration taken is that of tail shape. Unless wind tunnel facilities are available (which would be unusual for a microlight certification programme) general rules may be applied. The most important aspect of the design of the tail is that at-least 1/3 of the rudder must remain outside the wake from the horizontal stabiliser. Experience has shown that if a line is drawn on a side view of the aircraft upwards at 60° above the chord line from the leading edge of the surface, and a second at 30° above the trailing edge of the surface, the area between these two lines may be considered the wake, and sufficient rudder area must lie outside that. The cruciform shape of tail, as found on the Thruster, AX and X'Air series of aircraft for example are very good in this respect since at-least 50% of the rudder will invariably lie outside

the wake. Other designs such as the Spectrum T1 offer significant concerns as to the safety of spin recovery. These issues of tail shape are illustrated briefly in **Figure 30** below, and in greater depth at reference [81].

Figure 30, Tail shape considered with relation to rudder blanking and thus spin recovery (diagrams are illustrative only and not to scale)

<p>Low-fwd horizontal stabiliser</p>  <p>Considered high risk, almost total blanking of the rudder.</p>	 <p>(Example, EV-97 Eurostar)</p>
<p>Cruciform</p>  <p>Considered medium risk (usually acceptable), only partial blanking of rudder by horizontal stabiliser.</p>	 <p>(Example, X' Air Mk.2 Falcon)</p>

<p>Low—rear horizontal stabiliser</p>  <p>Considered medium risk (usually acceptable), low stabiliser but partial blanking of rudder through horizontal displacement of the horizontal stabiliser.</p>	 <p>(Example, Pegasus / Flightdesign CT2K)</p>
<p>T-tail</p>  <p>Considered low risk, a totally unblanked rudder. (Note, only the spinning perspective is considered here with respect to tailplane design and such tail shapes may present non spin-related handling deficiencies.)</p>	 <p>(Example, Shadow CD)</p>

Whatever mode seems least hazardous should always be flown first. This is in line with normal flight test practice of progressing from least to greatest risk in small steps. In practice, the planning team will tend to create, following their

best available judgement, a hierarchy of risk, and progress along the test plan towards the test considered to have greatest risk.

It is also important to make some estimation of the possible aileron effects before commencing spinning with mishandled aileron. In an aircraft with a particularly large wing, in-spin stick is likely to flatten and speed up the spin (and make recovery harder), whilst out-spin stick is likely to reduce the spin rate and push the nose down (assisting recovery). In an aircraft with a dominant fuselage, in-spin stick is likely to create a yawing moment aiding recovery; conversely out-spin (see section 4.6) stick may again make the spin faster and harder to recover from. Order of tests must take this into account.

5 The tumble departure mode in weightshift controlled microlight aeroplanes

5.1 Introduction to the tumble.

Since their appearance in the late 1970s, weightshift controlled microlight aircraft[82], have enjoyed a remarkable growth to become a large part of recreational aviation[83]. This has in part been due to their low cost, and in part due to an excellent safety record [84] consistently below 30 fatal accidents per million flying hours.

However, during investigations following a particular fatal accident in 1997, it was found that there had been a number of accidents, usually fatal, to weightshift controlled microlights, which could not be explained through any conventional cause. The reason for these accidents, which involved a departure from controlled flight followed by aircraft structural failure (generally including mechanical failure of the basebar, wingtips and leading edge), became known as the “tumble”.

There has been a previously published attempt to analyse the tumble, in that case for hang-gliders (where it had first been identified), at reference [85]. This section does not contradict that work, but does progress the analysis further than the previous work, introducing aeroelastic, transient aerodynamic, and induced camber effects.

References [86, 87, 88, 89, 90, 91, 92, 93, 94] report a number of accidents to Weightshift controlled Microlight Aircraft. With a few exceptions on specific points, these reports show a number of common factors.

- A departure from controlled flight either following gross mishandling, flight to the stall, or during flight in potentially highly turbulent conditions.

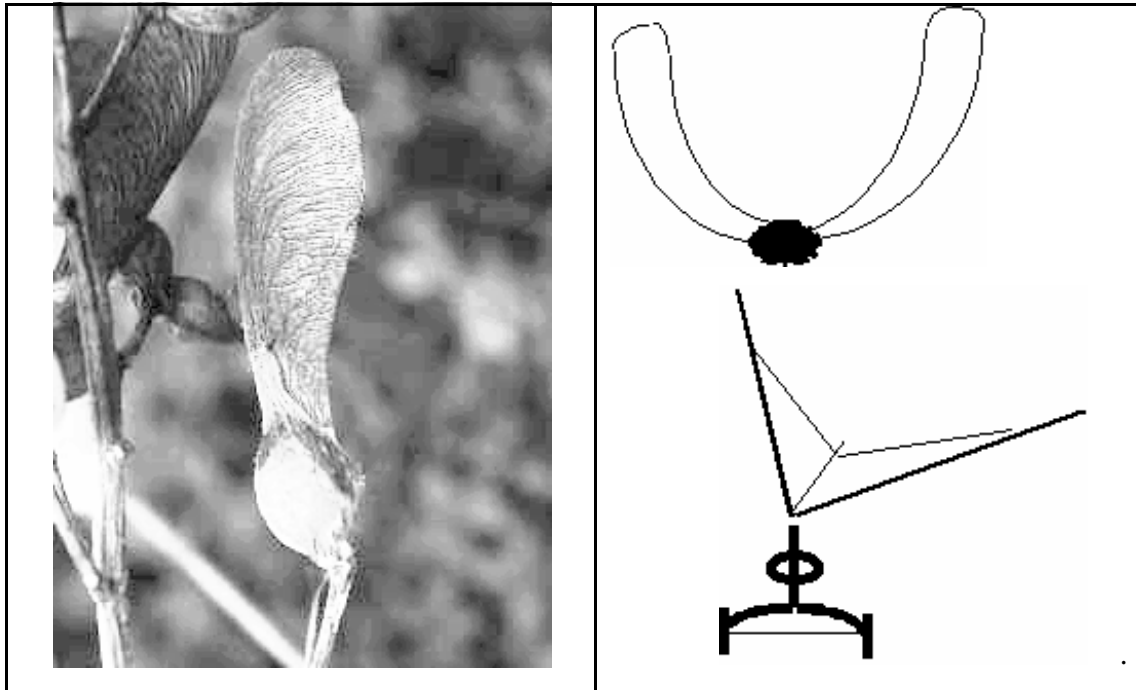
- In most cases, the aircraft was being flown at a comparatively low weight.

- Damage to the aircraft consistent with very large negative g overload of the wing (usually failure of the top wires, and also failure downwards of the wing-tips)
- Evidence of the wing being forced to a very high nose-up pitch attitude relative to the trike (impact of the basebar with the front strut, usually resulting in a failure of one of these two components, causing the propeller subsequently to impact the keel tube). Where a pilot has survived the departure it is normal that they have subsequently reported the basebar being “snatched from their hands” [95]. [The term “trike” is used here to describe all of the aircraft that is not the wing or hangbolt. The wing and trike are hinged in pitch and roll at the hangpoint, of which the hangbolt is the central component, whose removal allows the two to be separated for derigging.]
- Rapid autorotation of the aircraft in nose-down pitch, generally followed by ...
- Break-up of the aircraft in flight, preventing it from sustaining flight and usually resulting in a fatality.

*Note: Sycamoring failure mode. It has been recorded in a number of accidents that the wing basebar has failed following impact with the front strut. The result of this would appear to have been that immediately following this failure, the loss of structural integrity has caused a subsequent failure of the wing leading edge (and cross-tube), at the root on one side only. This has resulted in a new wingform that is approximately “L-shaped” as seen in forward view. It is reported that a wing which has failed in this way develops a spiral motion that tends to arrest the aircraft’s descent, in the manner of a sycamore seed (**Figure 31** below), hence the accepted term, “sycamoring” which has become adopted to describe the nature of descent. It is believed from anecdotal evidence, although documentary evidence to either support or dispute this case is weak, that all tumble accidents which have been survived have involved basebar failure and sycamoring descent. Similarly there does not appear to*

be any recorded tumble accident, where the front strut failed, which was survived. For this reason, all British microlight manufacturers eliminated any previous use of re-enforcing cables within the basebar from the late 1980s[96].

Figure 31, Sycamore Seed with wing casing, showing similarity to trike with damaged wing.

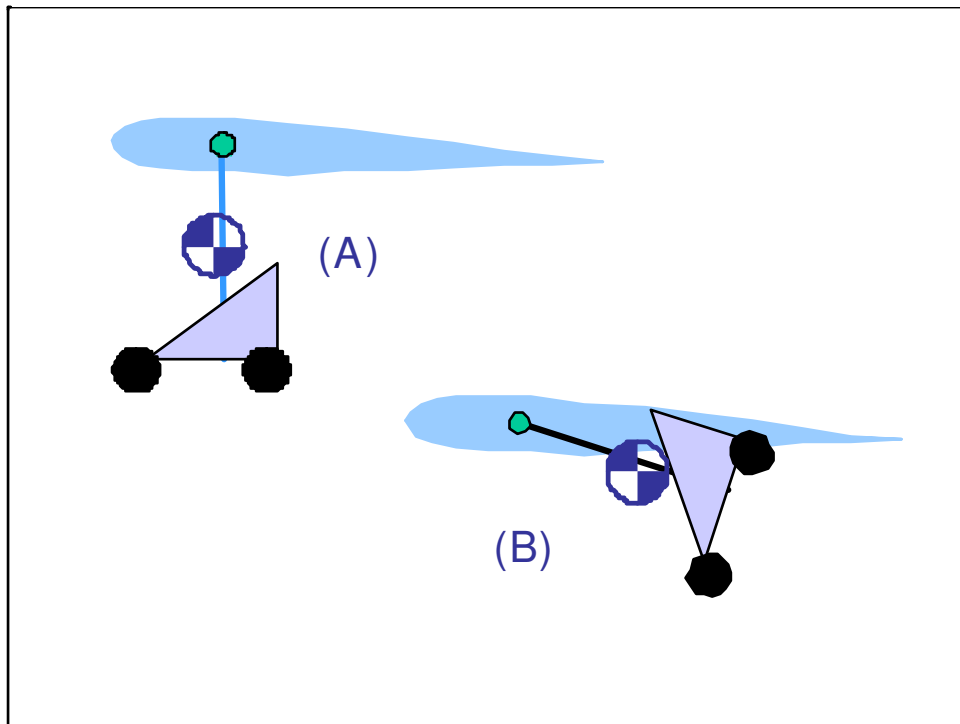


5.2 The mechanism of the established tumble.

The tumble behaviour of the two piece airframe that is a Weightshift Microlight contains what initially appears to be a paradox. The tumble rotation is known to be nose down whilst the basebar is known to be on the front strut – the control position associated with a nose-up pitching motion in normal flight. There must therefore be some mechanism which sustains these apparently contradictory conditions.

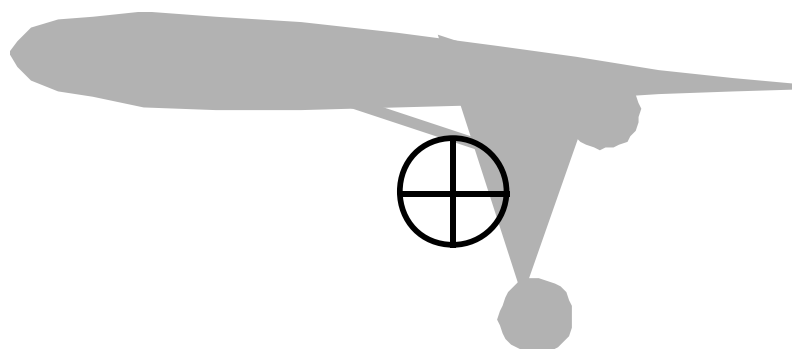
Figure 32 below illustrates the situation with the Microlight in normal attitude and when the wing is fully nose up relative to the pilot.

Figure 32. Positions of aircraft in normal flight(A) and tumble(B)



Whilst **Figure 33** shows diagrammatically the centre of gravity of the complete aircraft.

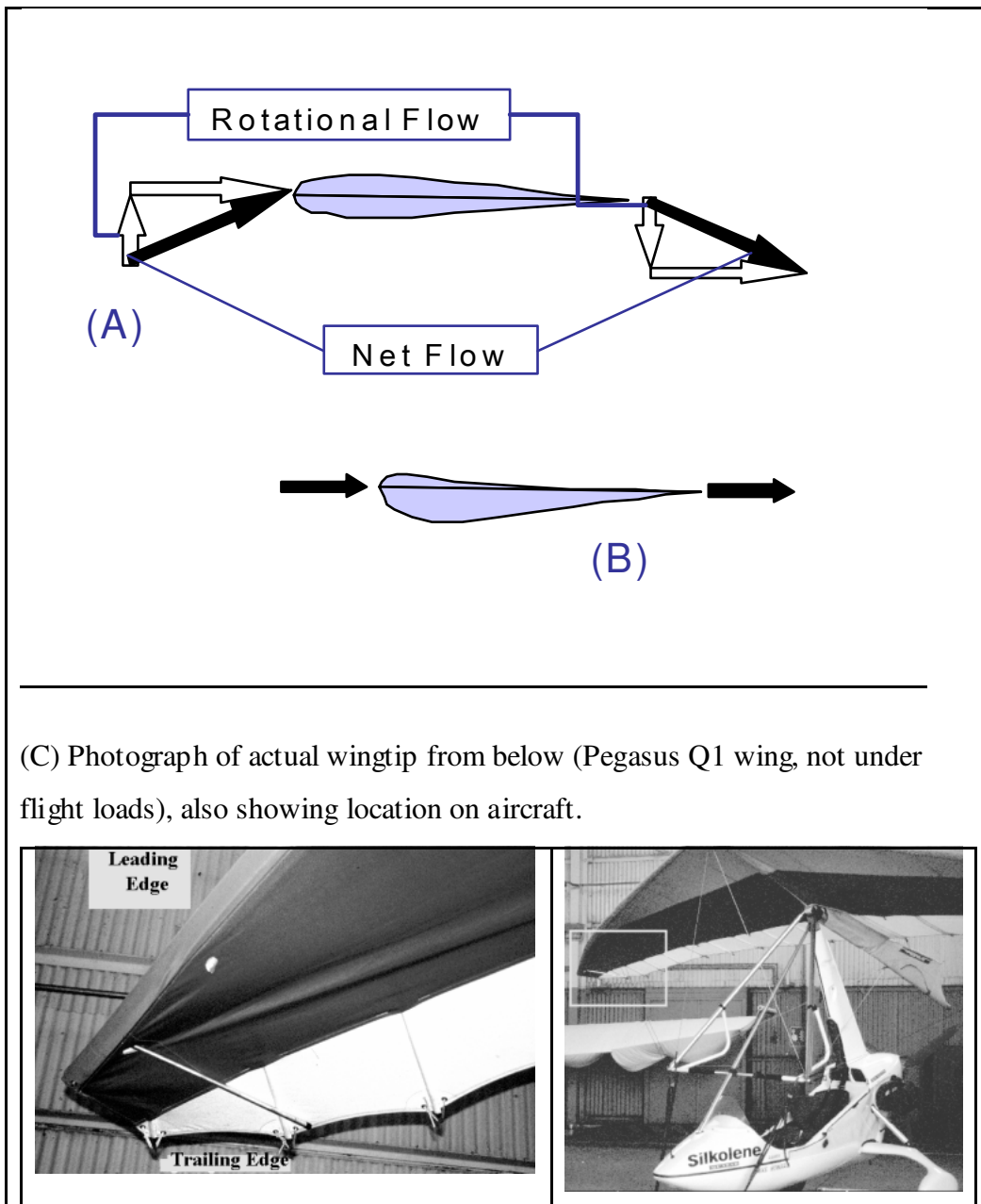
Figure 33, position of whole aircraft CG



The tumble therefore comprises a translational motion coupled with rotation about a point of the aircraft close to the centre of gravity and the incident airflow over the wing will be as shown in **Figure 34** (A) below. This type of

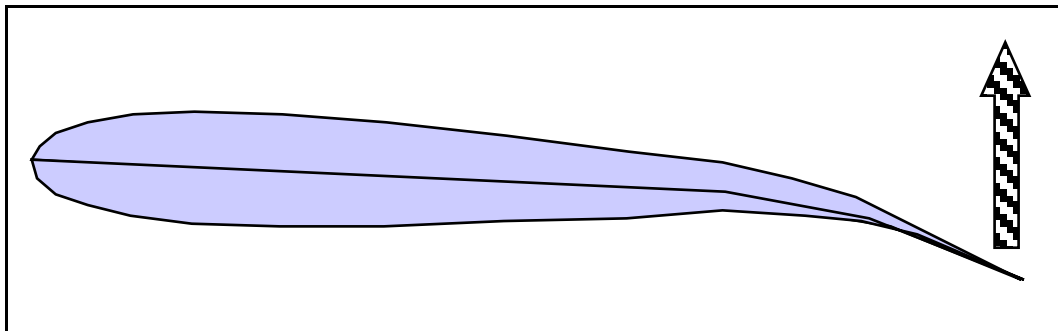
airflow can be experienced by a pitching wing in normal flight which gives rise to unsteady aerodynamic phenomena. In particular the airflow over the leading and trailing edges of the wing are appropriate to the incident flow over a sharply cambered wing as shown in **Figure 34 (B)**. This effect can be considered to be an induced camber and will generate negative lift. **Figure 34 (C)** shows a photograph of an actual wingtip.

Figure 34. illustration of induced camber during tumble



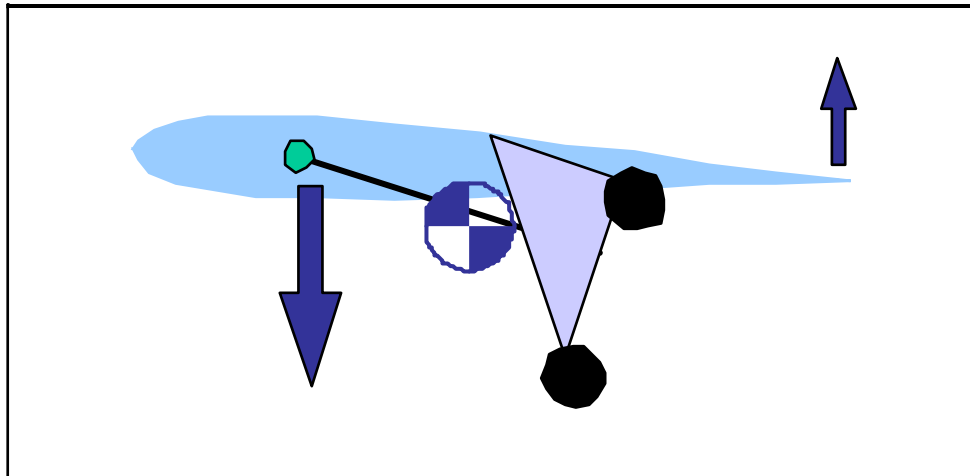
As the aircraft tumbles nose down, the inertial effects upon the wingtip trailing edge components will tend to force them in a direction from upper to lower surface. These trailing edge components are unlike those at the leading edge in that they are not constrained by a spar (although **Figure 34** (C) shows the “tipstick” extending from the leading edge, which is intended to limit deformation towards the lower surface). In consequence, the inertial loading will tend to deform the trailing edge structure towards the lower surface and therefore produce a localised positive camber. This will generate an additional positive lift in the trailing edge region which will, in turn, increase the nose down pitching moment. This is illustrated in **Figure 35**; it is also worthy of note that the wreckage of most aircraft which have suffered a tumble-related structural failure have shown failure of the wingtips, in the sense of the tip bending towards its lower surface.

Figure 35. Illustration of the effect of localised induced camber



This therefore shows the situation of a wing-trike combination locked into a configuration with the wing fully nose-up. The tumble rotation having begun causes the trailing edge panels to deflect downwards generating some additional localised trailing edge camber through aeroelastic effects. This camber will generate aerodynamic forces, which, in turn, will increase the nose down moment. This moment, when considered with the microlight’s centre of gravity location, causes the wing to rotate whilst translating. The wing sees the airflow as an effective camber, which therefore generates a downward lift force; this sustains the nose-down motion. **Figure 36** shows the combination of these aerodynamic effects, which helps to explain the phenomenon and the apparent paradox.

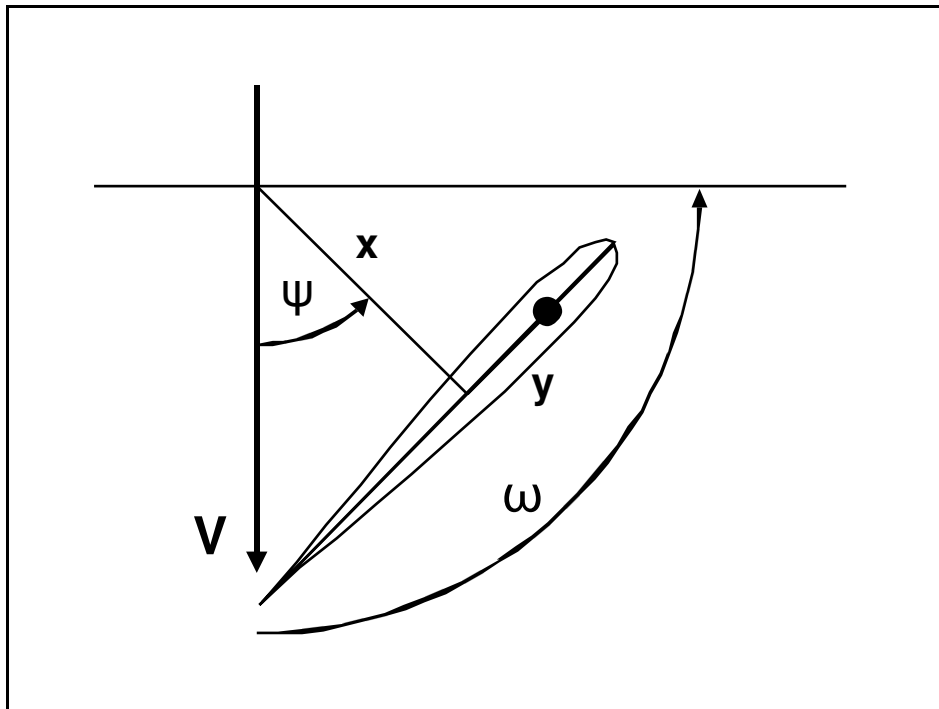
Figure 36. Illustration of aerodynamic forces sustaining the tumble



These comments about the unsteady aerodynamic effects are based on existing knowledge [97] of such phenomena. However, under normal circumstances a wing will see these effects as a small vertical wind perturbation superimposed on an essentially forward incident airflow. With the Microlight wing in a tumble we have the situation of a wing translating and rotating but with both motions of equivalent magnitude. The aerodynamics of such a wing motion is most unusual; what is known on the subject is discussed in section 5.5 following.

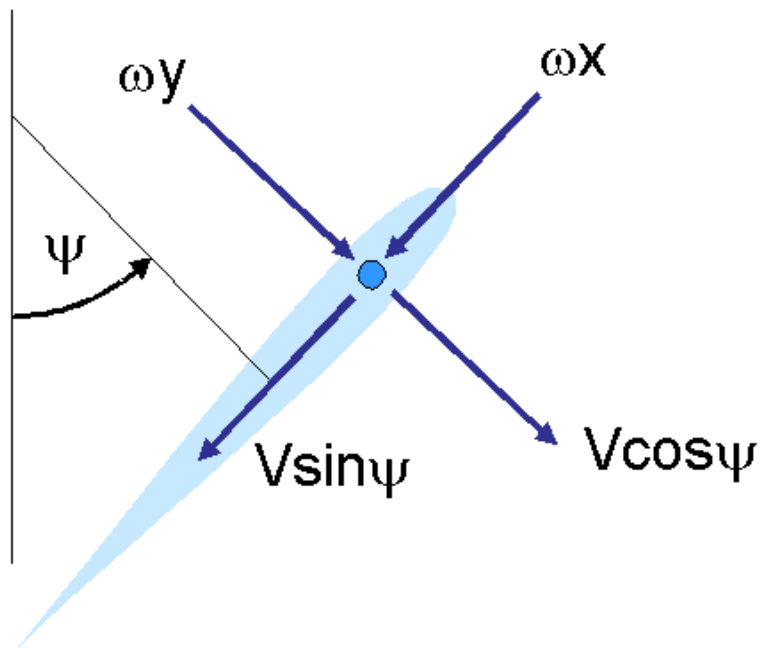
5.3 A simple estimate of the magnitude of induced camber during the tumble.

In order to estimate the degree of induced camber a short analysis is presented, using the terms shown in **Figure 37** below:-

Figure 37. Illustration of tumble parameters

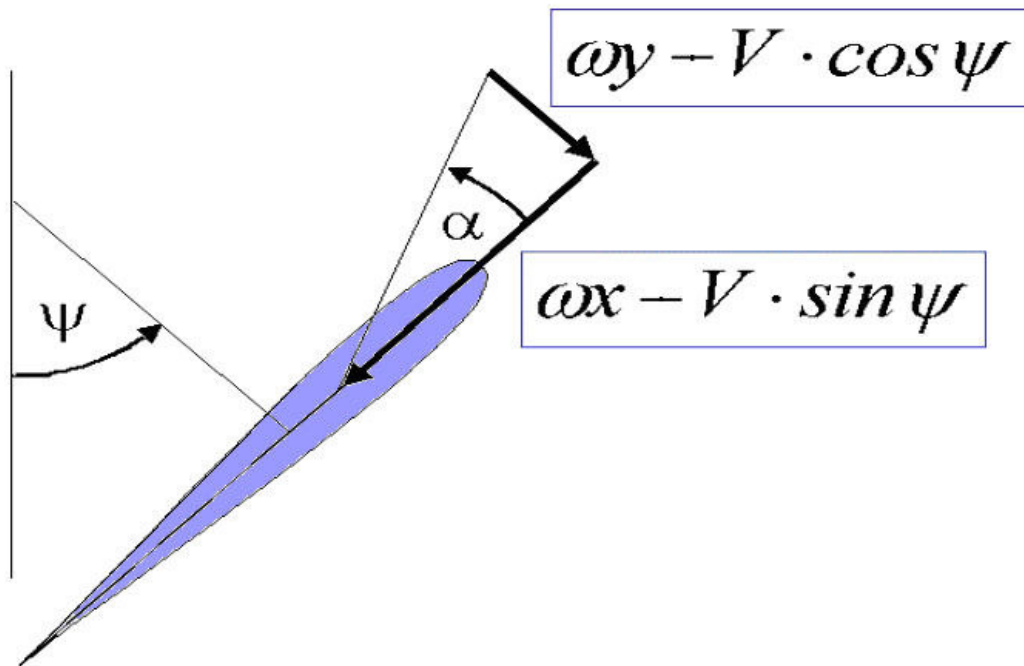
A wing section is fixed to an axis rotating about a point which is descending vertically. With reference to **Figure 37** above, by considering an element of the wing, which is distance y towards the leading edge from a reference point at which a radial line (length x) from the centre of gravity (CG) of the aircraft meets the wing chord line at 90° . This element is rotating about the CG at a rate ω and at any given moment the line between the CG and perpendicular to the wing chord, and the entire system direction of movement is $\psi = \omega t$, where ψ is the azimuthal co-ordinate. The rate of vertical, translational movement is V . The motion of this element may therefore be expressed by the various components of translation and rotation as indicated in **Figure 38** :-

Figure 38. Local velocity components of airflow over a wing element



With this information, the local angle of attack can be determined at (x,y) , as shown in **Figure 39**:-

Figure 39. Determination of local angle of attack.



From these, the following expression may be written for the local angle of attack:-

$$\alpha = \tan^{-1} \left(\frac{\omega y - V \cos \psi}{\omega x - V \sin \psi} \right) \quad (5-1)$$

or

$$\alpha = \tan^{-1} \left(\frac{\frac{y}{x} - \frac{V}{\omega x} \cos \psi}{1 - \frac{V}{\omega x} \sin \psi} \right) \quad (5-2)$$

(An alternative form, in terms of time would be:-)

$$\alpha = \tan^{-1} \left(\frac{\frac{y}{x} - \frac{V}{\omega x} \cos \omega t}{1 - \frac{V}{\omega x} \sin \omega t} \right) \quad (5-3)$$

From (5-2) a typical incident flow angle variation across the wing chord is given by **Table 12**, which is based upon conditions given in **Table 11** preceding it.

Table 11, Conditions used for tumble simulation

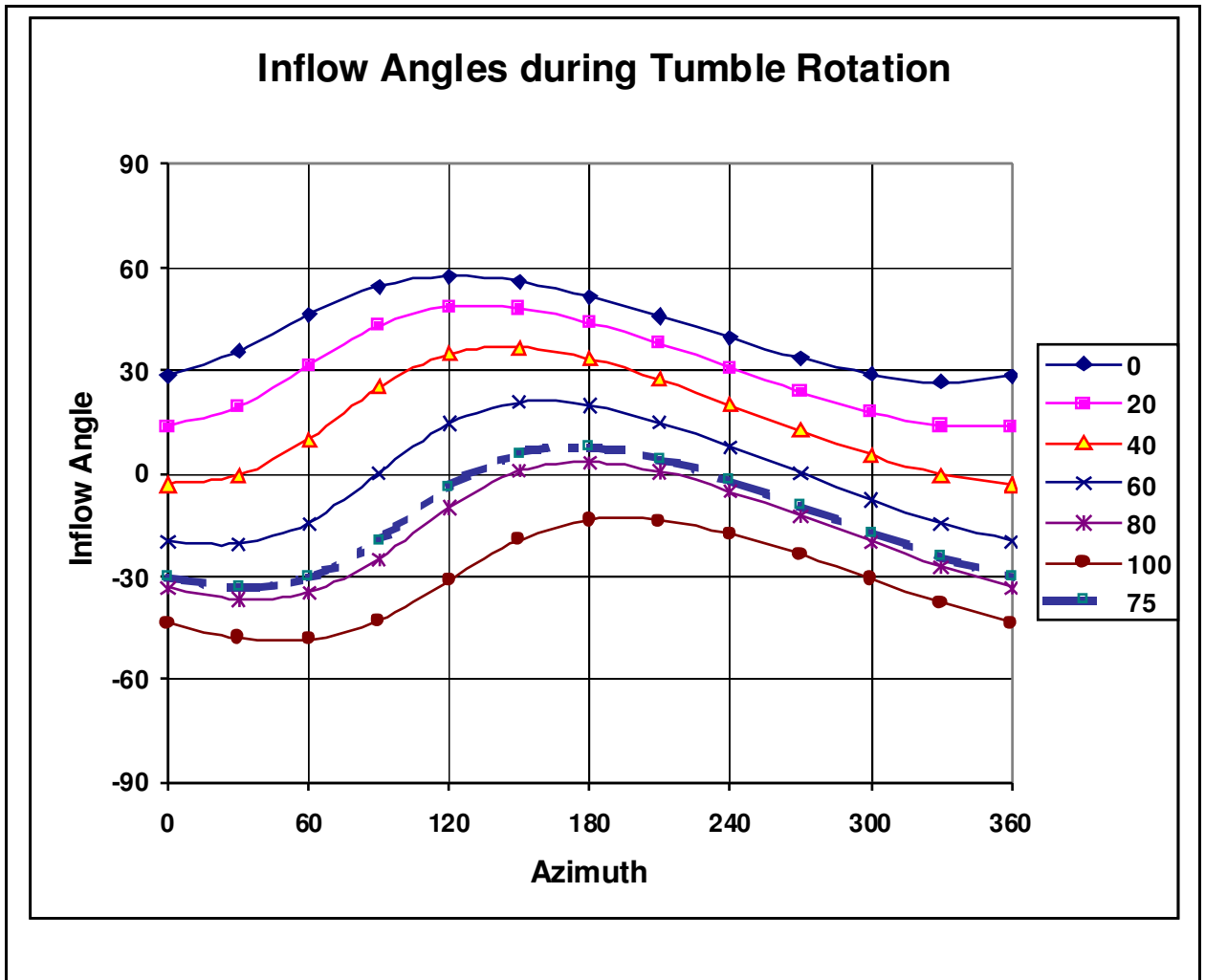
Tumble Rotation Rate	400°/sec
Tumble Translation Speed	5 m/s
Wing Chord	3m
Perpendicular distance from CG to wing chord	2.0m, intercepting at 0.6 smc.

Table 12, Local angle of attack (degrees)

Azimuth (°)	Chordwise Station (%)					
	0	20	40	60	80	100
0	28.45	13.60	-3.33	-19.70	-30.25	-33.35
30	35.70	19.45	-0.71	-20.69	-33.10	-36.62
60	46.26	31.39	9.94	-14.55	-30.36	-34.78
90	54.50	43.07	25.05	0.00	-19.32	-25.05
120	57.41	48.47	34.78	14.55	-3.81	-9.94
150	55.85	47.95	36.62	20.69	5.92	0.71
180	51.52	43.77	33.35	19.70	7.58	3.33
210	45.75	37.67	27.36	14.74	4.13	0.49
240	39.48	30.74	20.09	7.78	-2.01	-5.27
270	33.53	23.84	12.46	0.00	-9.41	-12.46
300	28.82	17.81	5.27	-7.78	-17.14	-20.09
330	26.58	13.81	-0.49	-14.74	-24.41	-27.36
360	28.45	13.60	-3.33	-19.70	-30.25	-33.35

This may be illustrated graphically as shown in **Figure 40** below.

Figure 40. Local angle of attack variation



Thus a significant induced camber effect may be seen throughout the sustained tumble.

The 75% chord result is highlighted in **Figure 40** above. Analysis of a pitching and plunging aerofoil using thin aerofoil theory [98], indicates that the lift force can be considered to be acting at the 25% chord based on an incidence determined by conditions at the 75% chord. In addition, a pitching moment is generated in opposition to the pitching rate and thus acts as a viscous aerodynamic damper. This figure shows that for approximately 80% of the rotation cycle the rotation imparts a negative incidence, giving a negative lift. This negative lift force sustains the nose down tumbling motion of the aircraft. The variation of the 75% incidence shows that the pitching

moment is not constant and a “pulsing type” of rotation rate would be likely. Observation of the tumbling incident described in **Figure 61** appears to confirm this behaviour.

5.4 Longitudinal static stability of a weightshift microlight: development of a model intended to aid analysis of tumble entry.

A weightshift controlled microlight aeroplane may under normal conditions be treated as having two separate and distinct longitudinal stability modes: that of the wing, and that of the trike. In normal flight, when the basebar is between the pilot and front strut, but touching neither, these are separate. When pitching moments are taken about the hangpoint, the aerodynamic pitching moment of the wing is balanced by the wing’s own weight. Similarly, the pitching moments of the trike about the hangpoint (due to weight, drag and thrust) must sum to zero.

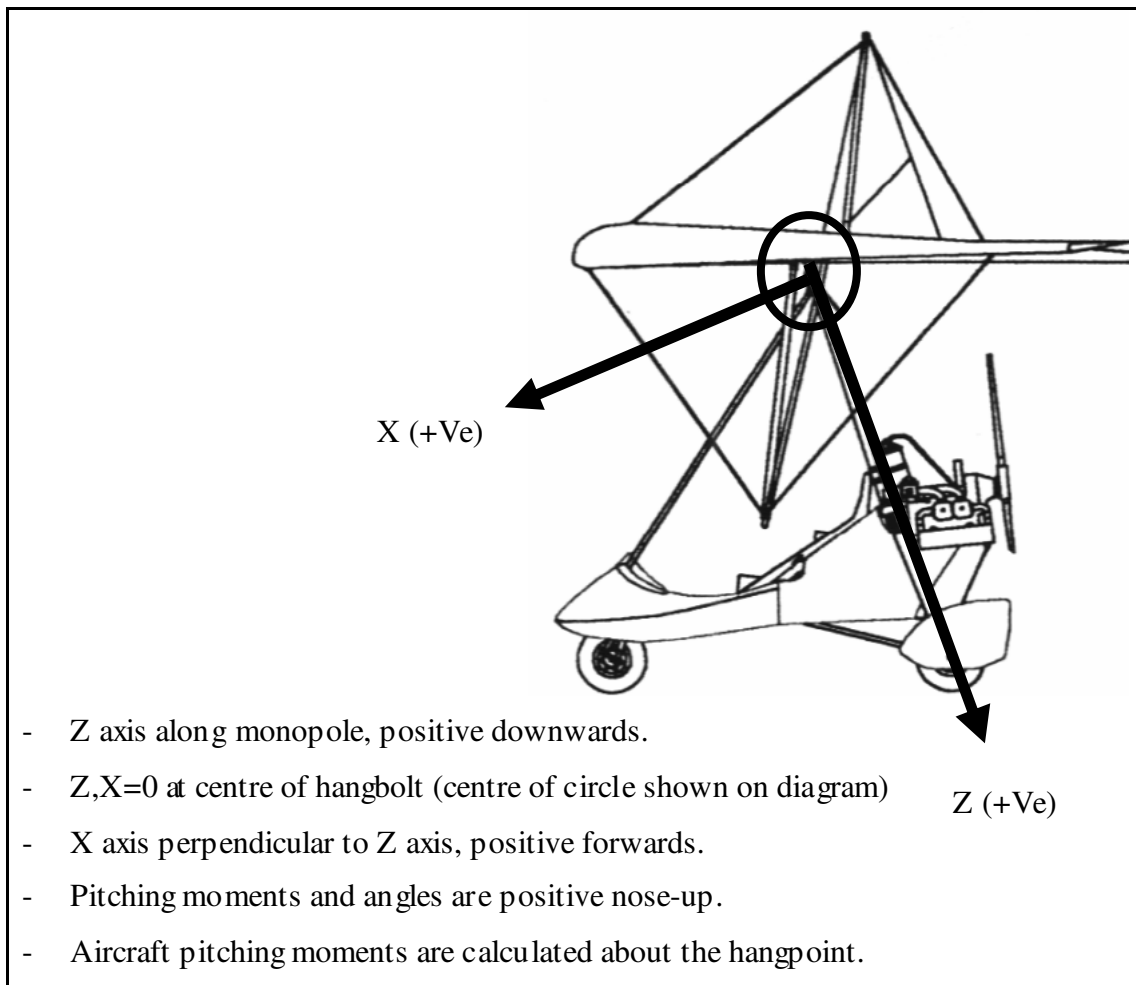
It is believed, mostly from the evidence of accident investigation reports, that the tumble occurs when some combination of conditions causes the basebar to be pushed against the front strut (equivalent to the control input used by a pilot to apply the maximum nose-up pitching moment), whilst the sum of pitching moments upon the aircraft cause are strongly nose-down. Wing aerodynamic data is available from tests using the BHPA test facility at Rufforth, Yorkshire (**Figure 41**). However, a theoretical model is required for the whole aircraft that predicts C_M as a function of aircraft pitch attitude. It should then be possible to combine the data for both wing and trike, to indicate at what combination of conditions the aircraft may continue to rotate nose-down, initiating and sustaining the tumble. This may then be used to determine whether an aircraft design offers any significant risk of tumble entry, given knowledge of the wing’s aerodynamic characteristics, and the desired or existing flight and manoeuvre envelope.

Figure 41. BHPA hang-glider test facility at Rufforth, Yorkshire



Consider the following model of a weightshift microlight in side view, disregarding for the time being the aerodynamic pitching moment of the wing. All pitching moments will be taken about the hangpoint.

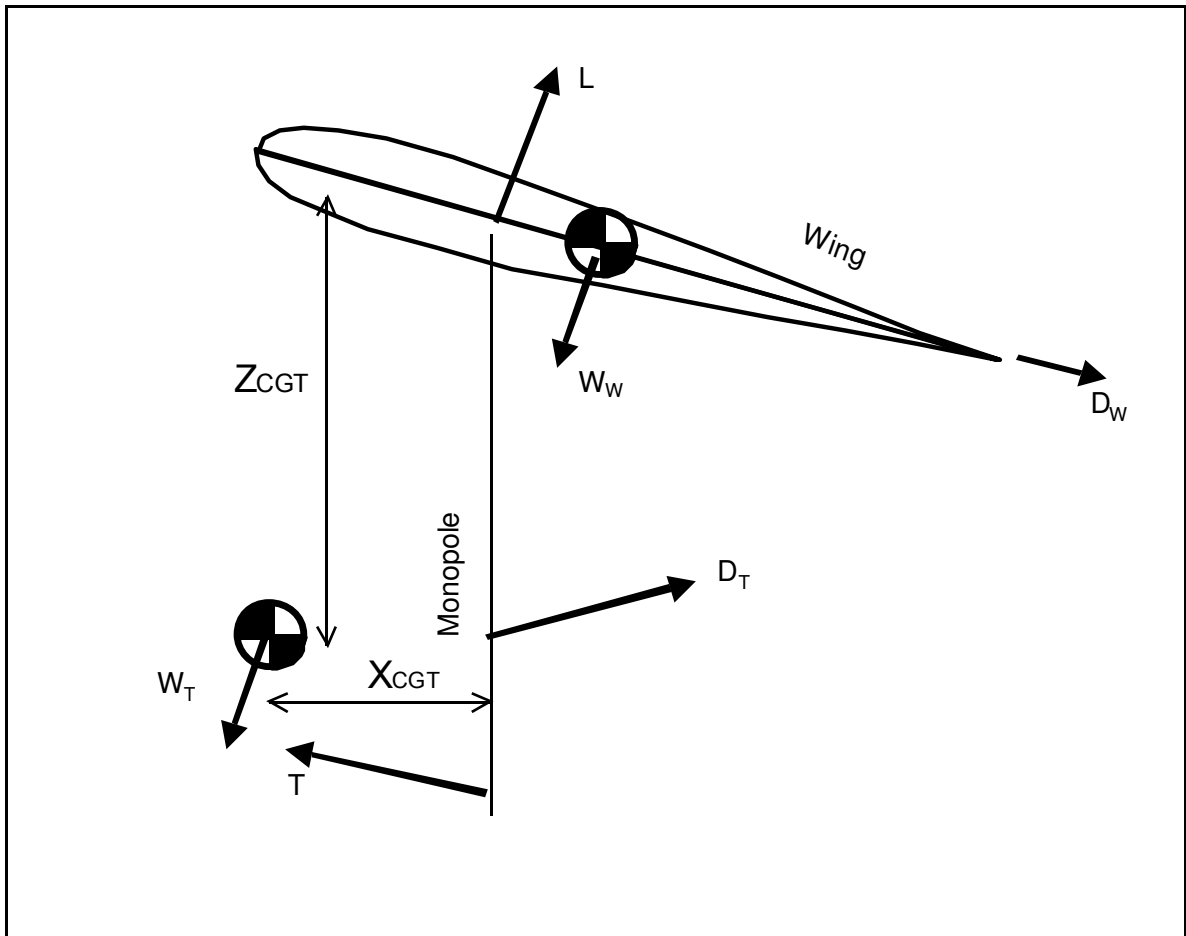
Figure 42. Sign conventions used in tumble analysis

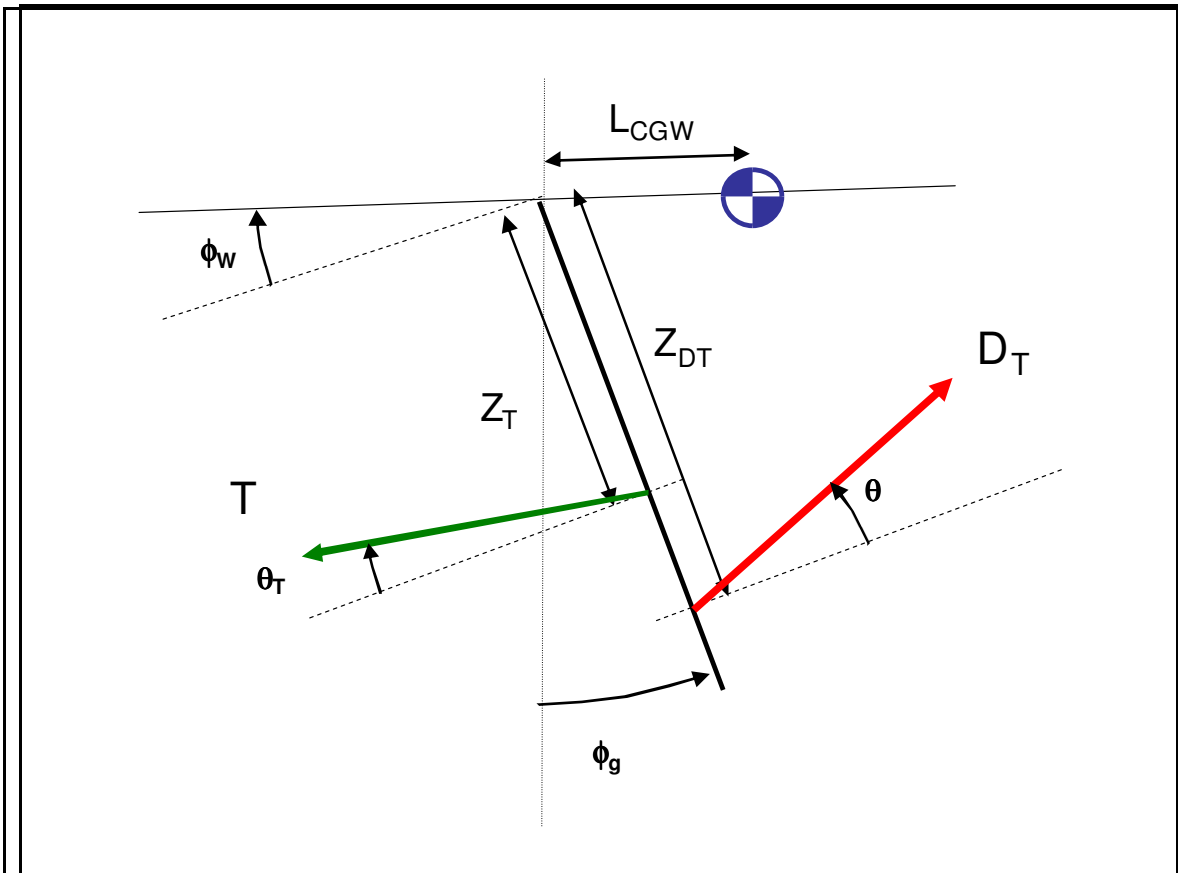


The model will make use of the following assumptions and variables:-

- The aircraft is in an unaccelerated state.
- Trike drag acts in the wind axis
- Wing lift and drag act at the hangpoint.

Figure 43. Forces, distances and angles relevant to the longitudinal stability model





\mathbf{W}_T is the weight of the trike. As shown in **Figure 43**, it acts through the trike CG, which is located Z_{CGT} below the hangpoint (in a direction parallel to the monopole), and X_{CGT} forward of the monopole axis (in a direction perpendicular to the monopole). The weight acts at an angle ϕ_g relative to the monopole axis. $\phi_g = 0$ when the monopole is perpendicular to the surface of the earth increasing with the aircraft's nose-up attitude.

\mathbf{T} is the thrust due to the engine. It acts through the monopole at a point Z_T below the hangpoint, and at an angle θ_T relative to a perpendicular to the monopole such that if $\theta_T = 0$ the thrustline is perpendicular to the monopole. θ_T is positive as the thrustline becomes more nose-up.

\mathbf{D}_T is the drag due to the trike. It acts through the monopole at a point Z_{DT} below the hangpoint, and at an angle θ relative to a perpendicular to the monopole such that if $\theta = 0$ the monopole is perpendicular to the relative airflow, and if θ is positive the monopole is more nose-up.

\mathbf{W}_W is the weight of the wing. It acts through the wing centre of gravity which is on the

wing keel a distance L_{CGW} behind the hangpoint. The wing itself is at an angle ϕ_w nose-up compared to a perpendicular to the monopole. The weight acts at an angle ϕ_g relative to the monopole axis. $\phi_g = 0$ when the monopole is perpendicular to the surface of the earth, becoming more positive with the aircraft's attitude increasing nose-up.

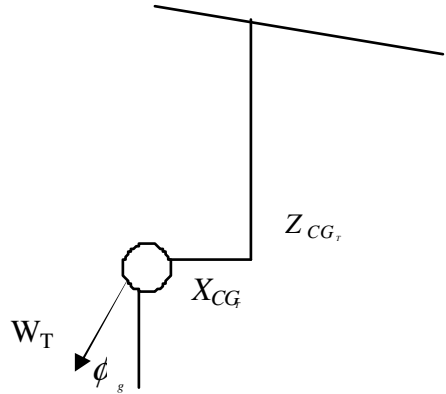
L is the lift due to the wing. It acts through the hangpoint at an angle perpendicular to the wing and is positive when acting towards the upper surface of the wing.

D_w is the drag due to the wing, it acts through the hangpoint in a direction parallel to the wing keel and is positive when acting towards the trailing edge.

Pitching moments of the whole aircraft (except for the present the wing aerodynamic pitching moments) about the hangbolt, are shown in the following **Table 13**.

Table 13. Pitching moments about hangpoint

Moment due to wing aerodynamic pitching moment:	Disregarded in this analysis because the wing freely articulates in pitch relative to the trike. Therefore any wing aerodynamic pitching moments will influence the wing pitch attitude only <u>within the aircraft</u> and will not directly influence pitching moments acting upon the whole aircraft.
Moment due to effect of wing lift:	=0, since lift is considered to act through hangpoint
Moment due to effect of wing drag:	=0, since wing drag is considered to act through hangpoint
Moment due to effect of wing weight:	$=W_w L_{CG_w} \cos[\phi_w - \phi_g] \quad (5-5)$

<p>Moment due to the drag of the trike</p>	$= -D_T Z_{D_T} \cos[\theta]$ $= -K_{D_T} V^2 Z_{D_T} \cos[\theta]$ <p>(Since $D_T = K_{D_T} V^2$)</p> <p style="text-align: right;">(5-6)</p>
<p>Moment due to thrust</p>	$= T Z_T \cos[\phi_T]$ <p style="text-align: right;">(5-7)</p>
<p>Moment due to the weight of the trike</p>	<div style="text-align: center;">  </div> <p style="text-align: center;">Taking moments about hangpoint</p> $= W_T (-X_{CG_r} \cos[\phi_g] + Z_{CG_r} \sin[\phi_g])$ <p style="text-align: right;">(5-8)</p>

Summing these components, we achieve the following expression for the pitching moment acting upon the entire aircraft.

$$M_{TOTAL} = W_w L_{CG_w} \cos[\phi_w - \phi_g] - K_{D_T} V^2 Z_{D_T} \cos[\theta] + T Z_T \cos[\phi_T] + W_T (-X_{CG_r} \cos[\phi_g] + Z_{CG_r} \sin[\phi_g]) \quad (5-9)$$

However it is difficult to predict the value of thrust during a departure from controlled flight, and also the effect of thrust is to pitch the aircraft nose-up; hence when considering the risk of a nose-down departure, zero thrust will be

regarded as the worst case. Therefore, it is conservative and appropriate to disregard it from the above formula, simplifying further to the following.

$$M_{TOTAL} = W_w L_{CG_w} \cos[\phi_w - \phi_g] - K_{D_r} V^2 Z_{D_r} \cos[\theta] + W_T (-X_{CG_T} \cos[\phi_g] + Z_{CG_T} \sin[\phi_g]) \quad (5-10)$$

This formula may then be used to estimate the total pitching moment on the trike. The data required use this formula to find M_{TOTAL} are:-

- W_w, W_T are basic design values of the aircraft; however, it should be borne in mind that whilst for a specific aircraft type W_w is fixed, W_T will vary according to occupancy and fuel state. However, for any given type, the minimum and maximum permitted loadings are published, allowing analysis to bracket the range of possible conditions.

- $Z_{D_r}, \theta, X_{CG_T}, Z_{CG_T}, K_{D_r}$ are functions of aircraft geometry and may be obtained from design data.

- ϕ_w, ϕ_g, θ are flight variables. Considering known flight conditions such as are shown in **Figure 44**, it may be determined that in level flight $\phi_g \approx -15^\circ$, and $\phi_w \approx 30^\circ$ (i.e. the monopole is canted about 15° forward of vertical, and the wing is about 15° nose-up from the horizontal, or 30° nose-up compared to a perpendicular line to the monopole). The range of values of ϕ_w will be approximately $\pm 10^\circ$ compared to this value (defined by the geometry of the trike, which restricts basebar movement). Also, normal (and usually placarded) operating limitations for an aircraft in this class are $\pm 30^\circ$ pitch attitude, compared to the normal level flight attitude. Therefore it may be considered that during flight within the normal envelope, $-[45^\circ < \phi_g < 15^\circ]$, and $[20^\circ < \phi_w < 40^\circ]$.

Figure 44. typical aircraft (Mainair Gemini Flash 2a) in flight



For the purposes of modelling, it is possible to examine a wider range of values of ϕ_g than might be experienced within the normal envelope, so values of $-105^\circ < \phi_g < 75^\circ$ will be considered [equating to attitudes between vertically upwards and vertically downwards, as seen by the pilot]. The significant case is the one where the pilot would not be able to prevent a nose down departure; assuming then a full nose-up pitch inceptor input, it can be further assumed that $\phi_w = 40^\circ$. θ , the trike angle of attack is relevant insofar as the drag due to the trike acts in a nose-down direction, therefore it will be considered to be 0° , again because this is the worst case for a nose-down pitching departure.

Therefore, the relationship describing the pitching moment acting upon the whole aircraft is given by:-

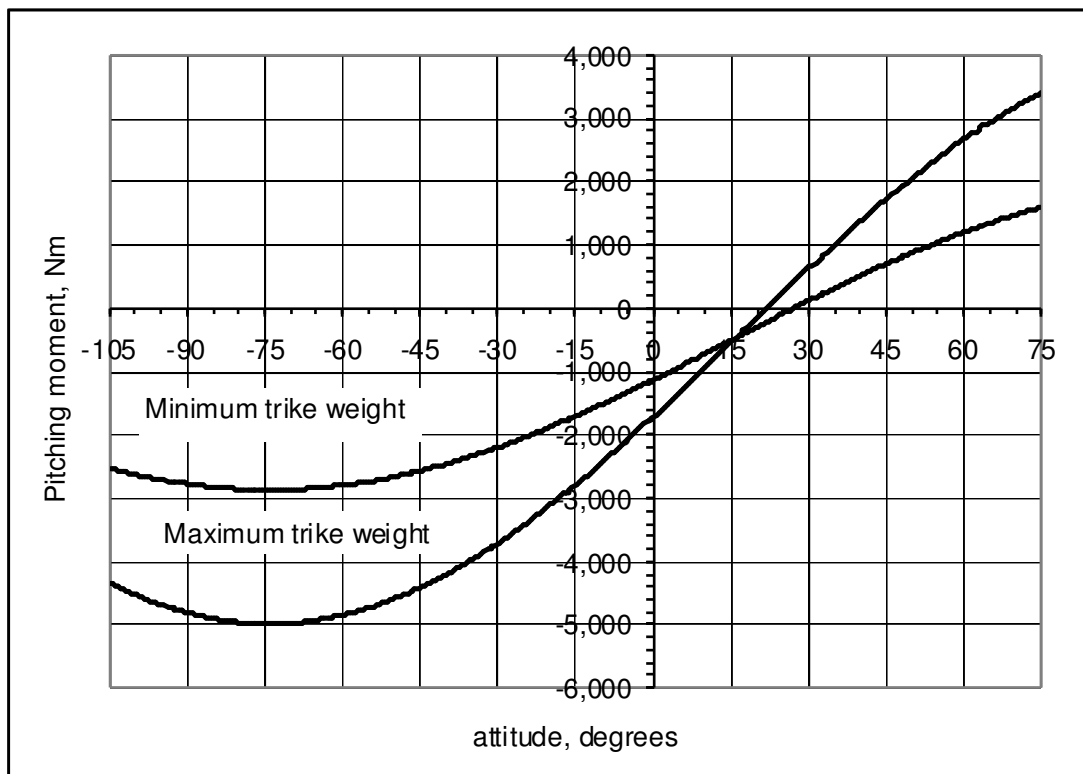
$$M_{TOTAL} = W_w L_{CG_w} \cos[40^\circ] \cos[\phi_g] + K_{D_T} V^2 Z_{D_T} \cos[6^\circ] - W_T \sqrt{X_{CG_T}^2 + Z_{CG_T}^2} \sin\left(\phi_g - \sin^{-1}\left(\frac{X_{CG_T}}{Z_{CG_T}}\right)\right)$$

(5-11)

Although for the purposes of considering the trike alone, the first term of this equation is omitted.

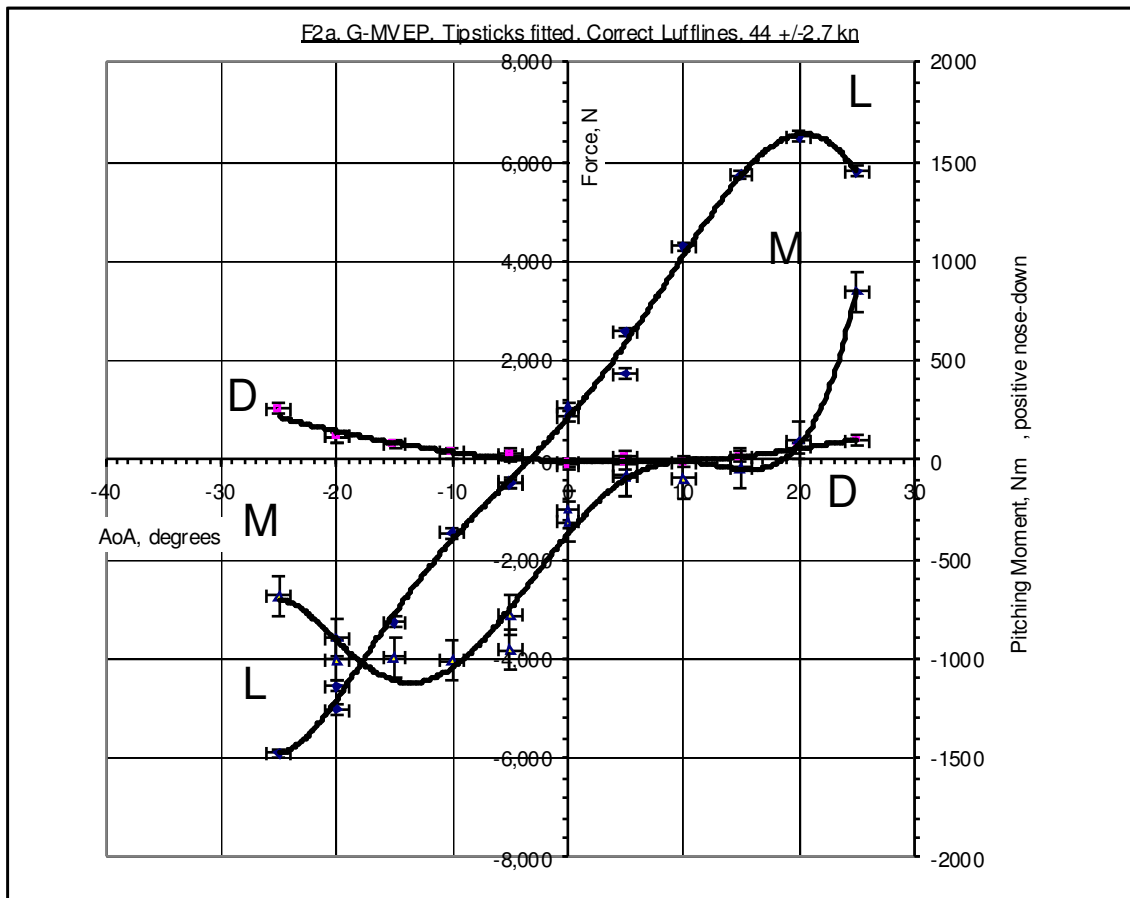
The graph below shows the value of M_{TOTAL} as a function of ϕ_g for a Mainair Gemini trike (**Figure 44**) for both it's maximum and minimum permitted loadings. V is assumed to be 43 knots, since this is a typical cruising airspeed, and also the speed around which the best quality wing aerodynamic test data is available.

Figure 45. Pitching Moment of trike about hangpoint, zero thrust



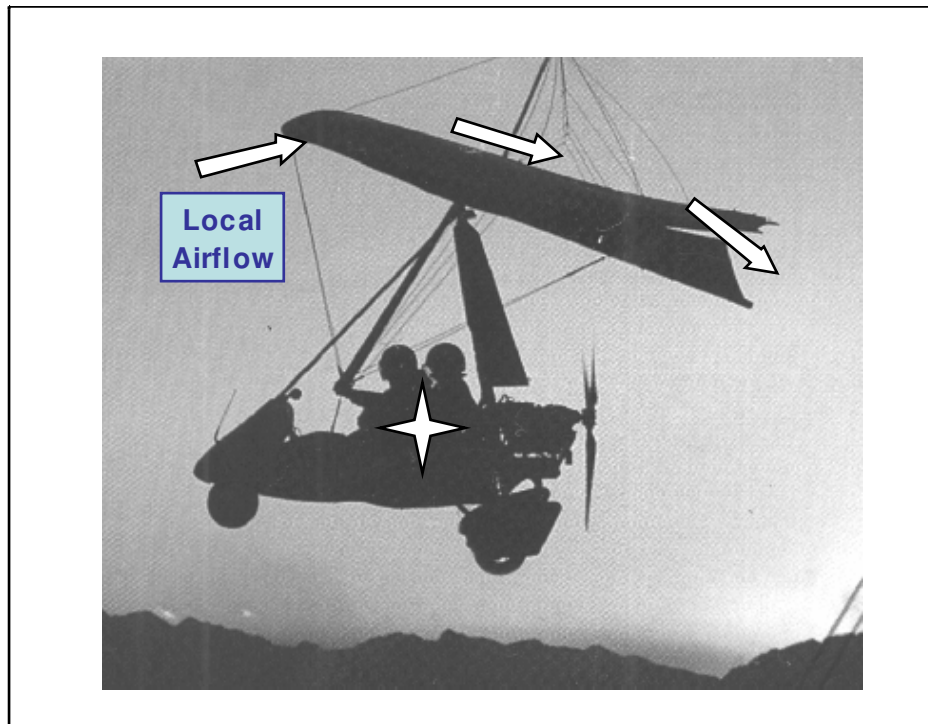
This may be compared to the following graph for a correctly adjusted Mainair Flash 2 alpha wing, which might typically be fitted to this trike.

Figure 46. Characteristics of Mainair Flash 2 alpha wing



If the wing is pushed through the stalling angle of attack to about 25° AoA, then the aerodynamic pitching moment will be about 600Nm nose-down. However, considering the wing, an equal pitching moment is reached at about 20° nose-up, regardless of weight (which equates approximately to 35° nose-up as seen by the pilot). If the aircraft was stalled at a greater nose up pitch attitude of, for example, 30° nose up (45° as seen by the pilot) then whilst the wing pitching moment will remain about 600 Nm the trike, depending upon weight, will have a pitching moment of $1,000 - 1,500\text{ Nm}$ nose-down. This will, once the basebar has been touched by the front strut - creating a rigid system, force the whole aircraft, in a rigid state, nose-down, rotating about the whole aircraft CG, which will, due to the relative masses, be close to the trike CG. The effect of this is to induce an apparent reverse camber at the wing:

Figure 47. Illustration of induced flow, superimposed upon aircraft image (Pegasus Quantum 15-912)



This induced reverse camber is likely to cause a reversal in pitch stability, and thus both a tendency to further pitch down; a negative lift force will also “lock” the trike to the aircraft, maintaining the a rigid system.

5.5 Wind tunnel testing of a scaled model to consider the flow around a tumbling aircraft.

Research has been carried out to investigate the flow around a tumbling aircraft [99]. This made use of a rigid scaled model based upon the shape (and in particular the 3-dimensional wing shape) of the Gemini Flash 2 alpha aircraft [100]; this model is shown in **Figure 48** below.

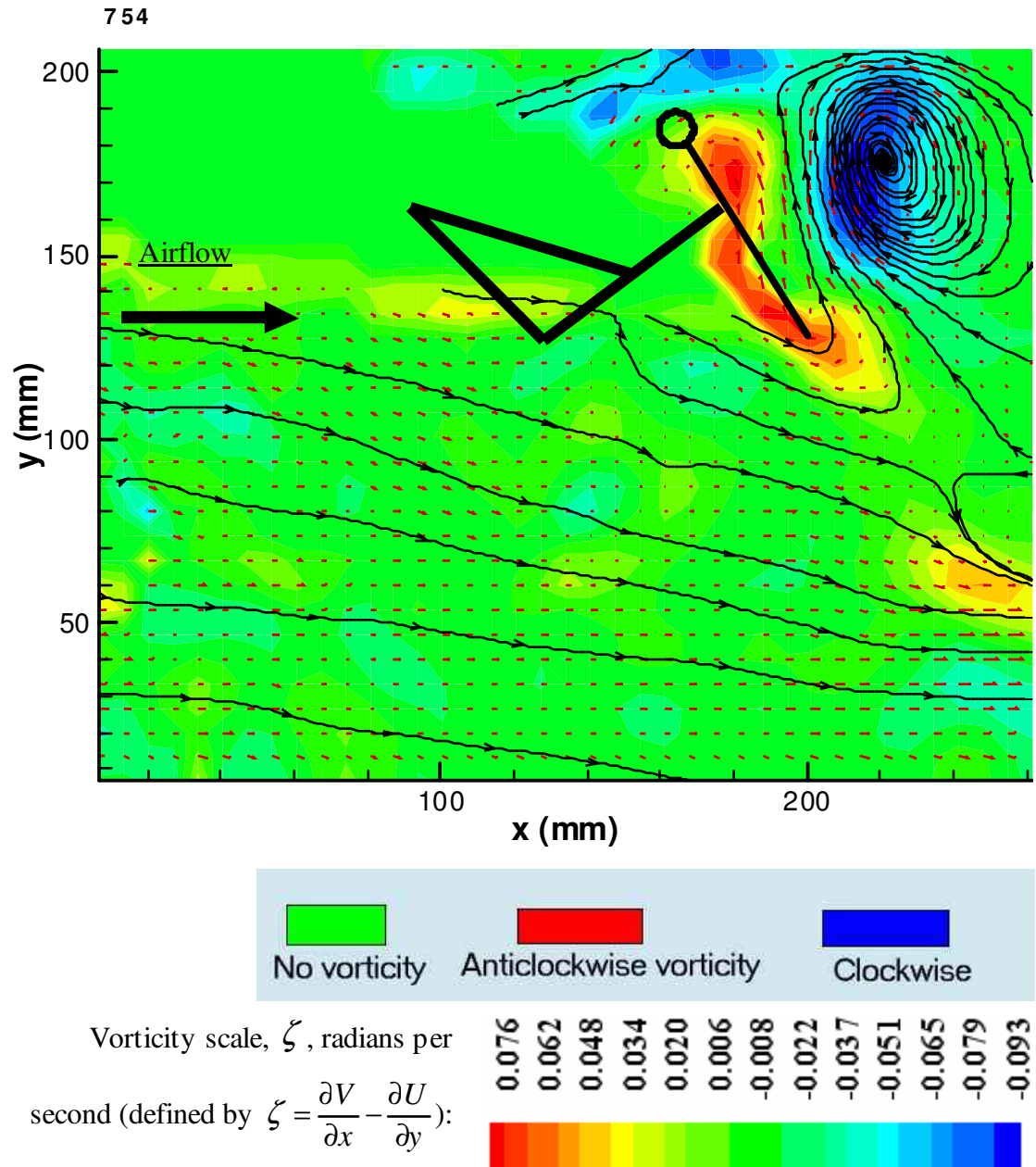
Figure 48. Scale model of Mainair Gemini Flash 2 alpha aircraft, used in wind tunnel tests



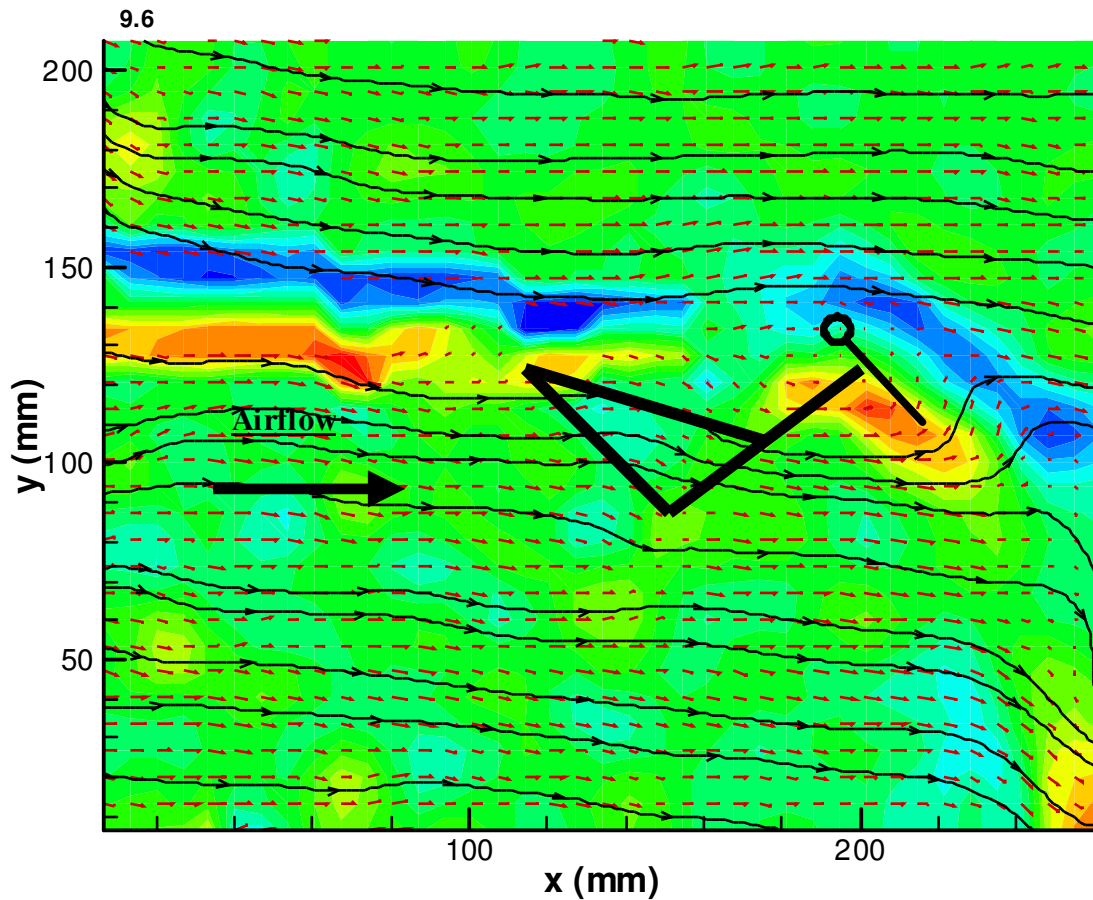
Photograph courtesy of Oliver Moncrieff

This model, which was 1:30 scaled down from the actual aircraft and set with geometry resembling an aircraft with the basebar against the front strut, was rotated in pitch within the University of Southampton's 7' x 5' (2.1m x 1.5m) low-speed wind tunnel which is fitted with Particle Image Velocimetry (PIV) equipment. No attempt was made to create a self-sustaining tumble, the subject of interest being the qualitative flow characteristics around the aircraft rather than quantitative effects. The airspeed and rotation rate were varied between 0.13-0.26m/s and 310-775°/s. Initial testing with smoke and a video camera showed the primary area of interest being 1 wing chord before and after the rotating aircraft in the direction of ambient airflow. **Figure 49** below shows the flow at two spanwise stations:-

Figure 49. Illustration of flow near¹⁶ the wing root during nose-down tumble rotation



¹⁶ 10mm outboard of wing root of model

Figure 50. Illustration of flow near the wing tip¹⁷ during nose-down tumble rotation

It may be seen from these flow visualisations that there is evidence of a significant (nominally spanwise) vortex formation occurring near to the wing root, but very little significant effect near the tip. Further investigation showed that the most readily visible vortex formation occurred at about 1/3 semi-span outboard of the root – partly because of well developed vortex shapes, and partly because at stations more inboard, partial blanking of the laser occurred due to the trike. The series of diagrams in **Figure 51** following are from Moncrieff [99] ; these show the flow around this station during a single tumble rotation at $620^\circ/\text{s}$ in a steady airflow of 0.26m/s ; symbology and orientation are identical to **Figure 49**, except that the trike diagram and wind vector are omitted for clarity.

¹⁷ 10mm inboard or wing tip on model.

Figure 51, Series of illustrations of flow around aircraft during one tumble cycle.

(All illustrations in same orientation)

Common Data Block for Figure 51

Rotational velocity = 620 °/s (10.8 rad/s)
 Free stream velocity = 0.26m/s
 Nominally ISA sea-level conditions, ambient air.
 Reynolds number $\sim 1.8 \times 10^{-3}$ (based upon centreline chord and free stream velocity)

0.076 0.062 0.048 0.034 0.020 0.006 -0.008 -0.022 -0.037 -0.051 -0.065 -0.079 -0.093

Vorticity scale, ζ  rad/s

All illustrations within this figure from Moncrieff [99]

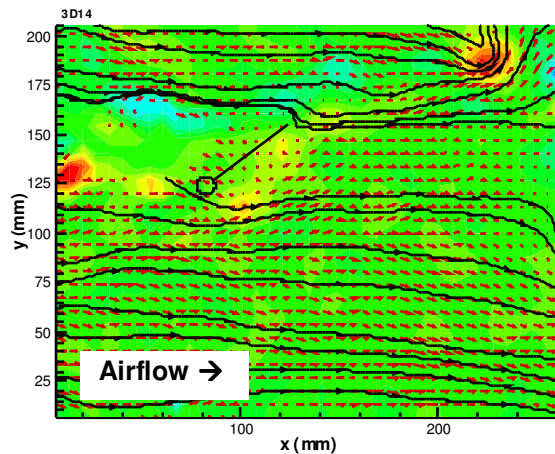


Figure 51(a)

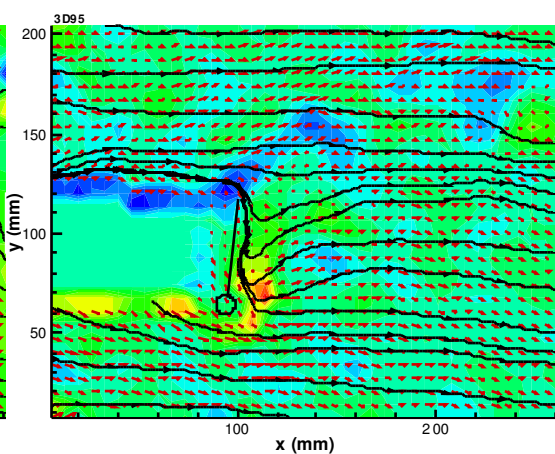


Figure 51(b)

The flow is steadiest when the wing is in the position shown in Figure 51(a) which is approximately 135° nose-down compared to the level flight attitude, this provides a convenient starting point from which to analyse the tumble. Figure 51(b) following shows the major impact the wing has on the freestream flow as it moves cross stream (inverted compared to the level flight attitude, the trike is to the right of the wing in the diagram), resulting vorticity is visible: clockwise at the trailing-edge and anti-clockwise to leeward of the leading-edge.

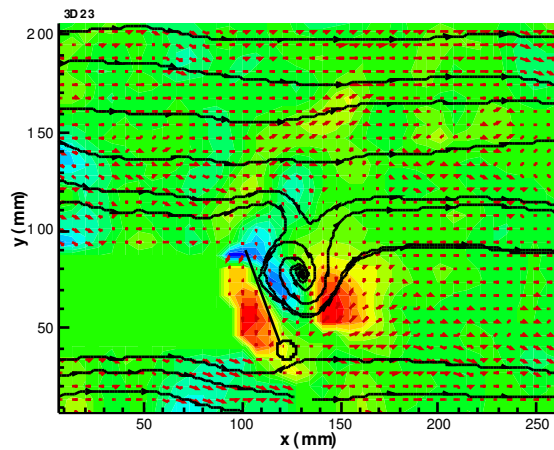


Figure 51(c)

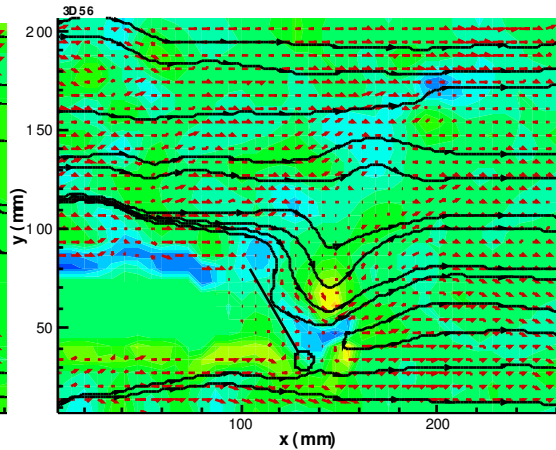


Figure 51(d)

In Figure 51(c) a vortex forms in the area between the leading edge and trailing edge but rapidly dissipates – as may be seen in Figure 51(d). Because of the short life of this vortex, it is assumed to have only small effect upon the wing – although it may create briefly an area of low pressure below the wing, generate, briefly, a force acting towards the aircraft CG.

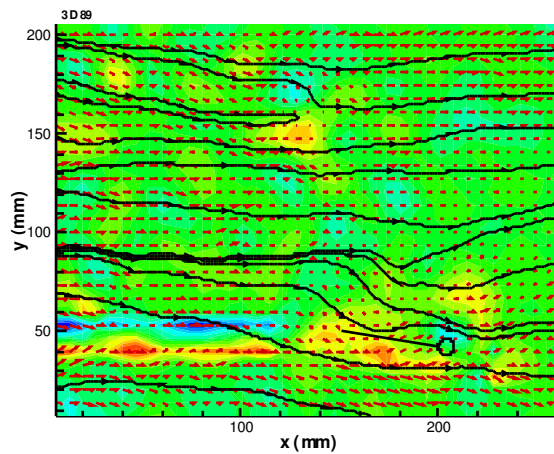


Figure 51(e)

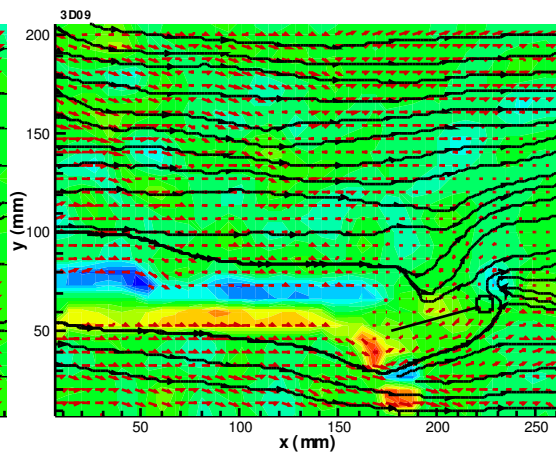
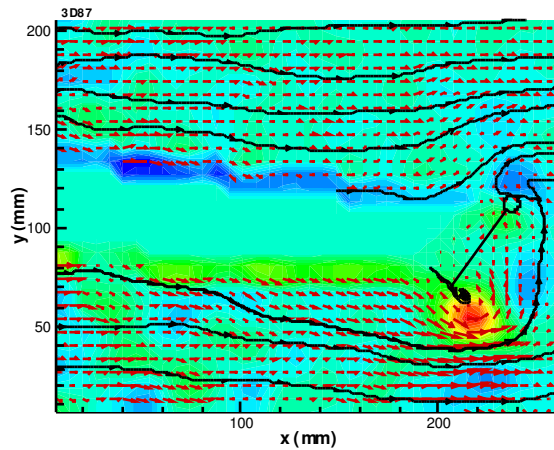
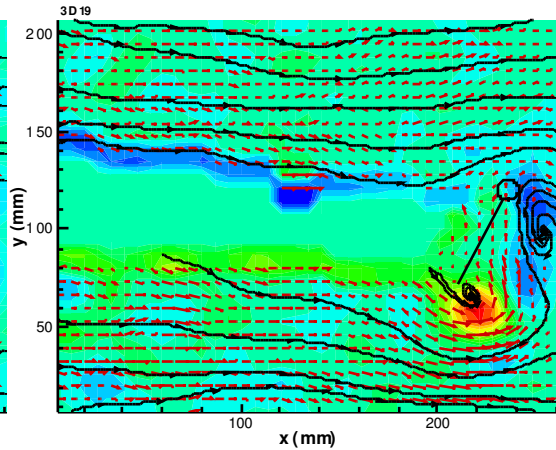
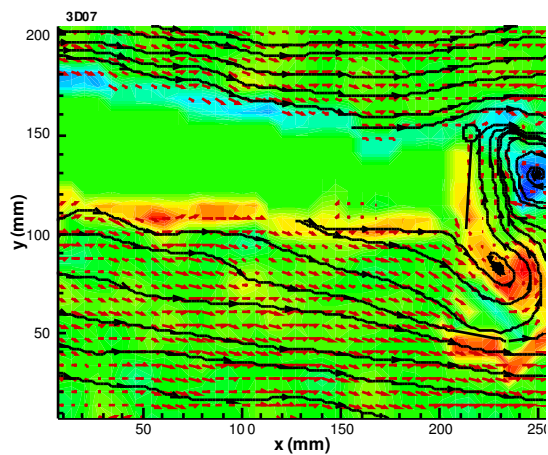
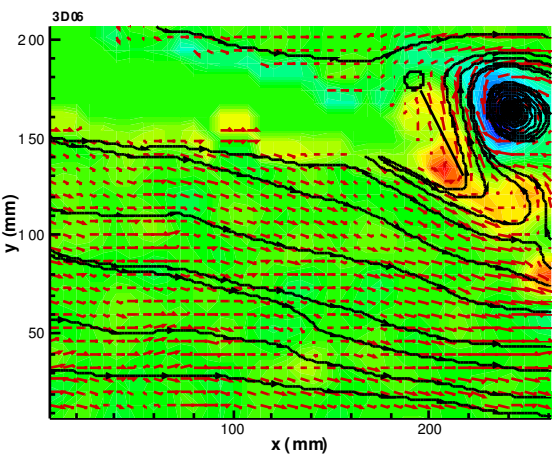


Figure 51(f)

As the wing passes through the condition approximately 90° nose-up compared to the level flight condition, the flow smooths out as the wing effectively moves downstream, travelling at approximately three times the freestream velocity. As the wing begins to pitch up into the flow, the flow initially remains attached to the wing (Figure 51(f)).

**Figure 51(g)****Figure 51(h)**

Flow separation at the leading-edge takes place at the same time as the formation of a trailing-edge clockwise vortex as the aircraft approaches something equivalent to a steep climbing attitude. Simultaneously, a smaller vortex in the opposite sense forms above the trailing edge.

**Figure 51(i)****Figure 51(j)**

As the aircraft passes through the level flight attitude, the clockwise vortex has now detached itself from the trailing-edge; meanwhile, the anti-clockwise vortex created above the leading edge is growing rapidly and appears to move along the upper surface of the aerofoil towards the trailing edge as the wing continues its nose-down rotation.

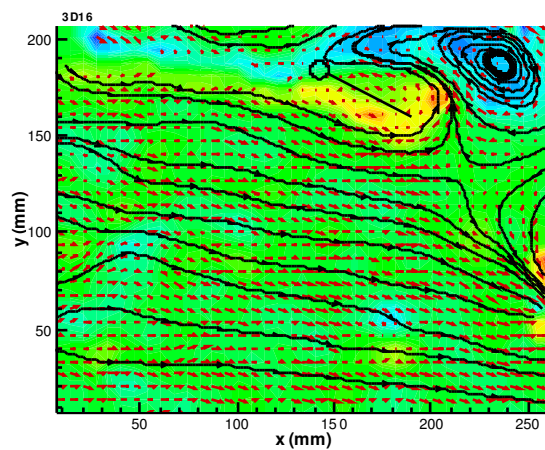


Figure 51(k)

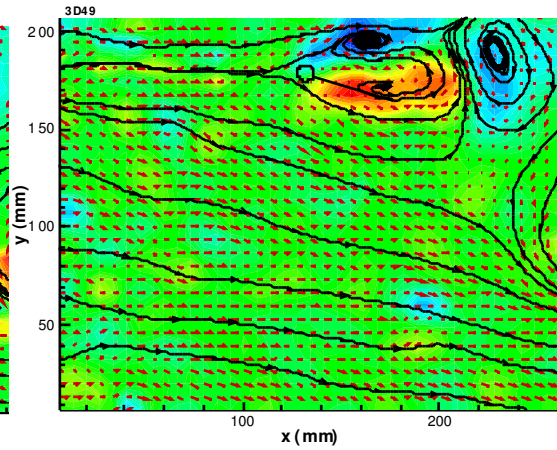


Figure 51(l)

As the aircraft approaches an attitude approximately 90° nose-down from the level flight attitude, the suction force at the trailing edge of the wing is still present as the aerofoil moves forward into the free-stream. Figure 51(l) shows classical von Kármán vortex shedding [101], as the inflow sweeps the alternating clockwise and anti-clockwise vortices downstream.

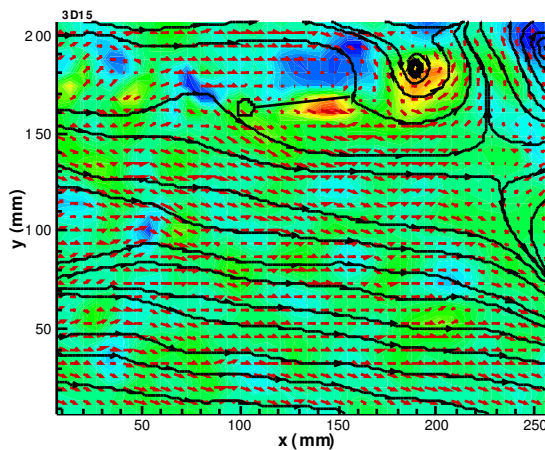


Figure 51(m)

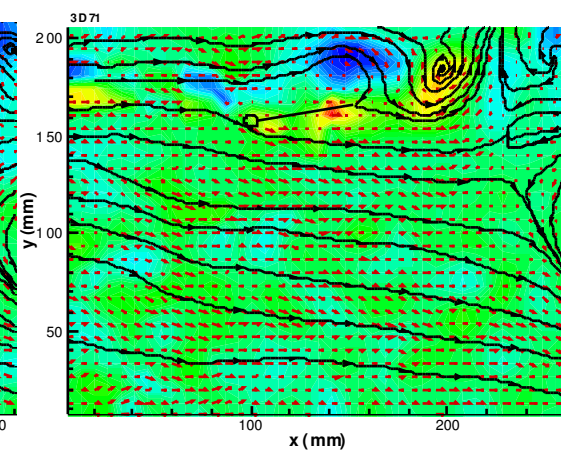


Figure 51(n)

The remains of the vortex shedding are still visible in Figure 51(m) as the flow becomes steadier via Figure 51(n), returning to smoother flow of the initial image for the rotation Figure 51(a).

5.6 Discussion, induced inflow and vortex generation during the tumble entry.

Since all experience is that the tumble is not survivable, and the level of maturity of knowledge of this mode is insufficient to discuss recoveries, the most important phase of the tumble must in current analysis be the entry. This will occur during initial nose-down rotation through (although not commencing at) the level flight attitude. The analysis above, shows two views of the aerodynamics at this phase in an initial nose-down pitching motion.

Figure 40 indicates that it is only for a short period around approximately 45° either side of the level flight attitude that the net force acts from the lower to upper surface of the wing; throughout the rest of the tumble cycle, the net force acts strongly from the upper to lower surface (nominally towards the aircraft CG).

Considering in addition to this the wind tunnel results, **Figure 49** and Figure 51(k) show formation of a large vortex that has moved to the trailing edge, with a diameter similar to that of the wing chord, and direction of rotation opposite to that of the wing. This vortex will create a large nose-down pitching moment during the phase of the tumble around the level flight attitude.

Therefore, it may be deduced that during the phase of the tumble (or tumble entry) between that corresponding to a steep climb and that corresponding to a steep dive, whilst the wing is subject to an aerodynamic force acting from the lower to the upper surface, there is also a large nose-down pitching moment sustaining the tumble. At all other phases of the tumble motion, the wing is subject to a force from the upper to lower surface, nominally towards the aircraft CG and thus also tending to sustain the tumble. This would be consistent with a continuation of the tumble after initial entry (which the evidence of accident reports supports), and with an increase in pitch rate

between around 45° nose-up and 45° nose-down relative to the normal level flight attitude. This is supported by **Figure 61** following).

It is therefore concluded that the most critical part of the tumble, and in particular the tumble entry, is that phase of nose-down rotation about 60° either side of the level flight attitude, and that all efforts towards avoiding the tumble entry (or should future work progress to this, recovery from the established tumble) should concentrate upon avoidance of rapid nose-down rotation at these pitch attitudes.

5.7 Discussion – behaviour of the aircraft during the sustained tumble.

Considering the evidence above in sections 5.4 and 5.6, both indicate that the forces acting upon the wing are not steady. The limited analysis in 5.4 shows a maximum force likely to act upon the wing between attitudes equivalent to 45° nose-up from the level flight attitude, to approximately 90° nose-down from the level flight attitude. Wind tunnel results given in 5.6 indicate that the wing is likely to also experience a large nose-down pitching moment during the first part of this phase. Therefore it is to be expected that the aircraft will display a pro-tumble acceleration (that is downwards, and also nose-down in pitch) during that part of the cycle. It will be seen in **Figure 61** following, that this is the observed behaviour, with the pitch rate peaking around this part of the tumble cycle, and reaching a minimum about 180° later (when the aircraft is inverted, and the analysis and test results from 5.4 and 5.6 above show much an effective angle of attack close to zero, and only very short term vortex formation).

5.8 Avoiding the tumble.

The analysis above indicates that a tumble can potentially occur if the aircraft enters a flight condition where the nose-down pitching moment due to the weight of the trike is greater than that of the pitching moment of the wing, locking the trike to the wing and thereby forcing the entire aircraft to pitch nose-down as a rigid body. This may be entered initially with the aid of

engine thrust, creating this situation when thrust is lost either deliberately (through throttle closure) or inadvertently (through engine failure). Alternatively the aircraft may if inverted also be in a position where the trike may “fall” towards the wing, leading it’s motion, creating a similar effect if the motion of the trike has a significant pitching component.

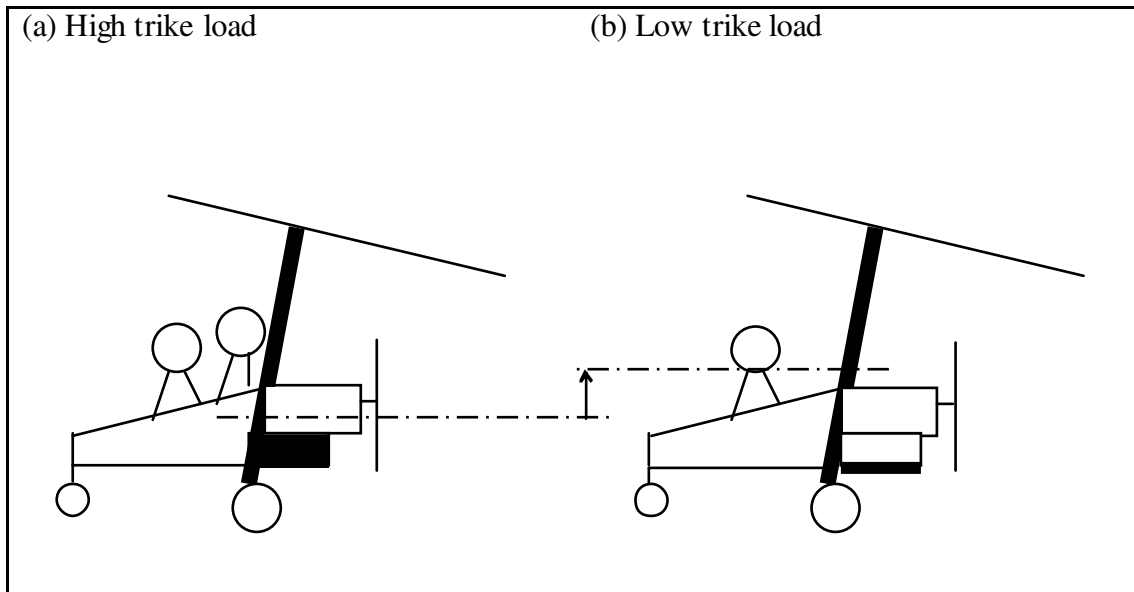
Using the simple model of the trike longitudinal stability given above, added to the aerodynamic characteristics of the trike, it becomes possible to predict the conditions at which the tumble might occur. It should be borne in mind that the tumble might not necessarily occur, since the rate of pitching must be sufficient to cause the inverse camber and upper surface vortex on the wing that is associated with the sustained tumble.

From this analysis, the tumble appears to be a function of both the wing and trike characteristics. A trike with a long monopole for example, will have a greater pitching moment at a steep nose-up attitude, and therefore a greater tendency to tumble.

5.9 Effect of aircraft mass upon the tumble.

It is known from the history of tumble accidents, that the more highly loaded the trike is, the less the aircraft will tend to tumble. At first sight of the graphs above, this does not make sense. However once the nose-down pitch departure occurs, a more lightly loaded trike will result in a whole-aircraft CG closer to the wing, and thus a greater angle of inflow into the wing – this is illustrated below. So, at a lower trike mass, the induced camber at the wing will be greater since the point of rotation will be closer to the wing. Also at lower trike mass, the rotational inertia in pitch will be less.

Figure 52. Illustrating the shift in vertical CG with passenger and fuel loading changes.



Taking an aircraft with a wing mass of 50 kg, trike mass 150kg, and distance between CGs, 1.5m; the total rotational inertia therefore is 87.5 kg.m² and the wing is 1m from the aircraft CG. If however the same aircraft has an increased trike mass of 300kg, then the rotational inertia is 96.5 kg.m² and the wing is 1.3m from the aircraft CG. Thus, with the same pitching moment applied, and disregarding aerodynamic damping (which at present, data does not exist to quantify); if a net nose-down pitching moment of 500 Nm is assumed, the following simple analysis may be carried out.

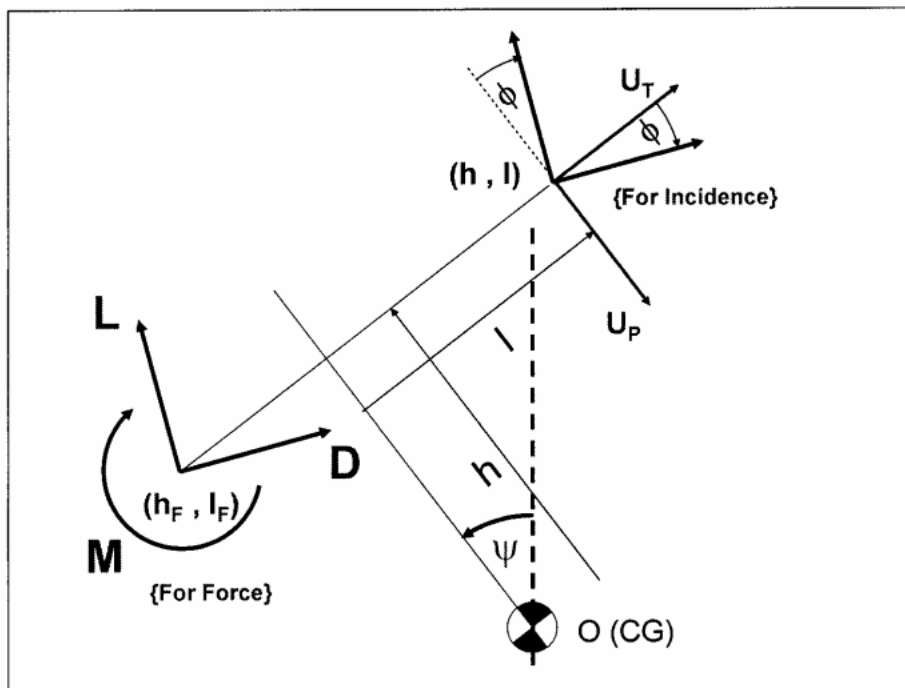
Table 14. Effect of trike mass upon inflow angle for constant pitching moment

	<u>Lighter aircraft</u>	<u>Heavier aircraft</u>
Total rotational inertia	87.5kg.m ²	96.5 kg.m ²
Rotational acceleration, assuming 500 Nm nose-down pitching moment and no aerodynamic damping,	5.73 rad/s/s	5.18 rad/s/s
Resultant rotational velocity after 1 second, α	328 °/s	296 °/s
Downward velocity of nose, assuming it is a nominal 1 m in front of the hangpoint.	9.38 m/s	7.23 m/s
Nominal aircraft stalling speed at this weight $\approx V_{so} \sqrt{\frac{MTOW}{W}}$	15 m/s	18 m/s
Approximate angle of resultant flow, at wing leading edge, at stalling speed	32°	21°

It is thus demonstrated that a reduced trike weight will result in a significantly greater induced camber following an aircraft stall at a high nose-up attitude. Therefore, the risk of the sustained tumble occurring, following a nose-up stall, is considerably greater.

5.10 A simple model of the tumble equations of motion

Figure 53. Co-ordinate system for tumbling aircraft

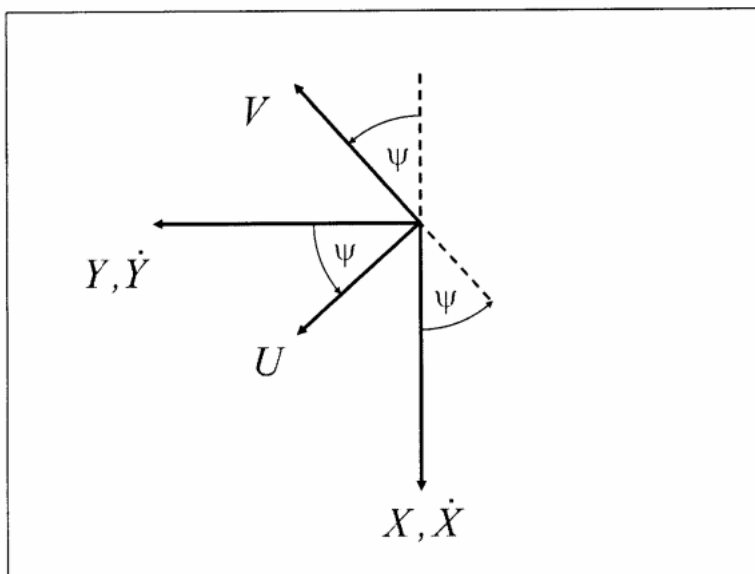


Notes

h_f, l_f , define points on wing at which net force acts.

h, l , define points on wing at which effective incidence (as defining aerodynamic loads on wing) occur.

Figure 54. Defining motion of the wing



Incident velocities due to CG translation may be written as:-

$$\begin{aligned} U &= \dot{X} \sin \psi + \dot{Y} \cos \psi \\ V &= -\dot{X} \cos \psi + \dot{Y} \sin \psi \end{aligned} \quad (5-12)$$

Whilst incident velocities due to CG rotation may be written as:-

$$\begin{aligned} \Delta U &= h \dot{\psi} \\ \Delta V &= l \dot{\psi} \end{aligned} \quad (5-13)$$

Combining these components,

$$\begin{aligned} U_T &= U + \Delta U \\ &= \dot{X} \sin \psi + \dot{Y} \cos \psi + h \dot{\psi} \end{aligned} \quad (5-14)$$

And:

$$\begin{aligned} U_P &= V + \Delta V \\ &= -\dot{X} \cos \psi + \dot{Y} \sin \psi + l \dot{\psi} \end{aligned} \quad (5-15)$$

From **Figure 53** the inflow angle ϕ is given by:

$$\phi = \tan^{-1} \left(\frac{U_P}{U_T} \right) \quad (5-16)$$

Now consider the vertical and horizontal motion of the wing; resolving vertically:-

$$m\ddot{X} = mg - L \cos(\psi - \phi) - D \sin(\psi - \phi) \quad (5-17)$$

Whilst resolving horizontally:-

$$m\ddot{Y} = L \sin(\psi - \phi) - D \cos(\psi - \phi) \quad (5-18)$$

Now, taking clockwise moments about the aircraft CG (and introducing the term k , to describe radius of gyration):

$$\begin{aligned}
 mk^2 \ddot{\psi} &= -M \\
 &+ L \cdot (l_F \cos \phi - h_F \sin \phi) \\
 &- D \cdot (h_F \cos \phi + l_F \sin \phi)
 \end{aligned} \tag{5-19}$$

Combining velocity components gives:

$$\bar{V}^2 = U_T^2 + U_P^2 \tag{5-20}$$

Lift, Drag and Pitching Moment are given by:

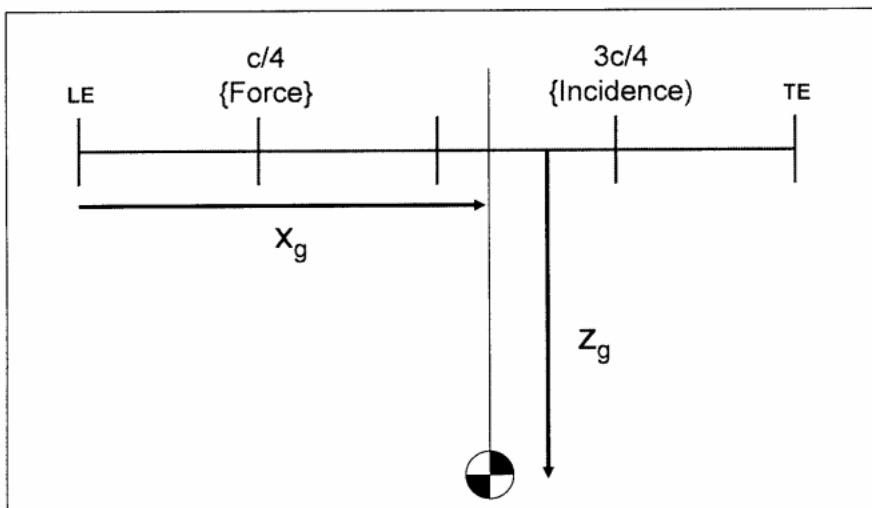
$$\begin{bmatrix} L \\ D \\ M \end{bmatrix} = \frac{1}{2} \rho \bar{V}^2 \cdot S \cdot \begin{bmatrix} C_L \\ C_{D0} \\ c \cdot C_M \end{bmatrix} \tag{5-21}$$

The pitch damping is given by the standard result:

$$C_M = \frac{c\pi}{8\bar{V}} \dot{\psi} \tag{5-22}$$

To ease the data input, the wing coordinate system is shown in Figure 3. The coordinates used in equations of motion are derived in (12).

Figure 55. Coordinate System in Wing



From these coordinates, we have the following results:

$$\begin{aligned}l &= \frac{3c}{4} - x_g \\h &= z_g \\l_F &= \frac{c}{4} - x_g \\h_F &= z_g\end{aligned}\tag{5-24}$$

Now considering the behaviour over a finite period of time, Δt :-

$$\begin{aligned}\Delta X &= \dot{X} \cdot \Delta t + \frac{1}{2} \ddot{X} \cdot \Delta t^2 \\ \Delta Y &= \dot{Y} \cdot \Delta t + \frac{1}{2} \ddot{Y} \cdot \Delta t^2 \\ \Delta \psi &= \dot{\psi} \cdot \Delta t + \frac{1}{2} \ddot{\psi} \cdot \Delta t^2 \\ \Delta \dot{X} &= \ddot{X} \cdot \Delta t \\ \Delta \dot{Y} &= \ddot{Y} \cdot \Delta t \\ \Delta \dot{\psi} &= \ddot{\psi} \cdot \Delta t\end{aligned}\tag{5-25}$$

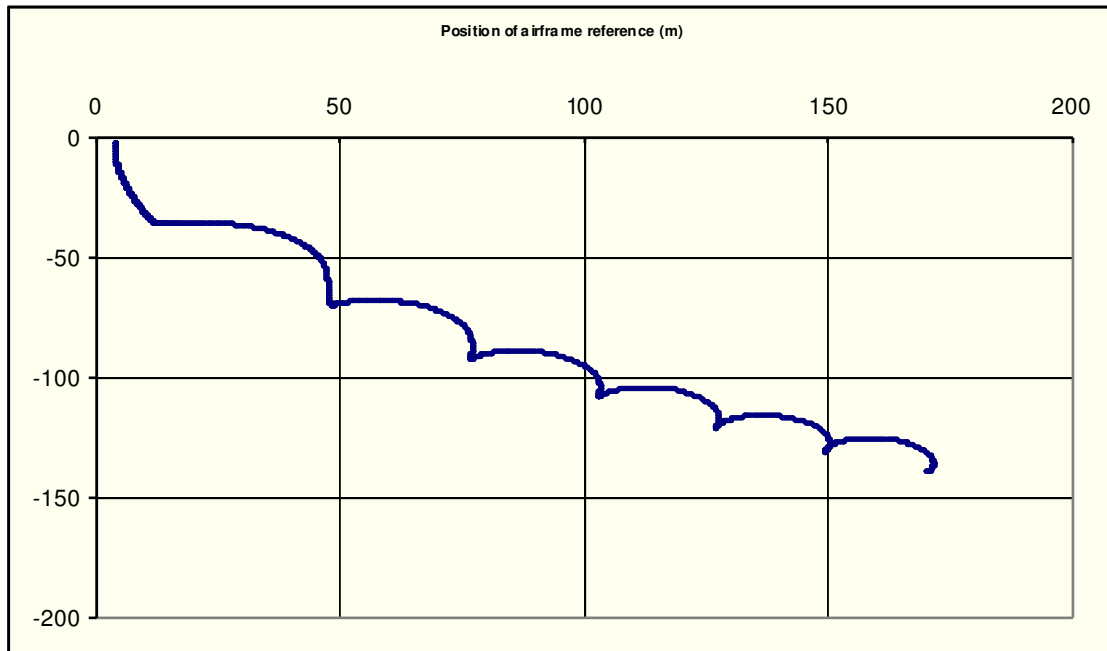
Using a tool such Microsoft Excel, this may then be used to generate an illustration of the motion of the aircraft during the developed tumble. This will not offer a reliable prediction of the aircraft's motion during the tumble, but does allow the aircraft's behaviour, as a function of the various input parameters to be considered generally. For example, if a sample set of aircraft characteristics are input as shown in **Table 15** below:-

Table 15. Characteristics of typical aircraft

M = 300kg
Radius of gyration = 1.5m
Wing area = 15 m ²
Chord = 1.5m
$\frac{\partial C_L}{\partial \alpha} = 5.8$ per radian
C _{Do} = 0.5
X _{CG} = 0.5
Z _{CG} = 0.5
h = 0.5
l = 0.625
h _F = 0.5m
l _F = -0.325m

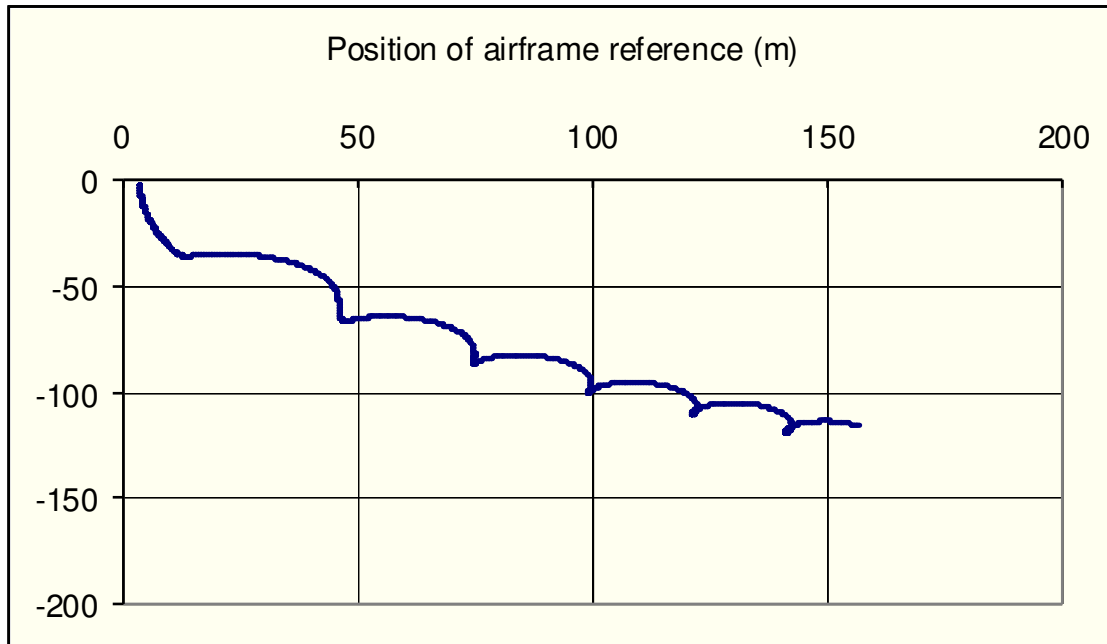
Then the motion of a nominal reference point (at position X=5m, Z=0) on the body of the aircraft may be represented by a diagram such as that shown in

Figure 56. Illustration of tumble motion, X_{CG}=0.5m



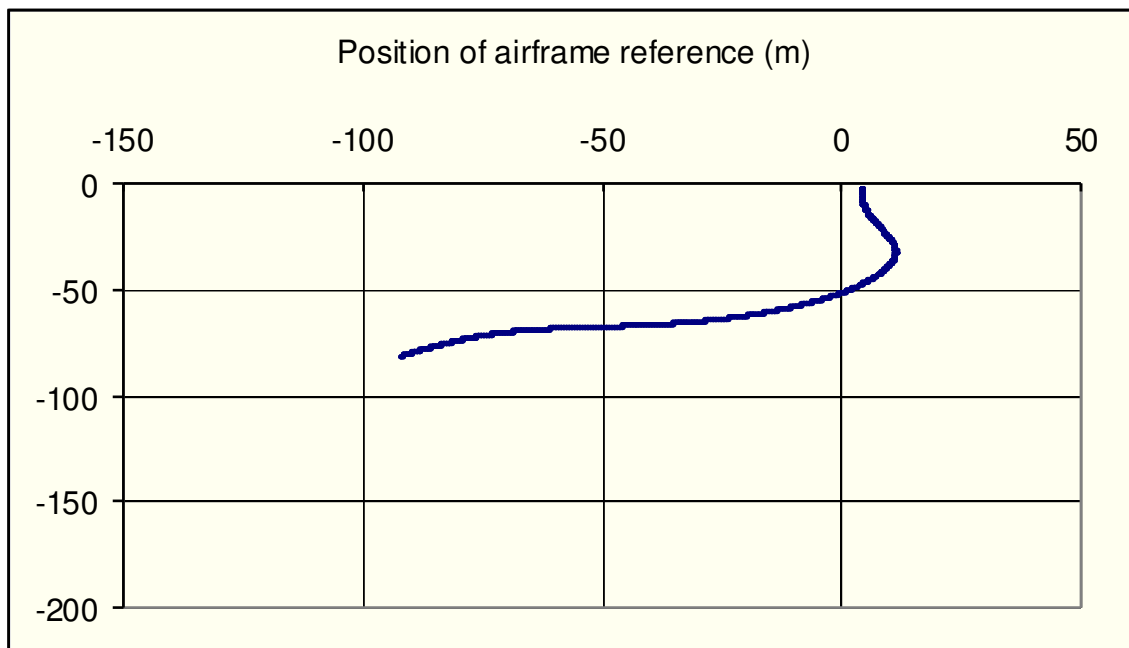
Yet by changing, for example, the value of X_{CG} from 0.5m to 0.7m (that is, moving the CG further forward on the aircraft), the result may be modified to that shown in **Figure 57**.

Figure 57, Illustration of tumble motion, $X_{CG}=0.7m$



This is a very similar result; however, if the CG is instead moved a similar distance rearwards, to a position $X_{CG}=0.3m$, then the behaviour is markedly different, as shown in

Figure 58. Illustration of tumble motion, $X_{CG}=0.3m$

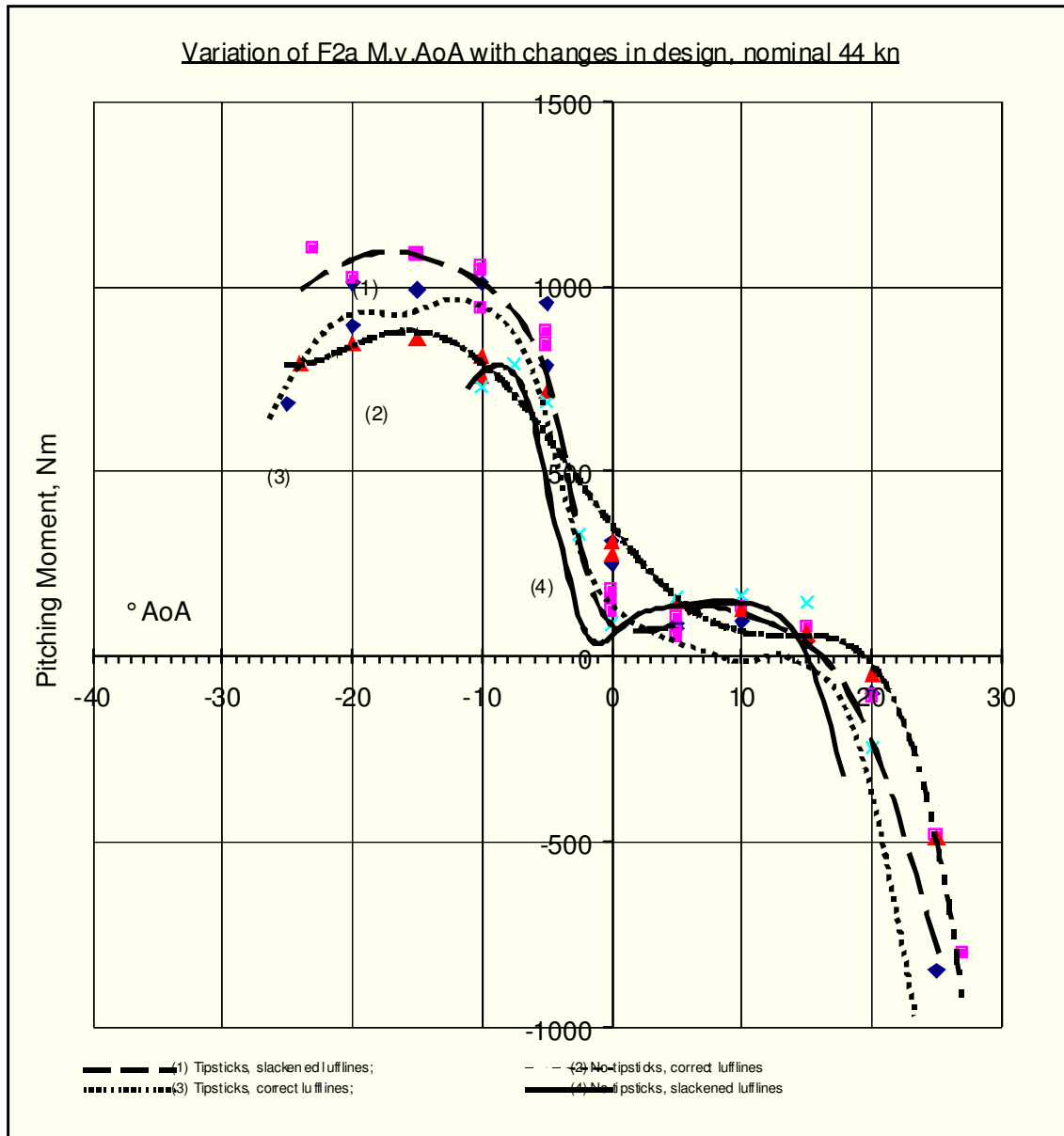


This is sufficient to illustrate that the tumble behaviour is a function of the longitudinal CG position of the aircraft. It would be appropriate for future wind tunnel or free-flight model testing to be planned using this tool, so as to identify those design variables which are potentially of greatest interest.

5.11 Effect of wing settings.

There is anecdotal evidence (although no formal record since wing settings are not normally recorded, and very hard to determine after an accident has occurred) to suggest that a mis-rigged wing, particularly one in which the luffline tension is insufficient, will display a greater tendency to tumble. The **Figure 59** below shows 4 curves for the Mainair Flash 2a (See above) wing already discussed, at a variety of conditions.

Figure 59. Effect of different rigging conditions upon Mainair Flash 2 alpha wing



These plots vary in three ways:-

The wings with insufficient luffline tension display a flat curve (indicating very low apparent longitudinal static stability) around the trimmed condition.

Without either tipsticks or correct luffline tension, the wing displays a pitch stability minimum about zero AoA. It is believed, from previous work by Kilkenny [102] on hang-glider stability and from discussions with microlight

wing designers, that this is related to the luffing dive (a mode of flight where unsatisfactory longitudinal stability characteristics cause a constant speed or accelerating descent which may be unrecoverable) and not to the tumble. Specifically, if this condition is achieved then because the $C_M:\alpha$ curve is at a minimum, the aircraft will remain at a stable angle of attack unless a sufficiently large pitching moment can be applied to move the angle of attack to above the maximum (seen in the plot above at about 10°). Given the low angle of attack, the aircraft will tend to descend (due to lack of lift) and either continuously accelerate or stabilise at a relatively high speed – which unless recovery actions are taken (probably by use of violent rolling manoeuvres) are likely to continue until impact with the ground.

Whilst all such wings may display an apparent tendency towards a nose down pitching moment at very low angles of attack (well below anything likely to be experienced within the permitted manoeuvre envelope) this is at a higher angle of attack for a wing without tipsticks and with incorrect luffline tension. [The lack of data at lower angles of attack than is shown in the graph is due to a physical limitation of the BHPA test rig; the only other known facility in the world (located in Germany) is of similar design and thus at present there is no means of determining exactly what happens at these angles of attack).

This last characteristic is considered significant to tumble initiation. It is only possible, due to the difficulty in obtaining either experimental data or a combined aerodynamic and aeroelastic model of such a wing, to postulate as to exactly what happens to the forces and moments acting upon the wing during the initial pitch down of tumble initiation. However, it is a reasonable assumption that the mis-rigged wing shown in curve (4) of **Figure 59** above, will show a greater tendency to pitch down as the reduction in AoA occurs than does the correctly rigged wing (irrespective of any induced reverse camber). In surveying these plots, it appears that correct luffline tension is important in preventing the tumble, but the presence of tipsticks provides a valuable backup – if luffline tension ceases to be correct, then the tipsticks appear likely to maintain a large margin between the normal cruise condition and the normal flying range of positive angles of attack. The graph above

gives reasonable grounds to believe that pitch stability reversal will occur at angles of attack less than -20° , which previous analysis indicates might potentially occur with sufficient mishandling in a lightweight aircraft.

5.12 Initiation of the tumble.

The description of the tumble initiation above shows that for the tumble to occur, it is most likely that the aircraft will be steeply nose-up with a low throttle setting or failed engine. There are several ways in which this might occur, which are discussed below.

5.13 First proposed mechanism, the whip-stall.

The whip-stall is an aggressive entry to the aerodynamic stall (at a high deceleration rate, well in excess of the 1kn/s normally recommended), followed by an equally aggressive recovery initiation by the pilot (pulling in the control bar rapidly). This is a manoeuvre which may be used by test pilots (with great care) to allow them to demonstrate V_{NE} or V_{DF} in this class of aircraft[**103**], which are otherwise control limited and unable to demonstrate high speed flight for certification purposes. However, there is absolutely no need for a pilot, other than a test pilot in the course of their duties, to ever carry out this manoeuvre in normal flight; the whip-stall is specifically prohibited by all microlight manufacturers, and by the UK pilot training syllabus[**104**]. It is considered likely (and several eyewitness reports of fatal accidents bear this out - most recently the October 2000 fatality to a Pegasus Quantum [**86**]) that this mechanism can lead to the tumble.

The sequence of actions in the whip stall is detailed below.

- The pilot places the aircraft in a climbing attitude, and pushes the control bar out rapidly to achieve a high deceleration rate. At the steepest possible nose-up attitude, the throttle is closed.

- The airspeed decreases rapidly, with nose-up rotational inertia pitching the aircraft nose-up past the normal AoA than would normally be expected for the stall, associated loss of airspeed will also occur. As a consequence, the aircraft will reach a state where the AoA is greater and the airspeed lower than would normally be expected at the stall. This point, when the maximum nose-up attitude is reached is the stall as perceived by the pilot.
- At the point of stall, the wings aerodynamic pitching moment becomes strongly nose down. Due to the low airspeed, this is likely to be less than if the stalling angle of attack is reached in a less dynamic manoeuvre.
- The trike, which had been held in a steep nose-up attitude by thrust, pitches down and pushes against the wing (front strut against basebar) creating a rigid system upon which a net nose-down pitching moment is acting.
- The aircraft is then rotating nose-downwards, with the entire system rotating about the whole aircraft CG (rather than the wing alone rotating about the hangpoint). This can initiate the tumble, as previously discussed.

5.14 Second proposed mechanism, Spiral instability combined with loss of visual horizon.

Weightshift Microlight aircraft are approved in all countries of which the author has knowledge only for flight in Visual Meteorological Conditions (VMC). This implies a guaranteed visual horizon which the pilot may use as a reference when correcting small rolling departures (such as may be caused by temporary inattention, or by turbulence). However, it is possible through ill-luck or poor judgement for an aircraft to enter Instrument Meteorological Conditions (IMC), where a defined horizon cannot be guaranteed (most commonly by entering cloud). If this happens, any pilot will attempt to

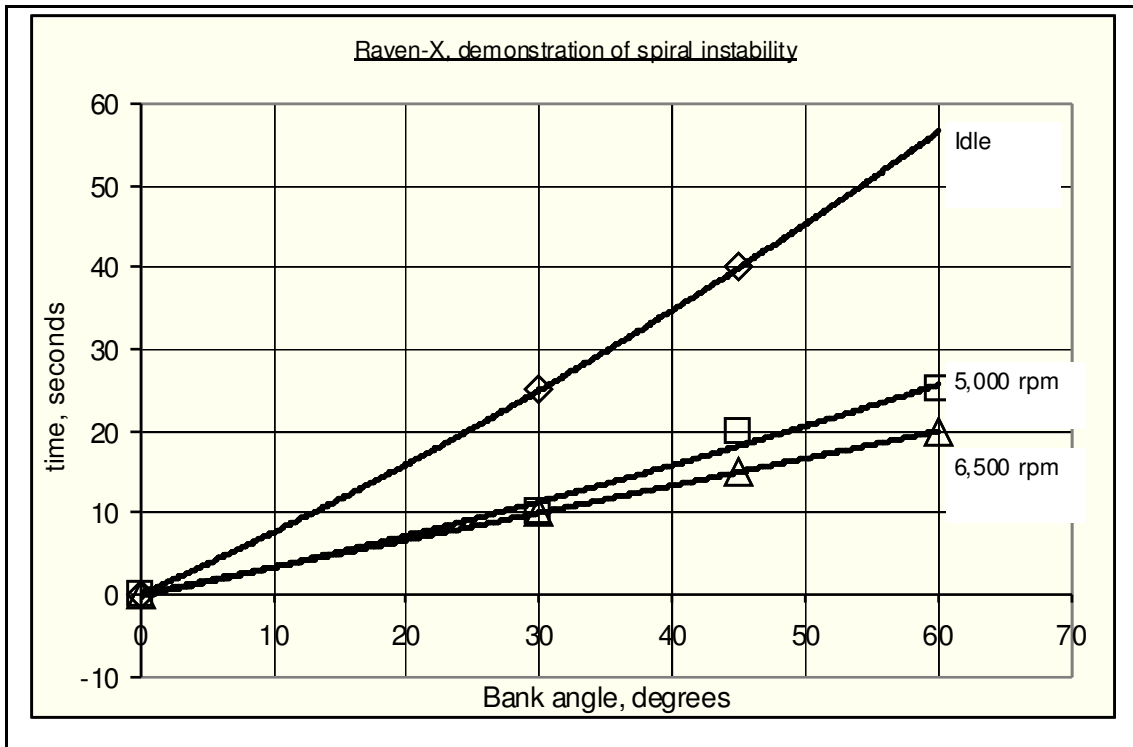
remove the aircraft from this condition as quickly as possible; however, if the pilot is unable to extract themselves from this situation it is almost inevitable that some cause (most likely the turbulence commonly found inside or near to most clouds) will initiate an undemanded rolling manoeuvre. Unlike most conventional fixed wing aeroplanes, many weightshift microlight aircraft are spirally unstable (particularly at higher power settings); thus, an initial small bank angle is likely to increase without (unless a horizon reference is available) the pilot's knowledge or ability to control it. The aircraft would then enter a divergent rolling manoeuvre, potentially through 90° of bank to a condition where the pendulum stability which keeps the trike below the wing will cease to act, and the wing angle of attack will reverse sense – inevitably causing some loss of control. It is then possible that the aircraft will find itself in an unsustainably steep nose-up attitude. It is noticeable that some tumble accident reports, particularly that to G-M VEP [87], have occurred in conditions where the horizon was known to be poor, and where the subsequent damage to the aircraft showed that the basebar had fractured (in contact with the front strut) at the end. This implies a rolling component to the departure from controlled flight, which would be consistent with this mechanism.

Table 16 shows the results of a brief test carried out to demonstrate the spiral instability of a weightshift aircraft. A Raven-X weightshift microlight (the actual aircraft used is shown in **Figure 96**), flown solo was trimmed in moderately turbulent conditions and the controls released. The resultant bank angle was estimated based upon a visual horizon and the time to reach given bank angles. This demonstrates that following flight into IMC such a departure could readily happen within 60 seconds (obviously, the presence of spiral instability will vary between aircraft types, and with power setting).

Table 16. Results of test to demonstrate weightshift spiral instability

Aircraft: Southdown Raven-X (Rotax 447 engine) + 60" 3-blade Ivoprop propeller @ 9° pitch (Propeller approved by MAAN 1076)			
Registration: G-MNKZ			
Crew: Gratton (solo)			
Conditions: CAVOK, light turbulence, nil Wx, OAT +5°C, No.3 from front hangpoint setting giving 48 mph IAS trim.			
Date: 13 Feb 2001			
Test: Aircraft flown in light but perceptible turbulence over woodland, nominal 1000ft on QFE 1024 hPa			
<u>Results:</u>			
<u>Power</u>	<u>Time at 30° bank</u>	<u>Time at 45° bank</u>	<u>Time at 60° bank</u>
3000 rpm (Flt Idle)	25 seconds	40 seconds	Test abandoned due to ground proximity
5000 rpm (PLF)	10 seconds	20 seconds	25 seconds
6,500 rpm (MCP)	10 seconds	15 seconds	20 seconds

Figure 60. Illustration of spiral instability as a function of engine power: Raven-X



In the case of G-MVEP referred to above, it would in light of this be a reasonable deduction that having lost the visual horizon the pilot (who was still under training) might have rolled beyond permissible limits in under 60 seconds.

A further comment may be made concerning the results above. This is that given that aircraft in this class appear to show the greatest spiral stability at low power settings, pilots should be taught, in the event of inadvertent flight into IMC, to descend out of it in idle power where possible, rather than attempting to climb out or maintain level flight.

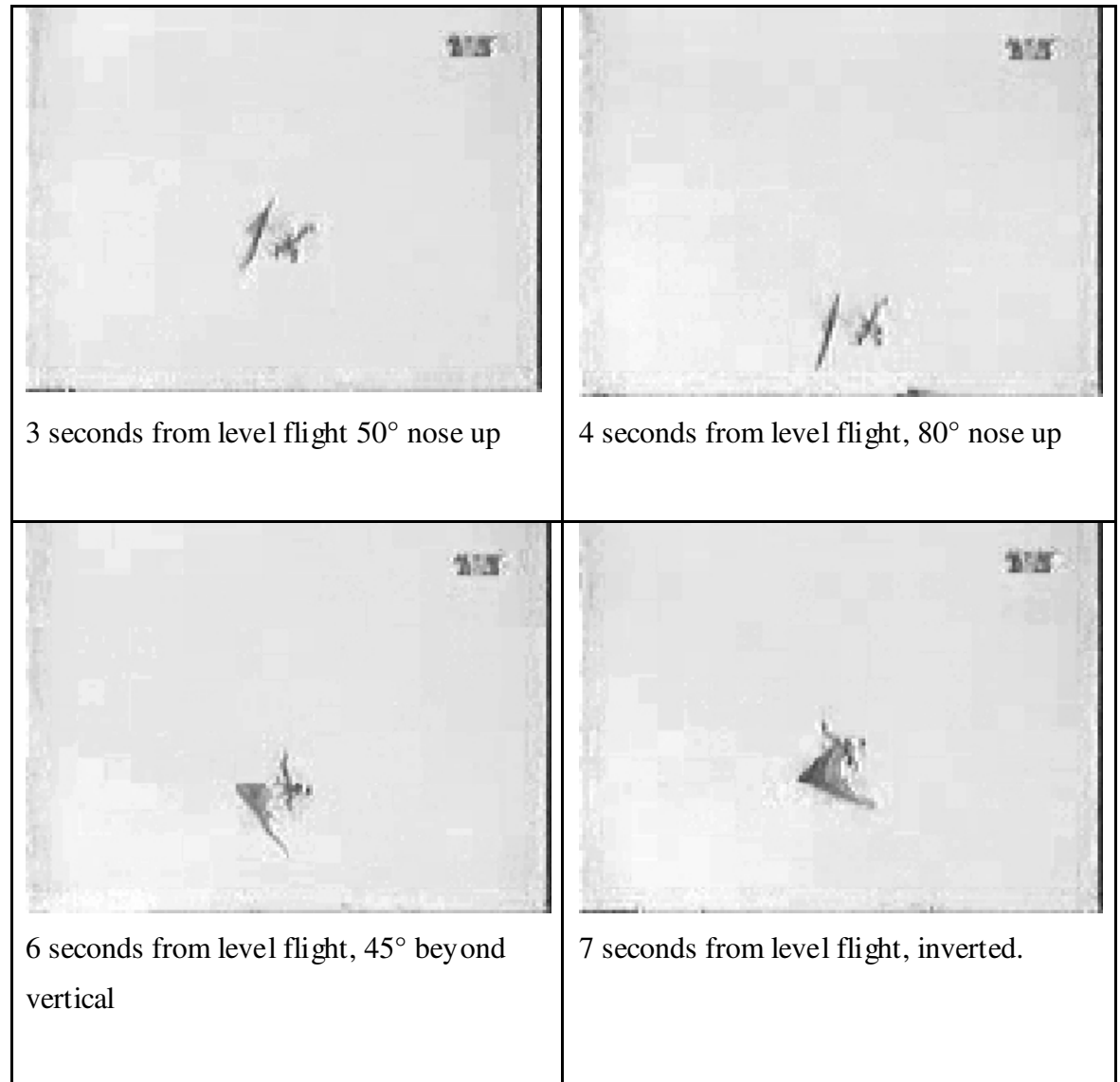
5.15 Third proposed mechanism – failed loop manoeuvre.

Whilst weightshift microlight aircraft are neither approved, nor should be, for aerobatics, it is occasionally known for a pilot to attempt aerobatic manoeuvres. There are several reported instances of pilots attempting to conduct a loop in such an aircraft. If positive normal acceleration is maintained throughout this manoeuvre then it can be executed as safely as in

any other aircraft. However, as with any other aircraft, if the aircraft runs out of kinetic energy near to the top of the loop, then the pilot will find themselves inverted without sufficient airspeed to complete the manoeuvre. In this case, the inevitable consequence will be a negative angle of attack, leading to a tumble. **Figure 61** shows a sequence of frames from the film taken of a French Cosmos aircraft. The aircraft was flying an air display sequence that included a loop, which failed. The result was a tumble resulting in the aircraft's destruction and death of the pilot on collision with the ground.

Figure 61. Illustration of a fatal tumble after a failed loop

Note: The origin of this piece of video is not entirely clear. It is believed to have been taken at an airshow in Europe, the aircraft being identifiable as a French “Cosmos” type. The exact date, location and source cannot be verified.





8 seconds from level flight, inverted with nose approximately 45° below the horizon. At this point the “nose-up” (in aircraft axes) motion pauses.




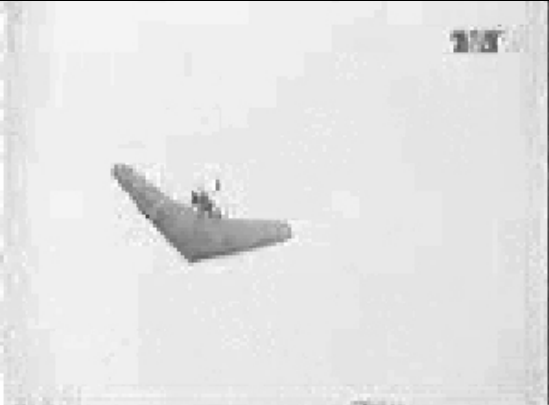




9 seconds from level flight, pitch rotation has reversed and the aircraft has rotated “nose down” (in aircraft axes) back to inverted.








$9\frac{1}{2}$ seconds from level flight, the wing is continuing to pitch “nose-down”, note that the trike can be seen to be very “nose down” compared to the wing. It is likely that the front strut or basebar has failed at this point.



10 seconds from level flight, the wing is now pointed almost straight upwards.

	
<p>10 $\frac{1}{3}$ seconds from level flight, the aircraft passes through a level attitude. It can be seen that the pitch rate between this frame and the previous is over 400°/s</p>	<p>10 $\frac{2}{3}$ seconds from level flight, the aircraft is now pointed downwards. Pitch rate must at this point be 200 - 300°/s</p>
	
<p>11 seconds from level flight, the aircraft passes through inverted.</p>	<p>11 $\frac{1}{3}$ seconds from level flight, 45° nose down.</p>
	
<p>11 $\frac{2}{3}$ seconds from level flight, the trike is very nose down compared to the wing - also there is considerable wing distortion.</p>	<p>12 seconds from level flight, inverted. Pitch rate appears to be slowing, note very large washout at tips. This may indicate tip failure.</p>

	
<p>12 $\frac{1}{3}$ seconds from level flight, passing through a level attitude.</p>	<p>12 $\frac{2}{3}$ seconds from level flight, aircraft is pointed downwards. Wing planform can be seen still intact.</p>
	
<p>13 seconds from level flight, passing through a level attitude.</p>	<p>13 $\frac{1}{2}$ seconds from level flight, passing through a vertical nose-down attitude.</p>
	<p>14 $\frac{1}{2}$ seconds from level flight, impact with the ground.</p>

5.16 Fourth proposed mechanism, flight through own wake vortex.

It is well known that a minimum safe separation should be ensured between landing aircraft, particularly behind larger aircraft which tend to generate very large vortex wakes that can normally be expected to remain for up to 80 seconds [105, 106] in normal conditions, rather longer in very still air. The

weightshift microlight using, as it does, a delta wing tends to generate a particularly large wake vortex for the size of the aircraft capable of generating considerable upset [107]. For this reason, pilots of weightshift aircraft are taught that level turns should never be continued beyond 270° and preferably not beyond 180° without climbing or descending during the turn.

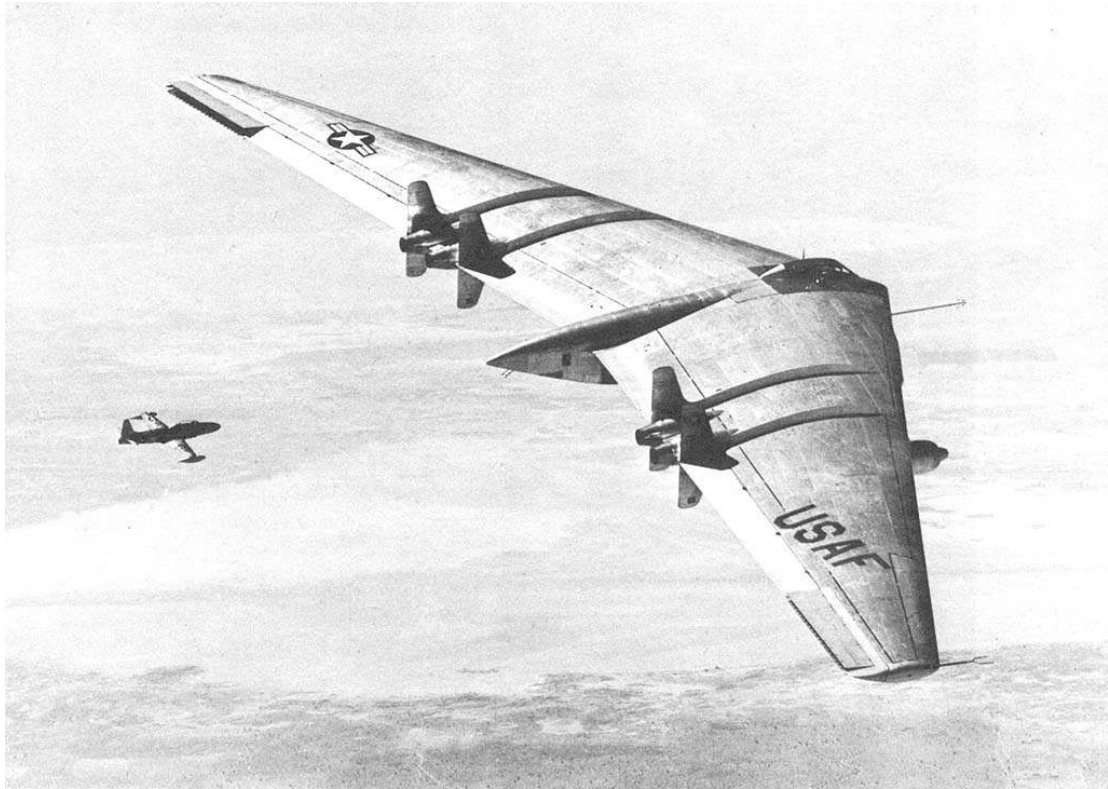
Considering a typical turning manoeuvre at 45 kn CAS, 60° bank, 2000ft it can be shown that the turn rate will be 40°/s. Hence, if the pilot were to fly a continuous tight balanced turn, the aircraft's own wake vortex would be met in less than 9 seconds - scarcely time for the vortex to have significantly dispersed in even moderately disturbed airflow. It is known that aircraft flying through the wake vortex of another can suffer a large magnitude undemanded roll. It is then reasonable to assume that the same mechanism, as was described above, for a loss of visual horizon may also occur – although it is likely that the onset will be more rapid.

The fatal accident to G-MVDO in 1992 was considered by the AAIB investigation report [108] to have been a tumble and in-flight break-up following a pilot flying what were observed from the ground to have been extremely tight turns of 360° or more.

5.17 Historical note 1 – the Northrop YB-49 “Flying Wing Bomber”

During the 1940s and 1950s there was a great deal of interest in the development of flying wing aircraft, particularly in the USA for military purposes. One such aircraft was the Northrop YB-49 (**Figure 62**). Although attributed at that time primarily to inertia coupling, there are a number of notable incidents where these aircraft suffered a pitching departure from controlled flight.

Figure 62. Northrop YB-49 experimental flying wing bomber.



Photograph courtesy of Northrop Grumman Corporation

The following account is by a USAF Test Pilot working in 1948 upon evaluation of the YB-49 aircraft [109], and describes a pitching loss of control in this aircraft. The use of the word “tumble” is that selected by the Test Pilot at the time.

“23 February YB-49 #368 one landing local Muroc----- 0:35 mins.

Recommended no intentional stalls due to the fact that during the final phase of the stall entry maneuver it lurched over backwards into a tumble. Had to use asymmetric power to recover. Submitted a full report and thankful that the throttles were hanging down from the ceiling rather than in a normal position since G forces had my arms locked upwards and my rear off the seat. Flight test engineers told me later that I had encountered inertial coupling”

“the results of my one Stall Test during which the aircraft had assumed a very high angle of attack without a stall warning and then pitched over backwards.... The

rotation was severe and made it difficult to keep my hands and feet on the controls. The engineers called it a lateral roll but I was experiencing a tumble! I was lucky that the designers had put two throttles hanging down from the upper surfaces, each connected to four engines. I applied full power with the left throttle and resolved the "tumble" with asymmetric power and elevon control."

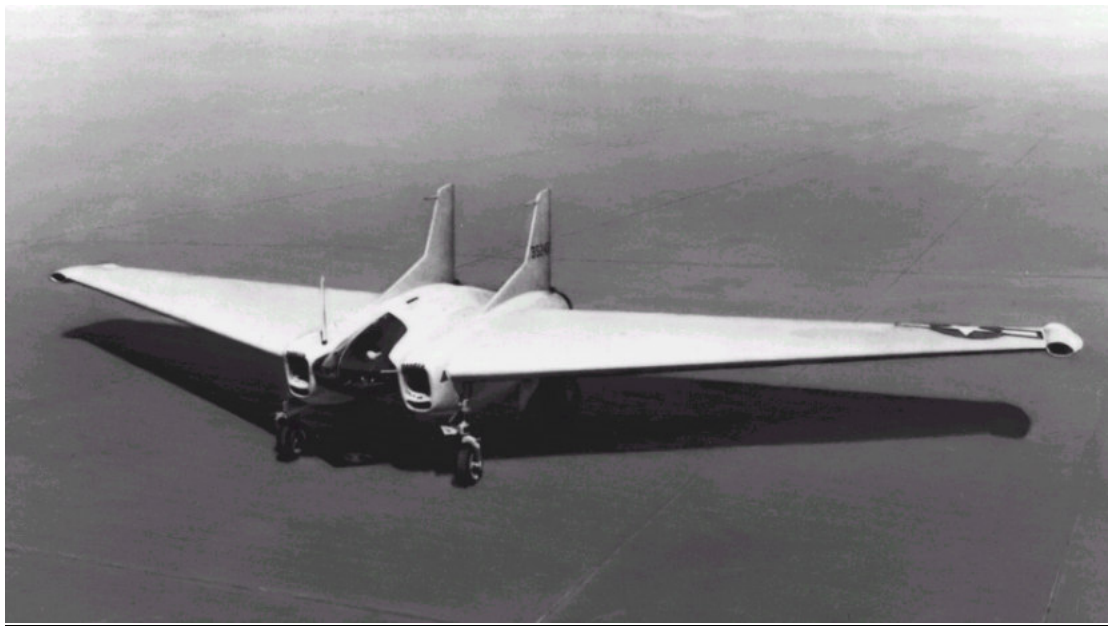
The aircraft was subsequently lost on 15 June 1948 whilst under the control of another Test Pilot and was destroyed killing all on board. Available reports indicate that the aircraft lost control in pitch at about 40,000ft[110], with the wingtips detaching from the airframe at a high altitude under loading which exceeded 4.8g[111]. The aircraft descended almost vertically, impacting inverted, whilst the wingtips were found several miles away. It is interesting to note that this is consistent with microlight tumble accidents, in that the departure from controlled flight was in pitch, descent was vertical from departure from controlled flight, and there was structural failure of the wingtips before impact with the ground. There are two obvious differences, which is that the aircraft had a CG which was within the airframe (rather than below), and that the rotation was nose-up (rather than nose-down). However, this only negates the mechanism described in 5.3 and 5.4 above and not the aerodynamics of the established tumble shown in 5.5 above; therefore, whilst it is not reasonable to assume a similar entry mechanism to that shown for a weightshift controlled microlight, there is no obvious reason why the aerodynamic characteristics that sustain this pitch autorotation are not similar in each case.

It is therefore indicated that the tumble as discussed in this section, and the tumble as described in the Test Pilot's account when describing loss of control in the Northrop YB-49, may well be closely related.

5.18 Historical Note 2, the Northrop XP-79 “Flying Ram” experimental fighter

A later experimental aircraft, also developed by Northrop, was the XP-79 (Figure 63), which was a tailless experimental fighter produced for the USAF. This aircraft was lost on its first flight on 12 September 1945. Very little information is available as to the reason why this aircraft was lost; however, it is known that the aircraft suffered a departure from controlled flight during which the pilot was subject to sufficient forces that he was unable to abandon the cockpit (where he was located in a “prone” position) before ground impact, causing loss of both the aircraft and pilot.

Figure 63, Northrop XP-79B "Flying Ram"



Photograph courtesy of Northrop Grumman Corporation

It is not known the specific nature of the departure from controlled flight that led to loss of the aircraft, and it is highly unlikely now that any new information will become available. However, it is again interesting to note that this is a further departure from controlled flight of a tailless delta winged aircraft, where high forces are likely to have been a significant factor. This *may* have been a tumbling departure, similar to that suffered by the YB-49.

5.19 Historical Note 3, The de Havilland DH108 “Swallow”

The de Havilland DH108 (Figure 64 below, also reference [112]) was a British research aircraft of which three examples were built, all in the late 1940s. The aircraft was a high performance tailless delta-winged aeroplane, designed specifically for research into the control of flying-wing aeroplanes, and into the transonic flight regime. All three of these aircraft were lost in fatal flight testing accidents.

Figure 64, de Havilland DH108 Swallow



Reproduced courtesy of 1000aircraftphotos.com

The first of these accidents [113, 114, 115], which was to aircraft TG306 occurred on 27 September 1946 is well known, having resulted in the death of Geoffrey de Havilland Jr., who was Chief Test Pilot of de Havilland at that time. The aircraft was investigating high speed controllability in a dive when the aircraft broke up “following violent divergent instability at Mach 0.9”, which is believed to have been in pitch. Technical investigation of the wreckage of the aircraft which had impacted into soft mud and therefore were able to be inspected (although unfortunately the accident data recorder fitted was destroyed by immersion in the same mud) showed that both wings had

failed in download. Therefore there are certain common threads here with known tumble departures, specifically :-

- A loss of control in the pitch axis from which recovery could not be effected.
- Forces acting upon the aircraft which apparently were so great that the pilot was unable to successfully abandon the aircraft.
- A structural failure in the air, which included a download failure of the wings.

The second such accident [113] was on 15 February 1950 to aircraft VW120 and was during a sortie from the Royal Aircraft Establishment at Farnborough to evaluate longitudinal stability and aero-elastic distortion at high Mach numbers. However, the aircraft did not achieve its intended initial test altitude of 38,000ft instead departing from controlled flight at 27,000 ft following the onset of divergent longitudinal oscillations. The aircraft is then reported to have descended at a very high rate, before breaking up somewhere between the surface and 10,000ft. Whilst it cannot be certain that the tumble was a factor (and contemporary reports indicate that the pilot had most likely lost consciousness due to an oxygen system failure), this accident again shows several common factors to those identified as part of the tumble, specifically :-

- A departure in pitch from controlled flight.
- A very rapid, apparently near-vertical, descent.
- A structural failure in the air (note, compared to TG306 the structure of VW120 was strengthened).

It seems likely, therefore, that VW120 had entered something similar to the tumble as previously described. The departure mechanism from controlled flight was certainly unrelated to those which affect weightshift microlight aeroplanes, but the aerodynamics sustaining the tumble, as identified in section 5.5 above may reasonably be considered to apply equally to this aircraft.

The third accident to the DH108 was on 1 May 1950 to aircraft TG283 also flying from RAE Farnborough; however, in this case the aircraft entered an inverted spin, which was identified and reported by the pilot. The aircraft spin recovery parachutes failed, as partially did the pilot's personal parachute – resulting in a fatal accident. However, this appears unrelated to the tumble, and therefore not of interest in the context of this study.

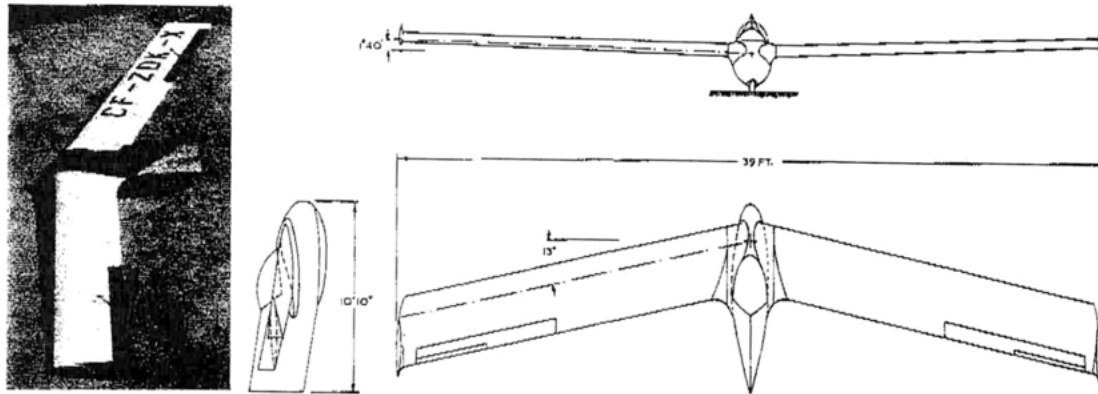
5.20 Historical Note 4, the BKB-1

The BKB-1, which is shown in **Figure 65** and **Figure 66** below was an experimental tailless swept-wing glider developed in Canada in the 1950s[**116**, **117**], which was later developed in the USA into a powered microlight aircraft known as the Kasperwing. Both the BKB-1 and the Kasperwing were shown to be able to enter a manoeuvre which was referred to at the time as a tumble, this was displayed extensively in the USA during the 1960s. It has been reported that the sustained tumble in these aircraft was believed due to “a strong vortex occurring just above the wing” [**118**]. The unique characteristic of the tumble in these aircraft was that it could be entered deliberately, and subsequently recovered from.

It is reported [**119**] that the method used to enter the tumble in this aircraft was to pull the aircraft into a vertical climb (effectively the first part of the loop), pause the pitching motion by moving the stick forwards with the aircraft pointed vertically upwards, then to pull the stick fully backwards (pitching nose-up), and that this would initiate a nose-up pitch autorotation. The pitch rate was recorded at approximately $360^\circ/\text{s}$, with the pilot experience positive normal accelerations of about 2g. The pilot of the aircraft reported that it was possible to tumble forwards only by moving the CG significantly forwards in the aircraft, and that in this instance the pitch rate increased to about $720^\circ/\text{s}$ whilst the acceleration forces upon his body became high and disorienting (as well as sufficient to damage the seat structure). In both cases centralisation of the pitch control was reported to recover the aircraft from the tumble with minimal height loss.

This appears to be further evidence that a rigid tailless aircraft is capable of entering a tumble, and also that this motion is rapid and can cause structural damage to the aircraft. Commonly with the evidence of the YB-49 it indicates a nose-up tumble as the most readily entered mode, and also shows that recovery is possible – in this case symmetrically using elevon control.

Figure 65. Illustration of BKB-1



Type designation	BKB-1
Country of design	Canada
Designer	S. K. Brochocki
Date of first flight of prototype	10 October 1959
Number produced	1

Dihedral	1,5°
¼ chord sweep	13,0°
Aero. twist root/tip	5,0°
Taper ratio (C_t/C_r)	1,0
Construction	Single spar, wood construction

Wings	
Span (b)	11,9 m
Area (s)	14,4 m ²
Aspect ratio (b^2/s)	10
Wing root chord (C_r)	1,22 m
Wing tip chord (C_t)	1,22 m
Mean chord ($C = s/b$)	1,22 m
Wing section, root	NACA 8-H-12
Wing section, mid	NACA 8-H-12
Wing section, tip	NACA 8-H-12

Ailerons	
Type	Upper surface hinge (elevon)
Span (total)	4,88 m
Area (total)	1,34 m ²
Mean chord	0,275 m
Max. deflection up	30°
Max. deflection down	30°
Mass balance degree	100%
Mass balance method	Bob weight
Construction	Wood. Fabric covered.

Reproduced courtesy of Mr S Brochocki, Air Progress

Figure 66. BKB-1 in flight



Reproduced courtesy of Mr D Webb

5.21 Conclusions concerning the tumble.

This section has explained that the tumble mode in a weightshift controlled microlight is sustained by induced flow as an aircraft rotates in pitch about its CG. It has demonstrated that the mode may be initiated by a rapid nose-down rotation of the whole aircraft rotating about its CG, and that this is most likely to be caused by a loss of power in a steeply nose-up pitch attitude, causing the rotation of the trike about the hangpoint to push the wing nose-down, via contact of the front strut and basebar.

Four possible methods of entry have been explained, through a whip-stall, rolling departure in IMC, a failed aerobatic manoeuvre, or flight through the aircraft's own wake vortex. All of these occasions are shown to be avoidable through good judgement on the part of the pilot; however equally it is possible with the knowledge of these entry mechanisms to avoid handling characteristics in a new aircraft design which will tend to make the aircraft tumble prone.

The tumble is a potential “killer” mode in microlight aircraft, as has been demonstrated by history. However, it is shown that through an understanding of tumble entry mechanisms in both pilot training, and in the investigation of the handling characteristics of new types, it is possible to avoid the tumble.

It is also shown that a tumble mode, apparently related to that seen in weightshift controlled microlights, can also occur in tailless rigid wing aircraft of any size, controlled using moving control surfaces – most commonly in a nose-up pitching motion. Although entered by different means, similarly to the weightshift tumble, this appears to be self-sustaining. There is sufficient evidence presented to indicate that this departure should be considered as part of the assessment of any such aircraft, particularly if the aircraft is to be used in any mode requiring rapid manoeuvring in pitch (e.g. display aerobatics, or as a fighter aeroplane).

6 Conclusions

6.1 Stall entry rates in the planning of flight testing.

Because stalling characteristics are a function of deceleration rate, it is important to ensure that the deceleration rates used in certification testing of aeroplanes are representative of the range of rates which may be met in service. For microlight aeroplanes, the maximum anticipated deceleration rate is that associated with a sudden loss of power following which the pilot attempts to maintain altitude, sacrificing airspeed to do so. The deceleration rate may be described by (2-27):-

$$\frac{dV_{ind}}{dt} = \frac{9.54\tau_d \sqrt{\sigma}}{G} \left(\frac{V_S^2}{V_E^2} + \frac{V_E^2}{V_S^2} \right)$$

Where τ_d is a function of aircraft characteristics, but has a maximum value given by (2-28):-

$$\tau_d = 1.74 - 0.036 \frac{W}{S}$$

6.2 Form of the O-A curve in Rogallo winged microlight aeroplanes.

For a conventional (Rogallo) flexwing microlight aeroplane, the stall speed with wing loading, comprising the O-A curve within the classical flight envelope (V-N) diagram has the form (3-2):-

$$V_S = V_{SO_{MTOW}.1g} \left(\frac{W}{MTOW} N_Z \right)^{C_{Ae}}$$

This relationship may be used to modify V_A and N_1 , so as to optimise operating limits and structural lightness, without unacceptably degrading the conservatism of structural reserve factors.

This form of the O-A curve is believed to be due to increased washout as wing loading is increased (through increasing weight and/or increasing N_Z).

Current facilities and available theory only permit determination of C_{Ae} for a particular wing through flight testing.

6.3 Spinning evaluation of 3-axis controlled microlight aeroplanes.

A set of spin recovery actions, comprising:-

- Close throttle,
- Centralise primary flying controls,
- Wait for spin to stop,
- Roll wings level,
- Ease out of any ensuing dive, applying power as the level flight attitude is reached,

is appropriate to a fixed wing microlight aeroplane which will be operated by pilots lacking training in spin-mode recognition and recovery, and/or availability of instrumentation which would assist in identifying spin direction.

Methods by which the suitability of these actions for an individual aircraft, and the acceptability of that aircraft's spinning characteristics are shown within this thesis.

6.4 The tumble mode.

The tumble mode in a weightshift controlled microlight is sustained by induced flow as an aircraft rotates in pitch about its CG. The mode may be initiated by a rapid nose-down rotation of the whole aircraft rotating about its CG; this being most likely to be caused by a loss of power in a steeply nose-up pitch attitude, causing the rotation of the trike about the hangpoint to push the wing nose-down, via contact of the front strut and basebar.

There are four known modes of tumble entry, through a whip-stall, rolling departure in IMC, a failed aerobatic manoeuvre, or flight through the aircraft's own wake vortex. All of these are avoidable through good judgement on the part of the pilot; however equally it is possible with the knowledge of these entry mechanisms to avoid handling characteristics in a new aircraft design which will tend to make the aircraft tumble prone.

Whilst the tumble is a potential “killer” mode in microlight aircraft, through an understanding of tumble entry mechanisms in both pilot training, and in the investigation of the handling characteristics of new types, it is possible to avoid the tumble.

A tumble mode, related to that seen in weightshift controlled microlights, can also occur in tailless rigid wing aircraft of any size, controlled using moving control surfaces – most commonly in a nose-up pitching motion. Although entered by different means, similarly to the weightshift tumble, this appears to be self-sustaining. There is sufficient evidence presented to indicate that this departure should be considered as part of the assessment of any such aircraft, particularly if the aircraft is to be used in any mode requiring rapid manoeuvring in pitch (e.g. display aerobatics, or as a fighter aeroplane).

7 Scope for further work in the fields of research described in this thesis.

7.1 Use of stall entry rates in the planning of flight testing.

Use of this work.

This work presents a tool by which the greatest deceleration rate in the event of an inadvertent stall of a microlight aeroplane may be predicted. Since existing test schedules for microlight aeroplanes already cover a range of decelerations from 1kn/s to 5kn/s it is unlikely that test planning would commonly be changed by this. However, it provides a tool by which the validity of the test conditions, for a particular type, may nonetheless be checked, and in this context usefully ensure the validity of test results in ensuring the suitability of the aircraft for normal use.

Further research.

This work has potential to be adapted to other classes of lightweight aircraft – for example to consider the immediate deceleration and consequent effects upon rotor speed of a gyroplane following an engine failure, or to consider the potential consequences of a launch-cable failure in a glider. It is very likely that such further work will require the researcher to investigate the physical significance of, and factors affecting the deceleration time constant, τ_d .

7.2 Form of the O-A curve in Rogallo winged microlight aeroplanes.

Use of this work

The research presented shows a form of the O-A curve which may, at the discretion of certification Engineers for particular projects, potentially be used either to increase V_A thus expanding the proven-safe flight envelope for a flexwing microlight, to justify reduced normal acceleration limits thus permitting reduction in structural weight, or potentially a combination of the two.

Further research

Although the general mechanism of increasing washout under load is understood – no rigorous aeroelastic model exists for a Rogallo type wing, which would allow prediction of spanwise and chordwise shape and pressure distribution. Such a tool might not only allow extrapolation of a valid O-A curve with less flight test data than is currently required, but in modelling the 2-dimensional loading of the wing, would be valuable for designers attempting structural optimisation and the maximum operating angle of attack (and thus speed) range for new microlight and hang-glider wings.

7.3 Spinning evaluation of 3-axis controlled microlight aeroplanes.

Use of this work

The main content of this work has entered use as guidance and planning material in the certification of microlight aeroplanes in the United Kingdom; this has included acceptance of the “controls centralised” spin recovery.

Published guidance material [78] however, does not yet reflect the complexity of some recently introduced types, and should be expanded as shown in Table 19 and the preceding text to include the added complexity of conducting spin-testing of flapped aeroplanes.

Further research

Whilst the guidance developed during this research is appropriate to the current types of microlight aeroplane being certified in the United Kingdom, the standard of aircraft is not static. It is likely in the future that the range of aircraft configurations will expand; this may for example include unswept rigid weightshift microlights, multi-engined aeroplanes or aircraft with retractable undercarriage – such aircraft already exist in other countries such as Germany and the Czech republic [Error! Bookmark not defined.], where no requirement for a spinning assessment exists. It is therefore important that as either such aircraft are introduced into Britain, or conversely should requirements for spinning assessment be introduced into countries using such

aircraft, the research is conducted to maintain appropriate guidance material. Similarly, whilst there is a high confidence in the methods proposed, as applied so far, it is important that this guidance is kept under continuous review, so that confidence may be maintained in the method's validity, or else published best practice modified in light of lessons learned in future programmes.

In addition, it has been noted during the course of this research that although a great deal of published material exists concerning the geometry of the spin, and a lesser amount exists (to which this research has added) concerning the conduct of spinning assessments, very little analysis exists with regard to prediction of either the spin-entry, or the spin recovery. A tool whereby spin entry and spin recovery characteristics could be reliably predicted would be both a new and original piece of work, and of enormous use throughout the aircraft industry, reducing both risk and cost during flight test programmes. The subject is commended to future researchers.

7.4 The tumble mode.

Use of this work

The primary use of this work has so far been, and is likely to continue to be, education of microlight pilots in the avoidance of tumble entry mechanisms. Through this alone however, it is hoped that lives will be saved through the avoidance of future fatal accidents.

In addition however, the knowledge which has been developed of the tumble entry mechanisms can also be used during the certification process for new aircraft types to identify and solve any areas of tumble susceptibility. In particular, determination of an operationally acceptable minimum full-power climb speed (or maximum climb attitude) to ensure that the wing always leads the trike during the stall event, and avoidance of strong spiral instability should ensure relatively tumble resistant aircraft.

Further research

The wind tunnel results shown in Section 5.5 are the first laboratory-level investigation of the flow affects around a tumbling aircraft; they are however brief and leave considerable potential for future work. In particular, the true 3-dimensional flow affects are unknown, as are the effects of Centre of Gravity (CG) position on the flow around an aircraft in the developed tumble (i.e. whether the movement of CG from below the wing as in a microlight, to within the wing, as in a flying wing aeroplane is significant, and if-so how). There is also currently only limited understanding of the magnitude of pitching moment during the tumble, or of the scale laws which might be applied when converting between a wind tunnel model and various full-sized aircraft.

This may be of particular significance for any future development of higher aspect ratio flying-wing aircraft, of any size – as it has been shown that such aircraft can tumble, and in some circumstances will also recover. This is not well understood, but there is sufficient evidence to indicate that this understanding should be developed as part of any new development of flying wing aircraft – particularly those which may be flown aerobatically. This significance is not only that of understanding the tumble entry resistance or recovery, but equally importantly of determining the structural loads upon the airframe during the developed tumble.

In summary, the work so far on the tumble mode whilst a considerable step forward in understanding of the mode, can only be considered a beginning to this subject, and there is considerable scope for future, useful, research.

8 Acknowledgements

No researcher in an established field, such as airworthiness, can or should attempt to work in isolation. The researches which have led to this thesis are no exception. Listed below are individuals without whose input, this work would not have reached the current stage of fruition.

<u>Name</u>	<u>Position</u>	8.1.1.1 <u>Contribution</u>
Brooks, Dr William	Chief Test Pilot (weightshift) BMAA, Technical Director Pegasus Aviation.	Discussions on flexwing design and testing
Cardenas, Brigadier General Robert L. USAF, Rtd	Former USAF Test Pilot	Discussions on loss of control issues in Northrop YB-49
Culling, Mr Stuart	Senior Engineering Inspector, AAIB (now retired)	Assistance with, and funding for, early tumble investigations circa 1998.
Dale, Mr. Mark	Technical Officer, BHPA	Provision of BHPA test rig, and assistance in it's use, for various flexwing tests
Dell, Ms. Liz	<i>Above all others</i> , my long suffering partner and fiancé, who has with remarkable patience, put up with my spare time occupation of completing these Doctoral studies over more than seven years.	
Dewhurst, Mr. Paul	Chief Instructor, Flylight Airports, and Test Pilot & Senior Inspector, BMAA	Thorough reporting of numerous test programmes.

<u>Name</u>	<u>Position</u>	8.1.1.1 <u>Contribution</u>
Dyde, Sqn.Ldr. Simon	Former Test Pilot, A&AEE	Assistance in the development of spinning methodologies during testing of the Tucano T1 circa 1995
Farley, John	Retired Test Pilot, writer	Access to, and discussion of, privately held historical flight test records.
Finnigan, Lt Col. (Rtd) Chris	Chief Executive, BMAA	Allowing the facility for research work within the BMAA's working programme.
Finn-Kelcey, Mr Nigel	Owner, Aviasud Mistral G-MWIB	Use of his aircraft
Grimwood, Mr Robert	Test Pilot, Flylight Airports	Thorough reporting of iXess test programme
Hamer, Mr. John	Test Pilot and Senior Inspector, BMAA	Active participation in numerous airworthiness evaluation programmes.
Howes, Mr Jonathan	Head, CAA Loads and dynamics section.	Useful discussions on structural implications of airworthiness evaluation methods.
Mulcahy, Capt. Paul	Test Pilot, CAA Formerly Test Pilot, A&AEE	Close co-operation on numerous flight test programmes.
Newman, Dr. Simon	Senior Lecturer, University of Southampton	Academic supervisor and collaborator on analysis of the tumble.

<u>Name</u>	<u>Position</u>	8.1.1.1 <u>Contribution</u>
Patrick, Mr. Roger	Chief Designer, Mainair Sports	Assistance in rig tests upon several flexwings, provision of F2a design data.
Payne, Mr Alan	Technical Administrator, BMAA	Ensuring the smooth progress of numerous engineering programmes.
Porteous, Capt. Tom	Chief Test Pilot (Fixed Wing), BMAA and Chief Test Pilot, Thruster Air Services	Assistance in several spinning test programmes.
Scott, Mr Philip	Owner, HM 1000 Balerit G-MZIC	Use of his aircraft
Steele, Capt. Dick	Owner, N3N-3 G-ONAF	Assistance in obtaining verified take-off and landing performance data.
Stinton, Dr. Darrol	Consultant, Author, retired Test Pilot	Author of volumes on aircraft design and testing, and informal discussions on the conduct of various test programmes.
Venton-Walters, Mr Roy	Formerly Chief Designer, Southdown	Discussions concerning stall characteristics of flexwings.
Walsh, Ms Joan	Engineer and Microlight Pilot	Informal input into discussion on mechanisms of the tumble.

<u>Name</u>	<u>Position</u>	8.1.1.1 <u>Contribution</u>
Welch, Mrs Ann,	Writer; president, BMAA and other organisations; retired pilot. Deceased December 2002.	Discussions concerning wartime ferry flying and 1950s glider test flying.
Welsh, Dr. Paul	Airworthiness Engineer, Flylight Airsports Ltd, Chief Designer, Bella Aviation.	Discussions concerning the tumble mode and participation in flexwing stall speed testing.

APPENDIX A

OTHER TEST TECHNIQUES DEVELOPED TO ASSIST IN THE INVESTIGATION OF AIRCRAFT FLYING QUALITIES.

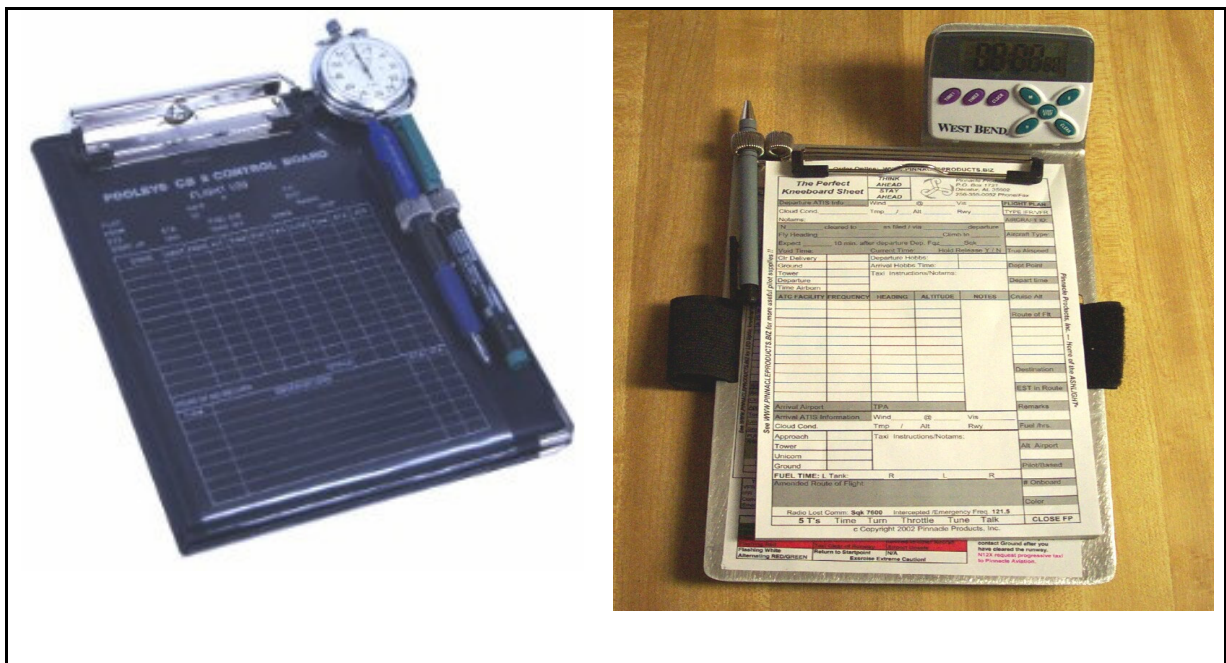
Introduction

This appendix does not primarily concern the most significant safety issues concerning microlight aeroplanes. However, much of the task of safety assessment requires verifiable performance data. This is partly for the purposes of operating data, and partly because this data is essential to the conduct of a certification programme (to allow proper reporting, repeatability and progression of test conditions). This section describes methods that have been developed or refined during the period of this research for the purposes of assessing microlight aeroplanes. Whilst they do not solve problems which have not previously been soluble by other methods, they do offer methods for the determination of aircraft performance which can be performed with less manpower, cost and infrastructure than has traditionally been the case, whilst ensuring an acceptable level of rigour. Specifically the methods developed have been used to determine PEC (and in particular ASI errors, which are most significant in microlight operations), take-off and landing performance and spinning characteristics. The methods described have been specifically developed to use with microlight aeroplanes, but they may equally be used (albeit with consideration of the underlying assumptions and if necessary amendment of the method) for other classes of aeroplanes.

A1 Manual methods for data recording

Traditionally most pilots will routinely fly with a kneeboard (such as shown in [Figure 67](#) below) on which both the plan for the flight, and data generated during the flight are recorded. An additional piece of equipment commonly carried is a stopwatch. Since these must normally be carried regardless of the purpose of a flight, it is unsurprising that these pieces of equipment are also primary to the conduct of a test flight. Those shown are approximately of A5 size, which is most common but not universal. The type and dimensions of kneeboard selected will often be a function of the specific cockpit environment.

Figure 67. Typical kneeboards



Two additional pieces of equipment which are routinely added, for test-flying purposes, are a force gauge and a ruler or tape-measure. These are used for measuring control inceptor forces and deflections. Whilst customised devices for this purpose do exist and may particularly be found in use at military test centres such as

Boscombe Down, the majority of flight testing is conducted using a simple spring-balance (**Figure 68**) and domestic tape measure.

Figure 68, Typical spring balance



Fundamental then to the testing process is the effective use of these simple tools. Whilst there are obviously safety rules inherent to their use, these are within the province of flight training and outside the scope of this appendix. However, a tool whose use it is helpful to describe is the “test card”. Test cards are sheets of paper (or card) developed by the test management team and carried in the air for the following purposes:-

- Showing the aircrew the order and condition of tests (and other flight actions such as positioning) required.
- Providing opportunity for manual recording of data (manual recording of data is considered essential in all flight test activities, even where automatic data recording is in use).
- Showing special checklists or safety data (such as provisional or absolute operating limitations).
- Combining as much as possible of the information that the Test Pilot or Flight Test Engineer will require in flight at a single source. (Thus enhancing both efficiency and safety in the conduct of the test sortie.)

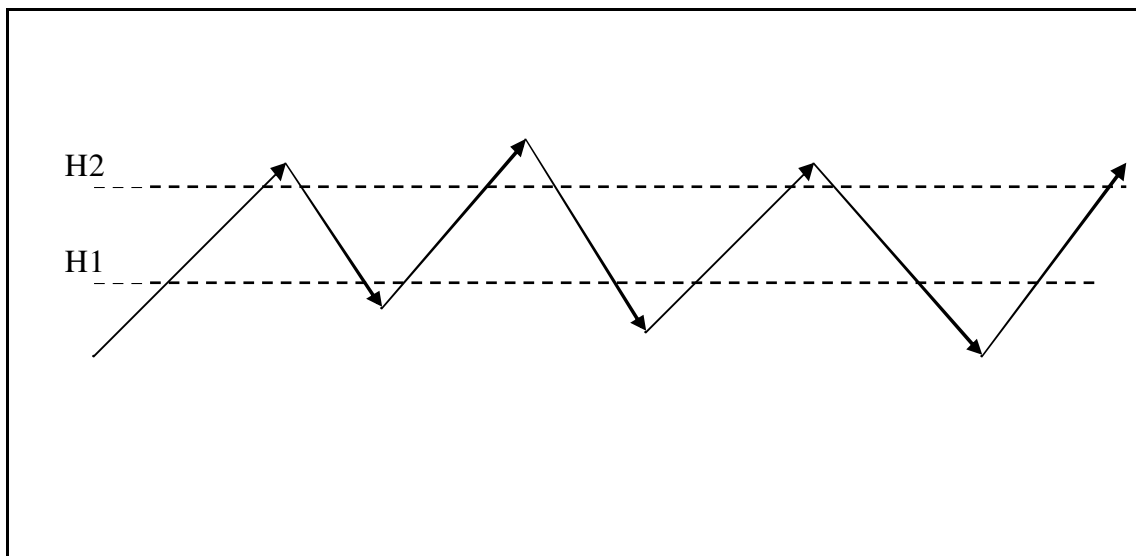
There are no firm and accepted rules concerning how test cards should be prepared. In most civil flight testing (including that of microlight aeroplanes) they are usually prepared by the Test Pilot, in most military aircraft testing they are prepared by the Flight Test Engineer in consultation with the Test Pilot, whilst in major military programmes (such as Eurofighter or F/A-22 [120]) they will be prepared by a committee including all parties interested in the conduct of a particular sortie. However, the general principles detailed above remain and the card must ultimately

remain useable by the crew for the intended purpose, which inevitably gives the captain of the aircraft (the test pilot) ultimate control over their content.

In order to illustrate the use of test cards, below is described a typical test – that of using test cards to determine the climb and glide performance of a hypothetical aircraft type.

The first part of the determination of climb and glide performance is to determine the speeds at which those performance values are determined. The method used for this will be “sawtooth climbs” and “sawtooth glides”. The title of these manoeuvres (usually flown together) implies a flightpath consisting of a number of steady condition climbs and descents, following a flightpath as illustrated in **Figure 69** below.

Figure 69. Illustration of sawtooth flightpath

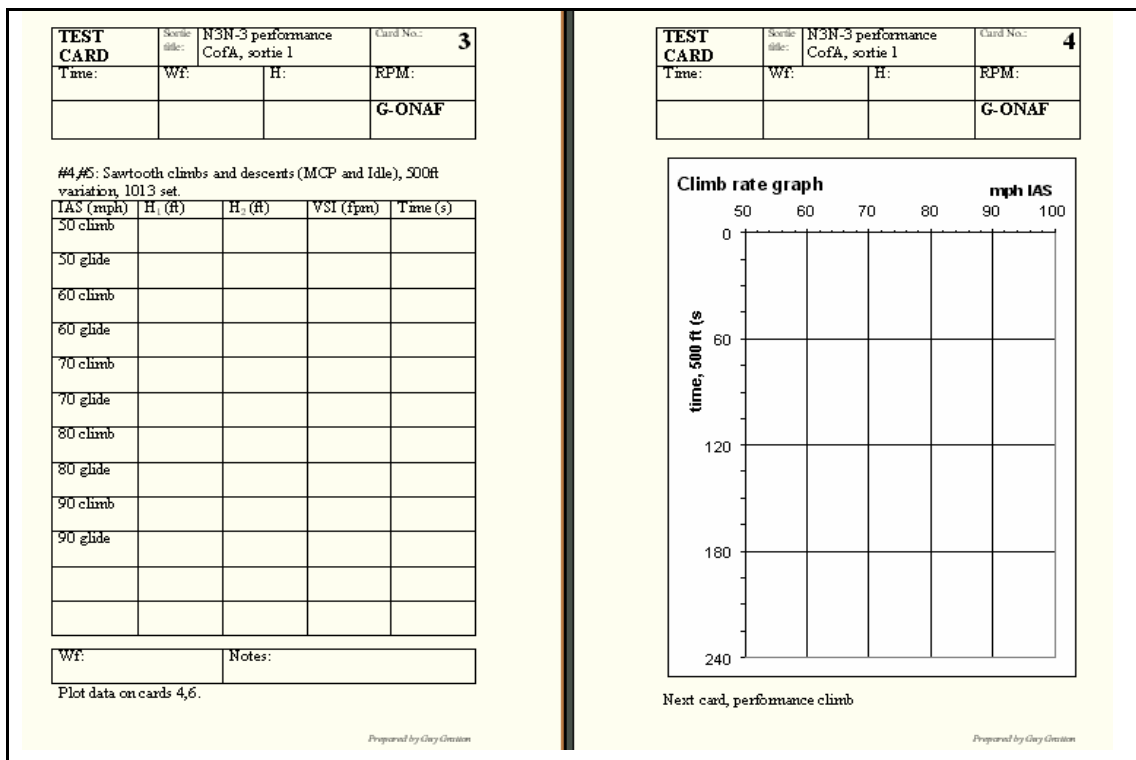


It will be noted that although the individual segments nominally show a continuous climb, the overall shape of the flightpath is uneven, obviously the climb and descent angles will vary with airspeed, but also the lower and upper bounds of the sawtooth will vary with operational necessity. What is critical is that the aircraft remains “on condition” (constant speed and known weight) throughout pre-determined height

bands, shown here as H1 and H2. These two heights would typically (for a microlight aeroplanes) be about 500ft apart although it is normal to make them further apart for a higher performance (greater climb rate) aircraft, and closer together (perhaps 200ft or even 100ft on occasion) for a very low performance (low climb rate) aircraft. This test might be illustrated on test cards similar to that shown in

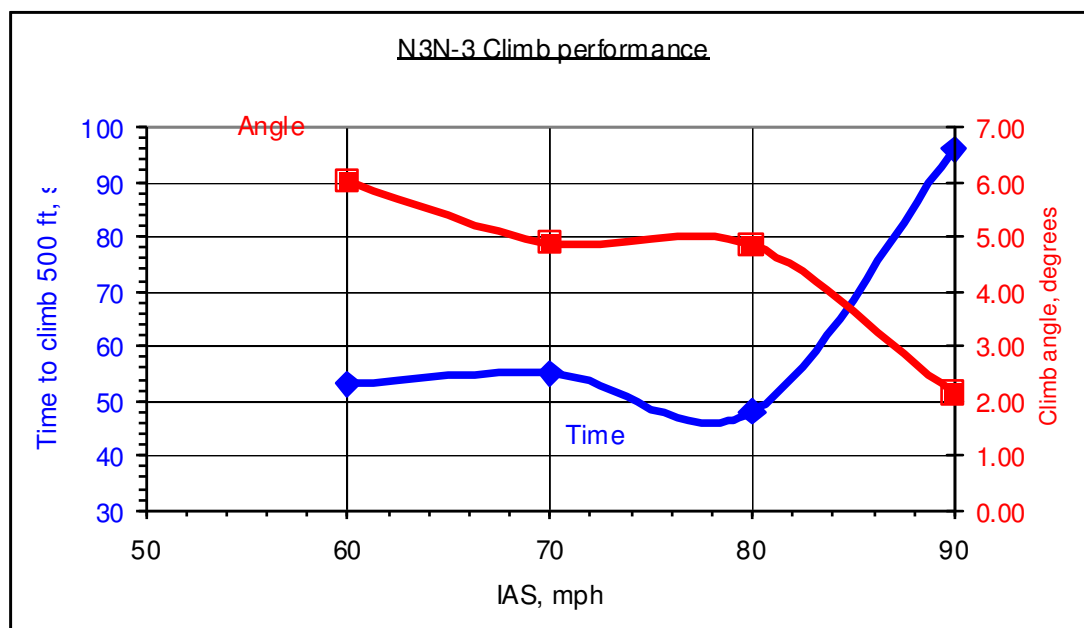
Figure 70 below – it will be noted that the cards below (which were originally used for assessment of a Naval Aircraft Factory N3N-3 aircraft) allow the test crew discretion concerning what heights and speeds are to be flown. This is normal since it is not considered good practice to constrain the specific test conditions prior to flight; a test pilot and/or FTE will make these decisions during the sortie dependent upon local conditions. For example, heights must permit flight without intruding into IMC conditions, controlled airspace, or transient meteorological conditions (e.g. turbulence, updraft, downdraft or inversion) which might affect the test results, and it is often necessary to determine the exact speeds (and conduct some limited analysis) in flight so as to ensure that the maxima and minima of the climb/glide curves are correctly identified – hence the inclusion of a simple graph pro-forma within the test cards.

Figure 70. Typical test cards showing sawtooth climbs and glides



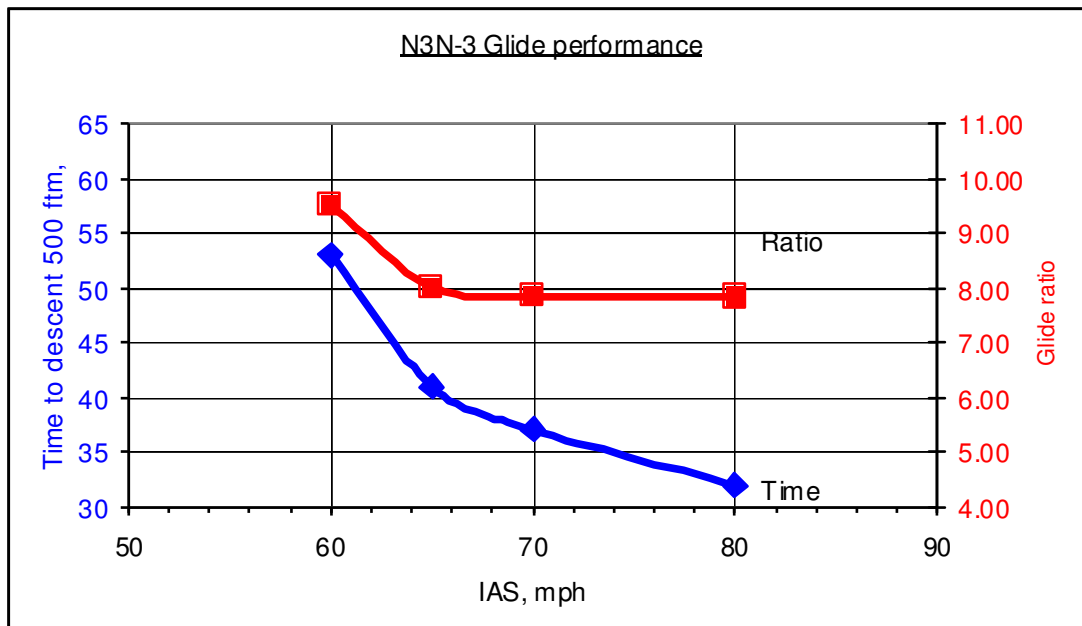
Once flown, this data must be analysed and reported. In **Figure 71** and **Figure 72** below is the plotted and analysed data obtained during this testing for issue of a public transport certificate of airworthiness of this N3N-3 aircraft (extracted from reference [121] but for details of the aircraft also see Section 0 in the main body of the thesis). It should be noted that the sole purposes of these specific tests was to determine the best climb and glide speeds, (which should not vary significantly with altitude or weight) and not the absolute performance. Also, although the data plotted below shows performance against Indicated Air Speed (IAS) analysis of climb and glide gradients is of-course carried against TAS (True Air Speed), which in turn is a function of IAS, the Airspeed Indicator (ASI) calibration curve (see section A2 below) and density altitude.

Figure 71, Analysed results of sawtooth climbs for N3N-3 aircraft



This indicates that the best climb rate speed lies between 75 and 80 mph IAS. It also indicates that the best angle climb speed lies at or below 60 mph IAS.

Figure 72. Analysed results of sawtooth glides for N3N-3 aircraft

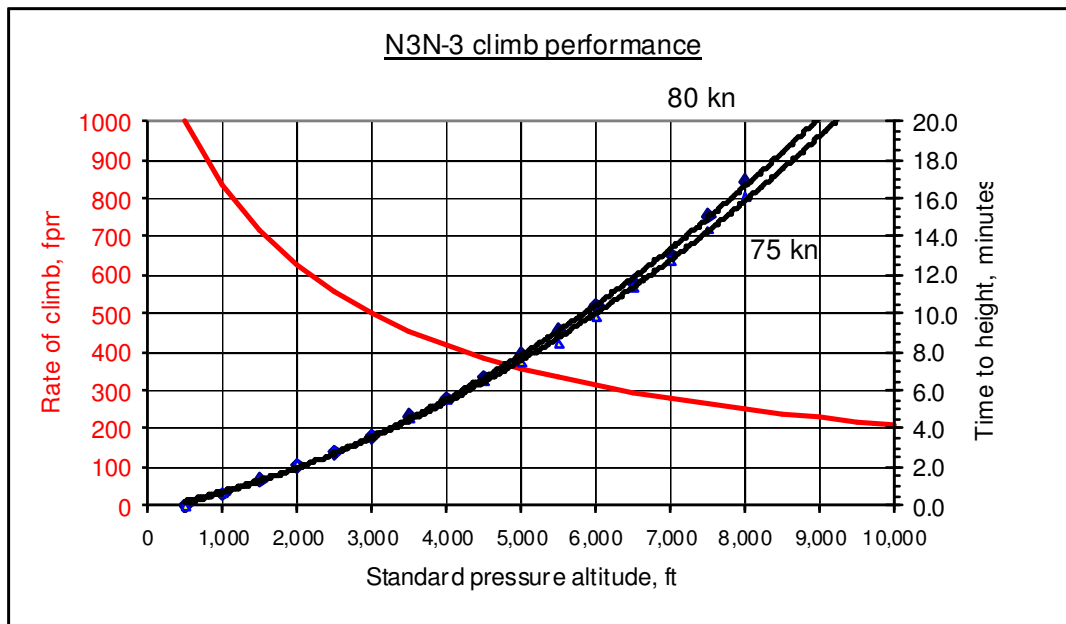


This indicates that the best glide angle speed lies at or below 60 mph IAS. Given that the stall speed is 53 mph IAS, it was considered in post flight discussion that a common best glide speed of 60 mph IAS should be used, and not any speed closer to the stall, which it was considered would lead the aircraft into an unacceptable risk of inadvertent stall (in addition the presence of pre-stall buffet commonly prevents the pilot from obtaining good performance data at speeds close to the stall).

Following this analysis, the speeds determined are used to allow the aircraft to be flown through a continuous long climb (or series of climbs, often on reciprocal crosswind headings so as to negate any wind gradient effects), at a mass no less than 95% MTOW (a constraint imposed by best practice in ensuring that only small corrections are made to MTOW, at which performance results are conventionally quoted for smaller aeroplanes, and also the requirements of BCAR Section K [122] which although technically obsolete is used throughout the UK industry and often mandated by CAA as technical guidance).

Shown in **Figure 73** are the analysed results for the N3N-3 previously described.

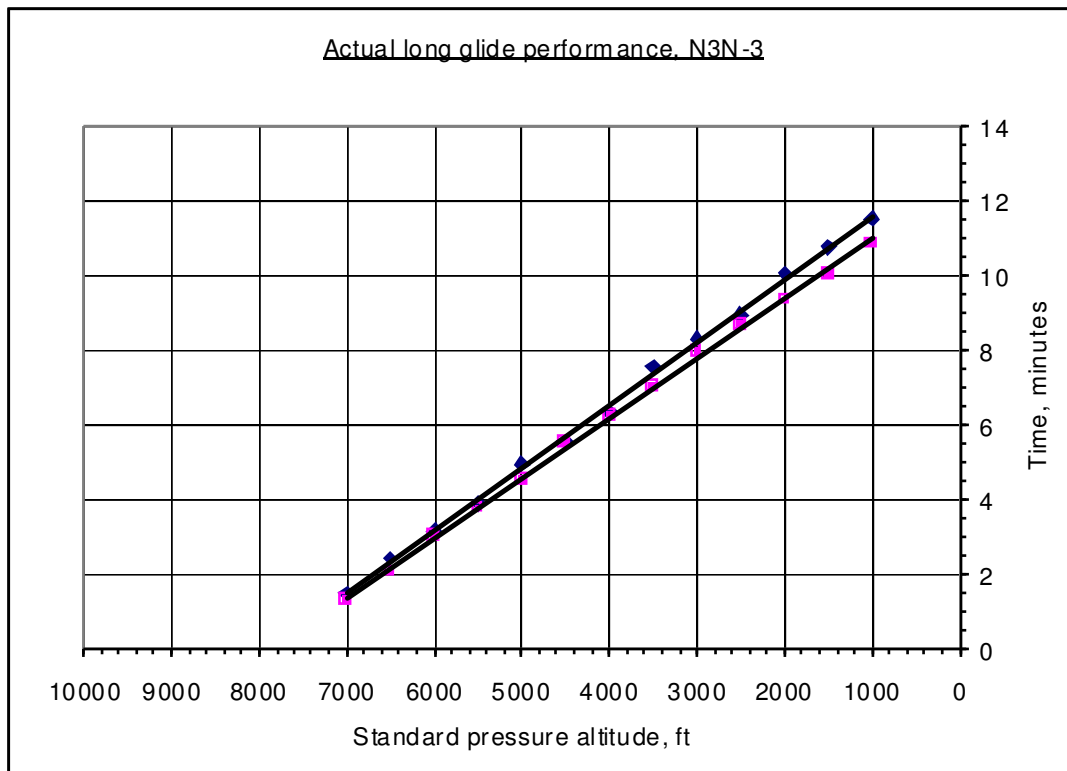
Figure 73. Results from a continuous climb for the N3N-3 aircraft



Notes: Two performance climbs were flown, one at 2830lb / 4.1" / 80mph IAS, the second at 2790lb / 4.2" / 75 mph IAS. The results plotted above were obtained. The best fit curve to each is a quadratic, and the climb rate curve given was obtained by differentiating each with respect to time, giving the same result to 2 significant figures. Data was only obtained between 500ft sHp and 8,000 ft sHp, portions of the curve below and beyond that are extrapolation.

Similarly, a continuous glide is flown (in practice, usually at-least two – one each at the best glide angle speed and one at the minimum sink speed). Results again are shown below.

Figure 74. Results from two continuous long glides for N3N-3 aircraft



Notes: Two continuous performance glides were flown at 60 mph IAS, from above 8,000 ft sHp through 1000 ft sHp, the first was at 2,800 lbf / 4.13", the second at 2780 lbf / 4.2". The engine was warmed at approximately 1500ft intervals. The following results were obtained. Of these, the poorer performance is afforded by the lower line of the graph above, which reduces to a steady descent rate of 580 fpm or 8.6:1 at sea-level (improving to a ratio of 10:1 at 10,000 ft).

Best climb rate speed is to be 80 mph IAS. This gives a climb rate at about 2800 lbf which is represented by :

$$\frac{1}{4 \times 10^{-7} H + 0.0008} \quad (\text{A1-1})$$

It is necessary to adjust to MTOW. Climb rate is represented conventionally for a piston-prop aircraft[123] by the following correction:

$$-\frac{dH}{dt} = \frac{550.P.\eta_p - D.V}{W} \quad (\text{A1-2})$$

Where, H = altitude

t = time

P = Engine power output (in horsepower)

η_p = Propeller efficiency

D = Drag

V = True Air Speed

W = Weight

this, taking all others as fixed, shows rate of climb as being inversely proportional to weight. Thus, the climb rate at MTOW, may be represented by:

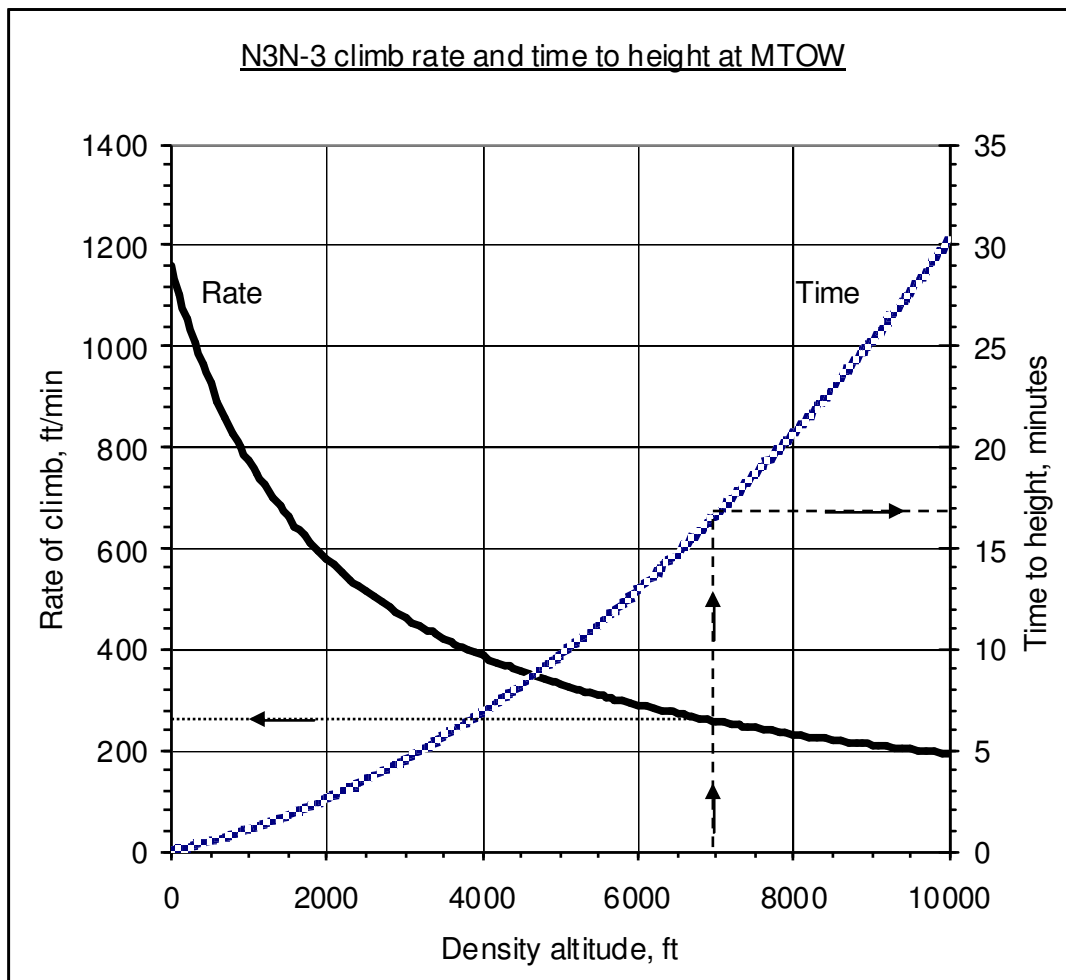
$$\frac{0.927}{4 \times 10^{-7} H + 0.0008} \quad (\text{A1-3})$$

where $0.927 = 2080 \text{ lbf}/3020 \text{ lbf}$. This could then be used to prepare a climb rate graph for inclusion in the Pilots Operating Handbook (POH). **Figure 75** Below shows an extract from the POH for the public transport version of the N3N-3.

Figure 75. Climb performance section from N3N-3 operators manual (UK public transport version)

Climb

The best climb-rate speed is 80 mph IAS. The graph below shows the climb performance at this speed for given density altitudes at MTOW. To calculate the time to climb between two heights, subtract the time at the lower height from the time at the greater height. Climb performance will be no poorer at lower weights.



Example shown, 7000 ft, climb rate is 240 fpm, time from sea-level is 17 minutes.

The speed for best climb angle is 63 mph IAS.

A2 Use of GPS for airspeed indicator calibration. (The racetrack method)

It is essential in all performance flight testing and much handling flight testing to know accurately the relationship between Indicated Air Speed (IAS) and Calibrated Air Speed (CAS). Historically, this relationship has been determined by a series of methods, including trailing statics, range-course methods, and tower flybys with high speed photography. All of these methods have disadvantages, in that they can be inaccurate, expensive, or require modification to the aircraft. The advent of inexpensive lightweight GPS (Global Positioning System) units, with exceptionally good levels of both precision (± 1 metre in 3 dimensions) and accuracy (± 15 metres in 3 dimensions) offered the potential for another method of determination. These units (examples illustrated below) have become standard equipment for most pilots, and thus are very readily available for any test programme.

Figure 76. Typical modern handheld GPS receivers



The method developed can be flown quickly; experience has shown that in good conditions, a thorough calibration for a low speed aeroplane such as an X' Air can be flown in as little as 30 minutes, or in poor conditions (such as where there is localised turbulence, or airspace restrictions) perhaps an hour. It may also be flown, if necessary, by a single pilot without any modification to the aircraft or requirement for external data recording. Required are turbulence-free conditions, accurate knowledge of outside air temperature, a GPS unit, and approximate wind heading data. The latter can be obtained from a meteorological office forecast, or readily estimated by any qualified pilot using a pressure chart. (See figures below).

Figure 77. Met office form 214 wind forecast, showing (columns from left) altitude, wind heading, wind strength, and OAT at specific locations.

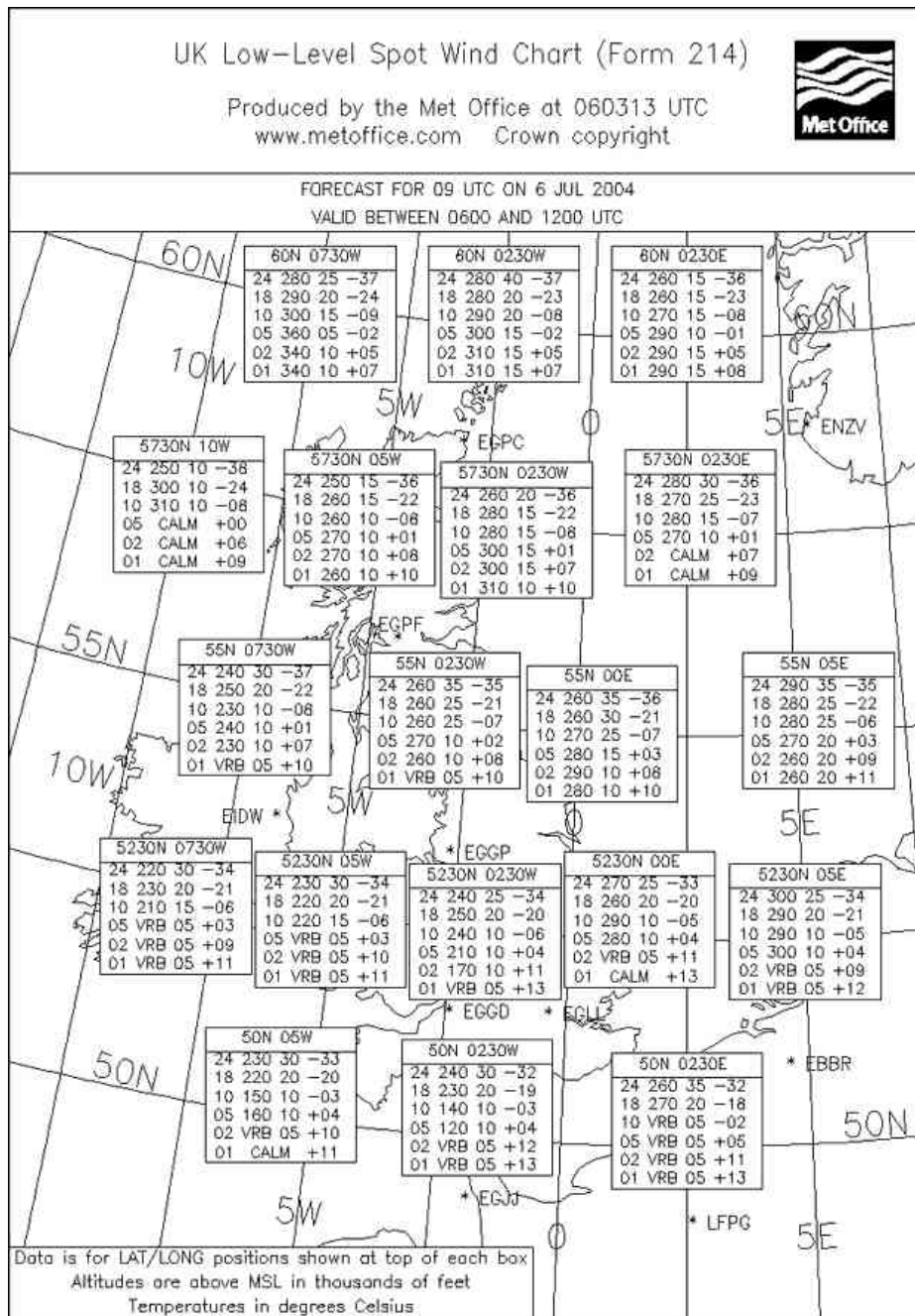
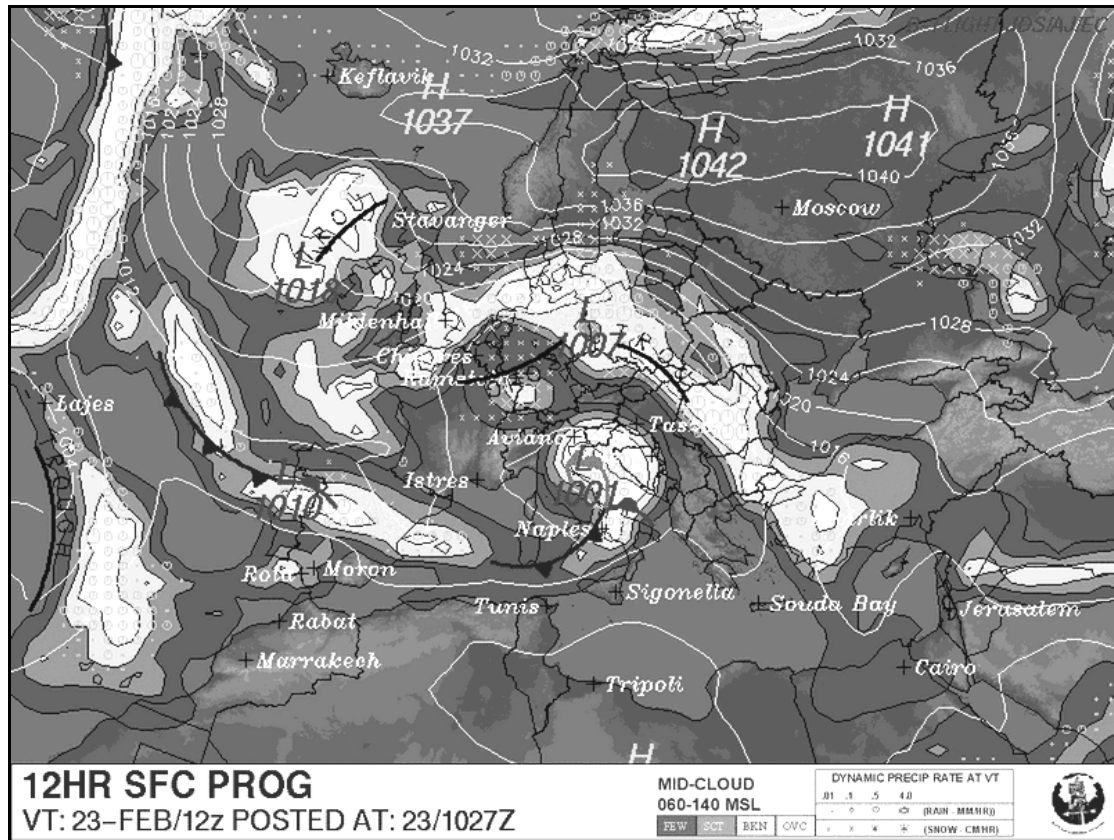


Figure 78. Typical pressure chart (USAFE type)



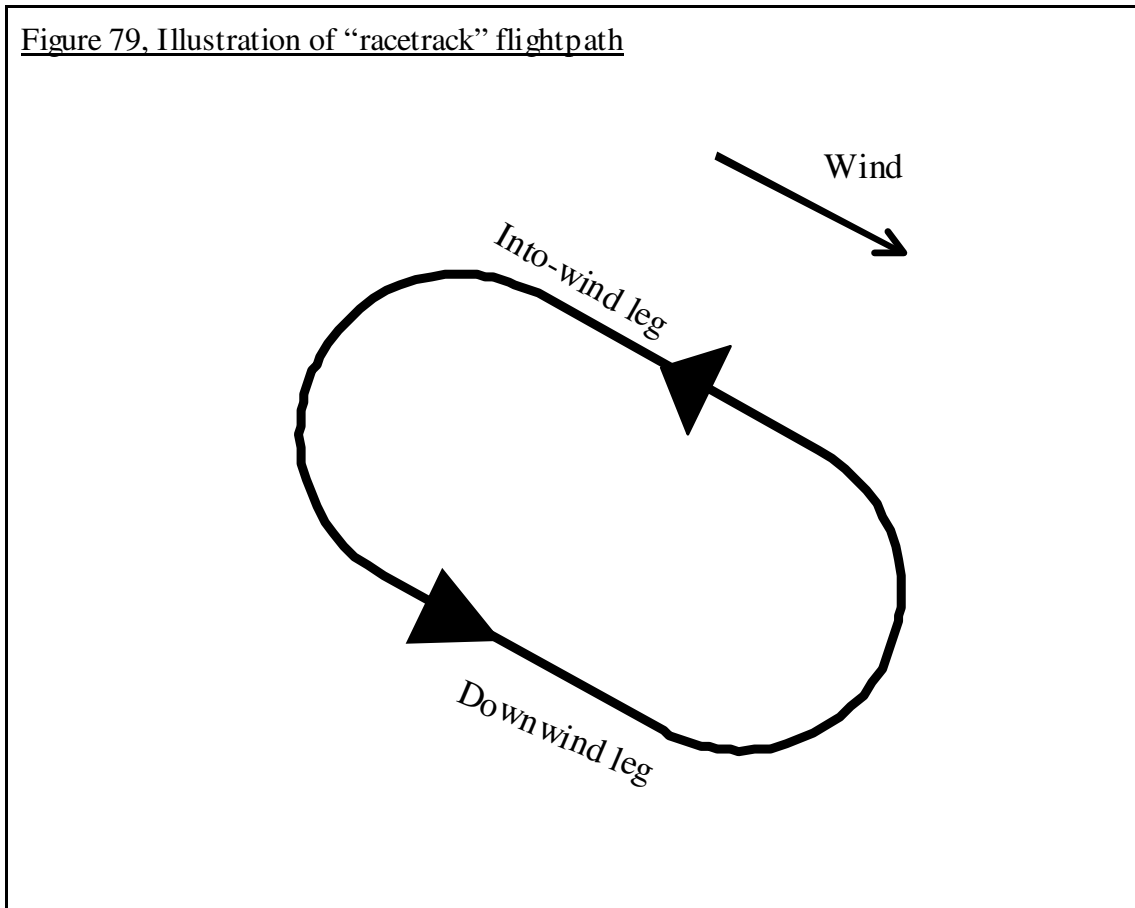
The following method is used to obtain data:-

The aircraft is pointed as accurately into wind as the forecast will allow. Precise wind heading is then obtained by varying heading slightly whilst maintaining constant speed and height. The aircraft is known to be exactly into wind when the lowest indication is obtained of GPS groundspeed. This heading is noted.

The aircraft is flown at a range of speeds from just above the stall, to at-least V_H (often to V_{ne}) with GPS groundspeed being noted against indicated airspeed at each increment. Where the airspeed exceeds V_H , and thus the aircraft is forced to descend, the time between two heights (normally about 200 ft, greater altitude changes potentially causing significant changes in the TAS:CAS relationship) is recorded to allow correction during subsequent analysis.

The aircraft, maintaining a constant nominal height, is then turned (using GPS so as to not be affected by any magnetic anomalies) onto a reciprocal heading, and this exercise repeated. If necessary (limitations of available airspace tend to control the flightpath) multiple turns are flown in a “racetrack” method as indicated below.

Figure 79, Illustration of “racetrack” flightpath



The data is then reduced, using a table such as that given below:-

Table 17. ASI calibration data reduction table

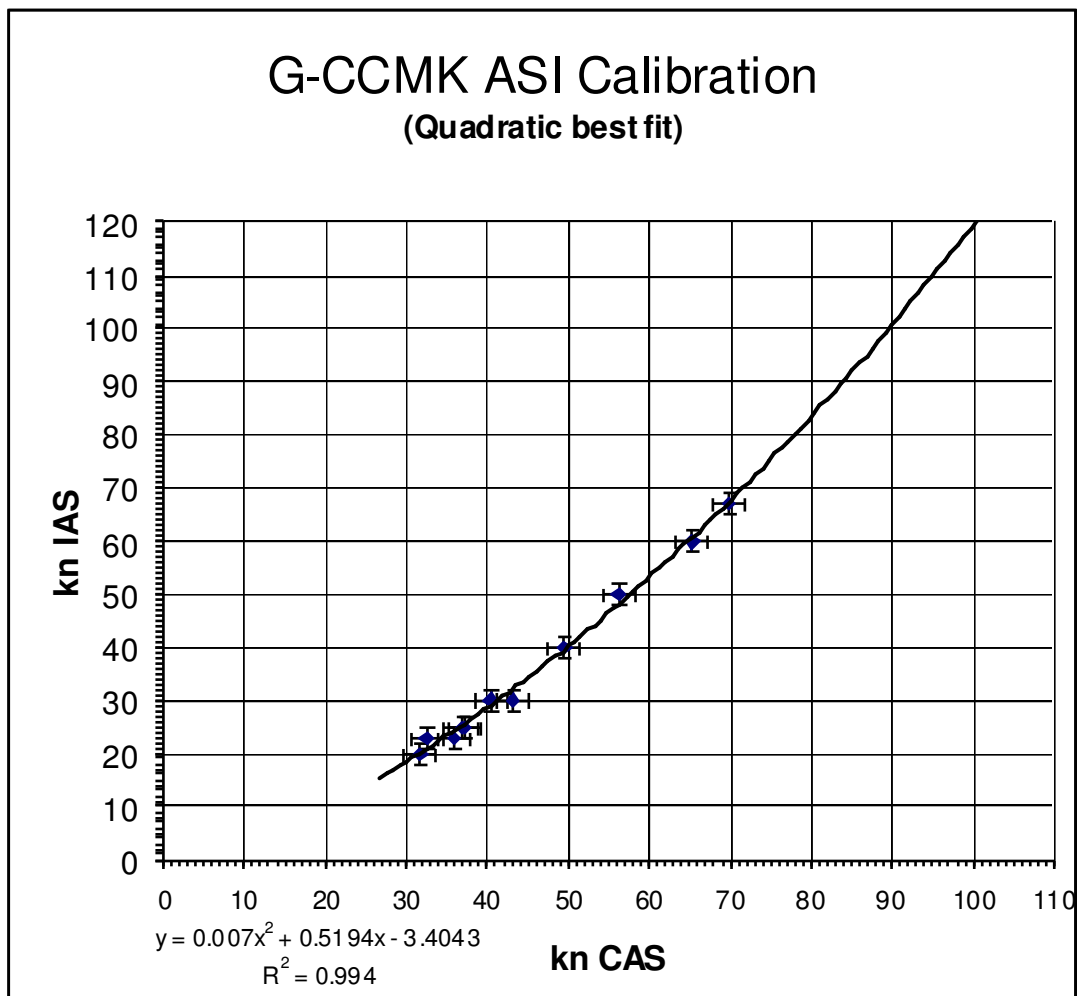
[Based upon reference [124].

IAS (any unit) (a)	GS Into wind (knots) (b)	time per 200 ft (s) I	Adjusted GS into wind (knots) (d)	GS downwind (knots) (e)	time per 200 ft (s) (f)	Adjusted GS downwind (knots) (g)	TAS (knots) (h)	CAS (knots) (i)
	from GPS	from stopwatch	$\sqrt{(b)^2 + \left(\frac{118}{(c)}\right)^2}$ or (b) if not descending	from GPS	from stopwatch	$\sqrt{(e)^2 + \left(\frac{118}{(f)}\right)^2}$ or (e) if not descending	$\frac{(d)+(g)}{2}$	$(h) \times \sqrt{\sigma}$
30								
40								
etc.								

σ , relative air density may be estimated from local OAT, pressure altitude, and ISA tables.

Finally this data is plotted to produce an ASI calibration chart. A typical example chart is shown below, for an X' Air Mk.1. Error bars are used, typically of ± 1 kn or ± 2 kn, depending upon the pilots opinion of the quality of data recording during a sortie. Normally the line fit used is then the least complex curve that fits within all the error bars. As will be seen below, the degree to which a low (normally 1st or 2nd) order curve may be fitted to reasonably low value error bars is good. No attempt has been made to try and fit any particular theoretical basis to these line fits, although it has been noted that in most cases (including that shown below) ASIs fitted to this class of aircraft will tend to underread at low speeds, overread at high speeds, and tend to read approximately correctly at around 45-65 kn. It has been found important, to use at-least 5 points, down to as near the stall as is reasonably achievable (because of the likelihood of low-energy discontinuities, and hence the desire to allow as little extrapolation into this potentially uncertain area as possible). At higher speeds, discontinuities or significant changes of curve form have not generally been noted above V_H and this area can be treated with less rigour.

Figure 80. Sample ASI calibration plot from GPS method



A3 Alternative GPS based methods for ASI calibration: the triangular, and box-pattern methods, also the non-GPS based ground course method.

An alternative method to the above is believed to have been used primarily by pilots carrying out test flying on behalf of the Popular Flying Association (PFA). This uses a similar means for groundspeed determination, but instead uses three legs, separated by 120°. The “folklore” associated with this method is that the mean of these three speeds will give the TAS. In practice this is untrue since the losses of groundspeed due to crosswind factors will cause the mean speed to be less than TAS (although trigonometry may be used to correct this, see [125]). It is also an inefficient method since the time spent flying an additional leg for each speed more than compensates for the time

spent accurately determining the wind heading. An additional consideration is that continuously flying a triangular course with 120° between legs is an internationally accepted procedure by which an aircraft which has suffered a failure of radio and navigation equipment, indicates its need for assistance [126] in the form of a “shepherd” aircraft. So, to fly a course which might unnecessarily indicate distress to a radar controller, would be highly irresponsible, particularly since the aircraft under test may well not be in contact with that radar controller (particularly given that even during flight testing, microlight aircraft rarely carry transponders which might display to a controller whether the aircraft is, or is not, in any form of distress.)

A variant method was devised independently and published by J T Lowry [127] and referred to as the “Box Pattern” method. This flies three legs at 90° spaced magnetic headings (one being due North), and then by trigonometry (reproduced below, using Lowry’s terminology) the TAS is determined at each speed.

Three groundspeeds are recorded for each IAS value, these are g_1 (flown due magnetic North), g_2 (flown on magnetic heading 90°) and g_3 (flown on magnetic heading 180°). Variables p , q , α used within the calculation have no physical significance.

$$p = \frac{g_1^2 + g_2^2}{2} \quad (\text{A3-1})$$

$$\alpha = \tan^{-1} \left(\frac{2g_2^2 - g_1^2 - g_3^2}{g_3^2 - g_1^2} \right) \quad (\text{A3-2})$$

$$q = \frac{g_3^2 - g_1^2}{4 \cos \alpha} \quad (\text{A3-3})$$

$$TAS = \sqrt{\frac{p + \sqrt{p^2 - 4q^2}}{2}} \quad (\text{A3-4})$$

V_w , the wind strength, may be determined as:-

$$V_w = \left| \frac{q}{TAS} \right| \quad (\text{A3-5})$$

This is clearly demonstrated in the reference to be a valid method, the box-pattern method uses three rather than two speeds (giving greater opportunity for error in an individual datum to be reduced by calculation) and also does not present the risk of inadvertently appearing to declare an emergency posed by the triangular method, it is however considered less efficient than the racetrack method for the following reasons:-

- Being reliant upon magnetic heading, the box-pattern method requires a currently calibrated compass, which is not a requirement of the racetrack method where GPS headings are used. Most microlight aircraft, whilst fitted with a magnetic compass, do not have them calibrated.
- Again, three legs are flown rather than two, so requiring a greater minimum time to fly than the racetrack method.
- It is more efficient to make use of methods that can be used unsupervised by pilots without deep technical training. Any method which reduces the amount of calculation, and thus potential for error introduction, is preferred.

A further variation upon this method was published by the National Test Pilots School (NTPS) at Mojave, California in reference [128] and in turn appears to be based upon reference [129]. This method is similar, but does not require any of the headings to use any particular value. The strengths and weaknesses applied to the method published by Lowry will also apply to this method except that it is based upon GPS ground track (rather than compass heading) and therefore any errors due to inaccuracies in the compass are eliminated.

The ground course method

The ground course method (also sometimes called the range-course or speed-course method) is a variant upon (and predecessor of) the racetrack method given above. Instead of using GPS to provide truth data, the aircraft was flown overhead two points on the ground which were in-line with the wind heading. This was used worldwide for many years, and prior to the advent of GPS was one of only three common methods available (the others being a trailing static and use of a chase aircraft with previously calibrated instruments). It is mentioned here for completeness, and because it is sometimes still used, primarily by test centres where it has become a familiar tool. Assuming the availability of suitable landmarks and the guarantee of empty airspace between them, this method has one major disadvantage. To accurately time between points, it is necessary to fly comparatively low (normally below 500 ft). Except in particularly unusual circumstances, such as over open sea with no significant land masses for a considerable distance into wind, air at this low level will be comparatively turbulent. This turbulence makes accurate control over the aircraft difficult, and also can cause fluctuations in pressure instrument readings. The consequence is greater scatter in the data, requiring acceptance of either a lower confidence in the results, or many tests at each condition to allow scatter to be reduced sufficiently during data reduction.

The earliest known publication describing the use of the ground course method is reference [130], which also shows the data reduction methods used in this technique. Although clearly not a recent paper, the method published therein is consistent with that used up until the advent of inexpensive GPS units.

A4 Methodology for Spin-Testing of Microlight Aeroplanes.

Section 4 to this thesis describes the general philosophy and practice reached in the course of this research concerning the spin-testing of microlight aeroplanes. However, in practice, what is important to the Engineers and Pilots conducting a spinning assessment is the minutiae of planning, conducting and reporting a spinning trial. This section (based partly upon reference [78]) describes much of this important detail, additionally to which several sample spinning test grids are presented, as are summaries of the conduct and results of a number of spinning assessments carried out.

Executing a spinning trial

The worst case for both entry and recovery will normally be with the CG at its aft limit. Therefore, tests shaded in the grids below should initially be carried out at the forward CG limit, then mid CG and finally at aft CG before progressing further. Later tests need then only be flown at aft CG. This approach is time-saving but only valid because the worst case spin and recovery are being sought out; trials of an aircraft to be approved for deliberate spinning will necessarily be more rigorous in exploring every possible combination.

Each spin mode should always be executed at least twice (once left once right). However, more spins are often required simply to record everything – see under “the flight” below.

If the testing is to be carried out by more than one pilot, the later pilot should not launch straight into the most “high risk” areas of the programme already flown, they should always repeat some of the more basic spins for familiarisation first.

Depending upon aircraft, between 10 and 20 spins per flight is normal. The deciding factor is a combination of available climb rate, and height loss per

spin; the greatest proportion of time during a spinning sortie is in the climb before and between spinning, not the spins themselves.

Turbulence must be light or nil, to prevent inadvertent disturbance with the stall.

There must be a clear horizon and clear sight of the ground. Without this, the pilot lacks a clear visual reference during the spin or spin recovery.

It must be possible to climb to at least 5,000 ft (preferably higher) without the cloud layers being such that there is any risk of descending through cloud or losing a horizon reference.

Under no circumstances must spinning be carried out over any human habitation. This is a requirement for safety to third parties.

If there is tolerance on the flying controls settings, the controls must be set to give the lowest permitted range of movements. If the aircraft proves spin resistant, this should be changed to the widest permitted range and the tests repeated.

Because of the risk of engine failure during the spin, if an electric starter is fitted it must be ensured that the battery is fully charged. An engine which requires external action to start (for example by prop swinging) will necessitate all spinning being flown in glide range of an airfield suitable for landing and a radio powered independently of the engine driven power supply.

Because spinning tends often to be flown above broken cloud (in which case, pilots will always enter spins above large “holes”) there is a significant risk of a loss of locational awareness. For this reason use of a GPS or other radio location device (e.g. a VHF radio incorporating a VOR receiver) has been found highly advantageous.

Abandonment / BRS deployment criteria must be well understood and briefed before the flight. A typical brief for a 7,000 ft spin entry might be a return to

standard entry and recovery if not recovered by 5,000 ft, door release (which might assist spin recovery) by 4,000 ft, and abandonment at 3,000 ft.

Sample test grid – Simple flapless aeroplane

Table 18 was originally developed for use with the X'Air Mk.1 aeroplane (See Appendix B9), but with slight modifications has proven suitable for other types. Despite the relative simplicity of the aircraft and that the aircraft will not be approved for deliberate spinning, a large number of spins (a minimum of 48) are required, which with some repetition and a mean rate of 15 spins per 1 hour sortie, equates to around 5 flying hours to complete the spinning assessment. Whilst progressing from initial quarter or half turn incipient spins to a maximum of 2 turns, also both mishandled spins and mishandled recoveries are flown. No more than one aspect of mishandling at a time is considered – given that the spin entry itself may be considered in service to be a result of mishandling, this is equivalent to the systems engineering philosophy of considering the single or double failure case, but not greater numbers of simultaneous failures (or in this case, simultaneous mishandling).

The shaded area of the grid indicates the range of spin entries which may be attempted. The progression of test is that this section is attempted firstly at fwd CG, then repeated at mid CG, then finally completed at aft CG. If after completion of this section a spin has not been induced, and it is confirmed that testing was carried out with the elevator set to give the greatest nose-up pitch authority available, and rudder to give the greatest rudder authority available, then the aircraft may be considered to be spin-resistant [131]. However, this is extremely rare; in the course of this research the only aircraft found fully spin-resistant was the 2-axis controlled HM 1000 Balerit; if a spin has been achieved, then the rest of the test-grid is completed.

Table 18. Test grid for a simple flapless aeroplane

Spin No.	No. turns			Entry		Mishandled Spin				Mishandled recovery		
	$\frac{1}{4}$ - $\frac{1}{2}$ turn	1 turn	2 turns	std entry	Entry from steep turn	$\frac{1}{2}$ in-spin aileron	$\frac{1}{2}$ out-spin aileron	Cruise Power	Full Power	Stick held back	Full power	Full opposite rudder held in
(a)	(b)	(c)	(d)	(e)	(f)	(g)	(h)	(i)	(j)	(k)	(l)	(m)
#1	X			X								
#2		X		X								
#3			X	X								
#4		X			X							
#5		X			X			X				
#6		X		X				X				
#7		X		X					X			
#8			X	X					X			
#9		X		X			X					
#10		X		X		X						
#11			X	X						X		
#12			X	X								X
#13		X		X							X	
#14			X		X			X				

Minimum: 48 spins.

Sample test grid – High power flapped aeroplane.

The less simple 3-axis microlight aeroplanes, such as for example the Pegasus CT2K (See Appendix B15), tend to combine relatively high power and wing loading, with the use of high-lift devices (normally flaps) to bring V_{so} down within the 35 kn CAS threshold required for certification.

For such an aircraft, a more complex test grid, is necessary, although in order to keep the size of the test programme in proportion it becomes necessary to pick a representative and “role relatable” sample of possible conditions, since flying a full test grid, covering every conceivable condition, would be an unnecessary programme expense; nonetheless, up to 80 spins is not unusual for such a programme. The following, in a similar format, is an example, which was used for flight testing of the Sky Ranger (UK) aircraft (in this case, there is no “spin resistance” evaluation, since the aircraft was already known to spin from data in other countries – although no formal evaluation had taken place. However, repetition of tests 1-6. in a similar manner to that shown in **Table 18** above was used as indicated to move from the initial “safer” forward CG position, towards the aft position where the majority of testing was carried out.

Table 19. Test grid for a simple flapped aeroplane

	Configuration			No. Turns		Entry		Spin Mishandling				Recovery Mishandling		
	CR	TO	L	1	2	Std	Turn	½ in- spin ailer on	½ out- spin ailer on	Cruise Power	Max Cont. Power	Stick held back	Full power	Full oppos- ite rudder held in
#1	X	X		X		X								
#2	X	X			X	X								
#3	X			X			X							
#4	X			X			X			X				
#5	X			X		X				X				
#6				X		X					X			
#7	X				X	X					X			
#8	X					X			X					
#9	X			X		X		X						
#10	X				X	X						X		
#11	X				X	X								X
#12	X			X		X						X		
#13	X				X		X							
#14			X	X		X								
#15			X	X		X								
#16		X		X		X								
#17			X		X	X								

Equipment required during spinning trials.

The following have been found useful and are recommended equipment for any pilot / FTO engaged in spin testing. Some parts of this list are normal flight equipment in any case, others are intuitively less obvious.

A kneeboard. This is for purposes of both data recording and informing the pilot of the order of tests – it is vital that all planning is completed on the ground. A particular format of test card has been found particularly useful in addition to this, an example of which is shown in **Figure 81**.

Figure 81. Sample kneeboard test card for spinning tests

Falcon 2 Spinning Flight: <u>3</u> No: <u>5</u> <i>Dewhurst / Gratton 516199</i>		A standard card like this can be very useful, reproduced in a photocopier and then altered by hand for each test point. Always fly with spares.
Fuel: <u>45 L</u> Weight : <u>420 kg</u> CG: <u>MCD</u>		
Vs: 23 kn Vne: 92 kn Max 6,800 rpm		Text and spaces kept large
Mode: Left / Right		Basic limitations are useful
Entry: Standard / 60° turn		
Power: Idle / Cruise (5,000) / Max		Use of standard lists to prevent omissions.
No. Turns: 1/2 / 1 / 2		
Recovery: Central / Opposite rudder		
h1: <u>6,700</u> h2: <u>5,800</u> (1013 set!)		It isn't possible to get all the data each spin. Test repetition is often necessary.
time of spin: _____		Room left for comments.
time to recover: <u>4 s.</u>		
actual Vs: _____		
<u>Comments</u>		
<i>ABOUT 5 dall FWD STACK FORCE NO TENDENCY TO REVERSE SPM ABOUT 3q IN RECOVERY</i>		

A voice recorder. The easiest way to do this is to use a small sound recorder attached to a small microphone or magnetic coil pickup inserted inside the earpiece of the pilots helmet or headset.

A stopwatch. Perception of time during a spin by pilots and observers is very unreliable, and a stopwatch allows reasonable determination of the duration and rate of spins.

A fuel burn .v. W&CG plot for the aircraft as it will be flown. This allows determination of weight and centre of gravity for each test point, and inadvertent excursions beyond the normal safe iterative progression of test can be avoided.

A radio. This is for two reasons; firstly large and rapid changes in height can create a hazard to other air traffic, and thus other airspace users should be informed via ATC. Secondly, engine failures during the spin are not

uncommon, particularly with the non-aerobatic engines normally fitted to this class of aircraft. Thus, the risk of a need to “land-out” and possibly request assistance in recovery of the aircraft should be accounted for.

A hard shelled helmet. Although, in general, spin characteristics of microlight aircraft are non-oscillatory, some can be, and head injuries possibly incapacitating the pilot, can result. (Notwithstanding this recommendation, some aircraft have proven not to have enough cockpit room for a helmet, and a degree of risk may need to be accepted in the name of pragmatism).

A four or five point harness, a 3 point harness or lapstrap is not sufficient. This is for similar reasons to the requirement for a hard-shelled helmet above, and also because lateral accelerations tend often to try and force the pilot sideways from his seat; this can restrict his or her ability to properly control the aircraft unless fully restrained.

A g-meter (it is not unusual for the normal acceleration limit to be approach or occasionally exceeded during spin recovery, particularly with power) located in the cockpit as near as possible to the CG.

Some assessors [132] have found that a small **video camera**, mounted in the rear of the cockpit and showing the “forward view” and main instruments is helpful as an aid to later analysis. This must, be well secured and able to withstand at least 9g forward load, 4.5g downward load and 3g sideward load. (These are standard crash-integrity loads contained within BCAR Section S).

Experience has not shown that force gauges and tape measures are particularly useful during spin testing.

This is in addition to all normal flight equipment and either personal parachutes or a Parachute recovery system fitted to the aircraft (reference [133] also see **Figure 82**). If personal parachutes are to be used, the crew must satisfy themselves that they can exit the aircraft if required, and practice this on the ground.

The use of “spin-chutes” has not generally been regarded as a good practice. These are small rapid-opening parachutes located in the tail of the aircraft and designed to rapidly increase directional stability of a rapidly yawing aeroplane in the case of an unrecoverable spin. The problem with their use being that a point mass in the tail of the aircraft will significantly alter the ratio of yawing to rolling inertias, and thus the natural spinning characteristics of the aircraft – effectively negating the purpose of the trial. However, some recent experiences on larger (VLA class) aircraft [134] have not shown significant effects from the fitment of a spin chute – so there may be scope for their use, subject to confirmation following the main testing that there is no significant change in spinning characteristics. A preferred approach is nonetheless to make use of a “whole aircraft recovery parachute” such as shown in **Figure 82** below; this has two advantages, one is that it is relatively easy to fit internally to the aircraft (thus not affecting the external aerodynamic shape), the other is that it can readily be mounted close to the aircraft CG, thus having negligible affect upon the A/B ratio.

Figure 82. Photographs of a whole-aircraft recovery parachute being deployed

(A) Photograph from below of deployment from Eagle microlight aeroplane



(B) Photograph from above of deployment from Cessna 150 light aeroplane



Photographs above courtesy of BRS Inc.

Summary of results from test programmes.

Numerous test programmes have been flown since a spinning evaluation became mandatory in the United Kingdom on new microlight aircraft types. Since spin testing up until that change in requirement was an unknown factor, the microlight flight testing community under technical leadership of the author has shared data and aimed to achieve a common approach and level of rigour in this testing.

Results from several test programmes upon representative aircraft are given in the table below.

Table 20, Summary of known spinning test results

Type: Easy Raider (Jabiru 2200 engine)	Tests Conducted By: BMAA	No. Spins Flown: 24
Entries examined: Standard, turning (x configs CR, TO (15° Flap), LAND (40° Flap))		
Power settings considered: Idle, PLF, MCP		
Spin mishandling considered: in-spin aileron, out-spin aileron		
Basic spin recovery: Centralised.		
Mishandled recovery cases considered: None.		
General points of interest: Reduction in power prior to recovery from power-on spins, caused a marked nose-down change in apparent attitude.		
Where flap was selected during the spin, although it did not impede recovery, it was found necessary to raise the flaps immediately after recovery so as to avoid exceeding V_F during the resultant spiral dive.		

Type: Escapade (Tailwheel, Jabiru 2200 engine)	Tests Conducted By: BMAA	No. Spins Flown: 60
Entries examined: Standard, turning (x configs CR, TO (15° Flap), LAND (40° Flap) [All with doors on and off].		
Power settings considered: Idle, PLF, MCP		
Spin mishandling considered: in-spin aileron, out-spin aileron		
Basic spin recovery: Centralised.		
Mishandled recovery cases considered: Opposite rudder, stick held back, full power		
General points of interest: With in-spin aileron aircraft recovered immediately to a spiral dive. Back-stick recovery was immediate but accompanied by rapid pitch-up. Power-on during recovery did not delay recovery but caused aircraft to approach V_{NE} or V_{FE} during pull-out. Doors did not significantly affect spinning characteristics, but did markedly change cockpit environment during the spin. Use of opposite rudder recovery caused large yawing motion in direction of rudder application accompanied by severe pitch up. Tailwheel results were read-across to nosewheel aircraft without further testing.		

Type: Murphy Maverick	Tests Conducted By: PFA	No. Spins Flown: 42 attempts
Entries examined: Standard, turning		
Power settings considered: Idle, PLF, MCP		
Spin mishandling considered: Aircraft would not establish a developed spin, therefore no cases could be attempted.		
Basic spin recovery: Centralised.		
Mishandled recovery cases considered: Stick held back, pro-spin rudder kept in.		
General points of interest: Aircraft's stall was indicated by a coupled roll:yaw oscillation before full back-stick, with no pitch break and full control in all axes (other than the oscillation) remaining.		

Type : MXP740 Savannah	Tests Conducted By: BMAA	No. Spins Flown: 30
Entries examined: Standard, turning		
Power settings considered: Idle, PLF, MCP		
Spin mishandling considered: Ailerons (½ in-spin, ½ out-spin)		
Basic spin recovery: Centralised.		
Mishandled recovery cases considered: Opposite rudder,		
General points of interest: Would only spin with power selected and closing the throttle always caused recovery to a spiral dive.		

Type: Thruster T600N (Jabiru engine)	Tests Conducted By: Thruster Air Services	No. Spins Flown: 72
Entries examined: Standard		
Power settings considered: Idle, PLF		
Spin mishandling considered: in-spin aileron, out-spin aileron		
Basic spin recovery: Throttle closed, controls centralised		
Mishandled recovery cases considered: None.		
General points of interest: Aileron tended to affect rate of descent, from 30A5-400 ft for 1-turn + recovery with in-spin aileron, 40A5-500ft with ailerons neutral, and 50A4-100ft with out-spin aileron. Aircraft would not spin to the left, left entries resulted in an immediate spiral dive.		

Type: X' Air Mk.1 (Rotax 582 engine)	Tests Conducted By: BMAA	No. Spins Flown: 32
Entries examined: Standard entry, turning entry.		
Power settings considered: Idle, PLF, MCP.		
Spin mishandling considered: Power only.		
Basic spin recovery: Controls central, throttle closed		
Mishandled recovery cases considered: Opposite rudder, throttle closed.		
General points of interest: At fwd CG / idle the aircraft displayed what was termed a spin, but was probably a forced yawing motion, at about 8 seconds per revolution,		

this was sometimes accompanied by a 2A5-40° / 3-4s pitch oscillation. With increased power and further aft CG the aircraft was more ready to spin, but always then self-recovered to a spiral dive within 1½ turns.

Type: X' Air Mk.1 (Jabiru 2.2L engine)	Tests Conducted By: BMAA	No. Spins Flown: 26
Entries examined: Standard, turning		
Power settings considered: Idle, PLF, MCP		
Spin mishandling considered: Ailerons (½ in-spin, ½ out-spin)		
Basic spin recovery: Centralised.		
Mishandled recovery cases considered: pro-spin rudder, PLF remaining, stick kept aft		
General points of interest: Very slow (8-9 secs per turn), every recovery action led to a spiral dive.		

Type: X' Air Mk.2 (Rotax 912 engine)	Tests Conducted By: BMAA	No. Spins Flown: Approx. 50
Entries examined: Standard, turning. (Crossed against configs CR, TO, LAND, flaps were not retracted during recovery).		
Power settings considered: Idle, PLF, MCP		
Spin mishandling considered: ½ in-spin aileron, ½ out-spin aileron,		
Basic spin recovery: Controls centralised		
Mishandled recovery cases considered: Stick held back, power left on, opposite rudder held in.		
General points of interest: At fwd CG aircraft refused to enter a spin, at mid it would do so, but tended to self-recover within 1 turn into a spiral dive. At aft CG, recovered to a spiral dive immediately upon recovery action. Increased power tended to increase the rapidity of entry. In-spin aileron increased the rotation rate and apparent stabilised speed. Out-spin aileron slowed the rotation rate (to about 10s per turn) and gave a slowed apparent stabilised speed. Flap setting had no apparent effect on spin mode or recovery, but reduced height loss per turn from about 400ft to 250ft. Care was required however to avoid exceeding V_F		

during the recovery.

Type: HM1000 Balerit	Tests Conducted By: BMAA	No. Spins Flown: 12
Entries examined: Rudder (Yoke) doublets at low speed, stalls off shallow and steep turns,		
Power settings considered: Idle, PLF, Full Throttle		
Spin mishandling considered: -		
Basic spin recovery: -		
Mishandled recovery cases considered: -		
General points of interest: The aircraft, which uses “Flying Flea” style 2-axis controls proved wholly spin-resistant.		

Type: Sky Ranger 912	Tests Conducted By: BMAA	No. Spins Flown: 89
Entries examined: Standard, turning. (Crossed against configs CR, TO, LAND, flaps were not retracted during recovery).		
Power settings considered: Idle, PLF, MCP		
Spin mishandling considered: ½ in-spin aileron, ½ out-spin aileron,		
Basic spin recovery: Controls centralised		
Mishandled recovery cases considered: Stick held back, power left on, opposite rudder held in.		
General points of interest: Controls centralised recovery was effective in every case; however, where the stick was held fully back (mishandled recovery case), the recovery was delayed by a further ¼-½ turn at about 60°/s (reduced rotation rate) unless some opposite rudder was applied.		

The data above, summarising as it does the results and conduct of a large number of spinning trials, allows the validity of the method given to be assessed. Any such assessment is inevitably incomplete, since there is no guarantee that a more thorough assessment would not have caused a problem

within the spinning characteristics to be revealed. However, based upon the above data and subsequent operating experience of all of these types once certified, evidence so far is that the method proposed and used was a success. Specifically:-

- No spinning related accident (causing damage to an aircraft or injury to a crewmember) occurred during any of these test programmes.
- All of these test programmes were completed in at-most 3 working days, and none required any permanent modification to the aircraft in the form of the fitment of trials equipment.
- In each case the “controls centralised” spin recovery actions were effective with 100% success.
- None of these types have suffered any reported spinning accident in subsequent service.

Reporting the results for a spinning trial on an aircraft not intended for aerobatic operation.

Spinning results (similarly to spinning test plans) are particularly well suited to tabular presentation. It has been found by experience that spinning reports best present most information as tables, with prose only being used to describe any handling peculiarities, and conclusions and recommendations.

The most important part of the report is however the recommendations. This will comprise two parts:-

The aircraft recommendations.

The report must state (and support this statement) whether or not the aircraft is acceptable for use as a microlight aeroplane with regard to its spinning characteristics and compliance with BCAR S221. It is assumed in this context that the final form of the report will consider that the aircraft is acceptable.

The manual recommendations

Since the aircraft has been spun, and the spin and recovery characteristics in the final modification state satisfactory, it is necessary to introduce advice into the operators manual about the spin. Bearing in mind that the aircraft is not cleared for deliberate spinning, this wording must be carefully constructed to be sufficiently clear to a pilot with no spinning experience, yet not give the impression that he or she should ever attempt to spin the aircraft. Therefore, the assessing pilot or engineer should recommend in their report, words to be included in the operators manual. These words should be brief but include:-

- A warning that deliberate spinning is prohibited.
- Guidance on how to recognise a spin should one occur.
- A clear explanation of the spin recovery actions, and what should then occur.
- Instructions on what the pilot should do after recovery from the spin.

Excerpt from approved operators manual (Raj Hamsa X' Air Mk.1).

Departures from Controlled Flight.

The Spin. *Deliberate spinning of the X' Air is prohibited. However, it is possible through mishandling of the aircraft to inadvertently enter a spin, either through stalling the aircraft in a turn, or by failing to keep the rudder pedals straight at the point of stall. Should this happen, the spin can be seen by a steep nose-down pitch attitude (about 45° nose down) and the aircraft yawing to one side or the other, some higher than normal 'g' forces may also be experienced. Should this occur, close the throttle and centralise the stick and rudder pedals immediately. The aircraft will stop turning almost immediately and return over about 5 seconds to a normal glide attitude, from which normal flight may be resumed.*

Other Departures. Other departures from controlled flight are likely either to be due to damage to the aircraft, or hazardous flying conditions. In either case, land as soon as possible and examine the aircraft, particularly the flying controls, for any damage..

A5 A timed method for the conservative estimation of take-off distances, eliminating the requirement for external measurement devices.

This method divides the take-off into three distinct segments, the initial ground roll, the post-rotation ground roll, and the climb to screen height. It is based upon times and speeds and does not directly measure distances.

Heights are measured by an observer in the aircraft using a sighting device to the edge of the runway – this relies upon the pilot holding the centreline accurately, and accurate knowledge of the height of the observer above the wheels, location relative to aircraft lateral centreline, and runway width. Since the only height required is the screen height, the device can be as straightforward as a single mark upon a strut or canopy, although two marks in-line or a wire frame have proven most useful.

Complying with normal certification practice, which requires at least 6 data points [135], a minimum of 7 take-offs are carried out, and the results (times, speeds) tabulated. The least favourable 6 results will be taken, a mean of each time and speed value used, then distances calculated as shown below.

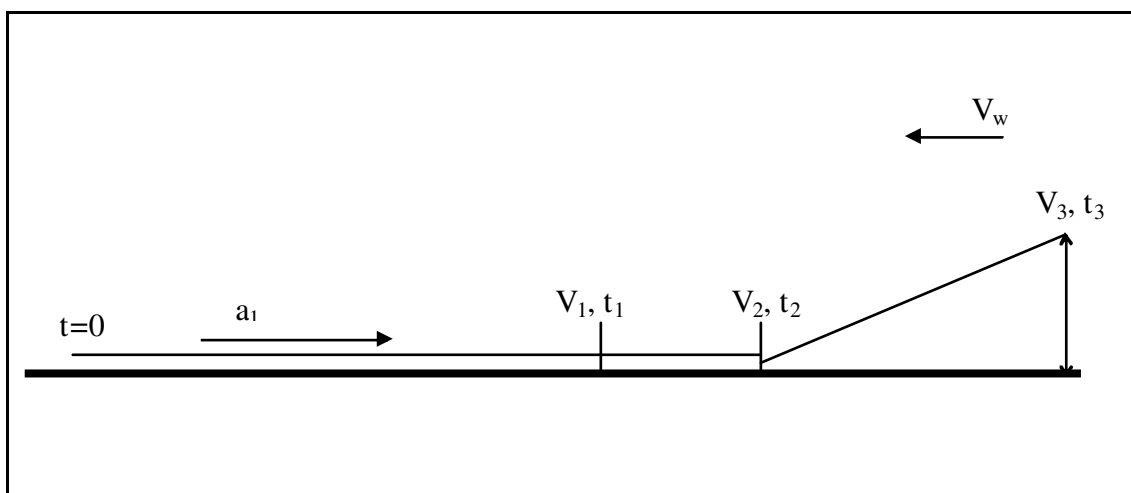
The following assumptions are made in this method:-

- During each segment, aircraft acceleration / deceleration is constant.
- Surface wind is constant between ground and screen height.
- During the air segment, the aircraft climbs in a straight line between the unstick point and screen height (for microlight aircraft particularly

this is a reasonable assumption, since the initial climb condition is established within 5-10ft of the ground, which is small within the 50ft climb to screen height).

- The following notation is used. Speeds at start, rotate, unstuck and screen height are 0, V_1 , V_2 , V_3 respectively. These are known in TAS by reduction from IAS values using determined PEC. Surface wind is V_w and is positive when a headwind. Times of each segment are t_1 , t_2 , t_3 . Note that if the aircraft has a very short distance from rotation to the unstuck point (such as a taildragger taking off in a 3-point attitude), then $t_2=0$, $V_1=V_2$ and the method is reduced to 2-segments. Lengths of each segment, measured along the ground, are S_1 , S_2 , S_3 . Straight line distance from unstuck to top of screen = S'_3 . Accelerations during each segment are a_1 , a_2 , a_3 . a_3 is acceleration along flightpath, not along the ground. Screen height is h . For calculation, all the above will be in consistent SI units (m, ms^{-1} , s).

Figure 83. Illustration of take-off segments



To determine actual length of first (pre-rotation) ground roll segment:-

Assuming that the aircraft is initially stationary

$$S_1 = \frac{1}{2} a_1 t_1^2 \quad (\text{A5-1})$$

$$V_1 - V_w = a_1 t_1 \therefore a_1 = \frac{V_1 - V_w}{t_1} \quad (\text{A5-2})$$

Inserting (A5-2) into (A5-1):

$$S_1 = \frac{t_1}{2} (V_1 - V_w) \quad (\text{A5-3})$$

To determine actual length of second (post rotation) ground roll segment.

$$S_2 = (V_1 - V_w)t_2 + \frac{1}{2}a_2 t_2^2 \quad (\text{A5-4})$$

$$V_2 - V_w = (V_1 - V_w) + a_2 t_2 \therefore a_2 = \frac{V_2 - V_1}{t_2} \quad (\text{A5-5})$$

Inserting (A5-5) into (A5-4)

$$\begin{aligned} S_2 &= (V_1 - V_w)t_2 + \frac{1}{2} \left(\frac{V_2 - V_1}{t_2} \right) t_2^2 \\ &= (V_1 - V_w)t_2 + \left(\frac{V_2 - V_1}{2} \right) t_2 \\ &= t_2 \left(\frac{V_2 + V_1}{2} - V_w \right) \end{aligned} \quad (\text{A5-6})$$

To determine actual length of air segment.

$$S_3^1 = t_3 \left(\frac{V_3 + V_2}{2} - V_w \right) \quad (\text{A5-7})$$

But by Pythagoras:

$$S_3 = \sqrt{S_3^1{}^2 - h^2} \quad (\text{A5-8})$$

And inserting (A5-7) into (A5-8)

$$S_3 = \sqrt{t_3^2 \left(\frac{V_3 + V_2}{2} - V_w \right)^2 - h^2} \quad (\text{A5-9})$$

Total take-off distance to screen height, in actual conditions, is then $S_1+S_2+S_3$, as determined above. Adjustments to standard conditions may be made using the usual variance factors [136].

However, this method does not take account of the errors which inevitably will exist in the variables. It is assumed that each of these factors are accurate to within the precision of recording (which is normally done manually, preferably by a Flight Test Observer (FTO) or exceptionally by the Test Pilot themselves). These precisions are usually taken to be ± 1 second for all time measurements, and $\pm 1 \text{ ms}^{-1}$ (about 2 knots) for all speed values including the headwind component. It is assumed that the height is correct, and that any errors in determining time to height are time errors alone. Using this, it is possible to conduct an error analysis starting with the following equation, which sums (A5-3), (A5-6) and (A5-8) above.

$$S = \frac{t_1}{2}(V_1 - V_w) + t_2 \left(\frac{V_2 + V_1}{2} - V_w \right) + \sqrt{t_3^2 \left(\frac{V_3 + V_2}{2} - V_w \right)^2 - h^2} . \quad (\text{A5-10})$$

Taking partial derivatives with respect to each component of (A5-10) in turn, the following series of factors are obtained.

$$\frac{\partial S}{\partial t_1} = \frac{V_1 - V_w}{2} \quad (\text{A5-11})$$

$$\frac{\partial S}{\partial t_2} = \frac{V_2 + V_1}{2} - V_w \quad (\text{A5-12})$$

$$\frac{\partial S}{\partial t_3} = \frac{t_3 \left((V_2 + V_3)^2 + 4(V_w^2 - V_w(V_2 + V_3)) \right)}{4 \cdot \sqrt{t_3^2 \left(\frac{V_3 + V_2}{2} - V_w \right)^2 - h^2}} \quad (\text{A5-13})$$

$$\frac{\partial S}{\partial V_1} = \frac{t_1 + t_2}{2} \quad (\text{A5-14})$$

$$\frac{\partial S}{\partial V_2} = \frac{t_2}{2} + \frac{t_3^2(V_3 + V_2 - 2V_w)}{4 \cdot \sqrt{t_3^2 \left(\frac{V_3 + V_2}{2} - V_w \right)^2 - h^2}} \quad (\text{A5-15})$$

$$\frac{\partial S}{\partial V_3} = \frac{t_3^2(V_3 + V_2 - 2V_w)}{4 \cdot \sqrt{t_3^2 \left(\frac{V_3 + V_2}{2} - V_w \right)^2 - h^2}} \quad (\text{A5-16})$$

$$\frac{\partial S}{\partial V_w} = \left[\frac{t_3^2(V_3 + V_2 - 2V_w)}{2 \cdot \sqrt{t_3^2 \left(\frac{V_3 + V_2}{2} - V_w \right)^2 - h^2}} + \frac{(t_1 + t_2)}{2} \right] \quad (\text{A5-17})$$

The estimated error due to each individual component will be the factor of that component's assumed error and the take-off distance's partial derivative with respect to that component. However it is also normal practice, based upon the assumption that errors are normally distributed, that the total error may be taken to be the square root of the sum of the squares of errors [137]. Thus, in any individual test, the estimated maximum error may be taken as.

$$\sqrt{\left(t_1 \frac{\partial S}{\partial t_1} \right)^2 + \left(t_2 \frac{\partial S}{\partial t_2} \right)^2 + \left(t_3 \frac{\partial S}{\partial t_3} \right)^2 + \left(V_1 \frac{\partial S}{\partial V_1} \right)^2 + \left(V_2 \frac{\partial S}{\partial V_2} \right)^2 + \left(V_3 \frac{\partial S}{\partial V_3} \right)^2 + \left(V_w \frac{\partial S}{\partial V_w} \right)^2} \quad (\text{A5-18})$$

(Note: combination of errors. Justifying the approach taken above, it is assumed that all errors, e are independent and follow a normal (Gaussian) distribution, with a mean of zero and variance σ^2 , then the sum of errors $\sum e = e_1 + e_2 \dots e_n$ is itself normally distributed with a mean of zero and a variance of $\sum \sigma_n^2$. This means that the standard deviation, which is proportional to the total error is defined by $\sigma^2 = \sum \sigma_n^2$. Written otherwise, this may be stated as Total error = $\sqrt{e_1^2 + e_2^2 \dots + e_n^2}$ which has an identical form

to (A5-18) above. Further examples of this method of combination of errors may be found in reference [138])

So, for a conservative analysis, the take-off distance should be calculated as shown in (A5-10) above. Then, the maximum error should be calculated, using (A5-18) and estimates of the accuracy to which each value was measured, and this added to the estimate for take-off distance. This sum, may then be used as a planning take-off distance value, with high confidence that the actual distance required is no greater than that.

Use of this may be demonstrated using the following worst 6 results for flight tests carried out for an increase in MTOW for the HM1000 Balerit aircraft [139]. The results (using a 2-segment method) were as follows:-

Table 21, Take-off test data for HM1000 Balerit at 420kg.

No.→	1	2	3	4	5	6
t ₁	11	15	15	12.5	14.5	13.5
t ₃	7.5	9	5	6	4.5	4.5
V ₂ , mph IAS	55	55	51	52	58	53
V ₃ , mph IAS	47	47	50	50	50	50
V ₂ , kn CAS (ms ⁻¹ CAS)	47 (24.2)	47 (24.2)	46 (23.6)	46 (23.6)	49 (25.2)	48 (24.7)
V ₃ , kn CAS (ms ⁻¹ CAS)	43 (27.2)	43 (27.2)	45 (23.1)	45 (23.1)	45 (23.1)	45 (23.1)
Mean time to unstuck= 13.6 s Mean climb time = 6.1 s Mean unstuck speed = 24.3 ms ⁻¹ Mean screen speed = 24.5 ms ⁻¹ Screen Height = 15m Surface wind – negligible.						

From (A5-10), the take-off distance is calculated (normally using a spreadsheet programme such as Microsoft Excel) to be 313m of which 165m was ground roll, and then using (A5-18), the maximum error is calculated to be 30m (or ±16%). Assuming that the worst case error applies, the take-off distance for planning may then be taken as 364m. (In practice, the

certification standard and normal working practice [140] requires the use of a 1.3 safety factor (+30%) in any case, which is clearly greater than the greatest predicted error from this test (and from most others); but, were the predicted error greater than that then it is conservative to use this in place of a 1.3 factor). It is most conservative to use both, which is what has become the most common practice.

A simple “reality check” upon this data may be obtained from the runway length and an external observer / camera. In this case the take-off tests were flown from Chilbolton (Stonefield Park) airfield in Hampshire [141], which has a runway length of 411m. A coarse check upon the results was provided by external observers and the pilot who estimated that about 75% of the runway was required to reach the 15m screen height, an observation which is consistent with the estimated distance.

A further check was made when this method was used during flight testing for issue of a Public Transport CofA of a Naval Aircraft Factory N3N-3 Aeroplane[142].

Qty 9 take-offs were flown from Isle of Wight (Sandown) airport, at conditions of 2870 lbf, 8kn headwind (4.1 m/s), no crosswind, 15°C OAT, QFE 1023, 60 ft amsl, short-dry grass. Using the 2-part segmented method (the rotation phase being extremely short, justifying this), the following results were obtained:-

Table 22. Take-off test data for N3N-3 Aeroplane

<u>No.</u>	<u>1</u>	<u>2</u>	<u>3</u>	<u>4</u>	<u>5</u>	<u>6</u>	<u>7</u>	<u>8</u>	<u>9</u>	<u>Mean</u>	<u>Mean,</u> <u>m/s</u> <u>CAS</u>
t ₁ , s	14.5	15	13.5	13.5	13	13	14	13.5	12.5	13.6	-
t ₁ +t ₃ , s	NR	22	19.5	18.5	20	17.5	19.5	20	19.5	19.6	-
t ₃ , s	-	7	6	5	7	4.5	5.5	6.5	7	6.1	-
V ₁ , mph IAS	52	52	52	52	52	55	53	52	52	52.4	23.6
V ₂ , mph IAS	30	60	60	60	58	60	58	58	57	55.7	25.3

(Headwind component 8 kn)

These values were reduced to calibrated SI units and input to a segmented method analysis model, and gave the following results at the tested conditions (shown to 3sf). Ground roll = 84.2m; Air segment distance = 123m along the ground; Estimated maximum total error in calculation = 46.2m (22.3%); Total conservative calculated take-off distance = 254m.

Verification of this data was performed using video analysis. A fixed video camera was used adjacent to the control tower, and a relationship established between aircraft position and height as seen in the camera, and relative to the runway, by comparing the geometry of 4 points in the field of view (two runway markers, a hangar, and a mid point) with that determined using an airfield plan. The two figures below show the geometry of this, and the relationship used to then relate from the video monitor to estimated values for take-off distance. Not all take-off ground-segments were recorded, due to an misunderstanding between the pilot and cameraman concerning the available field of view, nonetheless, sufficient data was obtained for reasonable verification purposes. From this, the following data were obtained: Ground roll, mean of 5 data points, 127m along the ground; Air segment distance, mean of 9 data points, 108m along the ground; Estimated maximum error, 14m based upon 10m accuracy for each data point; Total conservative take-off distance, 249m. This gives a slightly reduced take-off distance than that from

the timed method, thus the timed method is slightly more conservative. Correlation is fair, in that (before addition of error margins) the timed method gives 207m and the video method gives 235m (14% difference). The more elaborate error analysis of the timed method results in it being the more conservative method

Figure 84. Geometry of Sandown airport as used for N3N field performance estimation (not to scale)

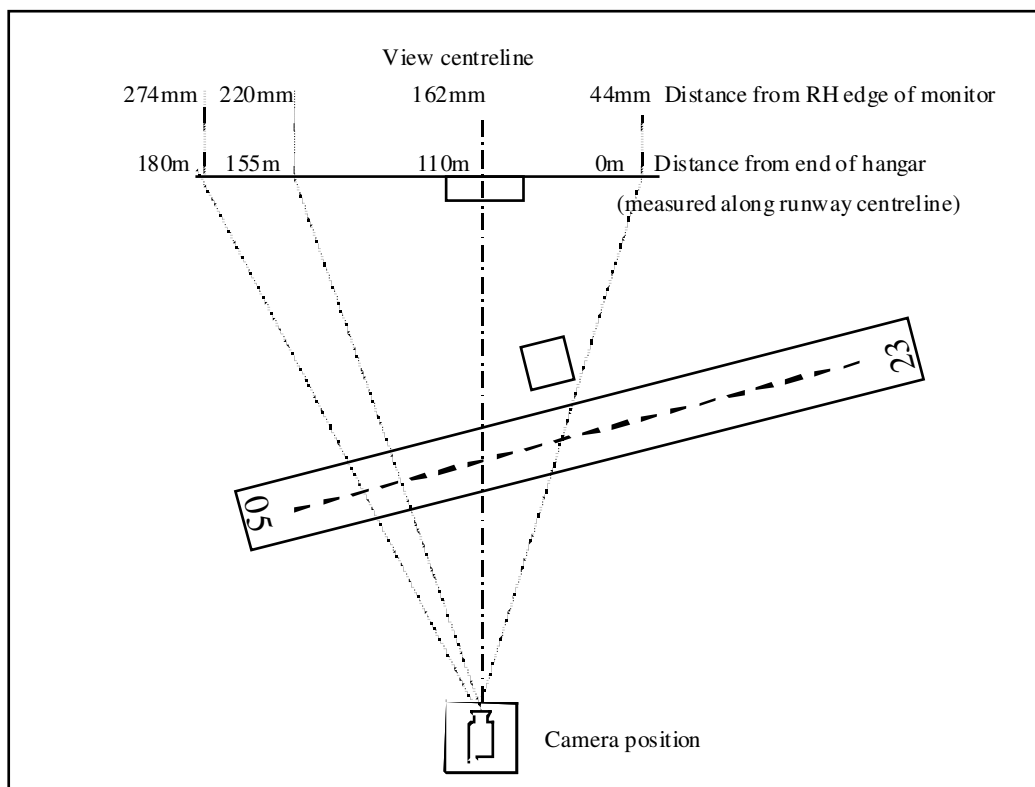
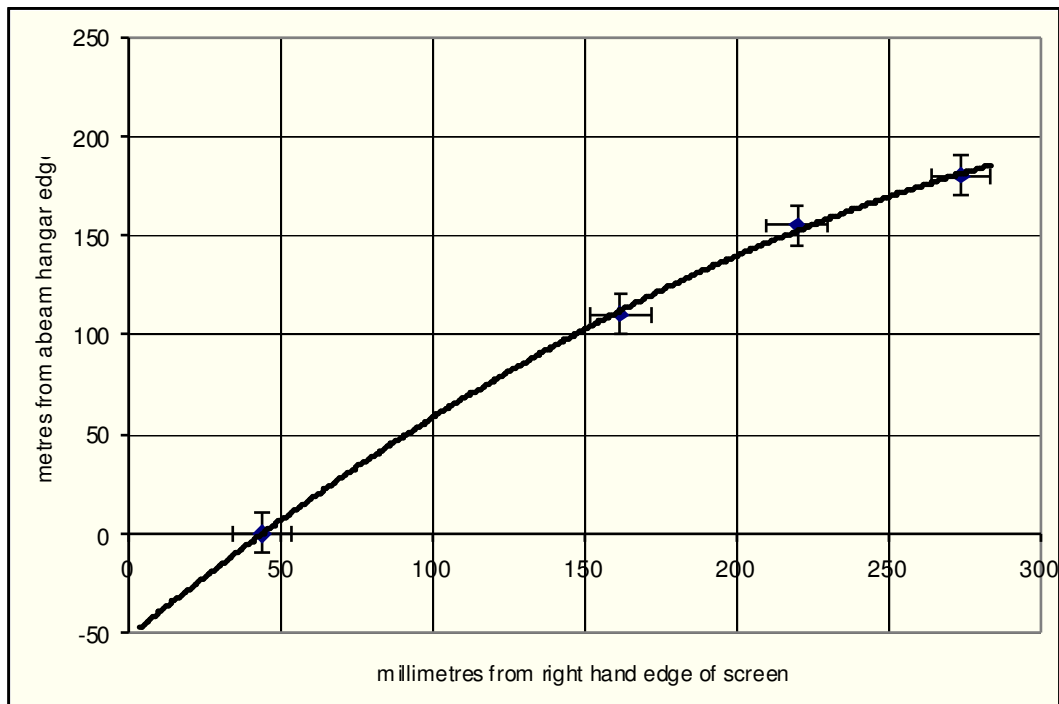


Figure 85. Aerial View of Sandown Airport, in similar orientation to figure above, showing approximate camera position



Figure 86. Chart of distance along runway centreline versus distance across video monitor screen, showing quadratic best fit curve.



A6 A timed method for the conservative estimation of landing distances, eliminating the requirement for external measurement devices.

Similarly to the method used for take-off distance estimation above, landing distances may also be estimated. In this case, the following notation is used: Speeds at screen height, touchdown, 3-wheels down, and stop are V_1 , V_2 , V_3 and 0 respectively. Surface wind is V_w and is positive when a headwind. The difference in V_w effect due to flightpath angle is assumed to be small. Times of each segment are t_1 , t_2 , t_3 . Note that in the case of a taildragger making a 3-point landing or other aircraft with an insignificantly short 2-wheel roll), then $t_2=0$ and the method is reduced to 2-segments. Lengths of each segment, measured along the ground, are S_1 , S_2 , S_3 . Straight line distance from top of screen to touchdown = S'_1 . Accelerations during each segment are a_1 , a_2 , a_3 . a_1 is acceleration along flightpath, not along the ground.

The total landing distance may be given by:-

$$S = \sqrt{t_1^2 \left(\frac{V_2 + V_1}{2} - V_w \right)^2 - h^2} + t_2 \left(\frac{V_3 + V_2}{2} - V_w \right) + t_3 \left(\frac{V_3 - V_w}{2} \right) \quad (\text{A6-1})$$

Similarly to the take-off case, it's essential to conduct an error analysis. This gives the following results:-

$$\frac{\partial S}{\partial t_1} = \frac{t_1 \left((V_2 + V_1)^2 - 4V_w^2 \right)}{4.2 \sqrt{t_1^2 \left(\frac{V_2 + V_1}{2} - V_w \right)^2 - h^2}} \quad (\text{A6-2})$$

$$\frac{\partial S}{\partial t_2} = \frac{V_3 + V_2}{2} - V_w \quad (\text{A6-3})$$

$$\frac{\partial S}{\partial t_3} = \frac{V_3 - V_w}{2} \quad (\text{A6-4})$$

$$\frac{\partial S}{\partial V_1} = \frac{t_1^2(V_1 + V_2 - 2V_w)}{4.2\sqrt{t_3^2\left(\frac{V_3 + V_2}{2} - V_w\right)^2 - h^2}} \quad (\text{A6-5})$$

$$\frac{\partial S}{\partial V_2} = \frac{t_1^2(V_1 + V_2 - 2V_w)}{4.2\sqrt{t_3^2\left(\frac{V_3 + V_2}{2} - V_w\right)^2 - h^2}} + \frac{t_2}{2} \quad (\text{A6-6})$$

$$\frac{\partial S}{\partial V_3} = \frac{t_2 + t_3}{2} \quad (\text{A6-7})$$

$$\frac{\partial S}{\partial V_w} = \left[\frac{t_1^2(V_1 + V_2 - 2V_w)}{2.2\sqrt{t_3^2\left(\frac{V_3 + V_2}{2} - V_w\right)^2 - h^2}} + t_2 + \frac{t_3}{2} \right] \quad (\text{A6-8})$$

Below is actual test data for an HM 1000 Balerit aircraft.

Table 23, Landing test data for HM 1000 Balerit at 420kg

<u>No.→</u>	<u>1</u>	<u>2</u>	<u>3</u>	<u>4</u>	<u>5</u>	<u>6</u>
t ₁	7	11.5	10	13.5	12	13.5
t ₃	43	20.5	28	26.5	25	29
V ₁ , mph IAS	50	53	48	50	50	55
V ₂ mph IAS	46	37	41	45	37	37
V ₁ , kn CAS (ms ⁻¹ CAS)	45 (23.1)	48 (24.7)	44 (22.6)	45 (23.1)	45 (23.1)	47 (24.2)
V ₂ , kn CAS (ms ⁻¹ CAS)	43 (22.1)	38 (19.5)	41 (21.1)	42 (21.6)	38 (19.5)	38 (19.5)
[The aircraft was stopped on the ground using moderate braking once at a fast walking pace].						
Mean time to from screen height to touchdown: 11.25						
Mean time to stop = 28.7 s						
Mean speed at screen height = 23.5 ms ⁻¹						
Mean touchdown speed = 20.6 ms ⁻¹						

Using this data, a total landing distance is derived of 364m, and a maximum estimated error of 54m (or 15%). This gives a total distance of 418m. Again this test was flown at Chilbolton with a 411m runway, and the pilot estimated

that the aircraft was stopped in about the full length of the runway – having descended through screen height before the threshold. In this case, the conservative estimate using this method matches well the visual estimate.

As for take-off distances (section A5), an opportunity also arose to use this method, and verify data using an external video source during testing of a Naval Aircraft Factory N3N-3 Aeroplane . The following test data was obtained.

Table 24, Landing test data for N3N-3 Aeroplane

<u>No.</u>	<u>1</u>	<u>2</u>	<u>3</u>	<u>4</u>	<u>5</u>	<u>6</u>	<u>7</u>	<u>8</u>	<u>Mean</u>	<u>Mean.</u> <u>m/s CAS</u>
t ₁ , s	15	13	10	10	10.5	8	8	10	10.9	
t ₁ +t ₃ , s	33	34	28	26.5	27.5	24.5	25.5	25.5	28.6	
t ₃ , s	18	21	18	16.5	17	16.5	17.5	15.5	17.6	
V ₁ , mph IAS	65	65	65	67	65	70	65	65	65.3	30.2
V ₂ , mph IAS	50	52	52	52	53	55	53	53	52.1	23.5

(Headwind component 8 kn)

These values were input to a segmented method analysis model, which gave the following results at test conditions. Air segment distance = 212m along the ground; Ground segment distance = 120m; Estimated maximum error = 48.8m (14.7%); Total conservative landing distance = 381m.

Verification of this data was again performed using video analysis and sufficient data was obtained for verification purposes. From this, the following data were obtained: Air segment distance, one data point only, 162m; Ground segment distance, 5 data points, mean 160m; Estimated maximum error, based upon assumed 10m accuracy in data, 14m; Estimated total landing distance, 336m. Thus the timed method is more conservative than the method of video analysis and may be accepted. There is an apparent mismatch between the ground and air segment distances – ground roll is somewhat longer on the video analysis compared to air segment, which is longer on the timed method. This is attributed to the difficulty in identifying the touchdown point from video analysis, nonetheless the total distance before addition of estimated errors (which effectively does not take into account this point) is extremely close (within 3%) and the timed method is made more conservative primarily by the larger value determined by the error analysis for that method.

APPENDIX B

CHARACTERISTICS AND
ILLUSTRATIONS OF THE MAIN
AIRCRAFT TYPES REFERRED TO IN
THIS THESIS

B1 Aviasud Mistral.

The Aviasud Mistral is a French designed 2-seat side-by-side tractor Aviasud configuration biplane with a tricycle undercarriage. Pitch and yaw control are through conventional elevator and rudder, but roll control is through differential movement of the entire lower mainplane.

Maximum permitted take-off weight (MTOW) is 390kg, with a typical empty weight of 190kg. Wing area is 17.9m², and V_{so} is 38 kn CAS.

The aircraft will be fitted either with the Rotax 532-2V engine, or the newer but similar 582/48-2V engine, both generating approximately 48kW maximum power. The Arplast 3-blade ground adjustable propeller of 65" diameter and 7.5° pitch is driven through a Rotax B-type gearbox with 1:2.58 ratio gearset.

The certification basis of the aircraft in the United Kingdom is BCAR Section S (initial working draft) plus some special limitations agreed at the time of approval between the BMAA and CAA.

Figure 87, Aviasud Mistral



B2 Eurowing Goldwing

The Eurowing Goldwing is a single-seat canard pusher aircraft derived from an earlier US design also called the Goldwing. Construction is primarily composite.

Maximum permitted take-off weight (MTOW) is 264kg, with a typical empty weight of 160kg. Total lifting surface area is 12.55m². V_{SO} is 30kn, whilst V_{ne} is 61kn; best glide ratio has found to be about 13:1

The aircraft may be fitted with any of a selection of 25-45 hp engines, driving 2-blade wooden propellers through a belt reduction. The most common engine fitted was the Fuji EC34PM which gives a climb rate of 428 fpm and a maximum level flight speed of about 50 kn.

The aircraft was approved for use in the UK on the basis of partial compliance with the March 1983 working draft of BCAR Section S, combined with operating experience prior to the introduction of mandatory safety regulations.

Figure 88. Eurowing Goldwing fitted with Rotax 377 engine



B3 Easy Raider.

The Easy Raider (formerly known as the Sky Raider II UK) is a derivative of an American single seat aircraft called the Sky Raider. The aircraft is a tandem 2-seat high wing monoplane taildragger with conventional flying controls. The aircraft is fitted with 4-position half span flaps, at 0, 15°, 30° and 40°.

Maximum permitted take-off weight (MTOW) is 450 kg, with a typical empty weight of 200 kg. Wing area is 9.8 m² and V_{so} is 34 kn CAS (full flap), V_{S1} is 36.5 kn CAS. V_{ne} is 115 kn CAS.

In the 503(1) configuration, the aircraft will be fitted with a Rotax 503-2V engine generating about 38 kW. Through a Rotax C-type gearbox with 3:1 gearset, this drives a Powerfin 3 blade composite ground adjustable propeller at 70" x 14°. In the J2.2(1) configuration, the aircraft will be fitted with a Jabiru 2200 engine, generating about 55kW, driving either a composite or wooden 2-blade propeller.

The certification basis is BCAR Section S issue 2, approval was under supervision of the author.

Figure 89. Easy Raider J2.2(1).



Photograph courtesy of Reality Aircraft Ltd

B4 KISS-400

The KISS-400 is a conventional 2-seat tandem weightshift controlled microlight aeroplane. The aircraft is one of a series manufactured by the French manufacturer *Air Creation*.

Maximum permitted Take-Off Weight (MTOW) is 400 kg, with a typical empty weight of 200 kg. Wing area is 13.3m² and V_{so} is 32 kn CAS. V_{ne} is 76 kn CAS.

The aircraft is normally fitted with a Rotax 582/48-2V engine generating approximately 48 kW. This drives an Arplast Ecoprop 170cm x 23° propeller through a Rotax E-type gearbox with 3.47:1 gearset.

The certification basis in the United Kingdom is BCAR Section S issue 2; approval was under supervision of the author.

Figure 90. Air Creation KISS-400



Photograph courtesy of Flylight Airsports

B5 Air Creation iXess

The iXess is a conventional (although relatively high performance) 2-seat tandem weightshift controlled microlight aeroplane. The aircraft is one of a series manufactured by the French manufacturer *Air Creation*.

Maximum permitted Take-Off Weight (MTOW) is 450 kg, with a typical empty weight of 200 kg. Wing area is 15m² and V_{so} is 33 kn CAS, V_{ne} is 84 kn CAS, V_A is 72 kn CAS

The aircraft is normally fitted with a Rotax 912UL engine generating approximately 59 kW. This typically drives an Arplast Ecoprop 166cm propeller through an integral gearbox.

The certification basis of the iXess in the United Kingdom was BCAR Section S issue 3 (which is identical in all technical content to issue 2).

Figure 91. Air Creation iXess



Photograph courtesy of Flylight Airsports Ltd

B6 Mainair Gemini Flash 2 and Flash 2a

The Mainair Gemini Flash 2 and Flash 2 alpha, are similarly conventional tandem weightshift microlight aeroplanes. The manufacturer, Mainair Sports, is based in Rochdale, Lancashire and still trade, although both types are now out of production. Both types are unusual in that the wings do not use “tipsticks” as part of their design. The Flash 2 was first approved in 1986, and the Flash 2a in 1991.

For both types, Maximum Take-Off Weight (MTOW) is 370kg, and wing area is 15.56m². Similarly, for both, V_{so} is 24 kn, and V_{ne} is 77 kn; these are IAS values and PEC are not known, but believed to be small.

Both types are approved for a wide range of powerplants, but a typical installation on either would be a Rotax 462 engine, generating about 40 kW, and driving a Warp Drive 3-blade composite ground-adjustable propeller at 62” diameter and 110° pitch measured at 12” diameter.

Approval of both types was to BCAR Section S Advance issue (March 1983).

Figure 92. Mainair Gemini Flash 2



B7 Mignet HM1000 Balerit.

The Mignet HM 1000 Balerit is a bi-wing pusher aircraft, with side-by-side twin seating. The aircraft is designed on the “Flying Flea” principle, in that pitch control is effected by varying incidence of the forward wing, and roll control is through secondary effect of yaw – the yoke drives the rudder, and there is no primary roll control.

The maximum permitted take-off weight is 406kg, wing area is 17.55 m², V_{so} is 39 kn CAS, V_{ne} is 77 kn CAS.

The aircraft as approved in the UK will be fitted with a Rotax 582/48-2V engine, which through a 3.5:1 belt reduction drives a 4 blade Cadeillan wooden propeller at 61” x 55”.

UK certification was originally to BCAR Section S issue 1 in 1994 with an MTOW of 390kg, but the type was subsequently re-certified at the higher weight of 406 kg to BCAR Section S issue 2 in 2001-2002.

Figure 93. Mignet HM1000 Balerit



B8 CFM Shadow

The CFM Shadow which comes in a number of variants is a British developed high wing tandem pusher aeroplane. All discussion here is of the Shadow CD and Shadow DD which are dual controlled microlight versions.

The Shadow CD has an MTOW of 374kg, a wing area of 15m², V_{so} is 35 kn IAS, V_{NE} is 94 kn IAS. The Shadow DD has an MTOW of 386kg, a wing area of 15.5m², V_{so} is 36 kn IAS and V_{NE} is 108 kn IAS. In both versions the ASI overreads by approximately 20% at high speeds.

As approved in the UK, the Shadow CD will normally be fitted with a Rotax 503-2V engine, generating about 55 hp driving a 52" 3 blade wooden propeller through a 2.58:1 Rotax gearbox. The Shadow DD will normally be fitted with a Rotax 582/48-2V engine generating about 65hp and also driving a 52" 3 blade wooden propeller through a 2.58:1 Rotax gearbox.

The Shadow CD was approved to BCAR Section S advance issue (1983). The Shadow DD was approved to BCAR Section S issue 1.

Figure 94. Shadow CD



B9 Raj Hamsa X' Air Mk.1 and Mk.2. (Falcon)

The Raj Hamsa X' Air Mk.1 is a derivative of the AX3, which itself is a French derivative of the Weedhopper – one of the earliest fixed wing microlight aeroplanes. The configuration is high wing, mid-tail, with a tractor engine and side-by-side seating. Control is through conventional ailerons, elevator and rudder. The aircraft is not fitted with flaps.

The X' Air Mk.2 (Falcon) is a derivative of the X' Air Mk.1. The tail structure is stiffened and the rear fuselage cone extended further aft. Most significantly however, the wing section is altered, wingspan reduced and half-span flaps introduced (requiring redesign of the aileron circuit).

Both aircraft have a Maximum Authorised Take-Off Weight of 450 kg. For the Mk.1, wing area is 16m², Vne is 83 kn CAS and Vso is 32.6 kn CAS. For the Mk.2 wing area is 14.3 m², Vne is 85 kn CAS and Vso is 35 kn CAS.

As approved in the UK, an X' Air Mk.1 is most likely to be fitted with a Rotax 582/48-2V engine generating 48kW, and a 65" Ivoprop propeller driven through a Rotax B-type gearbox with 2.58:1 ratio gearset. An X' Air Mk.2 is most likely to be fitted with a Jabiru 2200 engine generating 50kW and a 64" Arplast ecoprop direct-drive propeller.

Both aircraft are certified in the UK to BCAR Section S issue 2.

Figure 95. Raj Hamsa X'Air Mk.1 (UK) with Rotax 582/48-2V engine and Ivoprop propeller



B10 Southdown (now Medway) Raven-X.

The Southdown Raven-X (later manufactured by Medway Microlights) is a conventional 2-seat weightshift controlled microlight aeroplane. The aircraft is part of a family, and shares a trike with the earlier *Puma Sprint*, and a wing with various other “Raven” aircraft such as the *Hybred 44XL-R* and the *EclipseR*.

The aircraft has a Maximum Authorised Take-Off Weight (MTOW) of 367kg and a wing area of 15 m². V_{ne} is 87 kn and V_{so} is 30 kn (both are IAS values, and PEC are not known, but believed to be small).

A typical example of this aircraft might be fitted with a Rotax 447-1V engine generating about 31kW, driving a 3 blade 60”x9° Ivoprop through a Rotax A or B type gearbox using a 2.58:1 ratio gearset.

Certification of the type was to BCAR Section S advance issue of March 1983.

Figure 96. Southdown Raven-X with Rotax 447 engine.



B11 Spectrum T1

The Spectrum T1 is a two-seat tandem 3-axis tractor aeroplane of “fuse-tube” type construction. The type was developed from scratch in the UK in the mid 1980s.

The aircraft has an MTOW of 375kg, and a wing area of 15m². Vne is 83 kn CAS, Vso is 35 kn IAS, which is believed to be close to kn CAS.

Examples of the aircraft are fitted with Rotax 503-1V or -2V (34 or 37 kW) engines, driving a 2-bladed wooden 65” x 38” propeller or a 3-blade 62” Ivoprop composite propeller through a 2.58 reduction.

The aircraft was certified to BCAR Section S Advance copy (1983).

Figure 97. Spectrum T1



B13 Thruster TST Mk.1 and Thruster T300

The Thruster TST Mk.1 is a 2-seat side-by-side conventional tractor aeroplane derived from an Australian single seat aircraft also called the Thruster. The T300 is a very similar development of the earlier TST. Both variants are semi-open cockpit, with dual controls, and are taildraggers. The TST was the first 2-seat 3-axis training aeroplane readily available on the UK microlight market.

Both have an MTOW of 361kg which is commonly increased to 380kg by the addition of aerofoil section wing struts. Wing area is 25m². Both aircraft have a Vne of 80 kn, and a V_{S0} of about 35 kn.

The Thruster TST is normally fitted with a twin carburettor Rotax 503-2V engine generating about 55 hp; this will drive one of a wide range of 2 or 3-blade propellers through a 2.58:1 Rotax gearbox. The Thruster T300 may use this engine, or more commonly a Rotax 532-2V or 582-2V engine (the latter was a direct replacement for the former) generating about 65 hp and driving a similar range of propellers, also through a 2.58:1 Rotax gearbox.

Both of these early Thruster variants were certified to the 1983 Advance issue of BCAR Section S.

Figure 98. Thruster TST Mk.1



B12 Thruster T600 and T600 Sprint

The Thruster T600 is two-seat side-by-side conventional 3-axis tractor aeroplane with a high wing and mid tail. The aircraft is available in two undercarriage configurations, the T600N (nosewheel) and T600T (tailwheel). The type was derived via the Thruster T300 from the Thruster TST (Two-Seat-Trainer), an Australian aircraft which became the first readily available 3-axis training microlight in the UK.

The aircraft has an MTOW of 450kg and a wing area of 15.7m². V_{ne} is 102 kn IAS (exact correction is unknown, but slight overread is believed to occur) and V_{so} is 31.5 kn CAS.

A typical example of the aircraft might be fitted with a Jabiru 2.2L engine generating around 50kW. This is a direct drive horizontally opposed 2-cylinder 4-stroke engine, and is likely to be driving a Warp Drive 64" x 8.5° 2-blade composite propeller.

These aircraft were certified to BCAR Section S issue 2.

Figure 99. Thruster T600N Sprint



B13 Flightdesign / Pegasus CT2K

The CT2K is a British development of the German Flightdesign CT, which was originally designed for certification against the German microlight standard BFU-95. The type is a high (cantilever) wing side tractor, with side-by-side seating and dual controls. The aircraft is fitted with an electric flap system variable between -12° and 40° . Negative (high speed cruise) flap settings also reflex the ailerons.

The aircraft has an MTOW of 450kg and wing area of 10.8 m². V_{RA} is 115 kn, V_{NE} is 150 kn, V_{S1} is 43 kn and V_{S0} is 34 kn CAS.

At time of writing, all examples of the type are fitted with a Rotax 912ULS engine generating about 100 hp, driving a 1,66m 2-blade Neuform composite propeller through a 2.43:1 gearbox.

The aircraft was certified to BCAR Section S issue 2.

Figure 100, Flightdesign CT2K



B14 Sky Ranger UK

The Sky Ranger is a nosewheel configuration, single engine high-wing tractor monoplane. The UK version is slightly modified (by strengthening of the control circuits, addition of a ventral fin to enhance directional stability, and other smaller modifications from a similarly named aircraft originally designed and operated in France. The aircraft is fitted with dual controls, although in fact the control column, pitch trimmer and flap controls are fitted centrally in the cabin and shared between pilots, only the throttle and pedals being duplicated.

The aircraft has an MTOW of 450kg and wing area of 10.8 m². V_A is 72 kn, V_{NE} is 108 kn, V_{SI} is 36 kn and V_{S0} is 33 kn CAS.

Most examples in the UK are fitted with Rotax 912UL engines driving a 2-blade wood, or 3-blade composite propeller.

The aircraft is certified to BCAR Section S issue 2.

Figure 101, Sky Ranger UK



Photograph courtesy of Flylight Airsports Ltd

B15 Naval Aircraft Factory N3N-3.

The N3N-3 is a tailwheel configuration, single engine biplane with 2 seats in a tandem arrangement. It was originally built in 1941 by and for the United States Navy as a training aeroplane. The aircraft does not fall into the microlight category, but has been used during the report because take-off and landing performance testing carried out on it, and reported in Appendix A to this thesis, has relevance to microlight testing.

The aircraft has an MTOW of 1373 kg in public transport operation and a wing area of 28.3m². V_{so} is 46.5 kn CAS and V_{ne} is 142 kn CAS.

The sole example of the type in the UK is G-ONAF, which is fitted with a Wright R-760 radial engine generating about 170kW driving a fixed pitch 2.74m diameter propeller (original equipment, pitch setting unknown).

The original certification basis for the aircraft is uncertain, although BCAR Section K issue 7 was used for the transfer of the aircraft from private to public transport certification.

Figure 102. Naval Aircraft Factory N3N-3



APPENDIX C

REFERENCES

(Note: Some reference documents are repeated due to multiple reference within the text)

- 1 UK Civil Aviation Authority, British Civil Airworthiness Requirements, Section S, Small Light Aeroplanes, *CAP 482 issue 2*.
- 2 G B Gratton, "The weightshift-controlled microlight aeroplane", *Proc Instn Mech Engrs Vol 215 Part G pp147-154*
- 3 Source, data from statistics section, Civil Aviation Authority Safety Regulation Group.
- 4 UK Civil Aviation Authority, British Civil Airworthiness Requirements, Section S, Small Light Aeroplanes, *CAP 482 working draft, April 1983*.
- 5 G B Gratton, A dispersed airworthiness management system – the model of the British Microlight Aircraft Association, *International Journal of Aerospace Management, ISSN 1469-342, Vol.1 No.4, pp329-335 (Feb 2002)*
- 6 Joint Aviation Requirements, 1.1 General Definitions
- 7 Deutschen Aero Club e.V., Bauvorschriften für Ultraleichtflugzeuge, *BFU-95 dated 12 Oct 1995*
- 8 Luftfahrt-Bundesamtes, Bekanntmachung von Lufttüchtigkeitsforderungen für aerodynamisch gesteuerte Ultraleichtflugzeuge, *LTF-UL dated 30 Jan 2003*
- 9 Joint Aviation Authorities (JAA), Joint Airworthiness Requirements Part 22, Sailplanes and Powered Sailplanes, *JAR-22 AL8*
- 10 Joint Aviation Authorities (JAA), Joint Airworthiness Requirements Part VLA, Very Light Aeroplanes, *JAR-VLA AL1*
- 11 G B Gratton, BMAA Code of Practice for Microlight Hire, *BMAA Technical Information Leaflet No. 032 issue 1a, dated April 2003*.
- 12 British Microlight Aircraft Association, PPL(A) Microlight Training Syllabus, *Revision as at 14 Dec 1998*
- 13 Kilkenny, E., Longitudinal Static Stability of Hang-Gliders, *Phd Thesis, Cranfield University, 1988*
- 14 Source: author's personal notes from "qualeval" flight test assessment of Airborne XT912 / Streak III aircraft T2-22252 at Shifnal airfield, 14 May 2004.
- 15 Enzo Boschi, Il delta "intelligente", *Volare Sport Jan 99, pp32-33*
- 16 Air Accidents Investigation Branch, AAIB Bulletin No: 1/2000 Ref: EW/C99/8/5
- 17 British Civil Airworthiness Requirements, Section S, Small Light Aeroplanes *CAP 482*.
- 18 British Microlight Aircraft Association, Flight Test Schedule BMAA/AW/010b
- 19 British Microlight Aircraft Association, Microlight Maintenance Schedule MMS1 issue 2, *Technical Information Leaflet 020 issue 1*
- 20 Brooks, W.G., Flight Testing of Flexwings. http://www.raes.org.uk/light-av/brooks_p_1.htm

- 21 Cook, M V, The theory of the longitudinal static stability of the hang-glider, *Aeronautical Journal*, Oct 1994, pp292-304
- 22 Gratton, G.B. and Porteous, T, The Creation of a Formal Test Flying System Within The British Microlight Aircraft Association and a Discussion of the Spin Testing of Microlight Aircraft <http://www.setp.org/microlightaircraft.htm>
- 23 British Microlight Aircraft Association, BMAA Code of Practice for Microlight Hire, *TIL 032 issue 1a, April 2003*
- 24 EL Houghton and NB Caruthers, Aerodynamics for Engineering Students 3rd Edition, *ISBN 0-7131-3433-X*
- 25 Piper Aircraft Corporation, Cherokee Warrior II Information Manual, *Report VB-880*
- 26 ACI Stall Warning entry page, <http://homepages.which.net/~aci.stw/>
- 27 J M Pratt, Cessna 152 – A Pilots Guide, *ISBN 1-874783-30-6*
- 28 Empire Test Pilots School, Course Notes, No. 20 FTE Course 1996.
- 29 British Microlight Aircraft Association, Test Schedule for 3-axis performance and handling (Section S issue 2 compliance, Vd not exceeding 140 knots), *BMAA/AW/010a*
- 30 British Microlight Aircraft Association, Test Schedule for weightshift performance and handling (Section S issue 2 compliance, Vd not exceeding 140 knots), *BMAA/AW/010b*
- 31 H Glauert, The Elements of Aerofoil and Airscrew Theory, *Cambridge University Press, First Edition, 1926.*
- 32 M E Eshelby, Aircraft Performance, Theory and Practice. *ISBN 0-340-75897-X*
- 33 R Venton-Walters, Raven Operators Manual, *Southdown International Report R150 Issue 3 12 February 1986.*
- 34 R Venton-Walters, Re: Flexwing Stalling Speeds, *Email to G B Gratton dated 2 May 2002*
- 35 R Venton-Walters, Raven Operators Manual, *Report R150 Issue 3, 12 February 1986*
- 36 UK Civil Aviation Authority, Raven-X, *Type Approval Data Sheet No. BM13 issue 4.*
- 37 Joint Aviation Authorities (JAA), Joint Airworthiness Requirements Part 22, Sailplanes and Powered Sailplanes, *JAR-22 AL8*
- 38 Joint Aviation Authorities (JAA), Joint Airworthiness Requirements Part VLA, Very Light Aeroplanes, *JAR-VLA AL1*
- 39 Joint Aviation Authorities (JAA), Joint Airworthiness Requirements Part 23, Normal, Utility, Aerobatic, and Commuter Category Aeroplanes, *JAR-23 AL2*
- 40 Joint Aviation Authorities (JAA), Joint Airworthiness Requirements Part 23, Large Aeroplanes, *JAR-22 AL17*
- 41 UK Civil Aviation Authority, part K3-2 “Flight Manoeuvring Loads and Design Airspeeds) to British Civil Airworthiness Requirements Section K: Light Aeroplanes, *CAP 467 issue 7.*
- 42 B Cosgrove, Microlight Pilots Handbook, *ISBN 1-85310-808-1*

-
- 43 Nickel and Wohlhart (translated from German by Capt. E M Brown), *Tailless Aircraft in Theory and Practice. ISBN 1-56347-0942*
 - 44 J K Northrop, *The development of all-wing aircraft, 35th Royal Aeronautical Society Wilbur Wright memorial lecture, 1947.*
 - 45 B Cosgrove, *Pilots Weather, ISBN 1-84037-027-0 (pp45-46)*
 - 46 UK Air Accidents Investigation Branch, *Report of Fatal Accident to Pegasus XL-Q G-MYBR on 21 August 1999, AAIB Bulletin No: 1/2000 Ref: EW/C99/8/5*
 - 47 British Microlight Aircraft Association, *KISS-400(UK), Homebuilt Aircraft Data Sheet No. HM7 issue 1*
 - 48 Authorised by G B Gratton, PM Dewhurst, D Coupland, *KISS-400 (UK) Operators Manual, Issue 1 ALO*
 - 49 British Microlight Aircraft Association, *KISS-400(UK), Homebuilt Aircraft Data Sheet No. HM7 issue 1*
 - 50 Authorised by G B Gratton, PM Dewhurst, R Thomasson, *KISS-450 (UK) Operators Manual, Issue 1 ALO*
 - 51 Authorised by G B Gratton, P M Dewhurst, R J Grimwood, *Air Creation iXess operators manual, Issue 1, AL1*
 - 52 Source: conversations between author and Dr. W.G.Brooks, Technical Director, P&M Aviation, during 2003 and 2004.
 - 53 D Stinton, *Flying Qualities and Flight Testing of the Aeroplane, ISBN 0-632-02121-7*
 - 54 USAF Test Pilots School Notes, Part 10 High Angle of Attack Flight
 - 55 Empire Test Pilots School, *Fixed Wing Flight Test Manual, Chapter 2.8 - Spinning*
 - 56 UK Ministry of Defence, *Stalling Post-Stalling Gyration and Spins and Miscellaneous Flying Qualities – Post Stall Gyration and Spins. Def-Stan 00-970 Part 1 Section 2 Leaflet 52 issue 2 Dec 99*
 - 57 Yangos and Yangos, *Spin: Angles and Inertial Moments, Aeronautical Journal July/Aug 1981 pp270-276*
 - 58 T E Archer, *Are you ready for LOC?, Cockpit (magazine of the Society of Experimental Test Pilots), April/May/June 1991 pp5-12*
 - 59 A&L Welch, *Flying Training in Gliders, Published by British Gliding Association Sixth Edition 1975*
 - 60 UK Air Accidents Investigation Branch, *Report of Fatal Accident to Aviasud Mistral G-MYST on 23 June 2001, AAIB Bulletin No: 6/2002 Ref: EW/2001/6/9*
 - 61 UK Air Accidents Investigation Branch, *Report of Accident to Taylor J.T.1 Monoplane G-BEEW on 2 September 2001, AAIB Bulletin No: 11/2001 Ref: EW/G2001/09/03*

-
- 62 UK Air Accidents Investigation Branch, Report of Fatal Accident to Whittaker MW6S (modified) G-MZIN on 28 March 1999, *AAIB Bulletin No: 8/99 Ref: EW/C99/3/1*
 - 63 UK Air Accidents Investigation Branch, Report of Accident to Europa G-KWIP on 21 March 2000, *AAIB Bulletin No: 4/2001 Ref: EW/C2000/3/4*
 - 64 UK Air Accidents Investigation Branch, Report of Fatal Accident to Jodel D112 G-BCOG on 26 July 1998, *AAIB Bulletin No: 12/98 Ref: EW/C98/7/8*
 - 65 UK Air Accidents Investigation Branch, Report of Fatal Accident to Rallye Club 880B, G-AYKF on 26 August 1996, *AAIB Bulletin No: 2/97 Ref: EW/G96/8/9*
 - 66 UK Civil Aviation Authority, *LASORS 2005*
 - 67 Source, authors notes from flight test to Airborne XT912 / Wizard III aircraft T2-22252 flown at Shifnal, 14 May 2004.
 - 68 Source, conversations during the period of this research between author and Mr C J Draper, Proprietor, Medway Microlights.
 - 69 Piper Aircraft Corporation, Cherokee Warrior II Information Manual, *Report VB-880*
 - 70 Royal Air Force, Flying, *AP3456*
 - 71 N Williams, Aerobatics, *ISBN 0950454303*
 - 72 J S Denker, See How it Flies, <http://www.monmouth.com/~jsd/how/>
 - 73 R Stowell, Innovations in Stall/Spin Awareness Training, Presented to (USA) Second Annual Instructor Conference, Embry Riddle Aeronautical University, April 9-10, 1999. <http://www.richstowell.com/erau.htm>
 - 74 UK Air Accidents Investigation Board, Spectrum Microlight G-MWWY, *Bulletin 3/98 EW/C97/8/8*
 - 75 G Weighell, Quite Simple Really, *Microlight Flying Nov-Dec 01 pp44-45*
 - 76 UK CAA, *LASORS 2004*
 - 77 Minutes of the 24th meeting of the Airworthiness Requirements Board Light Aircraft Committee (Nov 1998)
 - 78 British Microlight Aircraft Association, Guidance on Spin Testing Microlight Aircraft, *TIL 025 issue 1 dated December 1999.*
 - 79 G B Gratton and S J Dyde, Tucano T Mk 1 - Assessment of possible unified spin recoveries, *Report D/A & E/BD/95/128, Dec 1995*
 - 80 G B Gratton, Bulldog T Mk 1 - Assessment of Lycoming modification 330 (Revised) engine inverted oil system, *PE/Bulldog/17*
 - 81 Philip W Neihouse, Jacob H Lichtenstein, Jacob H Pepoon, Tail-design requirements for satisfactory spin recovery, *NACA TN-1045(April 1946)*
 - 82 G B Gratton, "The weightshift-controlled microlight aeroplane", *Proc Instn Mech Engrs Vol 215 Part G pp147-154*

-
- 83 G B Gratton, "Less Weight More Fun", *Aerospace International*, Feb 2000, pp 30-32
 - 84 UK Civil Aviation Authority, Aviation Safety Review 1990-1999, CAP 701
 - 85 S J Morris, A Simplified Analysis of Tumbling Motion, *Hang Gliding*, Nov 1994, pp38-44.
 - 86 W G Brooks, "Report on an accident to a Pegasus Quantum Supersport 503, in Holland Michigan, USA, on 16 October 2000", <http://www.pegasusaviation.co.uk/pdf/Qtmacc.pdf>
 - 87 UK Air Accidents Investigation Branch; Bulletin 5/2000: EW/C97/10/5 (Mainair Gemini Flash 2a G-MVEP; Fatal Accident)
 - 88 UK Air Accidents Investigation Branch; Bulletin 1/97: EW/C96/7/8 (Mainair Gemini Flash 2a G-MTLA; Fatal Accident)
 - 89 UK Air Accidents Investigation Branch; Bulletin 8/92: EW/C92/5/1 (Pegasus XL-Q, G-MVCU; Fatal Accident).
 - 90 J Thomas, "Report of an incident that occurred on Sunday 21 July at Bedford Microlight Centre" (Unreferenced report of a recovered in-flight departure submitted to BMAA - Mainair Gemini Flash 2 G-MNNU).
 - 91 UK Air Accidents Investigation Branch; Bulletin 9/89: EW/C1108 (Mainair Gemini Flash 2a G-MTUW, Fatal accident)
 - 92 UK Air Accidents Investigation Branch; Bulletin 4/86: EW/C918 (Mainair Gemini Flash 2a G-MNEJ; Fatal Accident)
 - 93 Mainair Sports Ltd, Accident Investigation, Bulletin No. 20, 1 Sept 1986 (Mainair Gemini Flash 2 G-MNNF, survived in-flight break-up during flight testing)
 - 94 Mainair Sports Ltd, Accident Report, Bulletin No. 21, 15 Sept 1986 (Pegasus Flash 2, G-MNYY, survived in-flight break-up during initial testing of a newly built aircraft)
 - 95 Source: Multiple conversations between the author and (a) Check Pilot Brian Searle, and (b) Test Pilot John Hamer, both of whom had suffered in-flight breakups following tumble departures from controlled flight.
 - 96 Source: Multiple conversations between author and technical staff at Mainair Sports Ltd (in particular with Mr Roger Patrick, Chief Designer) between 1997 and 2002.
 - 97 Bisplinghoff, R.L., Ashley, A., Halfman, R.L. Aeroelasticity, *Addison-Wesley* 1955
 - 98 Y.C. Fung, An Introduction to the Theory of Aeroelasticity, *John Wiley*, 1955.
 - 99 O.Moncrieff, The Tumble Behaviour of Weightshift Controlled Microlight Aircraft, *University of Southampton Project report No. IP/211*, Oct 2003-Apr 2004
 - 100 UK Civil Aviation Authority, Mainair Gemini Flash 2 alpha, *Type Approval Data Sheet No. BM23 issue 11*

-
- 101 J F Douglas, J M Gasiorek, J A Swallowfield, Fluid Mechanics (second edition, pp306-310), ISBN 0-582-98861-6
 - 102 E A Kilkenny, An Experimental Study into the Longitudinal Aerodynamic and Static Stability Characteristics of Hang Gliders, *PhD Thesis, Cranfield Institute of Technology, September 1986*
 - 103 W G Brooks, Flight testing of flexwing aircraft, http://www.raes.org.uk/light-av/brooks_p_1.htm
 - 104 British Microlight Aircraft Association, PPL(A) Microlight Training Syllabus
 - 105 UK Civil Aviation Authority, Wake Turbulence, *General Aviation Safety Sense Leaflet No. 15A*
 - 106 UK Civil Aviation Authority, Wake Turbulence, *AIC 178/1993 (Pink 95)*
 - 107 B Cosgrove, Pilots Weather, ISBN 1-84037-027-0 (pp45-46)
 - 108 UK Air Accidents Investigation Branch, Report of Fatal Accident to Microlight, G-MVJU
 - 109 Source: correspondence between author, James Doolittle III and Brig.Gen. Bob Robert Cardinas, USAF(Rtd)
 - 110 http://www.check-six.com/Crash_Sites/YB-49_crash_site.htm
 - 111 D. Ford, "The Edwards Diaries", published in *Air and Space (Smithsonian Magazine)*, June/July 1997.
 - 112 H Matthews, DH.108 The sage of the first British supersonic aircraft, *HPM Publications 1997*
 - 113 D. Collier Webb , UK Flight Testing Accidents 1940-71, ISBN 0 85130 311 1
 - 114 G de Havilland Sr., Sky Fever, the Autobiography of Sir Geoffrey de Havilland, ISBN 0-905-778-405
 - 115 Article in Herts Advertiser and St Albans Times, week commencing 30 September 1946
 - 116 Stefanie Brochocki, Presentation to the July 15, 2000, TWITT meeting held in El Cajon, CA, <http://members.cox.net/rebid/Brochocki.html>
 - 117 Stefan Brochocki, A new tailless sailplane BKB-1, paper presented to the 8th OSTIV conference, Cologne, Germany, June 1960
 - 118 Stefan Brochoki, transcript of a lecture given to a branch of the Experimental Aircraft Association, St-Anne de Bellevue, Quebec, 1990. <http://members.cox.net/rebid/1990Lecture.html>
 - 119 J Mitchell, Witold Kasper and his aircraft, presentation to TWITT meeting November 21 1998, <http://members.cox.net/twitt/kasperminutes.htm>
 - 120 Flight Test Safety Committee, Test Card Creation and Approval, http://www.flighttestsafety.org/bestpractices/test_card_creation.htm
 - 121 G B Gratton (for Britten-Norman Group Ltd), Report recommending transfer of N3N-3 Reg: G-ONAF from private to public transport category certificate of airworthiness, *GBG/BNG/N3N/1, issue 2 dated 31 July 2002*
 - 122 UK Civil Aviation Authority, British Civil Airworthiness Requirements Section K, Light Aeroplanes. *CAP 467 issue 7 October 1992.*

-
- 123 F J Hale, Introduction to Aircraft Performance, Selection and Design, *ISBN 0-471-07885-9*
 - 124 British Microlight Aircraft Association, Form BMAA/AW/043 issue 1a
 - 125 Williams, Aviation Formulary, <http://www.best.com/~williams/avform.html>
 - 126 Royal Air Force No.1 AIDU, Flight Information Handbook (“The yellow book”), *this book carries no formal reference and is re-issued at 6 monthly intervals and referred to by title only.*
 - 127 J T Lowry, Performance of Light Aircraft, *ISBN 1-56347-33A-5*
 - 128 G Lewis (National Test Pilot School), Using GPS to determine pitot-static errors, 14 August 2003, <http://www.ntps.edu/Files/GPS%20PEC%20Method.doc>
 - 129 D Gray, Using GPS to accurately establish True Air Speed (TAS), Dated *June 1998 – privately published, no formal reference.*
 - 130 F L Thompson (Langley Memorial Laboratory, NACA), The measurement of air speed of airplanes, *NACA Technical Note No. 616, October 1937.*
 - 131 E Arnold, Certification of Spin Resistant Aircraft, *Society of Experimental Test Pilots – Report to the Profession 1999, pp58-73.*
 - 132 G B Gratton, Bulldog T Mk 1 - Assessment of Lycoming modification 330 (Revised) engine inverted oil system, *A&AEE Report No. PE/Bulldog/17*
 - 133 Sales literature by Ballistic Recovery Systems Inc, USA. <http://www.airplaneparachutes.com/>
 - 134 L G Janssens, J Russell, FAA Certification of the Liberty XL2, proceedings of the 2004 joint European Symposium of the Society of Experimental Test Pilots and Society of Flight Test Engineers.
 - 135 UK Civil Aviation Authority, British Civil Airworthiness Requirements, Section S, Small Light Aeroplanes, *CAP 482 issue 3.*
 - 136 UK Civil Aviation Authority, Take-off, climb and landing performance of light aeroplanes, *AIC 12/1996 Pink 120.*
 - 137 Empire Test Pilots School, Course Notes (No. 20 Flight Test Engineer Course, 1996).
 - 138 United Kingdom Accreditation Service, The Expression of Uncertainty and Confidence in Measurement, M3003
 - 139 G B Gratton, Post Flight Report, HM 1000 Balerit, Determination of take-off, climb, and landing performance, *1 Nov 01, Sortie 2, authorised by test schedule Special/MAAN 1562 / 1.*
 - 140 UK Civil Aviation Authority, Aeroplane Performance, *General Aviation Safety Sense Leaflet 7b.*
 - 141 R Pooley, R Patel, W Ryall; Pooleys Flight Guide United Kingdom, *ISBN 1-84336-0357-7*

- 142** G B Gratton, Report recommending transfer of N3N-3 Reg: G-ONAF from private to public transport category certificate of airworthiness, *GBG/BNG/N3N/1 issue 1 dated 26 May 2002 (Britten-Norman Group Ltd)*.